

**University of Alberta**

**Protein Separations in Capillary Zone Electrophoresis using Cationic  
Surfactant Coatings**

by

**Mahmoud Mohammad Yassine**



**A thesis submitted to the Faculty of Graduate Studies and Research in partial fulfillment  
of the requirements for the degree of Doctor of Philosophy.**

**Department of Chemistry**

**Edmonton, Alberta**

**Fall 2006**



Library and  
Archives Canada

Bibliothèque et  
Archives Canada

Published Heritage  
Branch

Direction du  
Patrimoine de l'édition

395 Wellington Street  
Ottawa ON K1A 0N4  
Canada

395, rue Wellington  
Ottawa ON K1A 0N4  
Canada

*Your file* *Votre référence*  
*ISBN: 978-0-494-23131-9*  
*Our file* *Notre référence*  
*ISBN: 978-0-494-23131-9*

#### NOTICE:

The author has granted a non-exclusive license allowing Library and Archives Canada to reproduce, publish, archive, preserve, conserve, communicate to the public by telecommunication or on the Internet, loan, distribute and sell theses worldwide, for commercial or non-commercial purposes, in microform, paper, electronic and/or any other formats.

The author retains copyright ownership and moral rights in this thesis. Neither the thesis nor substantial extracts from it may be printed or otherwise reproduced without the author's permission.

#### AVIS:

L'auteur a accordé une licence non exclusive permettant à la Bibliothèque et Archives Canada de reproduire, publier, archiver, sauvegarder, conserver, transmettre au public par télécommunication ou par l'Internet, prêter, distribuer et vendre des thèses partout dans le monde, à des fins commerciales ou autres, sur support microforme, papier, électronique et/ou autres formats.

L'auteur conserve la propriété du droit d'auteur et des droits moraux qui protègent cette thèse. Ni la thèse ni des extraits substantiels de celle-ci ne doivent être imprimés ou autrement reproduits sans son autorisation.

---

In compliance with the Canadian Privacy Act some supporting forms may have been removed from this thesis.

Conformément à la loi canadienne sur la protection de la vie privée, quelques formulaires secondaires ont été enlevés de cette thèse.

While these forms may be included in the document page count, their removal does not represent any loss of content from the thesis.

Bien que ces formulaires aient inclus dans la pagination, il n'y aura aucun contenu manquant.

  
**Canada**

## ABSTRACT

Capillary electrophoresis (CE) is a separation technique based on the differential migration of charged species in an electric field. The separation of proteins is not always possible since they tend to adsorb onto the capillary surface. Herein, cationic surfactants are employed to improve cationic protein separations in a simple and inexpensive way.

Surfactants such as didodecyldimethylammonium bromide (DDAB) adsorb onto fused silica capillaries to form semi-permanent bilayer coatings. However, initially such coatings had to be regenerated between runs to maintain efficiency and reproducibility. My studies demonstrate that reducing the capillary diameter and the volume of buffer flushed through the capillary enhance the coating stability. Chemical factors such as ionic strength and nature of the buffer anion, which decrease the critical micelle concentration (cmc) of the surfactant, improve the coating stability. The stability of the surfactant coating can also be increased with increasing the hydrophobicity of the surfactant monomers (i.e., increasing chain length and decreasing cmc). Over 60 successive separations were performed on a dimethyldioctadecylammonium bromide ( $2C_{18}DAB$ ) coated capillary over a 12-day period, without any regeneration of the coating. The separation efficiencies for four model cationic proteins ranged from 1.2-1.4 million plates/m for the dimethylditetradecylammonium bromide ( $2C_{14}DAB$ ) coating to 0.3-0.4 million plates/m for the  $2C_{18}DAB$  coating.

The enhanced stability of the surfactant coatings made possible their use to separate proteins at preparative scale levels using wide bore capillaries. At protein concentrations greater than 1 g/L, electromigration dispersion became the dominant source of band broadening, and the peak shape distorted to triangular fronting. Matching

of the mobility of the buffer co-ion to that of the analyte resulted in dramatic improvements in the peak shapes at preparative scales. The maximum sample loading capacity of 160 picomoles of each protein was achieved in a single run with a 100  $\mu\text{m}$ -2C<sub>14</sub>DAB coated capillary.

Finally, off-line coupling of preparative CE with the microwave-assisted acid hydrolysis (MAAH) for protein characterization was described. The protein separations and characterization were performed within an hour. Furthermore, the amino acid sequence of the protein can be read directly from one spectrum. The peptide sequence coverage achieved by CE/MAAH was 95%.

## ACKNOWLEDGMENTS

I would like to thank my supervisor, Dr. Charles A. Lucy, for his continual guidance, support and encouragement through out my graduate program, and for giving me the chance to carry out this research project in his lab. I am very grateful for his patience, kindness and valuable advice.

Present and past members of the Lucy group are gratefully acknowledged for their fruitful ideas, discussions and friendship. Also, I would like to thank Drs. Kimberly Roy and Nicole Baryla for their help with the CE system. My thanks are extended to Dr. Liang Li for the use of the MALDI/TOF MS. In particular, I would like to thank Nan Guo for her invaluable assistance with MAAH/MALDI data analysis and helpful discussions. I would also like to express my gratefulness to members of my thesis defense committee, Drs. John-Bruce Green, Jed Harrison, Todd Lowary, Anthony Yeung, and Annelise Barron, for their comments and critique on this thesis. Especial thanks also go to Dr. Monica Palcic for her support, comments and helpful discussions.

I should also express my deepest appreciation to my parents, brothers and sisters for their continued love, enthusiasm, and support. I am thankful to all my friends, in particular Drs. Mirwais Aktary and Abebaw Diress, for their encouragements and support. Warm thanks are also expressed to my wife, Mervat Elsiri, and my lovely children, Osama, Mohammad, and Mona. Mervat, without your love, encouragement, and unconditional support, this work would not have been successful.

Finally, I would like to thank the Department of Chemistry at the University of Alberta for the Dissertation Fellowship, Province of Alberta Graduate Fellowship and

General Research Award. I also would like to thank Novartis Pharmaceuticals Canada Inc for their generous scholarship.

The University of Alberta, the Natural Sciences and Engineering Research Council of Canada (NSERC) and Bristol-Myer Squibb provided financial support for this research.

*Dedicated to My Family*

# TABLE OF CONTENTS

## CHAPTER ONE: Introduction

1.1	History .....	1
1.2	Principles of Capillary Electrophoresis .....	3
1.2.1	Instrumentation .....	3
1.2.2	Electroosmotic Flow .....	5
1.2.3	Electrophoretic Mobility .....	9
1.2.3.1	Absolute Electrophoretic Mobility .....	11
1.2.3.2	Effective Electrophoretic Mobility .....	12
1.2.3.3	Apparent Mobility .....	14
1.3	Detection .....	16
1.3.1	On-line UV Absorbance .....	17
1.3.2	Mass Spectrometric Detection .....	18
1.3.2.1	ESI .....	18
1.3.2.2	MALDI .....	19
1.4	Band Broadening in CE .....	21
1.4.1	Extra-column Band Broadening .....	23
1.4.1.1	Injection .....	23
1.4.1.2	Detection .....	24
1.4.2	Longitudinal Diffusion .....	25
1.4.3	Thermal Effects .....	26
1.4.4	Electromigration Dispersion .....	28
1.4.5	Siphoning .....	31
1.4.6	Solute/Wall Interaction .....	32
1.5	Protein Separation in CZE .....	34
1.6	Capillary Wall Coatings .....	37
1.6.1	Covalently Bonded Coatings .....	37
1.6.2	Adsorbed Polymer Coatings .....	38
1.6.2.1	Non-ionic Polymer Coatings .....	39
1.6.2.2	Cationic Polymer .....	39
1.6.3	Adsorbed Surfactant Coating .....	41
1.7	Thesis Overview .....	46
1.8	References .....	47

## **CHAPTER TWO: Factors Affecting the Temporal Stability of Semi-permanent Bilayer Coatings in Capillary Electrophoresis Prepared using Double Chained Surfactants**

2.1	Introduction.....	54
2.2	Experimental Section.....	56
2.2.1	Apparatus.....	56
2.2.2	Chemicals.....	56
2.2.3	EOF Measurements.....	57
2.2.4	Coating Stability.....	58
2.2.5	cmc Determination.....	59
2.2.6	Protein Separations.....	60
2.3	Results and Discussion.....	61
2.3.1	Kinetic Model.....	64
2.3.2	Effect of Rinse Pressure.....	69
2.3.3	Effect of Capillary Diameter.....	72
2.3.4	Effect of Buffer Ionic Strength.....	75
2.3.5	Effect of Buffer Counter-ion Nature.....	78
2.3.6	Effect of Buffer pH.....	79
2.3.7	Role of cmc.....	81
2.3.8	Aging Time.....	82
2.3.9	Protein Separations.....	84
2.4	Conclusions.....	89
2.5	References.....	91

## **CHAPTER THREE: Enhanced Stability Self-assembled Coatings for Protein Separations by Capillary Zone Electrophoresis through the use of Long Chained Surfactants**

3.1	Introduction.....	94
3.2	Experimental Section.....	96
3.2.1	Apparatus.....	96
3.2.2	Chemicals.....	96
3.2.3	Preparation of the Surfactant Solutions.....	98
3.2.4	EOF Measurements.....	98
3.2.5	Coating Stability.....	99
3.2.6	Protein Separations.....	99

3.3	Results and Discussion .....	100
3.3.1	Effect of Buffer on EOF .....	101
3.3.2	Effect of Surfactant on EOF .....	103
3.3.3	Effect of pH on EOF .....	106
3.3.4	Effect of Surfactant Concentration on EOF .....	108
3.3.5	Protein Separations .....	111
3.4	Conclusions.....	117
3.5	References.....	120

#### **CHAPTER FOUR: Preparative Capillary Zone Electrophoresis using a Dynamic Coated Wide-bore Capillary**

4.1	Introduction.....	123
4.2	Experimental Section.....	126
4.2.1	Apparatus .....	126
4.2.2	Chemicals.....	126
4.2.3	Coating Procedure.....	127
4.2.4	Protein Separations .....	128
4.3	Results and Discussion .....	130
4.3.1	Protein Separation under Trace Conditions .....	130
4.3.2	Effect of Analyte Concentration under Preparative Conditions .....	133
4.3.3	Effect of Buffer Concentration .....	137
4.3.4	Effect of Buffer co-ion.....	139
4.3.5	Maximizing sample loading.....	140
4.4	Conclusions.....	144
4.5	References.....	146

#### **CHAPTER FIVE: Off-line Coupling of Preparative Capillary Zone Electrophoresis with Microwave-assisted Acid Hydrolysis for Protein Characterization**

5.1	Introduction.....	149
5.2	Background.....	151
5.3	Experimental Section.....	153
5.3.1	Apparatus .....	153

5.3.2	Chemicals.....	154
5.3.3	Coating Procedure.....	155
5.3.4	Protein Separations .....	155
5.3.5	CE Fraction Collection .....	155
5.3.6	Protein Digestion .....	158
5.3.7	Sample Preparation for MALDI-TOF MS Analysis.....	158
5.4	Results and Discussion .....	159
5.4.1	CE Fraction Collection .....	160
5.4.2	Determination of the Fractions Purity by MALDI-TOF MS.....	166
5.4.3	Sources of Contamination in the Bovine Protein Fraction .....	168
5.4.4	Microwave-assisted Acid Hydrolysis Analysis .....	173
5.4.5	MAAH/MALDI with Bis-tris Phosphate Buffer .....	177
5.4.6	Effect of 2C <sub>18</sub> DAB Surfactant on MAAH/MALD .....	182
5.4.7	Effect of Buffer Concentration on MAAH/MALDI.....	183
5.5	Conclusions.....	188
5.6	References.....	189

## CHAPTER SIX: Summary and Future Work

6.1	Summary.....	192
6.2	Future Work.....	196
6.2.1	On-line ESI-MS .....	196
6.2.2	EOF Control for Preparative CZE Applications.....	197
6.3	References.....	201

## LIST OF TABLES

<b>Table 2.1</b>	Effect of rinsing conditions on DDAB bilayer.....	70
<b>Table 2.2</b>	Effect of capillary inner diameter on DDAB bilayer .....	74
<b>Table 2.3</b>	Effect of ionic strength of sodium phosphate buffer at day 0 on DDAB bilayer.....	77
<b>Table 2.4</b>	Effect of buffer type and pH on DDAB bilayer .....	80
<b>Table 3.1</b>	Physico-chemical properties of cationic surfactants used as coatings .....	97
<b>Table 3.2</b>	Effect of hydrodynamic rinsing on DDAB bilayer .....	102
<b>Table 3.3</b>	Effect of increasing the capillary inner diameter on the stability of the DDAB and 2C <sub>14</sub> DAB surfactant bilayer coatings.....	107
<b>Table 3.4</b>	Effect of 2C <sub>14</sub> DAB concentration on the stability of the bilayer .....	110
<b>Table 3.5</b>	Migration time of the cationic proteins separated using 2C <sub>14</sub> DAB, 2C <sub>18</sub> DAB, and 3C <sub>12</sub> MAI .....	113
<b>Table 3.6</b>	Migration time reproducibility, peak height reproducibility, and efficiency reproducibility of the cationic proteins separated using 2C <sub>18</sub> DAB coating over a 12-day period .....	116
<b>Table 3.7</b>	Average migration time within the day for the cationic proteins separated using 2C <sub>18</sub> DAB coating over a 12-day period .....	116
<b>Table 3.8</b>	Migration time reproducibility, peak height reproducibility, and efficiency reproducibility of the cationic proteins separated using 3C <sub>12</sub> MAI coating over a 5-day period.....	118
<b>Table 3.9</b>	Average migration time within the day for the cationic proteins separated using 3C <sub>12</sub> MAI coating over a 5-day period .....	118
<b>Table 4.1</b>	Peak efficiency and peak asymmetry factor of h-cyt c separated in 25, 50 and 100 $\mu\text{m}$ i.d. capillaries coated with 2C <sub>14</sub> DAB.....	131
<b>Table 4.2</b>	Peak efficiency and peak asymmetry factor of h-cyt c at different concentrations separated using 100 $\mu\text{m}$ i.d. capillary coated with 2C <sub>14</sub> DAB .....	135

<b>Table 4.3</b>	Effective mobility of buffer co-ion, effective electrophoretic mobility, and peak asymmetry factor of b-cyt <i>c</i> and h-cyt <i>c</i> at different buffer concentrations separated by 100 $\mu\text{m}$ i.d. capillary using 2C <sub>14</sub> DAB coating .....	139
<b>Table 4.4</b>	Effective mobility of buffer co-ion, effective electrophoretic mobility, and peak asymmetry factor of b-cyt <i>c</i> and h-cyt <i>c</i> with different buffer co-ions separated by 100 $\mu\text{m}$ i.d. capillary using 2C <sub>14</sub> DAB coating .....	142
<b>Table 4.5</b>	Sample amount of each protein, resolution, and peak asymmetry factor of b-cyt <i>c</i> and h-cyt <i>c</i> separated by 100 $\mu\text{m}$ i.d. capillary using 2C <sub>14</sub> DAB coating at different sample concentrations .....	144
<b>Table 5.1</b>	Mass resolution and signal-to-noise ratio for 0.2 g/L h-cyt <i>c</i> at different 2C <sub>14</sub> DAB surfactant concentrations. ....	176
<b>Table 5.1</b>	Mass resolution and signal-to-noise ratio for 0.2 g/L h-cyt <i>c</i> at different concentrations of lithium and Bis-tris phosphate buffers.....	176

## LIST OF FIGURES

<b>Figure 1.1</b>	Schematic diagram of a capillary electrophoresis system.....	3
<b>Figure 1.2</b>	Schematic diagram of the electric double layer and the potential profile as a function of distance from the capillary wall.....	6
<b>Figure 1.3</b>	Schematic diagram of the flat profile of the electroosmotic flow.....	8
<b>Figure 1.4</b>	Schematic diagram showing a capillary zone electrophoresis separation and the resulting electropherogram at the detector.....	15
<b>Figure 1.5</b>	Schematic diagram illustrating the matrix-assisted laser desorption/ionization process with time-of-flight mass analyzer.....	20
<b>Figure 1.6</b>	Schematic diagrams illustrating the concentration profile of the analyte zone and the expected peak shape at the detector.....	29
<b>Figure 1.7</b>	Diagram showing the formation of micelle aggregates of CTAB in the solution and on the surface.....	44
<b>Figure 1.8</b>	Diagram showing the formation of vesicle aggregates of DDAB in the solution and the bilayer formation on the surface.....	45
<b>Figure 2.1</b>	Surface tension as a function of DDAB concentration in sodium acetate buffer.....	59
<b>Figure 2.2</b>	Effect of hydrodynamic and electro-kinetic rinsing on EOF of DDAB coated capillaries.....	63
<b>Figure 2.3</b>	Schematic diagrams of surfactant desorption process from silica surface.....	66
<b>Figure 2.4</b>	Effect of rinsing pressure on the decay rate constant.....	70
<b>Figure 2.5</b>	Effect of buffer volume that flow in the capillary during rinsing on the EOF.....	71
<b>Figure 2.6</b>	Effect of capillary inner diameter on reverse EOF of DDAB coated capillaries.....	73
<b>Figure 2.7</b>	Effect of capillary radius on the decay rate constant.....	74
<b>Figure 2.8</b>	Effect of buffer ionic strength on the reversed EOF of DDAB coated capillaries at day 0.....	76

<b>Figure 2.9</b>	Effect of cmc of DDAB on the decay rate constant.....	77
<b>Figure 2.10</b>	Effect of buffer type and pH on EOF of DDAB coated capillaries .....	80
<b>Figure 2.11</b>	Effect of aging time on EOF of DDAB coated capillaries in sodium phosphate buffer at ionic strength of $9 \times 10^{-3}$ M and pH 3.0 .....	83
<b>Figure 2.12</b>	Effect of aging time on the stability of DDAB coated capillaries in sodium phosphate buffer at ionic strength of $88 \times 10^{-3}$ M and pH 3.0 .....	85
<b>Figure 2.13</b>	Electropherograms of four proteins in acetate buffer at different concentration .....	87
<b>Figure 2.14</b>	Electropherograms of four proteins in 50 mM phosphate buffer at different voltage .....	88
<b>Figure 3.1</b>	Chemical structures of cationic surfactants used as coatings.....	97
<b>Figure 3.2</b>	Effect of hydrodynamic rinsing on the EOF of DDAB coated capillaries in different buffers .....	102
<b>Figure 3.3</b>	Effect of increasing the hydrocarbon chain length and the number of hydrocarbon chains of the surfactant monomer on the stability of the coatings.....	105
<b>Figure 3.4</b>	Effect of increasing the capillary inner diameter on the stability of the surfactant bilayer coatings.....	107
<b>Figure 3.5</b>	Effect of buffer pH on the stability of the double chained surfactants at pH 3.0 and pH 4.0 .....	109
<b>Figure 3.6</b>	Effect of surfactant concentration on the stability of the bilayer .....	110
<b>Figure 3.7</b>	Electropherograms of four proteins using 2C <sub>14</sub> DAB coatings at different pH .....	112
<b>Figure 3.8</b>	Electropherograms of four cationic proteins using 2C <sub>14</sub> DAB and 3C <sub>12</sub> MAI.....	113
<b>Figure 3.9</b>	Electropherograms of four cationic proteins with 2C <sub>18</sub> DAB coated capillary for 12-day period.....	115
<b>Figure 4.1</b>	Schematic diagram of a fronting peak showing parameters used to estimate the asymmetric factor.....	129
<b>Figure 4.2</b>	Effect of capillary diameter on electropherograms of trace concentrations of b-cyt <i>c</i> and h-cyt <i>c</i> using 2C <sub>14</sub> DAB coated capillaries .....	131

<b>Figure 4.3</b>	Electropherograms of b-cyt <i>c</i> and h-cyt <i>c</i> in 100 $\mu\text{m}$ i.d. capillary using $2\text{C}_{14}\text{DAB}$ coatings at different sample concentrations.....	134
<b>Figure 4.4</b>	Effect of buffer concentration on electropherograms of b-cyt <i>c</i> and h-cyt <i>c</i> using a $2\text{C}_{14}\text{DAB}$ coating.....	138
<b>Figure 4.5</b>	Effect of buffer co-ion on electropherograms of b-cyt <i>c</i> and h-cyt <i>c</i> using $2\text{C}_{14}\text{DAB}$ coatings at different buffer co-ions.....	141
<b>Figure 4.6</b>	Effect of sample concentration on preparative CZE separations of b-cyt <i>c</i> and h-cyt <i>c</i> using $2\text{C}_{14}\text{DAB}$ coatings. ....	143
<b>Figure 5.1</b>	Schematic diagram illustrate the position of the buffer level in the vials during <b>a.</b> separation; and <b>b.</b> fraction collection. ....	157
<b>Figure 5.2</b>	Electropherograms of <b>a.</b> b-cyt <i>c</i> ; and <b>b.</b> h-cyt <i>c</i> using $2\text{C}_{14}\text{DAB}$ coatings at 100 mM lithium phosphate buffer .....	162
<b>Figure 5.3</b>	Electropherogram of b-cyt <i>c</i> and h-cyt <i>c</i> at -10 kV using $2\text{C}_{14}\text{DAB}$ coatings at 100 mM lithium phosphate buffer .....	163
<b>Figure 5.4</b>	MALDI-TOF mass spectra of the protein fractions collected from electrophoresis run in Figure 5.3.....	167
<b>Figure 5.5</b>	Electropherogram of b-cyt <i>c</i> and h-cyt <i>c</i> at -5 kV using $2\text{C}_{14}\text{DAB}$ coatings at 100 mM lithium phosphate buffer .....	169
<b>Figure 5.6</b>	MALDI-TOF mass spectra of 10 fractions (A-J) for b-cyt <i>c</i> peak collected from electrophoresis run in Figure 5.5.....	170
<b>Figure 5.7</b>	The mass spectra of polypeptide ladders of h-cyt <i>c</i> fraction collected from electrophoretic run in Figure 5.3.....	174
<b>Figure 5.8</b>	Electropherograms of b-cyt <i>c</i> and h-cyt <i>c</i> at 100 mM Bis-tris phosphate buffer using two different coatings .....	178
<b>Figure 5.9</b>	Mass spectra of polypeptide ladders of h-cyt <i>c</i> fractions collect from electrophoretic runs using two different coatings .....	180
<b>Figure 5.10</b>	Electropherogram of b-cyt <i>c</i> and h-cyt <i>c</i> at 25 mM Bis-tris phosphate buffer using $2\text{C}_{18}\text{DAB}$ coatings .....	184
<b>Figure 5.11</b>	Mass spectrum of polypeptide ladder of h-cyt <i>c</i> collected from electrophoretic run in Figure 5.10.....	185
<b>Figure 6.1</b>	General structure of <b>a.</b> polyoxyethylene stearate; and <b>b.</b> dialkyl poly-oxyethylene ether surfactant of the $2\text{C}_n\text{E}_m$ family.....	199

## LIST OF ABBREVIATIONS

2D-gel	Two-dimensional gel electrophoresis
2C <sub>10</sub> DAB	Didecyldimethylammonium bromide
2C <sub>14</sub> DAB	Dimethylditetradecylammonium bromide
2C <sub>16</sub> DAB	Dihexadecyldimethylammonium bromide
2C <sub>18</sub> DAB	Dimethyldioctadecylammonium bromide
3C <sub>12</sub> MAB	Tridodecylmethylammonium bromide
3C <sub>12</sub> MAI	Tridodecylmethylammonium iodide
3C <sub>16</sub> MAB	Trihexadecylmethylammonium bromide
2C <sub>18</sub> E <sub>12</sub>	1,2-di-O-octadecyl-rac-glycerol-3-( $\omega$ -dodecaethylene glycol)
2C <sub>n</sub> E <sub>m</sub>	Dialkyl poly-oxyethylene ether
AFM	Atomic force microscopy
Bis-tris	Bis(2-hydroxyethyl)imino-tris(hydroxymethyl)methane
b-cyt <i>c</i>	Bovine heart cytochrome <i>c</i>
CE	Capillary electrophoresis
CHCA	$\alpha$ -cyano-4-hydroxycinnamic acid
CIEF	Capillary isoelectric focusing
cmc	Critical micelle concentration
<i>csac</i>	Critical surface aggregation concentration
CTAB	Cetyltrimethylammonium bromide
CZE	Capillary zone electrophoresis
DC	Direct current
DDAB	Didodecyldimethylammonium bromide
EMD	Electromigration dispersion
EOF	Electroosmotic flow
ESI	Electrospray ionization
h-cyt <i>c</i>	Horse heart cytochrome <i>c</i>
HPLC	High performance liquid chromatography
HCl	Hydrochloric acid

i.d.	Inner diameter
IEF	Isoelectric focusing
IHP	Inner Helmholtz plane
MAAH	Microwave-assisted acid hydrolysis
MALDI	Matrix-assisted laser desorption/ionization
MeOH	Methanol
MS	Mass spectrometry
NaOH	Sodium hydroxide
OHP	Outer Helmholtz plane
SDS	Sodium dodecyl sulphate
TBA	Tetrabutylammonium
TEA	Tetraethylammonium
TOF-MS	Time-of-flight mass spectrometry
Tris	Tris(hydroxymethyl)aminomethane
TTAB	Tetradecyltrimethylammonium bromide
UV	Ultraviolet-visible light

## ONE LETTER SYMBOL OF AMINO ACIDS

A	L-Alanine (89.09 Da)
C	L-Cysteine (121.16 Da)
D	L-Aspartic acid (133.10 Da)
E	L-Glutamic Acid (147.13 Da)
F	L-Phenylalanine (165.19 Da)
G	L-Glycine (75.07 Da)
H	L-Histidine (155.16 Da)
I	L-Isoleucine (131.17 Da)
K	L-Lysine (146.19 Da)
L	L-Leucine (131.17 Da)
M	L-Methionine (149.21 Da)
N	L-Asparagine (132.12 Da)
P	L-Proline (115.13 Da)
Q	L-Glutamine (146.15 Da)
R	L-Arginine (174.20 Da)
S	L-Serine (105.09 Da)
T	L-Threonine (119.12 Da)
V	L-Valine (117.15 Da)
W	L-Tryptophan (204.23 Da)
Y	L-Tyrosine (181.19 Da)

## LIST OF SYMBOLS

$A$	Absorbance
$A_1$	Fitting parameter
$A_\infty$	Asymptotic value
$a_h$	Electrostatic cross-sectional area of the head group of cationic surfactant
$b$	Optical path length
$C_{s,0}$	Solute concentration
$c_B$	Buffer concentration
$c_b$	Surfactant concentration
$D$	Diffusion coefficient
$E$	Electric field strength
$F$	Faraday constant
$f$	Friction coefficient
$F_E$	Electric force
$F_F$	Frictional retarding force
$g$	Gravitational acceleration
$H$	Theoretical plate height
$H_{Ad}$	Plate height due to adsorption
$H_D$	Plate height due to longitudinal diffusion
$H_{det}$	Plate height due to detection volume
$H_{EMD}$	Plate height due to electromigration dispersion
$H_{ex}$	Plate height due to extra-column band broadening
$H_{inj}$	Plate height due to injection plug length
$H_H$	Plate height due to siphoning
$H_T$	Plate height due to Joule heating broadening
$I$	Ionic strength of the solution
$J$	Flux of the molecule
$K$	Distribution coefficient of between solid phase and the bulk solvent
$K_a$	Acid dissociation constant

$k_a$	Adsorption rate constant
$k_b$	Thermal conductivity of the solvent
$k'$	Retention factor
$k_d$	Desorption rate constant
$k_{d,mic}$	Micelles dissociation rate constant
$k_{EMD}$	Electromigration dispersion factor
$k_{obs}$	Observed decay rate of the EOF
$l_c$	Maximum extended length of the hydrocarbon chain length
$L_d$	Capillary length to detector
$l_{det}$	Length of the detection window
$l_{inj}$	Injection plug length
$L_t$	Capillary total length
$M_r$	Molecular weight
$N$	Theoretical plate number
$P_0$	Intensity of the incident radiation
$P$	Intensity of transmitted radiation
$p$	Packing parameter
$pI$	Isoelectric point
$q$	Net charge of the ion
$R$	Gas constant per mole
$r$	Capillary inner radius
$R_s$	Separation resolution
$r_s$	Stokes' radius of the ion
$r_x$	Normalized radius variable at distance $x$ from the capillary central axis
$T$	Absolute temperature
$t$	Time
$t_{EOF}$	Migration time of the neutral marker
$t_{i,detector}$	Time when leading edge of the analyte band reaches the detector window
$t_{i,outlet}$	Time when leading edge of the analyte band reaches capillary outlet
$t_M$	Migration time of the ionic species
$t_r$	Retention time of the solute molecule

$t_m$	Retention time of the neutral marker (dead time)
$t_{ramp}$	Voltage ramp time (time for the voltage to change from zero to V)
$t_{rinse}$	Rinsing time
$T_w$	Temperature of the capillary inner wall
$V$	Applied voltage
$v$	Volume
$v$	Migration velocity
$v_{app}$	Apparent migration velocity
$v_{ave}$	Average apparent migration velocity
$v_c$	Volume of the hydrocarbon region
$v_{cap}$	Dimensionless units of capillary volumes
$v_{EOF}$	Velocity of the electroosmotic flow
$v_H$	Cross-sectional average of the hydrodynamic velocity
$v_{inj}$	Injection volume
$V_{prog}$	Voltage set by the instrument
$u_x$	Flow velocity at distance x from the capillary center axis
$w$	Base line width of the peak
$w_{1/2}$	Peak width at half-height
$w_{b,detector}$	Baseline width of the peak at the detector
$w_{b,outlet}$	Baseline width of the peak at the capillary outlet
$w_{collection}$	Time interval required for fraction collection
$x$	Distance
$z$	Charge on the solute ion
$\alpha$	Degree of ionization of weak acid
$\beta$	Slope of straight line
$\delta$	Thickness of the stagnant mobile phase
$\delta_1$	Sub-layer thickness in the stagnant mobile phase
$\Delta h$	Height difference
$\Delta P$	Pressure difference applied across the capillary
$\Delta v$	Apparent migration velocity difference
$\tau$	Injection time

$\eta$	Solution viscosity
$\sigma$	Standard deviation
$\sigma^2$	Variance
$\mu$	Electrophoretic mobility
$\mu_0$	Absolute mobility at the infinite dilution
$\mu_a$	Effective electrophoretic mobilities of the buffer co-ion
$\mu_{app}$	Apparent electrophoretic mobility
$\mu_b$	Effective electrophoretic mobilities of the buffer counter-ion
$\mu_e$	Effective electrophoretic mobility
$\mu_{EOF}$	Electroosmotic flow mobility
$\mu_{obs,corr}$	Corrected observed mobility
$\mu_s$	Effective electrophoretic mobilities of the sample
$\delta$	Thickness of stagnant layer of water under stirred conditions
$\delta_1$	Sub-layer in the stagnant layer
$\Psi_0$	Surface potential
$\Psi_d$	Potential at the outer Helmholtz plane
$\kappa$	Electrical conductivity
$\kappa^{-1}$	Thickness of the electric double layer
$\varepsilon$	Dielectric constant of the solvent
$\varepsilon_\lambda$	Molar absorptivity
$\lambda$	Wavelength
$\lambda_M$	Molecular conductivity at infinite dilution
$\zeta$	Zeta potential
$\rho$	Density
$\Gamma$	Surface excess

## CHAPTER ONE: Introduction

*Capillary electrophoresis* (CE) is an efficient analytical technique that can achieve extremely rapid and well resolved separations. The other advantageous characteristics including simplicity, high separation efficiency, small sample consumption and automation, make CE very popular in many research areas including biological, pharmaceutical, environmental and industrial analyses. The successful contribution of CE to the Human Genome Project illustrates the powerful capabilities of this technique [1]. Since it was an invaluable and powerful separation tool for the genome, it is predicted that CE could make a similar impact on the determination of the *proteome*– the map of the proteins encoded by the genome. For proteomic applications, large scale separation procedures are recommended to isolate and collect enough sample components for further studies including identification and characterization of the proteins. However, separation of proteins using CE is not always possible, and in some cases proteins fail to elute from the capillary. The primary objective of this thesis is to develop methods for protein separations by CE using simple and inexpensive coating technology to isolate and collect pure proteins for identification and characterization.

### 1.1 History

*Electrophoresis* is the migration of charged molecules in solutions under the influence of an electric field. Although the basic concepts of electrophoresis had been recognized for a long time, the moving boundary method developed by Tiselius had made feasible analysis of complex mixtures such blood plasma [2]. The electrophoresis experiments were performed in free solution in a quartz U-tube, and the analytes were

detected by UV-absorbance. In 1948, Tiselius was awarded by the Nobel Prize for the developing of this method. However, the separation of proteins was not possible due to thermal convection within the solution. Thus, supporting mediums such as filter paper or gels were employed to reduce the convective mixing [3, 4]. In the 1970s, isoelectric focusing (IEF) followed by electrophoresis of proteins in a gel slab containing sodium dodecyl sulphate (SDS) was introduced [5]. The SDS imparts a constant charge-to-mass ratio onto the proteins, and then the gel separates the proteins based on their sizes. Two-dimensional gel electrophoresis (2D-gel) is now one of the most important techniques for proteomic applications.

In 1967, Hjertén described an apparatus for free zone electrophoresis using high electric fields and capillaries of 300  $\mu\text{m}$  inner diameter [6]. The thermal convection effects were reduced by rotating the separation compartment about its longitudinal axis. Although this technique was novel and powerful, it failed to become a routine method due to its complexity. It was the pioneering work of Jorgenson and Lukacs in 1981 that demonstrated the significant potential of free solution electrophoreses in narrow capillaries (75  $\mu\text{m}$  i.d.) [7]. This technique of *capillary electrophoresis* (CE) became very popular due to its ease of automation and the commercial availability of high-quality narrow-bore capillary. Interest further increased after commercial CE instrumentations appeared on the market in 1989. Since then, CE continues to impact the separations of a wide variety of molecules including large biomolecules. In addition to providing extremely high separation efficiencies, CE offers substantial advantages over conventional gel slab electrophoretic techniques such as reproducibility, quantitative capabilities, and ease-of-automation. Furthermore, using narrow capillaries allows high

electric fields to be used. This shortens the separation time from hours for classical electrophoresis to minutes for capillary electrophoresis.

## 1.2 Principles of Capillary Electrophoresis

### 1.2.1 Instrumentation

A schematic diagram of the major components of a CE system is shown in Figure 1.1. The basic set-up of the system consists of: a narrow capillary extended between two buffer reservoirs to support the separating buffer; a high voltage source to provide an external electric field gradient across the capillary; and a detector to monitor the separated species from sample mixture. Typically, the capillaries are made of fused silica

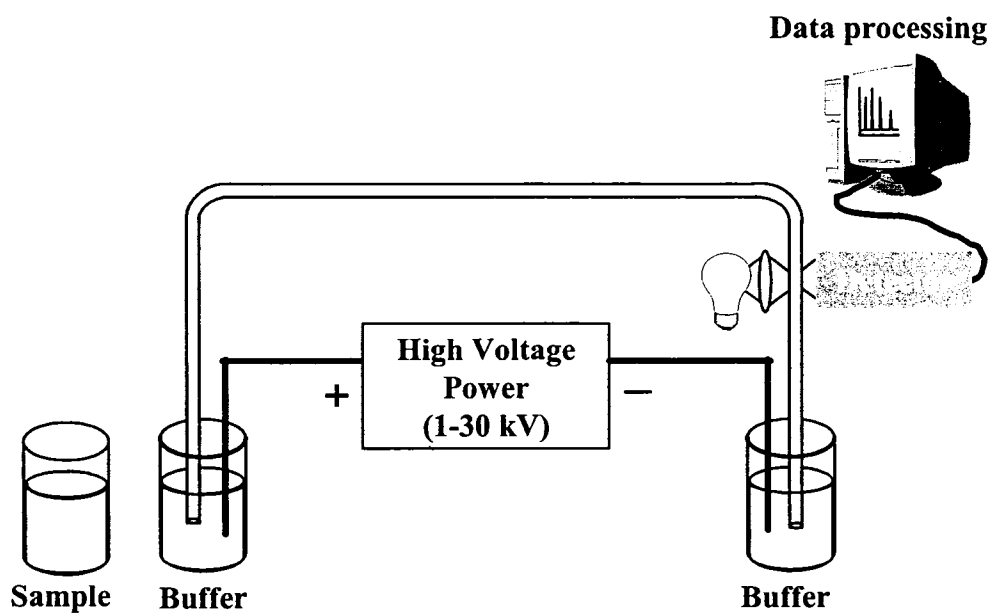


**Figure 1.1** Schematic diagram of a capillary electrophoresis system.

with inner diameters of 10-100  $\mu\text{m}$  and lengths 20-100 cm. The fused silica capillaries are externally coated with polyimide allowing them to be flexible. The most significant advantage of utilizing narrow capillaries is their effective dissipation of heat generated by the electrical resistance of the electrolyte within the capillary. The direct current (DC) power supply should provide voltages up to 30 kV across two electrodes, usually made up of platinum, inserted in the two distinct buffer reservoirs. Higher voltages (e.g., 40 kV) causes dielectric breakdown of the fused silica resulting in arc to the bench or student [8].

To perform a good separation, the capillary should be filled with separating buffer before sample injection. The sample injection is simply performed by replacing the inlet buffer reservoir with a sample vial. There are two injection techniques currently used in CE. The first is the hydrodynamic mode where the sample is injected by applying pressure or vacuum at one end of the capillary. The number of moles of the sample injected can be computed using Poiseuille's law multiplied by the sample concentration ( $C_{s,0}$ ):

$$amount = \frac{\Delta P \pi r^4 \tau}{8\eta L_t} C_{s,0} \quad (1.1)$$

where  $\Delta P$  is pressure difference applied across the capillary,  $r$  is inner radius,  $\tau$  is injection time,  $\eta$  is solution viscosity, and  $L_t$  is capillary total length. All experiments in this thesis used hydrodynamic injection.

The other mode is electrokinetic injection. Once the sample vial is in place, sample is introduced into the capillary by applying a voltage for a fixed period of time. The amount of sample loaded depends on the electrokinetic phenomena, in particular

electroosmotic mobility ( $\mu_{EOF}$ ) and solute's electrophoretic mobility ( $\mu_e$ ) (Section 1.2.2 and 1.2.3). The amount of the sample loaded can be computed using:

$$amount = \frac{(\mu_{EOF} + \mu_e)\pi r^2 V\tau}{L_t} C_{s,0} \quad (1.2)$$

where  $V$  is applied voltage, and the other terms are defined as for eq. 1.1.

After sample injection, the capillary ends should be well immersed in the buffer reservoirs prior to the application of the electric field. Also, the buffer in the two reservoirs should be at the same level to avoid siphoning (Section 1.4.5) [9]. Upon the application of electrical voltage across a capillary, electroosmotic flow is generated inside the fused silica capillary and sweeps the separated analytes to the detector side. The separation mechanism in CE is based on a molecule's electrophoretic mobility (Sections 1.2.2 and 1.2.3). Optical detection is typically performed on-column through a window created by removing (burning) the external polyimide coating from a segment of capillary a few centimeters before the outlet of the capillary. Most of the studies in this thesis use on-column UV detection for the protein separations. Mass spectrometric detection is performed on the material at the outlet of the capillary either on-line using electrospray ionization (ESI) mass spectrometry or off-line using matrix-assisted laser desorption/ionization (MALDI) mass spectrometry. In Chapter Five, off-line detection using MALDI will be employed for protein identification and characterization.

### 1.2.2 Electroosmotic Flow

*Electroosmosis* is the flow of liquid induced by an applied external electric field in the vicinity of a charged surface. It is usually explained using the Stern-Gouy-Chapman model of the electrical double layer at a charged interface. The surface of

fused silica, the most frequently used capillary in capillary zone electrophoresis (CZE), possesses about  $\sim 5$  silanols/nm<sup>2</sup> of weakly acidic silanol ( $-\text{SiOH}$ ) groups (average pKa  $\sim 5.3$ ) [10]. At pH above 3, some of the silanol groups are dissociated leaving an excess of negative charge on the capillary wall. To maintain charge balance, excess cations from the buffer solution are attracted to the immediate proximity of the capillary wall. Simultaneously, the co-ions in the vicinity of the solid surface are repelled away from the capillary surface due to electrostatic repulsion. This nonhomogeneous spatial distribution of charge is known as the *electrical double layer* and is shown in Figure 1.2 for a negative charged surface.

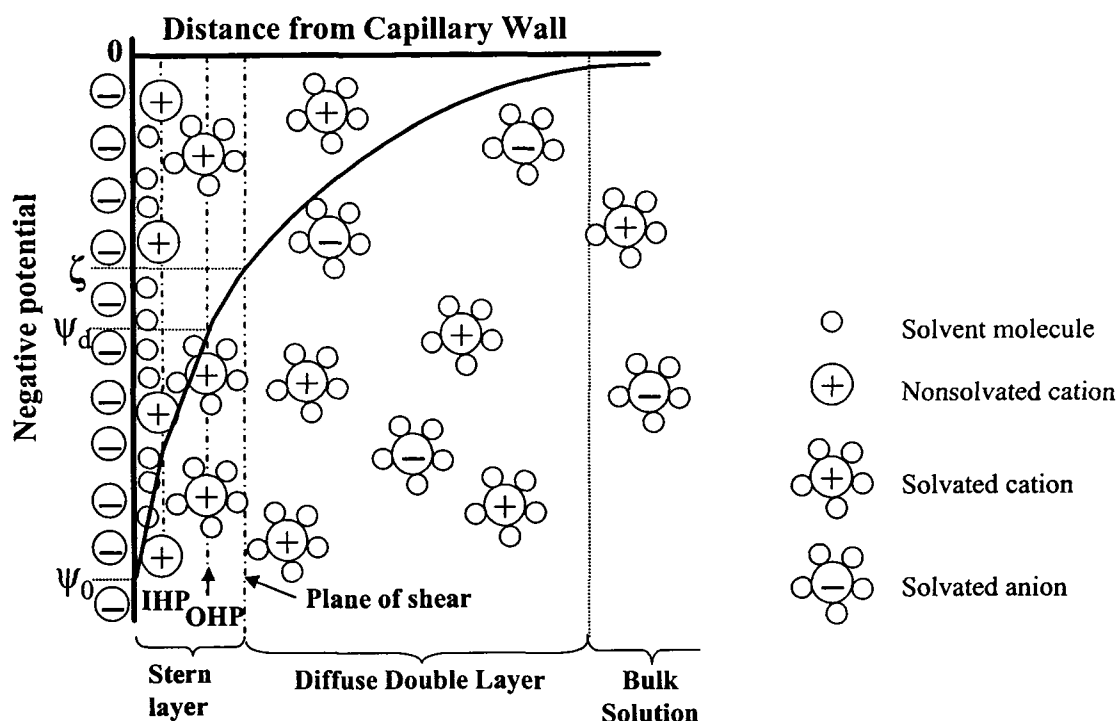


**Figure 1.2** Schematic diagram of the electric double layer and the potential profile as a function of distance from the capillary wall. Diagram is drawn for a negatively charged surface, such as the CE capillary, according to Gouy-Chapman-Stern Model.

According to the Stern-Gouy-Chapman model [11, 12], the double layer is divided into an immobilized compact layer and a mobile diffuse layer (Figure 1.2). The part of the compact layer adjacent to the surface contains strongly oriented solvent molecules and non-solvated cations that are strongly bound to the solid surface by electrostatic and other cohesive forces. The plane defined by the centers of the non-solvated cations is called the *inner Helmholtz plane* (IHP). In the compact layer, another plane known as the *outer Helmholtz plane* (OHP) is located just after the IHP and is defined by the centers of the immobilized solvated counter ions that are electrostatically adsorbed to the solid surface. The area between the wall and the OHP is referred to as the *Stern layer*. The *plane of shear* is formed at the outer edge of the compact layer, i.e., at or slightly beyond the OHP or Stern layer. The counter-ions in the immobilized Stern layer do not fully neutralize the surface charge. The excess negative charge at the plane of shear is compensated by the excess positive charge in the diffuse layer that extends from the OHP to the bulk solution. The ions in the diffuse part of double layer are mobilized because of the thermal agitation.

Within the Stern layer, the negative potential at the surface ( $\psi_0$ ) drops linearly to  $\psi_d$  at the OHP due to the strongly adsorbed non solvated and solvated cations, as depicted by the solid curve in Figure 1.2. Beyond the OHP, the potential decays exponentially within the diffuse layer until it reaches zero in the bulk solution. The corresponding potential at the plane of shear is referred to as *zeta* ( $\zeta$ ) *potential*. The thickness of the diffuse region of the double layer ( $\kappa^{-1}$  in m) is given by:

$$\kappa^{-1} = \frac{1}{F} \sqrt{\frac{\epsilon RT}{2000 I}} \quad (1.3)$$

where  $F$  is the Faraday constant (96485 coulombs/mole),  $\varepsilon$  is the dielectric constant of the solvent,  $R$  is the gas constant,  $T$  is the absolute temperature, and  $I$  is the ionic strength of the solution. In aqueous solution ( $\varepsilon = 78.49$ ) at 25°C, the values of  $\kappa^{-1}$  range from 4.3 nm at  $I = 0.005$  M to 0.96 nm at  $I = 0.1$  M [11].

Upon application the electric field across the capillary, the excess positive charged species in the diffused double layer are drawn to the negative electrode and drag the bulk solution along with them. This produces a flow referred to as the *electroosmotic flow* (EOF). The mobility of the electroosmotic flow ( $\mu_{EOF}$ ) is expressed by the Helmholtz-Smoluchowski equation:

$$\mu_{EOF} = \frac{v_{EOF}}{E} = -\frac{\varepsilon\zeta}{\eta} \quad (1.4)$$

where the  $v_{EOF}$  is the velocity of the electroosmotic flow, and  $E$  is the electric field strength. As shown in Figure 1.3, the velocity of the EOF increases radially from zero at

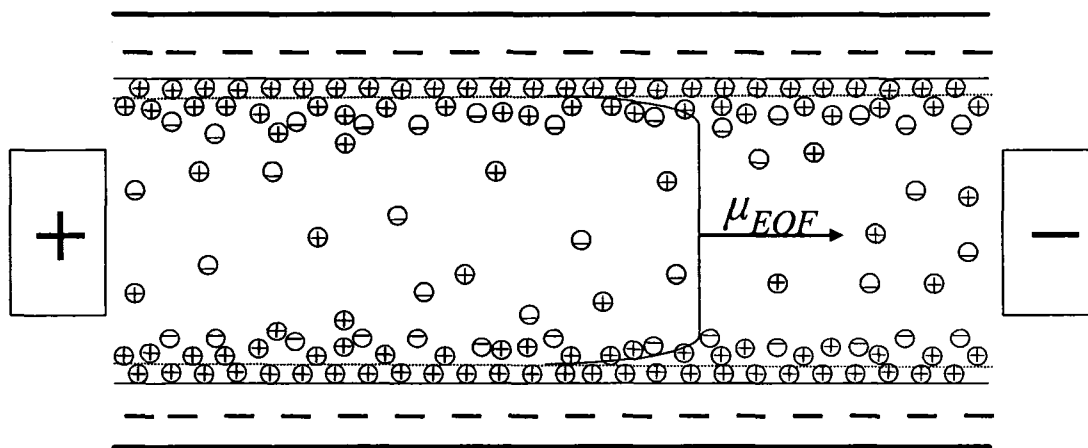


**Figure 1.3** Schematic diagram of the flat profile of the electroosmotic flow.

the immobilized Stern layer to its maximum velocity at the boundary between the double layer and the bulk solution. Since the thickness of the diffuse part of the double layer is negligible compared to the capillary inner diameter, the liquid within the tube is considered to move as a plug with a uniform velocity distribution across the capillary diameter.

Based on eq. 1.4, the EOF is directly dependent on the  $\zeta$  potential which is related to surface charge and the thickness of the double layer. These, in the case of fused silica, are highly affected by the buffer pH, the ionic strength and the nature of the ions in the double layer [10, 13-15]. Temperature has an indirect effect on the EOF via the viscosity. For instance, the electroosmotic mobility is calculated to increase by 2-3% per °C in the range 20-100 °C [16]. In general, the electroosmotic mobility is only dependent on the surface charge density of the capillary and the buffer conditions and not on the capillary dimensions such as the length and the inner diameter of the capillary, as long as the inner diameter is significantly greater than seven times the thickness of the double layer [17].

### 1.2.3 Electrophoretic Mobility

Under the influence of the external electric field, charged analytes migrate in the direction of that field. The difference in the migration rate of the analyte species is the basis of the separation mechanism by electrophoresis. Electrophoretic mobility ( $\mu$ ) is defined as the ratio of the migration velocity ( $v$ ) of analyte over the applied electric field ( $E$ ). That is,

$$\mu = \frac{v}{E} \quad (1.5)$$

The electrophoretic mobility for a certain ionic species in a given medium is a constant material property of that ion. This mobility is a function of the electric force that the ion experienced ( $F_E$ ) and its frictional retarding force ( $F_F$ ) through the medium it migrates. In a uniform electric field, the driving electric force of an ion is given by:

$$F_E = qE \quad (1.6)$$

where  $q$  is the net charge of the ion. As the ion migrates through the solvent, it is subjected to a dragging frictional force which is proportional to its velocity. From Stokes law, the friction coefficient ( $f$ ) opposing movement of a small spherical particle in a medium of viscosity ( $\eta$ ) is related to the Stokes' radius of the ion ( $r_s$ ), that is the radius of the solvated spherical ion (the sum of the crystallographic ion radius and the solvent shell surrounding the ion) as it migrates through the solution. Therefore,

$$F_F = -fv = -6\pi\eta r_s v \quad (1.7)$$

Under infinite dilution condition, it is assumed that there are no electrostatic interactions among the ions. When the steady state is attained during electrophoresis process, the retarding and driving electric forces are balanced, and the ion migrates at a constant velocity. Thus,

$$qE = 6\pi\eta r_s v \quad (1.8)$$

Rearrange the above equation:

$$\frac{v}{E} = \frac{q}{6\pi\eta r_s} \quad (1.9)$$

This proportionality yields the equation that describes the electrophoretic mobility in terms of physical parameters, i.e.,

$$\mu = \frac{q}{6\pi\eta r_s} \quad (1.10)$$

This is the most commonly used expression in CE, and it is known as the Hückel equation. The separation mechanism in CZE is based on the differences in the electrophoretic mobility of ionic species. This can arise from the difference in the net charge on the ionic species and/or the differences in the frictional properties, i.e., the size or shape, as inferred from eq. 1.10. In addition, the electrophoretic mobility is independent on the electric field gradient and capillary dimensions. However, the temperature, ionic strength and buffer pH have critical effects on the ion mobility [18].

### 1.2.3.1 Absolute Electrophoretic Mobility

The *absolute electrophoretic mobility* is the mobility of a fully charged species in a solution with zero ionic strength (at infinite dilution). It is a characteristic constant that depends on the intrinsic properties of the ionic species (charge and size) and the solvent. Accordingly, the solvent impact on absolute mobility is apparently due to its viscosity. The temperature has an indirect effect on the mobility via viscosity. Increasing the temperature reduces the viscosity and thus enhances the analyte electrophoretic mobility [18].

It is possible to correlate the molecular conductivity ( $\lambda_M$ ) and the absolute mobility at the infinite dilution ( $\mu_0$ ) [12] by:

$$\mu_0 = \frac{\lambda_M}{F} \quad (1.11)$$

where  $F$  is the Faraday constant. It is very beneficial to estimate the ion mobility using molecular conductivity data in the literature [19], as a starting step for theoretical calculations and stimulations of ion migration. Experimentally, the absolute mobility can be determined by using conductivity [20, 21] and capillary electrophoresis [22]. In capillary electrophoresis, for example, the absolute mobility can be determined by

measuring the mobility for full solute charge at different ionic strength and extrapolated the mobility to zero ionic strength, which gives the mobility at the infinite dilutions [23].

### 1.2.3.2 Effective Electrophoretic Mobility

The Hückel equation provides a useful description of the solvent effects on the ion mobilities at infinite dilution, i.e., absolute mobility. However, in practice CZE is always performed at finite ionic strengths and thus the analyte mobility is referred to as the *effective electrophoretic mobility* ( $\mu_e$ ). The effective mobility of charged ionic species can be calculated from the migration time of the analyte ( $t_M$ ) and the migration time of electroosmotic flow ( $t_{EOF}$ ) using the following equation:

$$\mu_e = \frac{L_t L_d}{V} \left( \frac{1}{t_M} - \frac{1}{t_{EOF}} \right) \quad (1.12)$$

where  $L_d$  and  $L_t$  are the capillary length to detector and total length respectively, and  $V$  is the applied voltage.

In an electrolyte solution, the effective charge of the solute is less than the net charge as a result of the screening influence of the counter-ions in the solution [24, 25]. As the reference ion moves under the influence of the electric field gradient, its ionic atmosphere lags behind the reference ion, resulting in a deformation of the ionic atmosphere to an egg shape. As a consequence, a *relaxation effect* is created due to the columbic interactions between the reference ion and its lagging ionic atmosphere. In addition, the ionic atmosphere introduces an *electrophoretic effect* resulting from the movement of the ionic atmosphere in response to the applied electric field. Both the relaxation and electrophoretic effects retard the motion of the reference ion, and these effects become more pronounced at high ionic strength. The contribution of the effects

of the ionic atmosphere on ion mobility of a fully ionized solute ion is described by Pitts' equation for ionic strengths up to 0.1 M [23]:

$$\mu_e = \mu_0 - Az \frac{\sqrt{I}}{(1 + 2.4\sqrt{I})} \quad (1.13)$$

where A is a constant, z is the charge on the solute ion,  $c_B$  is the buffer concentration, and I is the ionic strength of the buffer given by:

$$I = \frac{1}{2} \sum_k c_{B,k} z_k^2 \quad (1.14)$$

The pH also has a significant effect on the effective electrophoretic mobility for systems with weak acid or base functionalities. Under the condition  $pK_a - 2 < pH < pK_a + 2$ , for example, the buffer pH has a great impact on the degree of dissociation of a weak acid and thus on the effective charge of its ionic species. The equilibrium between the ionized and neutral component of weak acid is rapid. Therefore, the solute behaves as a single partially ionized entity [26]. The influence of the pH on the effective mobilities for a monovalent weak acid (HA) is described by [25]:

$$\mu_e = \alpha \mu_{A^-} = \frac{1}{1 + 10^{(pK_a - pH)}} \mu_{A^-} \quad (1.15)$$

where  $\alpha$  is the degree of ionization of the weak acid and  $\mu_{A^-}$  is the effective mobility of the fully ionized solute ( $A^-$ ). As a result of the sensitivity of the effective mobilities of weak electrolytes with the buffer pH, varying the buffer pH can alter the selectivity between weak electrolytes solutes with different  $pK_a$ .

Due to its amphoteric nature, the magnitude and the direction of the effective electrophoretic mobility of a protein depends mainly on the medium pH [27]. The pH at which a protein possesses no net electric charge is known as its *isoelectric point* (pI). At

this pH (buffer pH equivalent to the  $pI$ ), no effective electrophoretic mobility of the protein is attained. However, when the buffer pH is slightly higher than the  $pI$ , the protein's overall charge is negative as a result of the deprotonation of some of its basic functional groups. Under these conditions, its effective electrophoretic mobility is towards the anode. The electrophoretic mobility of the protein increases with increasing buffer pH until full deprotonation of all the basic functional groups occurs. On the other hand, when the buffer pH is slightly lower than the  $pI$ , the overall charged state of the protein is positive due to the partial protonation of its acidic functional groups. As the buffer pH decreases further, the protein's effective electrophoretic mobility increases until full protonation of the acidic functional groups takes place. The electrophoretic mobility of protein at low pH is directed towards the cathode. Protein separations in CZE will be discussed in depth in Section 1.5.

### 1.2.3.3 Apparent Mobility

The observed migration of ionic species in CZE is a combination of the effective electrophoretic velocity of species and the bulk electroosmotic velocity of the electrolyte buffer. The apparent mobility of the charged solute species is calculated by:

$$\mu_{app} = \frac{L_d L_t}{t_M V} \quad (1.16)$$

where  $L_d$  and  $L_t$  are the capillary length to detector and total length respectively,  $t_M$  is the migration time of the ionic species, and  $V$  is the applied voltage. The apparent mobility is also a function of both the effective mobility of the ionic species and the electroosmotic flow:

$$\mu_{app} = \mu_{EOF} + \mu_e \quad (1.17)$$

Since the neutral species experience no mobility under the influence of the electric field, their apparent mobility is equivalent to the EOF, and no separation between different neutral species occurs. As shown in Figure 1.4, the effective mobility of the

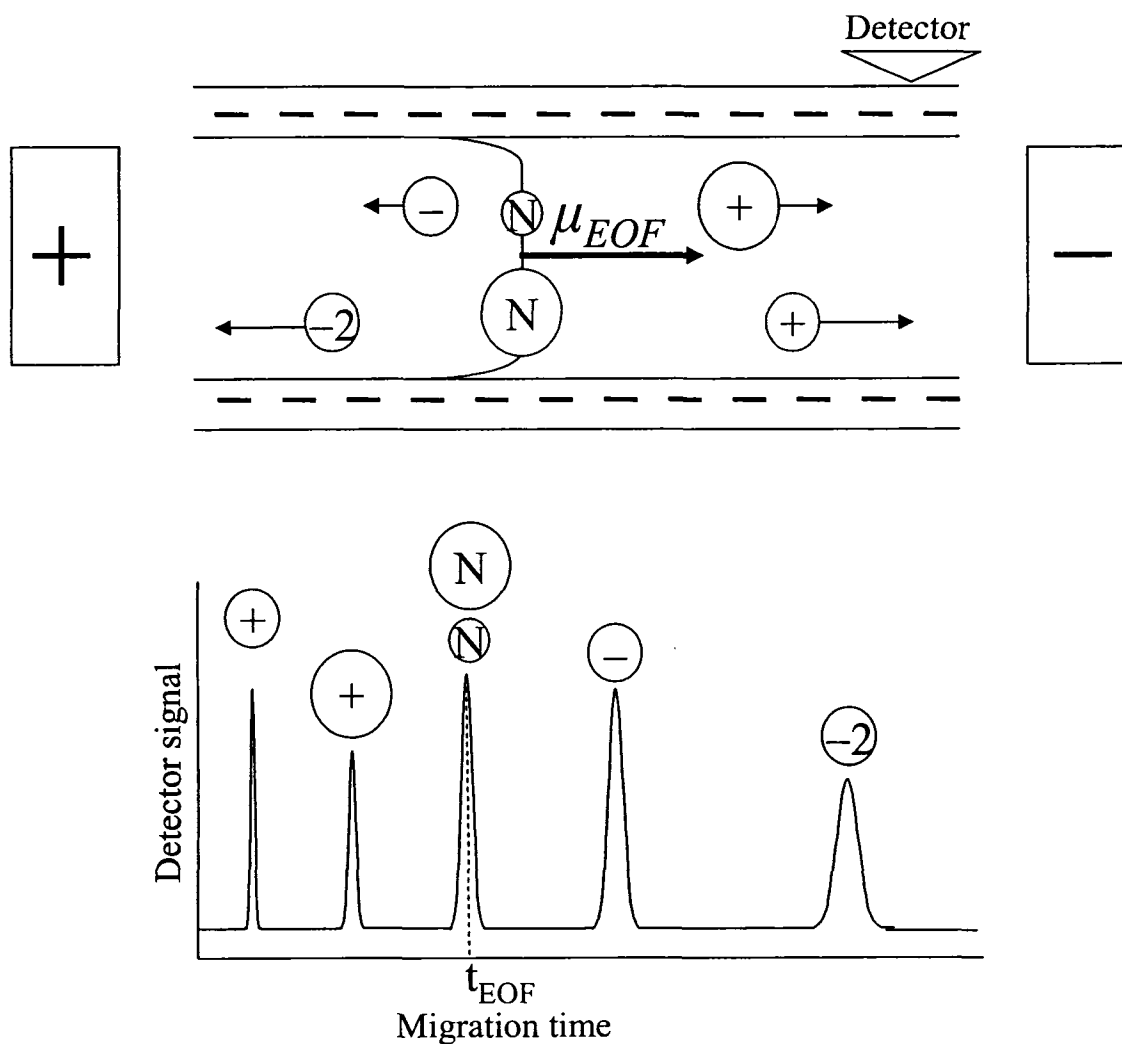


**Figure 1.4** Schematic diagram showing a capillary zone electrophoresis separation (top diagram) and the resulting electropherogram at the detector.

cations and the electroosmotic flow have the same direction (co-EOF), and so the mobilities of cations are enhanced by the EOF. Thus, the peaks for cations appear before the EOF peak. In contrast, the anions migrate against the EOF (counter-EOF). As long as the magnitude of the effective mobility of the anion is less than the EOF (which is commonly true), the anions will be swept towards the detector by the EOF and their peaks appear after the EOF peak. However, if the effective mobility of an anion is faster than that of the EOF, no peak will be detected in the direction of the EOF [28].

### **1.3 Detection**

The minute amount of sample injected into CZE makes the criteria for the detection system more challenging. The criteria that must be considered when choosing a detector for analysis include sensitivity, selectivity, linear range and cost. More importantly, the response of the detection system should be reproducible and proportionally related to either the amount or the concentration of the analytes. A wide variety of detection modes have been employed in CZE with varying degrees of success. Common detection modes include: absorbance; fluorescence [29]; electrochemical [30]; and mass spectrometric detection. In general, on-line UV absorbance is the most common detection method even though its sensitivity is low relative to other detection modes utilized for CZE. Mass spectrometric techniques have been given much attention in the recent years, in particular for biological analysis. In this thesis, my emphasis is centered on both on-line UV-absorbance (direct mode) and off-line mass spectrometric detection due to their importance in proteomic applications.

### 1.3.1 On-line UV Absorbance

UV absorbance detector is the most popular mode utilized to monitor the CZE separations due to its simplicity, robustness, easy to handle, and lack of chemical modification required for detection. The large majority of compounds absorb in the UV region in their native state. Furthermore, the analyte maintains its original identity after detection (nondestructive detection mode), and thus UV absorption can be used in conjunction with other analytical tools.

In the direct mode, the UV detector measures the analyte absorbance at a single wavelength. The light source is typically a deuterium lamp (190-600 nm). The UV cut-off for fused silica is about 170 nm [31]. Thus, the capillary itself acts as the cuvette. In the Beckman MDQ used in my work, the desired wavelength is selected by a filter. After the light passes through the transparent capillary window, the transmitted light is collected by photodiode detector to convert the photocurrent to voltage which in turn is converted to absorbance unit after amplification [32].

When the analyte absorbs light, it is promoted to an excited electronic state. As a consequence, the intensity of the transmitted light reaching the detector decreases. According to the Beer-Lambert's law, the amount of light absorbed by the analyte is proportional to its concentration ( $C$ ),

$$\log(P_0 / P) = A = \varepsilon_{\lambda} b C \quad (1.18)$$

where  $P_0$  is the intensity of the radiation incident on the analyte,  $P$  is the intensity of radiation transmitted by the analyte,  $A$  is the analyte absorbance,  $\varepsilon_{\lambda}$  is the molar absorptivity at the selected wavelength, and  $b$  is the optical path length. Since the capillary is cylindrical, the average optical path length is less than the inner diameter of

the capillary. As a result of short the optical path length, the detection limit is relatively high in the range of  $10^{-6}$ - $10^{-7}$  M with a linear dynamic range of three to four decades [33, 34]. Several approaches have been developed to enhance the detection sensitivity and decrease the detection limit such as utilizing a bubble cell [35], Z-type or U-type flow cell [34, 36], or multi-reflection cell [37]. However, these approaches are not very practical in the CE, since they trade off sensitivity with extra band broadening or add more complexity to the detection methods.

### **1.3.2 Mass Spectrometric Detection**

Mass spectrometry has the greatest potential among the detectors employed to CZE, since it can determine the molecular mass and structural information of the analyte. There are several types of MS detectors, among them ion trap, quadrupoles, time-of-flight (TOF), and Fourier transform ion cyclotron resonance. CZE can be coupled to any of the MS detectors either on-line such as electrospray ionization (ESI) [38] or off-line such as matrix-assisted laser desorption/ionization (MALDI) [39].

#### **1.3.2.1 ESI**

The electrospray ionization is a soft ionization process based on converting the analyte ions in solution into ions in the gas phase using a high electric field [40]. ESI is very effective in ionizing large biomolecules, such as proteins, because a solvent-aided transfer of analyte ions to the gas phase assists the formation of multi-charged analyte ions. Three common types of interfaces have been constructed for coupling CE with ESI-MS. These include coaxial liquid sheath-flow [41], sheathless [42] and liquid-junction interfaces [43]. The coaxial liquid flow has the advantage of simple and reproducible construction over the other interfaces. However, the external liquid flow

dilutes the analyte, reducing the sensitivity of the system. The sheathless and the liquid-junction interfaces are more sensitive. However, the construction of these interfaces is difficult to perform. The detection limit for the CE-ESI-MS was ranging from 100 [41] to 0.5 femtomoles [44] for proteins, depending on the type of the interface.

### 1.3.2.2 MALDI

Matrix-assisted laser desorption/ionization (MALDI) mass spectrometry is a soft ionization process introduced for the analysis of nonvolatile biomolecules such as proteins. A schematic diagram of the MALDI is presented in Figure 1.5. It employs the energy from a laser to ionize biopolymers from a dry mixture of the analyte and matrix [45]. The key to successful MALDI analysis is the proper combination of matrix material and laser wavelength. The matrix is usually a small organic molecule that absorbs at the wavelength of the laser. The roles of the matrix are: to entrap analyte into the matrix-analyte co-crystal; to isolate the analyte molecules so that they do not aggregate; to absorb energy from the laser beam and then readily evaporate into the gas phase; and to aid the analyte ionization process [46]. When the laser pulse strikes the dried well-mixed matrix-analyte mixture, the energy is mainly absorbed by the matrix molecules and rapidly converts the mixture into a plume of vaporized materials [47].

The exact mechanism by which the ionization process for proteins happens is still under debate, but the most plausible mechanism involves gas phase proton transfer from the matrix to the analyte [48, 49]. Generally, when proteins mixed with the matrix material, two major signals in the mass spectra, corresponding to singly and doubly protonated protein molecules, are produced, i.e.,  $[M+H]^+$  and  $[M+2H]^{2+}$  [50]. However, if buffer cations such as sodium or potassium are presented in the sample mixture,

proteins might appear as mixed ion species ( $[M+H]^+$ ,  $[M+Na]^+$ , or  $[M+K]^+$ ). As MALDI depends on pulsed laser radiation for ionization, the most common mass analyzer coupled with MALDI is time-of-flight (TOF) mass spectrometers [51].

Coupling of CE to MALDI-MS is usually performed off-line by fraction collection. The collected analyte is mixed with the MALDI matrix and deposited on the

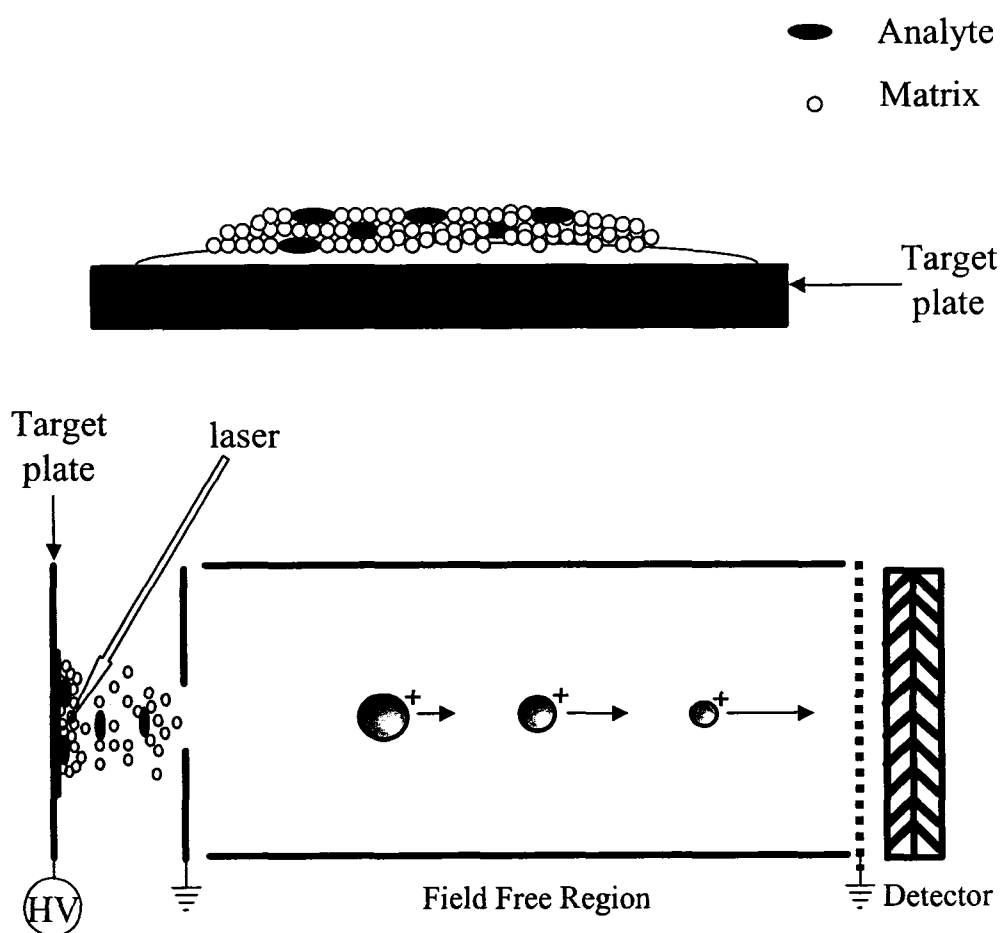


**Figure 1.5** Schematic diagram illustrating the matrix-assisted laser desorption/ionization (MALDI) process with time-of-flight (TOF) mass analyzer.

target plate prior to MS detection. Several features make MALDI suitable for biological sample separation by CE including simplicity of spectra, tolerance to a variety of separation conditions, and compatibility with inexpensive TOF mass spectrometers. The absolute sensitivity of analysis are in the low femtomole range [52]. Off-line MALDI-MS detection is used in Chapter Five of this thesis.

#### 1.4 Band Broadening in CE

In CE, like all other separation techniques, the separation resolution of two components is based on the difference of the migration velocity of the analyte species relative to the broadening effects. *Separation resolution* ( $R_s$ ) between two adjacent peaks is defined as [31, 53]:

$$R_s = \frac{2(t_{M2} - t_{M1})}{w_1 + w_2} \quad (1.19)$$

where  $t_M$  is the migration time, and  $w$  is the base line width of the peak. If the peak is Gaussian, the  $w$  is equal to 4 standard deviation ( $\sigma$ ) of the peak, and thus [31, 53],

$$R_s = \frac{t_{M2} - t_{M1}}{2(\sigma_1 + \sigma_2)} \quad (1.20)$$

The subscripts 1 and 2 refer to the two adjacent peaks.

The *separation efficiency*, expressed in number of theoretical plates ( $N$ ), is an important parameter to describe the separation performance and is given by:

$$N = \frac{L_d^2}{\sigma_{tot}^2} \quad (1.21)$$

where  $L_d$  is the capillary length to the detector, and  $\sigma_{tot}^2$  is the total variance of the analyte

peak. The resolution is also related to the square root of the theoretical plate number. In terms of apparent electrophoretic velocity, the resolution equation is given by:

$$R_s = \frac{1}{4} \sqrt{N} \frac{\Delta v}{v_{ave}} \quad (1.22)$$

where  $\Delta v$  is the apparent migration velocity difference between the two analytes, and  $v_{ave}$  is their average migration velocity [54]. Therefore, it is important that the dispersion phenomena be minimized to enhance the separation efficiency as well as the resolution. These dispersion factors include extra-column effects, longitudinal diffusion, thermal effects, electromigration dispersion, hydrodynamic effects, and adsorption of the analyte to the capillary wall.

In analogy to chromatographic methods, the peak height model can be utilized to estimate the contributions of the above dispersive factors to the peak broadening by computing the plate height associated with each factor. The *plate height* ( $H$ ) is related to the theoretical plate number and is defined as the variance ( $\sigma_{tot}^2$ ) of the peak per unit distance along the zone displacement distance, i.e., capillary length to the detector ( $L_d$ ),

$$H = \frac{L_d}{N} = \frac{\sigma_{tot}^2}{L_d} \quad (1.23)$$

The total variance represents all the individual variances generated from the dispersion factors that occur during the separation process. If each dispersion factor is assumed to act independently, the variances from each factor can be summed together to compute the total peak variance:

$$\sigma_{tot}^2 = \sigma_{ex}^2 + \sigma_D^2 + \sigma_T^2 + \sigma_{EMD}^2 + \sigma_H^2 + \sigma_{Ad}^2 \quad (1.24)$$

where  $\sigma_i^2$  is the variance generated from the extra-column effect, longitudinal diffusion,

thermal, electromigration, hydrodynamic and adsorption, respectively. Since the variance is directly proportional to the plate height (eq. 1.23), the contribution of the dispersion factors can also be expressed in terms of plate heights:

$$H = H_{ex} + H_D + H_T + H_{EMD} + H_H + H_{Ad} \quad (1.25)$$

#### 1.4.1 Extra-column Band Broadening

Extra-column band broadening ( $H_{ex}$ ) includes time-independent broadening factors due to injection and on-line detection. The injection and detection are considered to have the major contribution to the total plate height [55]. Therefore,

$$H_{ex} = H_{inj} + H_{det} \quad (1.26)$$

where  $H_{inj}$  is the plate height contribution to the injection plug length, and  $H_{det}$  is the variance due to detection volume.

##### 1.4.1.1 Injection

In CZE, the injection of sample plug into the capillary is performed either by applying pressure or voltage (Section 1.2.1). The shape and the length of the injection plug length have significant contribution to the overall peak broadening. For a rectangular plug length, the plate height contribution generated due to injection is given by:

$$H_{inj} = \frac{l_{inj}^2}{12L_d} \quad (1.27)$$

where  $l_{inj}$  is the injection plug length. However, the plate height expression due to injection will be different for non-rectangular injection profiles [56]. Upon applying pressure injection, for instance, a parabolic profile at the front of the injection plug would be inserted as a result of the laminar flow. This would add an extra broadening to the

solute zone [57]. However, consideration of this refinement to the injector band broadening is not necessary in the present discussion.

A reasonable approximation for the maximum permissible injection length (as defined by a 10% increase in the overall plate height [58]) is given by:

$$l_{inj,max} = \sqrt{2.4Dt_M} \quad (1.28)$$

where  $t_M$  is the migration time, and  $D$  is the diffusion coefficient of the analyte [59]. As inferred from the above equation, the injection plug length is significantly affected by analyte properties such as size and mobility. Thus, the injection plug length for fast migrating analytes should be smaller than the large slow migrating analytes to keep the injection broadening not pronounced. In practice, eq. 1.28 corresponds to the recommendation that the injection plug length should not exceed 1 to 2% of the total capillary length depending whether fast or slow migrating analytes are analyzed [60, 61].

#### 1.4.1.2 Detection

Using on-line UV-detection, the detection window is determined by the length of the slit along the column ( $l_{det}$ ). The plate height contribution resulting from on-column detection with a rectangular slit aperture is:

$$H_{det} = \frac{l_{det}^2}{12L_d} \quad (1.29)$$

Broadening due to detection can be reduced by decreasing the slit aperture, but this may reduce the radiant power ( $P_0$ ) reaching the detector and thus increasing the detector noise [33]. A reasonable approximation for the maximum permissible detection window (as defined by a 10% increase in plate height) is [59]:

$$l_{det,max} = \sqrt{2.4Dt_M} \quad (1.30)$$

Experimentally, the on-line UV-detection slit aperture length in the range of 0.1 to 1 mm is commonly utilized [34].

Another source of broadening that is related to the detector is *detection rise time* (the time required for the detector output to increase from 10 to 90%). Since the separation in CZE is rapid, the detector rise time should be minimal in order to guarantee a sufficiently quick response to not broaden the peaks. Additionally, the data sampling rate (data acquisition) should be sufficient to have actual representative of the peak. In the Beckman MDQ used in this work, the detector rise time is dictated by the data sampling rate selected (P/ACE System MDQ Software Reference Manual, page 2-129). For instance, if the data sample rate of 4 Hz is chosen, the detector rise time is 0.7 sec, whereas at sampling rate of 32 Hz, the detector rise time would be 0.08 sec.

#### 1.4.2 Longitudinal Diffusion

*Diffusion* is the movement of the analyte molecules under the influence of a concentration gradient. When a sample is injected into a capillary, analyte molecules start to diffuse away from the center of the sample zone where the analyte concentration is the highest. With time, the concentration profile as a function of distance becomes Gaussian. The Einstein equation (eq. 1.31) relates the variance caused by the molecular diffusion with the time allowed for the diffusion to occur (solute migration time,  $t_M$ , in the case of CZE),

$$\sigma_D^2 = 2Dt_M \quad (1.31)$$

where  $D$  is the diffusion coefficient of the analyte. Consequently, the plate height due to longitudinal diffusion ( $H_D$ ) is:

$$H_D = \frac{2Dt_M}{L_d} \quad (1.32)$$

The plate height is only dependent on the migration time, and thus it depends on the apparent migration velocity ( $v_{app}$ ) of sample zone in the capillary [62]. By substituting the migration time from eq. 1.16 into 1.32 yields:

$$H_D = \frac{2DL_t}{\mu_{app}V} = \frac{2D}{\mu_{app}E} = \frac{2D}{v_{app}} \quad (1.33)$$

In the absence of Joule heating (Section 1.4.3), increasing the applied electric field increases the apparent migration velocity of the analyte, which reflects a decrease in the contribution of longitudinal diffusion broadening factor [7].

### 1.4.3 Thermal Effects

The major limitation of increasing the electric field to speed up the analysis time and reduce the diffusional broadening is *thermal* or *Joule heating broadening*. Upon application the electric field across the capillary, heat is generated due to the passage of the current through the buffer within the capillary. As a consequence, the overall temperature of the buffer increases. However, heat loss through the capillary wall to the surrounding creates a radial temperature gradient within the capillary. It was assumed that the temperature profile is parabolic if the buffer resistivity within the capillary is independent temperature [63].

The temperature difference between the center of the capillary and its wall is increased by the amount of electric current generated within the capillary, i.e., increases with the electric field strength or the capillary inner diameter. Since the electrophoretic mobility increases with temperature (Section 1.2.3), the mobility of the analyte molecules

at the center of the capillary is faster than that of analyte molecules near the walls. The plate height contribution of Joule heating broadening to the total peak broadening ( $H_T$ ) is [64]:

$$H_T = \frac{E^4 r^6 \kappa^2 B^2}{24D(8k_b T_w^2 - E^2 \kappa r^2 B)^2} v_{app} \quad (1.34)$$

where  $D$  is the diffusion coefficient,  $B$  is a constant,  $r$  is the capillary radius,  $E$  is the electric field strength,  $\kappa$  is the electrical conductivity of the background electrolyte solution,  $k_b$  is the thermal conductivity of the solvent,  $T_w$  is the temperature of the capillary inner wall, and  $v_{app}$  is the analyte apparent velocity. The plate height contribution is strongly dependent on the capillary diameter, as shown in eq. 1.34. In addition, the electric field strength and the buffer conductivity significantly affect the plate height generated by Joule heating.

Experimentally, Joule heating is monitored by measuring the current across the capillary as the applied voltage is increased, i.e., generating an Ohm's plot. A linear relationship between the observed current and the applied voltage indicates that Joule heating broadening is not significant. However, at high voltage a positive deviation from linearity occurs. This disproportionate increase in current with voltage indicates that the temperature excessively increased in the capillary and the broadening contribution due to thermal dispersion will be significant [65].

To minimize the plate height originating from Joule heating, the apply voltage should be in the linear portion of the Ohm's plot. Using buffers with low conductivity such as borate, Tris, and Bis-tris buffer, or reducing the concentration of the buffers with high conductivities will extend the linear portion of Ohm's plot, and thus higher voltages can be applied. However, care must be taken for decreasing the buffer concentration

since one could obtain highly triangular peaks due to electromigration dispersion (Section 1.4.4) [66]. More importantly, decreasing the capillary inner diameter causes a dramatic decrease in temperature difference between the capillary center and its wall (sixth order dependence on radius in eq. 1.34). With narrow capillary, the surface-to-volume ratio is large resulting in efficient heat dissipation and thus decreases the broadening due to Joule heating. In practice, capillaries with inner diameter in the range of 25 to 100  $\mu\text{m}$  are most frequently employed in CE.

#### 1.4.4 Electromigration Dispersion

Under ideal conditions, symmetrical-shaped peaks are obtained where the broadening is mainly dominated by the longitudinal diffusion. Such symmetrical peaks are observed when the sample-to-buffer concentration ratio is below  $10^{-2}$  [67]. However, at high sample-to-buffer concentration ratio peaks often exhibit significant tailing or fronting with a typical triangular-shaped. Such triangular peaks indicate that the broadening is dominated by electromigration dispersion [68].

*Electromigration dispersion* results from changes in the local electric field strength in the analyte zone compared to the normal buffer [60]. The concentration profile of the analyte zone is strongly affected by the difference in the electrophoretic mobility between the analyte and the buffer co-ion. This mobility difference causes the local electric field strength inside the analyte zone to vary. Thus, analyte ions migrate at different velocities, and band broadening results.

When the analyte has an effective mobility higher than that of the buffer co-ion, the fast analyte ions outrun the buffer co-ions and exit the leading boundary of the original analyte zone into the buffer. When the analyte ions cross the boundary, the

concentration profile of the analyte becomes distorted with the concentration at the rear boundary being higher than that at the leading boundary. As a consequence, the electric field strength becomes low at high analyte concentration. Thus, the velocity of the analyte in the migration direction decreases at higher analyte concentration, whereas it speeds up at the regions with low analyte concentration. This results in the formation of sharp rear side and diffuse leading side in the analyte zone. Therefore, a fronting triangular peak is produced in the detector, as shown in Figure 1.6a. In contrast, the electric field gradient increases with analyte concentration when the analyte mobility is

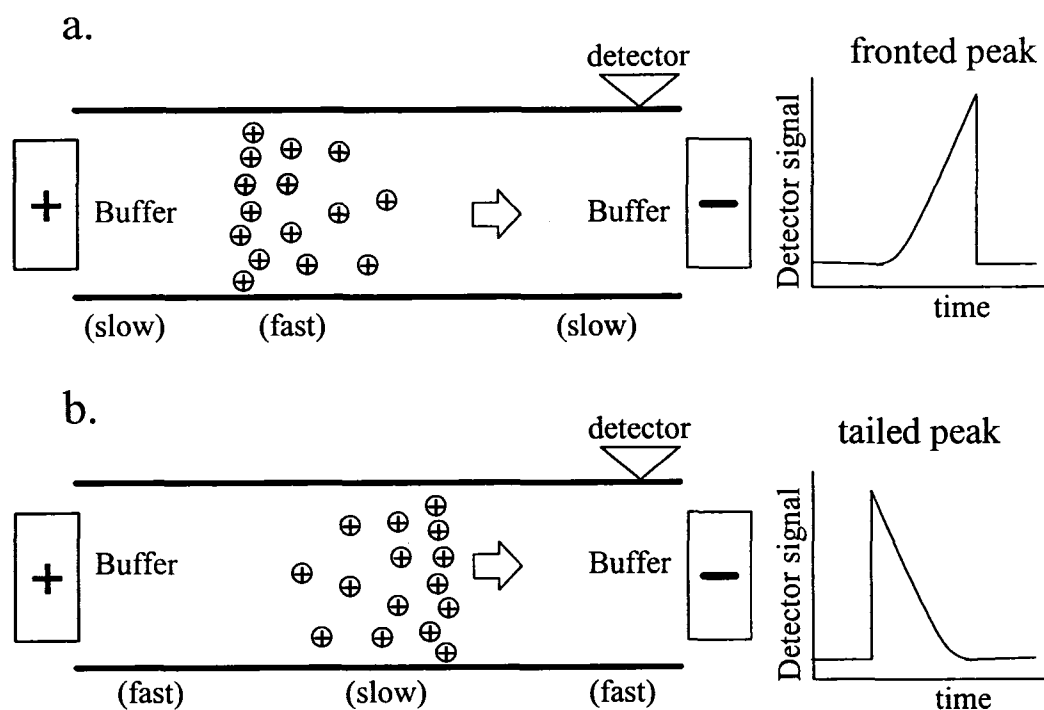


**Figure 1.6** Schematic diagrams illustrating the concentration profile of the analyte zone and the expected peak shape at the detector as a function of mobility difference between the analyte and the buffer co-ion.

slower than that of the buffer co-ion. This results in an increase in the analyte apparent velocity in the migration direction with concentration. Thus, a sharp side is formed at the front of the analyte zone, producing a tailing triangular peak at the detector (Figure 1.6b). No electromigration dispersion occurs if the mobilities of the analyte and the buffer co-ion are equivalent [67].

The plate height due to electromigration dispersion ( $H_{EMD}$ ) is [69, 70]:

$$H_{EMD} = \frac{2El_{inj}C_{s,0}|k_{EMD}|}{9c_B v_{app}} \quad (1.35)$$

where  $E$  is the electric field,  $l_{inj}$  is the analyte injection length,  $C_{s,0}$  is the initial analyte concentration,  $c_B$  is the buffer concentration,  $v_{app}$  is the apparent velocity of the analyte within the capillary, and  $k_{EMD}$  is the electromigration dispersion factor. The value of  $k_{EMD}$  can be calculated from the electrophoretic mobilities of the buffer constituents and the analyte ions. For non-protolyzing analyte ( $S^+$ ),  $k_{EMD}$  is given by [67, 71]:

$$k_{EMD} = \frac{(\mu_a - \mu_S)(\mu_b - \mu_S)}{(-\mu_a + \mu_b)\mu_S} \quad (1.36)$$

where  $\mu_a$ ,  $\mu_b$  and  $\mu_S$  are the mobilities of the buffer co-ion, the buffer counter ion and the sample, respectively. The  $k_{EMD}$  is constant for a sample zone in the electrophoretic buffer during the separation process. In case of protolyzing analyte, the increase in analyte concentration also causes a change in the pH in the analyte zone affecting the migration rate by the change in the effective mobility of the analyte in the sample zone. Thus,  $k_{EMD}$  for protolyzing analyte is dependent on the local conductivity as well as the relative changes of the effective mobility as a result of the pH change [69]. As shown in eq. 1.35, the broadening contribution from electromigration dispersion can be minimized by decreasing the sample-to-buffer concentration ratio. This can be performed by increasing

the buffer concentration or diluting the sample under investigation. The first approach is limited by Joule heating as the increased buffer concentration will increase the current generated within the capillary. The second approach is not very practical since it exerts more demands on the sensitivity of the detection system. The best approach to minimize the electromigration dispersion is to keep the  $k_{EMD}$  value as low as possible. This can be done by choosing a buffer with a co-ion effective mobility as close as possible to the mobility of the analyte [72]. Matching of the effective mobility of the buffer co-ion to that of the analyte results in dramatic reduction in the plate height and near symmetrical peak can be produced. This is illustrated in Chapter Four, where resolution and efficiency in preparative protein separations are strongly affected by the choice of buffer co-ion.

#### 1.4.5 Siphoning

The presence of hydrodynamic flow during the separation process can result in a devastating loss in separation efficiency. The *hydrodynamic flow*, also known as *siphoning*, is generated due to the difference in the buffer level in the vials at the inlet and outlet ends of the capillary. The velocity profile of siphoning flow, as all pressure driven flow, is characterized by its parabolic nature [9]. Since the siphoning flow occurs during the separation process, it might be added to or subtracted from the apparent velocity of the solute. The plate height contribution of the siphoning ( $H_H$ ) is [73]:

$$H_H = \frac{r^2 v_H^2}{24D(v_{app} \pm v_H)} \quad (1.37)$$

where  $r$  is the radius inner diameter,  $D$  is the diffusion coefficient of the solute molecules,  $v_{app}$  is the apparent velocity of the solute molecules in the absence of siphoning flow, and

$v_H$  is the cross-sectional average of the hydrodynamic velocity. Assuming that the height difference between buffer levels in the separating vials ( $\Delta h$ ) is constant, therefore,

$$v_H = \frac{\Delta h \rho g r^2}{8\eta L_t} \quad (1.38)$$

where  $\rho$  is the density of the buffer,  $g$  is the gravitational acceleration,  $\eta$  is the viscosity of the medium, and  $L_t$  is the total capillary length.

To avoid broadening due to siphoning, the driving force for hydrodynamic flow in the capillary should be eliminated. This can be performed by balancing the level of the buffer in the separating vials as well as employing narrow capillaries for separation. With very wide bore capillaries ( $> 100 \mu\text{m}$  i.d.), any small difference in the buffer height in the vials will cause a severe band broadening as inferred from eqs. 1.37 and 1.38. Similarly, it is apparent from these equations that siphoning will be more significant in microfluidic systems where  $L_t$  is smaller than in my work (where  $L_t$  is  $\geq 30$  cm).

#### 1.4.6 Solute/Wall Interaction

Since the separation mechanism in CZE depends on the difference in the migration velocity of the solute in the separating buffer, the capillary wall should not contribute to the electrophoretic separation. However, the solute molecules may interact electrostatically with ionized silanol groups on the wall. Besides, hydrophobic, hydrogen bonding and van der Waals forces may contribute to the adsorption mechanism [74]. Regardless, the solute adsorption onto the capillary wall may have a significant influence on the overall band broadening since it introduces chromatographic retention to the electrophoretic separation [75]. Solute adsorption has been noted to be more significant

for large molecular weight compounds, such as proteins, because they have many charges as well as hydrophobic moieties [76].

The extent of the wall adsorption could be described quantitatively using the retention factor ( $k'$ ). Jorgenson and co-workers predicted that  $k'$  values as small as 0.05 can increase the plate height of protein peak up to 20-fold [77]. The  $k'$  can be determined by running the CE system under chromatographic condition (apply pressure instead of voltage) for the solute and neutral marker separately, where:

$$k' = \frac{t_r - t_m}{t_m} \quad (1.39)$$

where  $t_r$  is the retention time of the solute molecule, and  $t_m$  is the dead time as defined by elution of the neutral marker [77]. In a liquid-solid separation system, the  $k'$  value is related to the distribution coefficient ( $K$ ) of the solute between solid stationary phase and the bulk solvent. In an open tube, the expression relating  $k'$  and  $K$  is:

$$K = \frac{rk'}{2} \quad (1.40)$$

where  $r$  is the capillary inner radius. The parameter  $K$  is also related to the adsorption and desorption rate constant  $k_a$  and  $k_d$ , respectively [78],

$$K = \frac{k_a}{k_d} \quad (1.41)$$

Slow adsorption/desorption kinetics will considerably distort the peak shape and increases the plate height contribution to the overall broadening. As the desorption process requires time, a portion of the solute zone will lag behind resulting in the formation of tailing peak. When the adsorption of the solute molecules to the supporting wall is very strong, i.e, extreme slow desorption kinetics, solutes may completely stick to

the capillary wall and never elute from the capillary. Assuming the adsorption isotherm is linear and that the adsorption is controlled by the rate of solute diffusion to the capillary wall surface, the plate height contribution from wall adsorption is [79]:

$$H_{Ad} = \left[ \frac{K^2 r}{D(r + 2K)} + \frac{4K}{(r + 2K)k_d} \right] v_{app} \quad (1.42)$$

where  $D$  is the solute diffusion coefficient, and  $v_{app}$  is the apparent velocity of the solute molecules.

Based on eq. 1.42, reducing the solute apparent velocity by decreasing the applied electric field strength would reduce the plate height due to adsorption. However, this approach will increase the analysis time and broadening due to longitudinal diffusion becomes significant. The best approach to minimize the broadening due to adsorption can be accomplished by deactivation of the inner surface of the capillary to suppress the adsorption. Many strategies have been employed to reduce the solute-wall interactions, especially for proteins. These include increasing the buffer ionic strength, operating the separation at extreme pH, and finally modifying the inner wall surface by permanent or dynamic coatings. Sections 1.5 and 1.6 provide more discussion regarding protein separations and wall coatings.

## 1.5 Protein Separations in CZE

*Proteins* represent a large and complex group of biomolecules. They consist of a chain of amino acids joined together by peptide bonds. Physical properties such as size, shape, hydrophobicity and isoelectric point ( $pI$ ) for a particular protein are determined, to a large extent, by the number, the nature and the sequence of the amino acid residues. In addition, proteins have both negative and positive functional groups. Because it has

amphoteric characteristics, the charge state of the protein depends on the medium pH [80]. The net charge of a protein is zero as the medium pH is equivalent to its  $pI$ . The overall protein charge is negative if the medium pH is higher than its  $pI$ , whereas if the pH is less the  $pI$ , the overall charge of the protein species is positive.

Traditionally, two dimensions gel electrophoresis (2D-gel) is frequently employed for protein separation due to its high resolving power. Although it is very popular for protein separations, 2D-gel electrophoresis is time-consuming, labor-intensive, difficult-to-automate, and has low reproducibility [81]. Capillary electrophoresis has many beneficial characteristics including fast, high resolution, high efficiency, and ease-of-automation that make it an attractive alternative to 2D-gel electrophoresis for protein separations. However, protein separations in CZE with untreated fused silica are not always possible at physiological pH. For protein bearing a net negative charge, the columbic repulsion could prevent interaction between the protein and the negatively charge wall surface and thus prevent adsorption. At physiological pH, for example, recoveries up to 90% can be achieved for proteins with low  $pI$  values such as pepsin ( $pI$  of 3.2) [80]. In contrast, positively charged proteins electrostatically interact with the negatively-charged fused silica surface. This leads to band broadening with severe peak tailing if slow reversible adsorption kinetics are dominant. Further, irreversible adsorption leads to diminished recovery, and even total loss of the protein onto the silica surface is a possibility [76]. The protein adsorption also causes a change in the zeta potential at the surface of the capillary wall which reflects a change in the EOF. The alteration of the EOF velocity changes the migration time of protein and thus reduce the separation reproducibility [80, 82].

Generally, high concentration buffers minimize protein adsorption. The buffer cations compete with the proteins for the cation-exchange (silanols) sites on the silica surface. Less hydrated cations are most effective in preventing protein adsorption. For example,  $K^+$  was more effective to minimize protein adsorption than  $Li^+$  ions [77]. However, this approach is limited by Joule heating broadening.

Another approach to minimize protein adsorption onto the silica surface is to use extreme buffer pH. When the operating pH was  $< 2$ , the EOF, and hence the surface charge, is drastically reduced as a result of progressive protonation of the silanols on the capillary wall [83]. Although protein separations can perform well in buffers with low pH, this method suffers from high conductivity resulting from the contribution of large ion concentration of the extremely high mobility hydronium ion. This may lead to deteriorate of protein separations due to Joule heating. Other disadvantage of utilizing acidic buffers is the limited selectivity due to the narrow pH range, as the proteins are fully ionized at low pH. Thus, separation of closely related proteins may not be possible under acidic conditions. Alternatively, using buffers with extremely high pH is fairly successful for protein separations [84]. At very high pH, almost all proteins will be anionic and repelled from the capillary wall. For effective elimination of protein adsorption it is recommended that the buffer pH be at least two pH units above the highest protein  $pI$  [85]. Unfortunately, application of this method is limited by chemical instability of the proteins and degradation of capillary inner surface. Also, protein separations at extreme high pH suffer from limited selectivity due to the narrow pH range as the proteins are fully ionized.

## 1.6 Capillary Wall Coatings

The most effective way to avoid protein adsorption onto the capillary surface is to alter or shield the surface charge of the capillary using a coating. In addition, it is also possible, by applying coating technology, to manipulate the EOF to optimize the separation efficiency, the speed of analysis and the resolution. Ideally, a wall coating should exhibit advantageous characteristics including high efficiency (theoretically, approaching 1-2 million plates/m), high recovery (approaching 100%), and good migration time reproducibility from run to run (ideally less than 1%) [86]. More importantly, the coating procedure should be easy to apply, inexpensive, and exhibit good stability over a wide range of buffer conditions [87]. Characterization of the properties of the coating is commonly assessed by the stability of the EOF as well as separation performance of basic proteins, in particular  $\alpha$ -chymotrypsinogen A, ribonuclease A, cytochrome *c*, and lysozyme, due to their high tendency to adsorb to the capillary wall [86]. Generally, coatings are classified into three major categories: covalently bonded coatings; non-covalently bonded polymer coatings; and adsorbed surfactant coatings.

### 1.6.1 Covalently Bonded Coatings

Covalently bonded coatings are usually achieved by attaching the polymer to the silica wall by covalent bonds. These coatings are generated by derivatizing the capillary wall with a bifunctional silane reagent, to produce an intermediate layer between the capillary wall and the polymer. The silane reagent serves as an anchor, in which one group reacts with the silica surface forming a siloxane bond (Si-O-Si) and the other with the coating monomers [88]. Due to the instability of siloxane bonds under alkaline conditions, the Si-O-Si can be replaced by Si-C linkage using Grignard chemistry. The

Si-C linkage shows good stability in the pH range of 2.7 to 9.5 [89]. In the final stage, the coating monomers are polymerized to form the top layer of the coating. The top layer of the coating should have strong hydrophilic nature to reduce protein-coating interactions. It is also possible to further cross-link the top layer of the coating to increase the stability of the coatings [90].

Neutral hydrophilic polymer coatings such as polyacrylamide [88], poly(vinyl pyrrolidone) [83] and poly(ethylene glycol) [91, 92] are extensively employed to separate protein mixtures. These coatings suppress the EOF and reduce protein adsorption. The suppression of the EOF is attributed to the shielding of the silanol groups and the increase in the viscosity near the capillary wall. The absence of the charge in these coatings eliminates the electrostatic interactions between the proteins and the capillary wall, and near symmetric peaks may be obtained [93, 94].

Permanent coated capillaries can provide efficiencies greater than one million plates/m for basic proteins [90, 93]. However, this strategy suffers from several disadvantages including: labor-intensive and lengthy derivatization procedures that significantly increase capillary cost; limited pH range over which separations can be performed due to the fragility of the siloxane bond; and possibly limited capillary life. Furthermore, the preparation of the coating comprises several chemical steps which are difficult to control. Therefore, reproducibility from capillary to capillary may be an issue [82, 95].

### **1.6.2 Adsorbed Polymer Coatings**

Adsorbed polymer coatings are an alternative method employed to overcome the major drawbacks of covalently bonded coatings. Its beneficial advantages over the

covalently bonded polymers are the simplicity of coating formation and the possibility of coating regeneration. Adsorbed polymer coatings are simply prepared by rinsing the capillary with buffer containing a polymer. The coating is formed as the polymer physically adsorbs to the capillary wall. The adsorbed polymer shields or alters the charged groups of the silica wall. These adsorbed coatings may be non-ionic or cationic polymers.

#### **1.6.2.1 Non-ionic Polymer Coatings**

Highly hydrophilic coatings such as poly(vinyl alcohol) are very effective for protein separations, and efficiencies of more than 1 million plates/m can be achieved [96]. Despite their effectiveness for protein separations, the stability of these polymers is limited to acidic buffer conditions, and the coating can be easily removed from the surface if the polymer is not present in the buffer. The presence of the polymer in the separating buffer would cause serious interferences with detection scheme, particularly mass spectrometry. Less hydrophilic polymer such as poly(ethylene oxide) shows better stability than poly(vinyl alcohol) in the absence of polymer in the buffer [82]. To increase the effectiveness of the poly(ethylene oxide) coating for protein separations, the capillary should be pretreated by 1 M HCl before flushing with acidified polymer solution followed by rinsing with the normal buffer. The coating, however, is unstable at alkaline pH ( $\text{pH} > 8.0$ ), and might be slowly degraded during the course of long runs due to electrolysis of the buffer ( $> 50$  min when the cathodic buffer vial contains 0.5 mL) [97].

#### **1.6.2.2 Cationic Polymer**

Cationic polymers such as polybrene [98], polyarginine [99] and polyethylene-

imine [100] have been widely used as non covalent coatings for protein separations. These polymers have high tendency to adsorb to the negatively charged silica surface by electrostatic interactions. Upon adsorption, they introduce positive charges onto the surface and thus reverse the EOF. Cationic polymer coatings are particularly appropriate for separation of proteins at pH less than their *pI*. Under these conditions, the proteins possess positive charges and thus are repelled from the coating surface. As a dynamic coating, polyarginine polymer is very efficient for the separation of basic proteins with plate numbers in excess of 1 million plates/m [99].

The strong binding of the polymer to the silica surface can keep the coating intact to the wall even after the polymer is removed from the buffer. Thus, adsorbed polymers can form semi-permanent or static wall coatings [76]. Separation efficiencies of 0.3 to 0.5 million plates/m were achieved for several cationic proteins using polyethyleneimine, as a static wall coating [100]. The absence of the polymer from the buffer avoids any possible interaction between the polymer and the proteins, and may enhance the signal-to-noise ratio [98]. However, the separation efficiency achieved by these coatings is significantly low compared to the theoretical predicted efficiency of 1-2 million plates/m [86]. Besides, the electroosmotic flow deteriorated during the run due to the bleeding of the polymer from the surface. For instance, the EOF of polyethyleneimine coated capillary decreased by 10% over 25 runs performed after coating the capillary [101]. Thus, recoating the capillary is required before each run to maintain reasonable migration time reproducibility. However, this extra recoating step (at least 15 min [101]) prior each protein separation is time consuming and impractical.

### 1.6.3 Adsorbed Surfactant Coating

Surfactants are becoming increasingly popular over both covalently and non-covalently polymer coatings due to their simplicity of application, versatility, and low cost. *Surfactants*, also known as surface-active agents, have a general structure of a hydrophilic (polar or ionic) headgroup and a hydrophobic moiety, generally one or more hydrocarbon chains. Based on the nature of the headgroup, the surfactants are classified as nonionic, zwitterionic, anionic and cationic surfactants. At a specific concentration, known as the *critical micelle concentration* (cmc), the surfactant monomers start to aggregate to minimize the interaction of the hydrophobic tails with water. In other words, the cmc is the concentration of surfactant monomer in equilibrium with micelles in the bulk solution. The value of the cmc depends mainly on the nature of the surfactant. In addition, buffer conditions such as ionic strength and the nature of the buffer counterion may influence the cmc value, especially for ionic surfactants. In this thesis, my discussion will be focused on cationic surfactants, in particular surfactants with quaternary ammonium headgroups.

At a concentration above the cmc, the surfactant monomers spontaneously aggregate into a wide variety of morphologies. The geometry of the aggregation structure is strongly dependent on the shape of the surfactant monomers. According to the theory of self-assembly of surfactant, the secondary structure of the surfactant aggregation can be predicted from the value of the packing parameter  $p$  given by [102]:

$$p = \frac{v_c}{l_c a_h} \quad (1.43)$$

where  $v_c$  is the volume of the hydrocarbon region,  $l_c$  is the optimal hydrocarbon chain

length related to its maximum extended length, and  $a_h$  is the electrostatic cross-sectional area of the headgroup.

In general, single chained cationic surfactants, such as tetradecyltrimethylammonium (TTAB) and cetyltrimethylammonium bromide (CTAB), have a packing factor of less than 0.33 in pure water. Due to the large cross sectional area of the headgroup of single chained surfactant, these molecules possess a conical shape. Thus, spherical micelles are favored. The packing factor can be increased by decreasing the electrostatic repulsion between the adjacent headgroups. For example, the addition of salts increases the packing factor for CTAB to 0.50 [103], resulting in the formation of cylindrical (rod-like) micelles. Similarly, addition of SDS to CTAB reduces the electrostatic repulsion between adjacent CTAB sufficiently to generate bilayer structures [104].

Alternatively, the packing factor of a surfactant can be increased by increasing the volume of the hydrocarbon region ( $v_c$ ) while maintaining the length of the hydrocarbon tail ( $l_c$ ). This is most easily accomplished by using surfactants possessing multiple hydrocarbon tails. The presence of two alkyl chains makes these surfactants cylindrical in geometry. The packing factor for double chained surfactants is in the range of 0.5-1. Double-chained cationic surfactants with alkyl chains longer than eight carbon atoms form bilayer (vesicle) structures in aqueous solutions [105, 106] and are favored to form bilayers on surfaces. The length of the alkyl chain has less effect on the aggregation morphology, as both the volume ( $v_c$ ) and the length ( $l_c$ ) of the hydrocarbon chain increase proportionally, and thus the packing parameters remains constant. For instance, didecyl-dimethylammonium bromide ( $2C_{10}DAB$ ), didodecyldimethylammonium bromide

(DDAB), dimethylditetradecylammonium bromide ( $2C_{14}DAB$ ), and dihexadecyldimethylammonium bromide ( $2C_{16}DAB$ ), all have packing factors of  $\sim 0.62$  [107]. Thus, all of these double-chained surfactants are expected to form bilayers.

Triple chained cationic surfactants possess a hydrophobic moiety consisting of three hydrocarbon chains. This enlarges the packing parameter to about 1 which is at the transition point between bilayer (vesicle,  $0.5 \leq p \leq 1$ ) formation and inverted structures ( $p > 1$ ). For instance, Kunitake *et al.* observed well-developed bilayer structures for trihexadecylmethylammonium bromide ( $3C_{16}MAB$ ), but did not see any bilayers with tridodecylmethylammonium bromide ( $3C_{12}MAB$ ) [105].

Traditionally, single chain surfactants have been utilized as dynamic wall coatings for protein separations [108]. In dynamic coatings, the surfactant is added to the electrophoretic buffer to maintain the coating intact to the surface. Upon rinsing the capillary with a CTAB solution, the monomers and micelles, which have high affinity to the silica surface, adsorbed onto the surface as a hemi-micelle layer and thus shield the bulk solution from the negative silanol groups [109]. Atomic force microscopy (AFM) imaging confirmed that CTAB adsorbed on the silica surface as spherical micelles spaced uniformly onto the silica surface, as shown in Figure 1.7 [110]. The cationic surfactant coating generates a reverse charge on the silica surface and thus reverses the direction of the EOF as well as prevents the adsorption of cationic proteins. Efficiency of cationic protein separated by CTAB dynamic coatings are relatively low, less than 0.35 million plates/m [108]. They attributed the lower efficiency to the interaction between the CTAB and the proteins. Besides, the presence of surfactant in the buffer makes CE incompatible with detection schemes such as mass spectrometry due to the drastic ion suppression of

sample ionization, and sensitivity limitation caused by the bulk flow of charged reagent into the mass spectrometer ion source [111].

Previous studies in our group demonstrated that DDAB formed semi-permanent wall coatings. The stability of these coatings was attributed to the formation of the bilayer coatings onto the silica surface, as confirmed by AFM imaging (Figure 1.8) [110]. Bilayers prepared from DDAB are sufficiently stable that the surfactant need not be in the separation buffer. These coatings are very effective for protein separations, achieving efficiencies in excess of 0.56 million plates/m and recoveries greater than 92% [87].

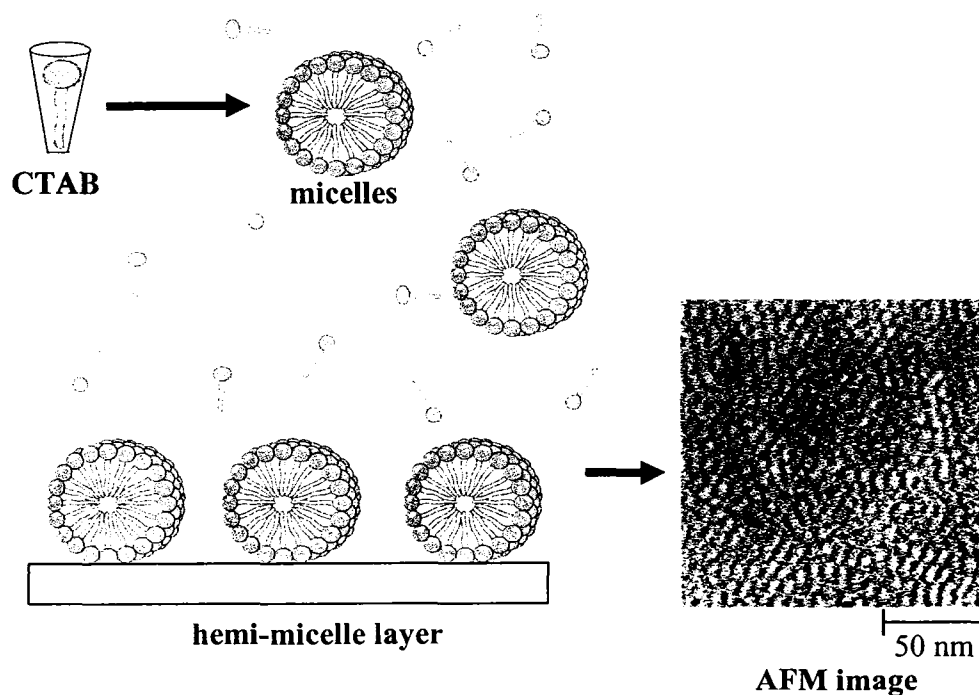


**Figure 1.7** Diagram showing the formation of micelle aggregates of CTAB in the solution and on the surface. AFM image (150 nm × 150 nm) of 0.5 mM CTAB in 10 mM phosphate buffer at pH 7.0 on fused silica (with permission reference [110]).

However, the efficiency and recoveries were highly reduced by performing replicate protein separations on the same coating. The deterioration of the separation performance using bilayer coatings is due to the gradual degradation of the DDAB during the separation as the running buffer passes through the capillary. For instance, the EOF decreased by 3% after 75 min under continuous electrophoretic conditions [110]. The bleeding of the bilayer may cause serious interference with detection, particularly with electrospray ionization mass spectrometry.

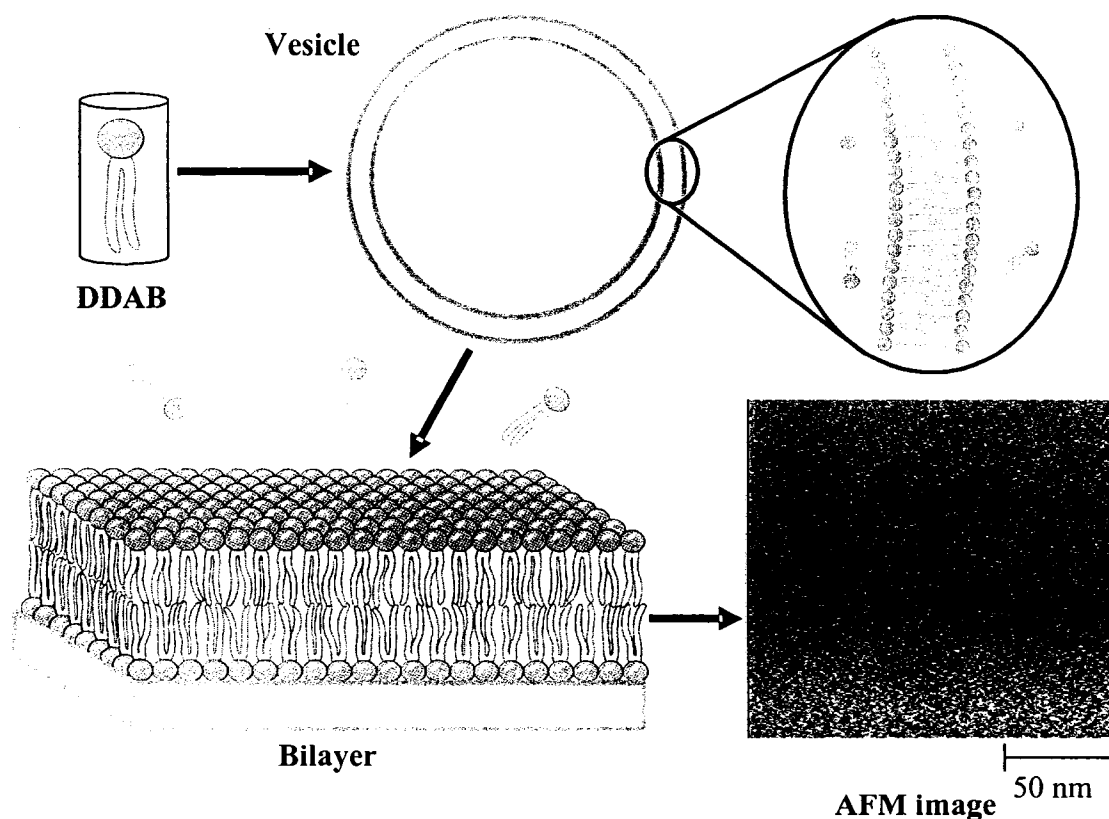


**Figure 1.8** Diagram showing the formation of vesicle aggregates of DDAB in the solution and the bilayer formation on the surface. AFM image (150 nm × 150 nm) of 0.1 mM DDAB in 10 mM phosphate buffer at pH 7.0 on fused silica (with permission, reference [110]).

## 1.7 Thesis Overview

The aim of this thesis is to develop a stable, efficient, inexpensive and robust capillary coating system to prevent protein adsorption onto the fused silica capillary wall. Surfactant coatings are attractive in preventing protein adsorption because of their simplicity, versatility and low cost. In Chapter Two, I investigate the factors which govern the stability of the semi-permanent coating formed by aggregations of double-chained surfactants on the capillary wall. Didodecyldimethylammonium bromide (DDAB) is used in this study. A simple means to enhance the stability of this semi-permanent coating is illustrated in Chapter Three. Long double chained cationic surfactants as well as triple chained cationic surfactant are employed to increase the stability of semi-permanent coatings. The high stability of these surfactant coatings enables preparative protein separations to be performed in wide bore capillaries (Chapter Four). Finally, Chapter Five describes a manual fraction collection for isolation of picomole quantities of pure protein using a commercial CE instrument for microwave assisted acid hydrolysis (MAAH) for protein characterization. MALDI-TOF MS are used to determine the purity of the isolated fractions.

## 1.8 References

- [1] Dovichi, N. J., Zhang, J., *Angew. Chem. Int. Ed.* 2000, 39, 4463-4468.
- [2] Tiselius, A., *Trans. Faraday Soc.* 1937, 33, 524-531.
- [3] Kunkel, H. G., Tiselius, J., *J. Gen. Physiol.* 1951, 35, 89-118.
- [4] Raymond, S., Weintraub, L., *Science* 1959, 130, 711-711.
- [5] Anderson, L., Anderson, N. G., *Proc. Natl. Acad. Sci. USA* 1977, 74, 5421-5424.
- [6] Hjertén, S., *Chromatogr. Rev.* 1967, 9, 122-219.
- [7] Jorgenson, J. W., Lukacs, K. D., *Anal. Chem.* 1981, 53, 1298-1302.
- [8] Hutterer, K. M., Jorgenson, J. W., *Anal. Chem.* 1999, 71, 1293-1297.
- [9] Jussila, M., Palonen, S., Porras, S. P., Riekkola, M.-L., *Electrophoresis* 2000, 21, 586-592.
- [10] Schwer, C., Kenndler, E., *Anal. Chem.* 1991, 63, 1801-1807.
- [11] Hunter, R. J., *Zeta potential in Colloidal Science. Principles and Applications*, Academic Press, New York 1981.
- [12] Bard, A. J., Faulkner, L. R., *Electrochemical Methods. Fundamentals and Applications*, John Wiley & Sons, Inc., Hoboken, NJ 2001.
- [13] Dickens, J. E., Gorse, J., Everhart, J. A., Ryan, M., *J. Chromatogr. B* 1994, 657, 401-407.
- [14] Vindevogel, J., Sander, P., *J. Chromatogr.* 1991, 541, 483-488.
- [15] Corradini, D., Spreccacenero, L., *Chromatographia* 2003, 58, 587-596.
- [16] Vinther, A., Sørensen, H., *J. Chromatogr.* 1991, 559, 27-42.
- [17] Stevens, T. S., Cortes, H. J., *Anal. Chem.* 1983, 55, 1365-1370.
- [18] Rush, R. S., Cohen, A. S., Karger, B. L., *Anal. Chem.* 1991, 63, 1346-1350.

- [19] "Handbook of Chemistry and Physics", Lide, D. R. (Editor), CRC Press, Boca Raton, FL, 2005-2006
- [20] Jones, J. H., Spuhler, F. J., Felsing, W. A., *J. Am. Chem. Soc.* 1942, 64, 965-968.
- [21] Jandik, P., Bonn, G., in: VCH (Ed.), *Capillary electrophoresis of small molecules*, New York 1993.
- [22] Fu, S., Lucy, C. A., *Anal. Chem.* 1998, 70, 173-181.
- [23] Li, D., Fu, S., Lucy, C. A., *Anal. Chem.* 1999, 71, 687-699.
- [24] Friedl, W., Reijenga, J. C., Kenndler, E., *J. Chromatogr. A* 1995, 709, 163-170.
- [25] Porras, S. P., Riekkola, M.-L., *Electrophoresis* 2003, 24, 1485-1498.
- [26] Smith, S. C., Khaledi, M. G., *Anal. Chem.* 1993, 65, 193-198.
- [27] Winzor, D. J., *Anal. Biochem.* 2004, 325, 1-20.
- [28] Melanson, J. E., Baryla, N. E., Lucy, C. A., *Trends Anal. Chem.* 2001, 20, 365-374.
- [29] Kuhr, W. G., Yeung, E. S., *Anal. Chem.* 1998, 60, 2642-2646.
- [30] Baldwin, R. B., *Electrophoresis* 2000, 21, 4017-4028.
- [31] Grossman, P. D., Colburn, J. C., *Capillary Electrophoresis: Theory & Practice*, Academic Press, Inc., San Diego, California, USA 1992.
- [32] Pentoney, S. L., Sweedler, J. V., in: Landers, J. P. (Ed.), *Handbook of Capillary Electrophoresis*, CRC Press, Inc. 1994.
- [33] Walbroehl, Y., Jorgenson, J. W., *J. Chromatogr.* 1984, 315, 135-143.
- [34] Bruin, G. J. M., Stegeman, G., Van Asten, A. C., Xu, X., Kraak, J. C., Poppe, H., *J. Chromatogr.* 1991, 559, 163-181.
- [35] Xue, Y., Yeung, E. S., *Anal. Chem.* 1994, 66, 3575-3580.

- [36] Chervet, J. P., Van Soest, R. E. J., Ursem, M., *J. Chromatogr.* 1991, 543, 439-449.
- [37] Wang, T., Aiken, J. H., Huie, C. W., Hartwick, R. A., *Anal. Chem.* 1991, 63, 1372-1376.
- [38] Smith, R. D., Goodlett, D. R., Wahl, J. W., in: Landers, J. P. (Ed.), *Handbook of Capillary Electrophoresis*, CRC Press, Inc. 1994.
- [39] Castoro, J. A., Chiu, R. W., Monnog, C. A., Wilkins, C. W., *J. Am. Chem. Soc.* 1992, 114, 7571-7572.
- [40] Buruins, A. P., *J. Chromatogr. A* 1998, 794, 345-357.
- [41] Smith, R. D., Loo, J. A., Barinaga, C. J., Edmonds, C. G., Udseth, H. R., *J. Chromatogr.* 1989, 480, 211-232.
- [42] McComb, M. E., Perreault, H., *Electrophoresis* 2000, 21, 1354-1362.
- [43] Lee, E. D., Muck, W., Henion, J. D., Covey, T. R., *Biomed. Environ. Mass Spectrom.* 1989, 18, 844-850.
- [44] Issaq, H. J., Janini, G. M., Chan, K. C., Veenstra, T. D., *J. Chromatogr. A* 2004, 1053, 37-42.
- [45] Vorm, O., Roepstorff, P., Mann, M., *Anal. Chem.* 1994, 66, 3281-3287.
- [46] Karas, M., Bahr, U., *Trends Anal. Chem.* 1990, 9, 321-325.
- [47] Gusev, A. J., Wilkinson, W. R., Proctor, A., Hercules, D. M., *Anal. Chem.* 1995, 67, 1034-1041.
- [48] Karas, M., Kruger, R., *Chem. Rev.* 2003, 103, 427-439.
- [49] Lane, C. S., *Cell. Mol. Life Sci.* 2005, 62, 848-869.
- [50] Beavis, R. C., Chait, B. T., *Anal. Chem.* 1990, 62, 1836-1840.

- [51] Ingendoh, A., Karas, M., Hillenkamp, F., *Int. J. Mass Spectrom. Ion Processes* 1994, 131, 345-354.
- [52] Yeung, K. K.-C., Kiceniuk, A. G., Li, L., *J. Chromatogr. A* 2001, 931, 153-162.
- [53] Kenndler, E., in: Khaledi, M. G. (Ed.), *High-Performance Capillary Electrophoresis*, John Wiley & Sons, Inc., New York 1998, pp. 25-76.
- [54] Giddings, J. C., *Sep. Sci.* 1969, 4, 181-189.
- [55] Otsuka, K., Terabe, S., *J. Chromatogr.* 1989, 480, 91-94.
- [56] Huang, X., Coleman, W. F., Zare, R. N., *J. Chromatogr.* 1989, 480, 95-110.
- [57] Peng, X., Chen, D. D. Y., *J. Chromatogr. A* 1997, 767, 205-216.
- [58] Grushka, E., McCormick, R. M., *J. Chromatogr.* 1989, 471, 421-428.
- [59] Lucy, C. A., Yeung, K. K.-C., Peng, X., Chen, D. D. Y., *LC.GC* 1998, 16, 26-32.
- [60] Foret, F., Deml, M., Bocek, P., *J. Chromatogr.* 1988, 452, 601-613.
- [61] Lee, H. G., Desiderio, D. M., *J. Chromatogr. B* 1994, 662, 35-45.
- [62] Giddings, J. C., *J. Chromatogr.* 1989, 480, 21-33.
- [63] Jones, A. E., Grushka, E., *J. Chromatogr.* 1989, 466, 219-225.
- [64] Grushka, E., McCormick, R. M., Kirkland, J. J., *Anal. Chem.* 1989, 61, 241-246.
- [65] Bello, M. S., Chiari, M., Nesi, M., Righetti, P. G., *J. Chromatogr.* 1992, 625, 323-330.
- [66] Bello, M. S., Righetti, P. G., *J. Chromatogr.* 1992, 606, 95-102.
- [67] Mikkers, F. E. P., Everaerts, F. M., Verheggen, T. P. E. M., *J. Chromatogr.* 1979, 169, 1-10.
- [68] Beckers, J. L., *J. Chromatogr. A* 1995, 693, 347-357.
- [69] Xu, X., Kok, W. T., Poppe, H., *J. Chromatogr. A* 1996, 742, 211-227.

- [70] Palonen, S., in Department of Chemistry, University of Helsinki, Helsinki University Printing House, Helsinki, 2005, pp. 13-42 (Thesis).
- [71] Cifuentes, A., Xu, X., Kok, W. T., Poppe, H., *J. Chromatogr. A* 1995, 716, 141-156.
- [72] Sustacek, V., Foret, F., Bocek, P., *J. Chromatogr.* 1991, 545, 239-248.
- [73] Grushka, E., *J. Chromatogr.* 1991, 559, 81-93.
- [74] Ermakov, S. V., Zhukov, M. Y., Capelli, L., Righetti, P. G., *J. Chromatogr. A* 1995, 699, 297-313.
- [75] Kennedy, R. T., *Anal. Chimica Acta* 1999, 400, 163-180.
- [76] Doherty, E. A. S., Meagher, R. J., Albarghouthi, M. N., Barron, A. E., *Electrophoresis* 2003, 24, 34-54.
- [77] Green, J. S., Jorgenson, J. W., *J. Chromatogr.* 1989, 478, 63-70.
- [78] Schure, M. R., Lenhoff, A. M., *Anal. Chem.* 1993, 65, 3024-3037.
- [79] Gaš, B., Stedry, M., Kenndler, E., *Electroporesis* 1997, 18, 2123-2133.
- [80] Towns, J. K., Regnier, F. E., *Anal. Chem.* 1992, 64, 2473-2478.
- [81] Wang, Y., Balgley, B. M., Rudnick, P. A., Lee, C. S., *J. Chromatogr. A* 2005, 1073, 35-41.
- [82] Iki, N., Yeung, E. S., *J. Chromatogr. A* 1996, 731, 273-282.
- [83] McCormick, R. M., *Anal. Chem.* 1988, 60, 2322-2328.
- [84] Lauer, H. H., McManigill, D., *Anal. Chem.* 1986, 58, 166-170.
- [85] Bonvent, J. J., Barberi, R., Bartolino, R., Capelli, L., Righetti, P. G., *J. Chromatogr. A* 1996, 756, 233-243.

- [86] Mazzeo, J. R., Krull, I. S., in: Landers, J. P. (Ed.), *Handbook of Capillary Electrophoresis*, CRC Press, Boca Raton, FL 1994, pp. Chapter. 18.
- [87] Baryla, N. E., Lucy, C. A., *Anal. Chem.* 2000, 72, 2280-2284.
- [88] Hjertén, S., *J. Chromatogr.* 1985, 347, 191-198.
- [89] Cobb, K. A., Dolnik, V., Novotny, M., *Anal. Chem.* 1990, 62, 2478-2483.
- [90] Srinivasan, K., Pohl, C., Avdalovic, N., *Anal. Chem.* 1997, 69, 2798-2805.
- [91] Bruin, G. J. M., Chang, J. P., Kuhlman, R. H., Zegers, K., Kraak, J. C., Poppe, H., *J. Chromatogr.* 1989, 471, 429-436.
- [92] Meagher, R. J., Seong, J., Liabinis, P. E., Barron, A. E., *Electrophoresis* 2004, 25, 405-414.
- [93] Cifuentes, A., Diez-Masa, J. C., Fritz, J., Anselmetti, D., Bruno, A. E., *Anal. Chem.* 1998, 70, 3458-3462.
- [94] Feldmann, A., Claubnitzer, U., Otto, M., *J. Chromatogr. B* 2004, 803, 149-157.
- [95] Wang, Y., Dubin, P. L., *Anal. Chem.* 1999, 71, 3463-3468.
- [96] Gilges, M., Kleemlss, M. H., Schomburg, G., *Anal. Chem.* 1994, 66, 2038-2046.
- [97] Preisler, J., Yeung, E. S., *Anal. Chem.* 1996, 68, 2885-2889.
- [98] Yao, Y. J., Khoo, K. S., Chungb, M. C. M., Li, S. F. Y., *J. Chromatogr. A* 1994, 680, 431-435.
- [99] Chiu, R. W., Jimenez, J. C., Monnog, C. A., *Anal. Chim. Acta* 1995, 307, 193-201.
- [100] Erim, F. B., Cifuentes, A., Poppe, H., Kraak, J. C., *J. Chromatogr. A* 1995, 708, 356-361.
- [101] Córdova, E., Gao, J., Whitesides, G. M., *Anal. Chem.* 1997, 69, 1370-1379.

- [102] Israelachvili, J. N., Mitchell, D. J., Ninham, B. W., *J. Chem. Soc., Faraday Trans. 2* 1976, 72, 1525- 1568.
- [103] Liu, J.-F., Ducker, W. A., *J. Phys. Chem. B* 1999, 103, 8558-8567.
- [104] Wang, C., Lucy, C. A., *Electrophoresis* 2004, 25, 825-832.
- [105] Kunitake, T., Kimizuka, N., Higashi, N., Nakashima, N., *J. Am. Chem. Soc.* 1984, 106, 1978-1983.
- [106] Svitova, T. F., Smirnova, Y. P., Pisarev, S. A., Berezina, N. A., *Colloids Surf. A* 1995, 98, 107-115.
- [107] Warr, G. G., Radha Sen, Evans, D. F., Trend, J. E., *J. Phys. Chem.* 1988, 92, 774-783.
- [108] Cifuentes, A., Rodriguez, R., Garcia-Montelongo, F. J., *J. Chromatogr. A* 1996, 742, 257-266.
- [109] Lucy, C. A., Underhill, R. S., *Anal. Chem.* 1996, 68, 300-305.
- [110] Baryla, N. E., Melanson, J. E., McDermott, M. T., Lucy, C. A., *Anal. Chem.* 2001, 73, 4558-4565.
- [111] Varghese, J., Cole, R. B., *J. Chromatogr. A* 1993, 652, 369-376.

## CHAPTER TWO: Factors Affecting the Temporal Stability of Semi-permanent Bilayer Coatings in Capillary Electrophoresis Prepared using Double Chained Surfactants

### 2.1 Introduction

Capillary electrophoresis (CE) is a powerful analytical technique for large biopolymers, as illustrated by CE's sequencing of the Human Genome [1]. Due to its beneficial features including high separation efficiency, high resolution, rapid separation time and ease of automation, it is envisioned that CE could make a similar impact on the determination of the proteome. However, the separation of proteins is complicated by their tendency to adsorb onto the negatively charged surface of the capillary. As discussed in Section 1.5, protein adsorption can lead to significant band broadening, poor migration time reproducibility [2] and low sample recovery [3]. There are a number of approaches for shielding or altering the surface charge of the capillaries, and thereby reducing protein interaction with the capillary wall. These include: the use of extreme pH [2, 4]; high ionic strength [5]; and zwitterionic additives [6]. However, the most common approach has been to coat the capillary wall [7]. Wall coatings are classified into [8]: covalently bonded/cross-linked polymers [9-12]; adsorbed cationic or nonionic polymers [13, 14], [15]; and adsorbed surfactants (dynamic coatings) [16-21]. These approaches were discussed in details in Section 1.6.

Dynamic coatings are attractive relative to the other wall modification approaches

---

\* Aversion of this chapter has been published. Yassine, M. M., Lucy, C.A., *Analytical Chemistry* **2004**, 76, 2983-2990.

due to their simplicity, versatility and low cost. As shown in Section 1.6.3, double chain cationic surfactants, such as didodecyldimethylammonium bromide (DDAB), have a packing factor ( $p$ ) of  $\sim 0.62$  and form bilayer wall coatings [17, 22]. These bilayer coatings are stable even after the surfactant has been removed from the run buffer. Thus, DDAB coatings are referred to as semi-permanent coatings, where surfactant need not be present in the run buffer and the coating is refreshed between each electrophoretic run.

The bilayer coatings, particularly DDAB, are very effective in the separation of cationic proteins, achieving efficiencies ranging from 0.56 to 0.75 million plates/m and recoveries of more than 92% in less than 8 minutes [22]. Successive measurements of a neutral marker (mesityl oxide), to assess the stability of the bilayer coating without refreshing the coating between the runs, showed that the electroosmotic flow (EOF) gradually decreased by 3% over 75 minutes. The drift in the EOF associated with DDAB coatings indicates that there is gradual loss of surfactant from the bilayer. This may cause serious interference with detection, particularly with electrospray ionization mass spectrometry (ESI-MS) [23-25]. Thus, an understanding of the desorption mechanism of the surfactant is essential to minimize the bleed of surfactant from the capillary and to maintain high migration time reproducibility.

This Chapter investigates the effect of chemical and physical factors on the stability of DDAB coatings. A model describing the degradation process of the DDAB bilayer has been proposed based on EOF measurements. Significant improvements in the coating stability can be achieved by altering experimental conditions, such that high migration time reproducibilities are achieved for protein separations even without regenerating the capillary between runs.

## 2.2 Experimental Section

### 2.2.1 Apparatus

All capillary electrophoresis experiments were performed on a Beckman-Coulter P/ACE™ MDQ instrument (Fullerton, CA, USA). The system was equipped with a UV absorbance detector. Detection was achieved by direct mode (Section 1.3.1) at 254 nm for stability studies and 214 nm for protein separations. Data acquisition (4 Hz) and control were performed using P/ACE station software (Version 2.3; Beckman) for Windows 95 on a 300-MHz IBM personal computer. Untreated fused-silica capillaries (Polymicro Technologies, Phoenix, AZ, USA) with a total length of 30 cm (20 cm to the detector), an inner diameter of 50  $\mu\text{m}$ , and an outer diameter of 360  $\mu\text{m}$  were used unless otherwise noted. The capillary was thermostatted at 25 °C.

### 2.2.2 Chemicals

Nanopure 18-M $\Omega$  ultra-pure water (Barnstead, Dubuque, IO, USA) was used to prepare all solutions. Generally, phosphate buffers were prepared from reagent grade orthophosphoric acid (BDH, Darmstadt, Germany) and adjusted to the desired pH with reagent grade sodium hydroxide (BDH). For the pH studies, the phosphate buffers were prepared from sodium dihydrogen phosphate salt (BDH), and the pH was adjusted using orthophosphoric acid. Acetate buffers were prepared using glacial acetic acid (BDH) and sodium acetate or sodium hydroxide (BDH). The cationic surfactant didodecyldimethylammonium bromide (DDAB) was used as received from Aldrich (Milwaukee, WI, USA) and dissolved in the desired buffer. A solution of 1 mM mesityl oxide (Aldrich) dissolved in water was used as the neutral EOF marker. Previous studies have indicated that mesityl oxide is an appropriate EOF marker for buffers containing low

concentrations of surfactant [19]. A mixture of 0.1 mg/mL of protein lysozyme (chicken egg white), ribonuclease A (bovine pancreas),  $\alpha$ -chymotrypsinogen A (bovine pancreas) and cytochrome *c* (bovine heart) were used as received from Sigma (St. Louis, MO, USA) and dissolved in water.

### 2.2.3 EOF Measurements

To avoid hysteresis effects, fresh capillaries were used with each new buffer system. New capillaries were rinsed with 1 M NaOH under high pressure at 138 kPa (20 psi) for 10 min, and then with distilled water at high pressure (138 kPa) for 2 min. After the preconditioning steps, the capillary was rinsed at 138 kPa for 10 min with 0.1 mM DDAB-containing solution to coat the capillary. For capillaries with i.d. other than 50  $\mu\text{m}$ , the rinsing times ( $t_{rinses}$ ) were adjusted according to Poiseuille's equation:

$$t_{rinses} = \frac{8\eta L_t v}{\pi r^4 \Delta P} \quad (2.1)$$

where  $\eta$  is solution viscosity,  $L_t$  is capillary total length,  $v$  is the volume of liquid flushed through the capillary,  $r$  is inner radius, and  $\Delta P$  is pressure difference applied across the capillary.

The neutral marker, mesityl oxide (1 mM in water) was injected into the capillary using hydrodynamic injection at 3.4 kPa (0.5 psi) for 3 s unless otherwise noted. The electroosmotic flow ( $\mu_{EOF}$ ) was calculated using:

$$\mu_{EOF} = \frac{L_d L_t}{t_{EOF} V} \quad (2.2)$$

where  $L_t$  and  $L_d$  are the total length of the capillary (30 cm) and the capillary length to the detector (20 cm) respectively,  $t_{EOF}$  is the migration time of the neutral marker (mesityl oxide) in s, and  $V$  is the applied voltage in volts.

#### 2.2.4 Coating Stability

The stability of the DDAB coatings was indirectly evaluated by monitoring the EOF as a function of time. The stability studies were performed in two manners. In the first method, *hydrodynamic rinsing*, the coated capillary was flushed with running buffer at a constant pressure of 138 kPa for an initial period of 0.5 min. The EOF was then determined, as in eq. 2.2. Next, the capillary was regenerated by rinsing with 1 M NaOH at high pressure (138 kPa) for 3 min, followed by 0.1 mM DDAB solution for 3 min at 138 kPa. The capillary was then flushed (138 kPa) with running buffer for a longer period of time, and the EOF was determined once more. This regeneration/elution procedure was repeated for flush times up to 60 min (corresponding to 415 capillary volumes). The stability of the coating (i.e., EOF) was reported versus the number of capillary volumes of run buffer flushed through the capillary.

The second method, *electro-kinetic rinsing*, is also known as the successive injection method [22]. After coating the capillary with DDAB solution as described in the hydrodynamic rinsing, the excess DDAB solution were removed by flushing the capillary with running buffer for 1.5 min at 13.8 kPa (2 psi), which corresponds to one capillary volume. Consecutive EOF determinations were then performed by injection of mesityl oxide and application of the voltage. The capillary was not rinsed with NaOH or DDAB between consecutive EOF determinations. The buffer reservoirs were changed every 12 successive runs to ensure that the buffer pH remained constant [26]. The stability of the coating (i.e., EOF) was reported versus the total time that the voltage was applied.

### 2.2.5 cmc Determination

To determine the critical micelle concentration (cmc), the surface tension of a series of buffer solutions containing increasing concentrations of DDAB (from 0.0001 to 0.1 mM) were measured using a Fisher Surface Tensiometer (Model 20, Fisher Scientific, Pittsburgh, PA, USA) at room temperature (25 °C). An example illustrating the changes of the surface tension versus increasing concentration of DDAB (mM) is shown in Figure 2.1. The cmc values were taken as the inflection point in a plot of surface tension versus

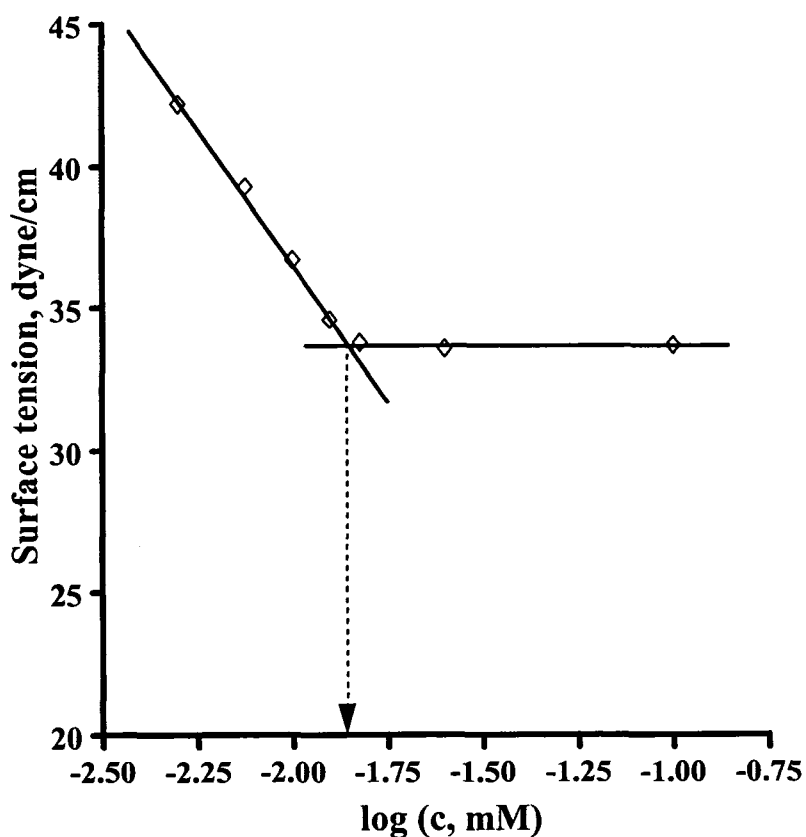


**Figure 2.1** Surface tension as a function of DDAB concentration in sodium acetate buffer.

the log of the surfactant concentration, i.e., at 0.014 mM in sodium acetate buffer at an ionic strength of 9 mM and pH 4.0 (Figure 2.1).

### 2.2.6 Protein Separations

For protein separations, a fresh capillary of length 30 cm (20 cm to the detector) and 25  $\mu\text{m}$  inner diameter (360  $\mu\text{m}$  outer diameter) was used. The capillary was flushed under high-pressure at 138 kPa with 1 M NaOH for 20 min, followed by rinsing with water for 5 min at 138 kPa. The coating procedure for the capillary consisted of a 20 min rinse with 0.1 mM DDAB in the running buffer, followed by a 1 min rinse (138 kPa) with the electrophoretic buffer to remove the excess surfactant monomers from the capillary. A protein mixture of 0.1 mg/mL was injected using 6.9 kPa (1 psi) for 5 s. The applied voltage was  $-3$  kV (for 50 mM phosphate buffer at pH 5.0) and  $-2$  kV (for 50 mM acetate buffer at pH 5.0). Detection for proteins was performed using the direct UV-mode at 214 nm.

The migration time reproducibility was calculated by performing 10 successive injections without recoating the capillary with the surfactant solution. Efficiencies were computed by the P/ACE Station software using the peak width at half-height method. In this method the efficiency ( $N$ , theoretical plates) is determined from the migration time of the analyte under consideration ( $t_M$ ) and its peak width at half-height ( $w_{1/2}$ ) according to:

$$N = 5.54 \times \left( \frac{t_M}{w_{1/2}} \right)^2 \quad (2.3)$$

The magnitude of the migration time and the peak width at half-height should have the same units, either of time or length.

## 2.3 Results and Discussion

As discussed in Section 1.2.2, the electroosmotic flow mobility ( $\mu_{EOF}$ ) is reflective of the zeta potential ( $\zeta$ ) at the surface of the capillary, as described by the Smoluchowski equation:

$$\mu_{EOF} = -\frac{\varepsilon\zeta}{\eta} \quad (2.4)$$

where  $\varepsilon$  is the dielectric constant of the eluent, and  $\eta$  is the viscosity of the eluent. Thus, monitoring the stability of the electroosmotic flow mobility over time allows one to infer the stability of a capillary coating. This approach has been used to monitor the stability of cationic polymer coatings [14], mixed surfactant coatings [10, 16], phospholipids liposomes [27, 28] and DDAB coatings [22, 29].

Two variants of the EOF stability technique were used in this study. The first is electro-kinetic rinsing, and is the procedure that has been used in previous studies [10, 14, 16, 22, 27, 28]. In the electro-kinetic rinsing procedure, the capillary is first rinsed (10 min at 138 kPa) with DDAB-containing buffer followed by a second rinse (1.5 min at 13.8 kPa) with the separation buffer (no surfactant). This second rinse is used to flush out non-adsorbed surfactant from the capillary. The time required to flush the entire length of capillary was determined by measuring the time required for an injection of mesityl oxide to be pushed to the detector (1.0 min) and then allowing for the 10-cm length of capillary after the detector. A series of injections of mesityl oxide are then made to monitor the change in EOF with time. The triangles ( $\blacktriangle$ ) in Figure 2.2 display the resultant reversed EOF (from cathode to anode) as a function of time for such an experiment.

The alternate means of determining the stability of the coatings is to use hydrodynamic rinsing. In this procedure, the capillary is again first rinsed with DDAB-containing buffer for 10 min at 138 kPa. Then, the capillary is rinsed with the separation buffer (no surfactant) for a fixed period of time. Mesityl oxide is injected and the EOF is determined. The capillary is then regenerated with NaOH, recoated with DDAB-containing buffer and then subjected to a longer rinse with surfactant-free separation buffer before determination of the EOF. The rhombus shape data ( $\diamond$ ) in Figure 2.2 displays the EOF observed using 12.4 kPa (1.8 psi) for these hydrodynamic rinses. This pressure yields the same flow rate as initially generated using  $-9$  kV in the electro-kinetic rinsing experiment.

The initial rates of decay (linear decrease in EOF over the first 3 minutes) is statistically equivalent for the electro-kinetic at  $-9$  kV ( $-4.0 \times 10^{-5}$  (cm<sup>2</sup>/Vs)/min) and hydrodynamic rinsing at 12.4 kPa ( $-(4.8 \pm 0.9) \times 10^{-5}$  (cm<sup>2</sup>/Vs)/min). However, by even 10 min of rinsing it is apparent that the rate of decay under electro-kinetic rinsing is slower than for hydrodynamic rinsing, as shown in Figure 2.2. This difference is believed to be due to the decrease in the capillary flow under electro-kinetic rinsing caused by the decrease in the EOF as the DDAB coating degrades. This change in flow rate, as the DDAB coating degrades, makes it difficult to model the degradation behavior using electro-kinetic rinsing. Therefore, the experiments below use hydrodynamic rinsing, unless specifically noted otherwise. The use of hydrodynamic rinsing enables better control over the linear velocity of flow over the course of the experiment, a variable that will be shown to be important below. Also, much greater linear velocities

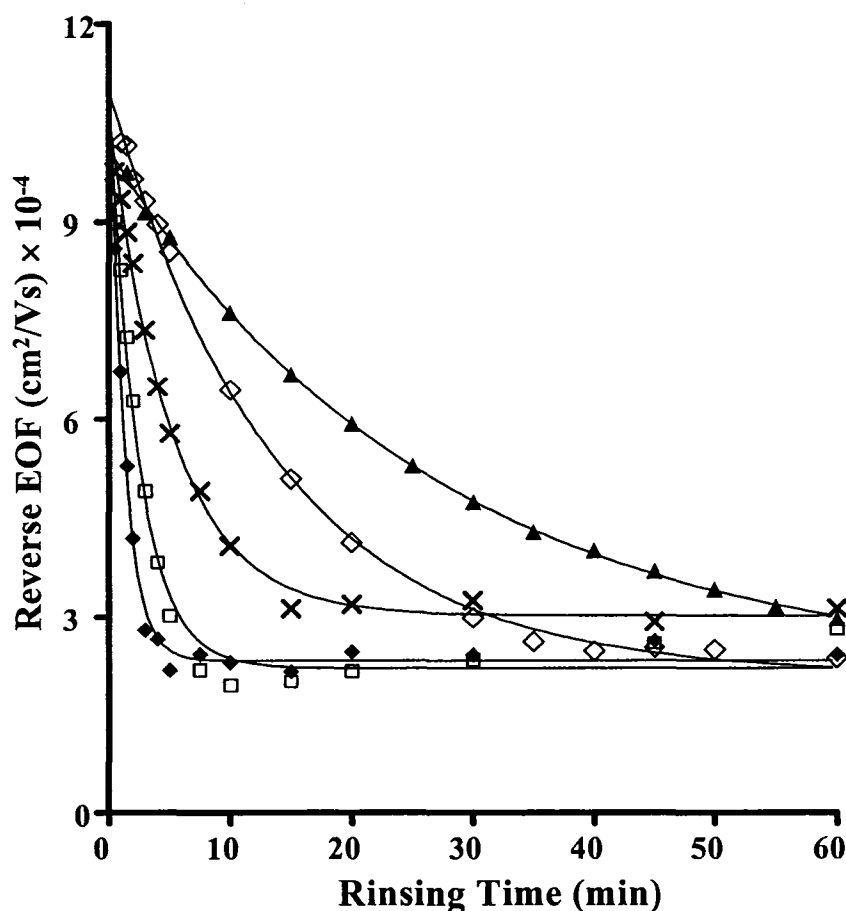


**Figure 2.2** Effect of hydrodynamic and electro-kinetic rinsing on EOF of DDAB coated capillaries. Rinses using 12.4 kPa (◇); 34.5 kPa (×); 69.0 kPa (□); 138 kPa (◆); and -9 kV (▲). **Experimental conditions:** applied voltage during EOF measurement, -9 kV; capillary, 30 cm × 50 μm i.d. (20 cm to detector); buffer, 10 mM sodium acetate at pH 4.0; neutral marker, 1 mM mesityl oxide; λ, 254 nm; and temperature, 25 °C. The capillary was rinsed with 0.1 mM DDAB-containing solution for 10 min at 138 kPa. After each run the capillary was regenerated by rinsing with 1 M NaOH then recoated again with DDAB solution. Curves are the fit of the data to equation 2.12. Note: with DDAB coating, the EOF is directed from anode to cathode and thus CZE is run in reverse mode.

can be achieved using applied pressure than voltage, which reduces the overall experiment time.

### 2.3.1 Kinetic Model

There have only been a limited number of studies of the kinetics of surfactant interactions with solids such as silica [30-33], and most of these focus dominantly on the adsorption step. The only previous study of desorption of a cationic surfactant from silica simply used initial rates to characterize the kinetics [30]. In this chapter, the kinetic models developed by Tiberg *et al.* are used to characterize the behavior of DDAB desorbing from the fused silica capillary [33]. Tiberg *et al.* assumed that under stirred conditions there was a stagnant layer of water of thickness  $\delta$  adjacent to the silica surface. Transport of surfactant within the stagnant layer is solely via diffusion of monomers and/or micelles. Beyond the stagnant film, the bulk solution undergoes rapid convective mixing. Thus, adsorption of surfactant to the surface involves a diffusive step followed by a chemical kinetic step involving interaction between the surfactant and the surface. Adsorption of the surfactant on the surface proceeds until the surface aggregate is completely formed.

With respect to the desorption process, Tiberg *et al.* [33] identified two limiting cases. If the desorption kinetics of the surfactant from the surface is fast (Figure 2.3a), there will be a local equilibrium between the surface aggregate and the solution immediately adjacent to it in the stagnant mobile phase ( $\delta_1$ ). The concentration of the free monomer in this region is a constant equal to the critical surface aggregation concentration ( $csac$ ). In other words, the  $csac$  is the concentration of surfactant monomer in solution that is in equilibrium with the surfactant aggregate at the solid surface. Thus,

the *csac* is analogous to the cmc discussed in Section 1.6.3. The bulk solution undergoes rapid convective mixing, and thus it is treated as an infinite sink, i.e., the concentration of surfactant in the bulk solution is zero ( $c_b \approx 0$ ). Under these conditions the surfactant monomers are transported by diffusion due to the difference in monomer concentration at  $\delta_1$  ( $c = csac$ ) and at  $\delta$  ( $c \approx 0$ ) as shown in Figure 2.3a. According to Fick's second law:

$$\frac{\partial c}{\partial t} = D \frac{\partial^2 c}{\partial x^2} \quad (2.5)$$

where  $D$  is the diffusion coefficient of the surfactant monomer. Equation 2.5 predicts how the concentration of the monomer varies with time ( $t$ ) as well as with distance ( $x$ ) from the surface within the stagnant layer. Assuming that the concentrations in the stagnant layer adjust quickly to steady-state values, i.e.,  $\frac{\partial c}{\partial t} \approx 0$ , then,

$$0 = D \frac{\partial^2 c}{\partial x^2} \quad (2.6)$$

The solution of eq. 2.6 is a straight line with equation:  $c = \beta x + constant$ , where the slope  $\beta$  is:

$$\beta = \frac{c(\delta) - c(\delta_1)}{\delta - \delta_1} = \frac{-(csac)}{\delta - \delta_1} \quad (2.7)$$

The flux ( $J$ ) of the monomer in this stagnant region is given by:

$$-J = D \frac{\partial c}{\partial x} = D\beta = D \frac{-(csac)}{\delta - \delta_1} \quad (2.8)$$

However, the desorption rate ( $\partial\Gamma/\partial t$ , where  $\Gamma$  is the amount of surfactant adsorbed, also known as the "surface excess") is given by:

$$\frac{\partial\Gamma}{\partial t} = -J \quad (2.9)$$

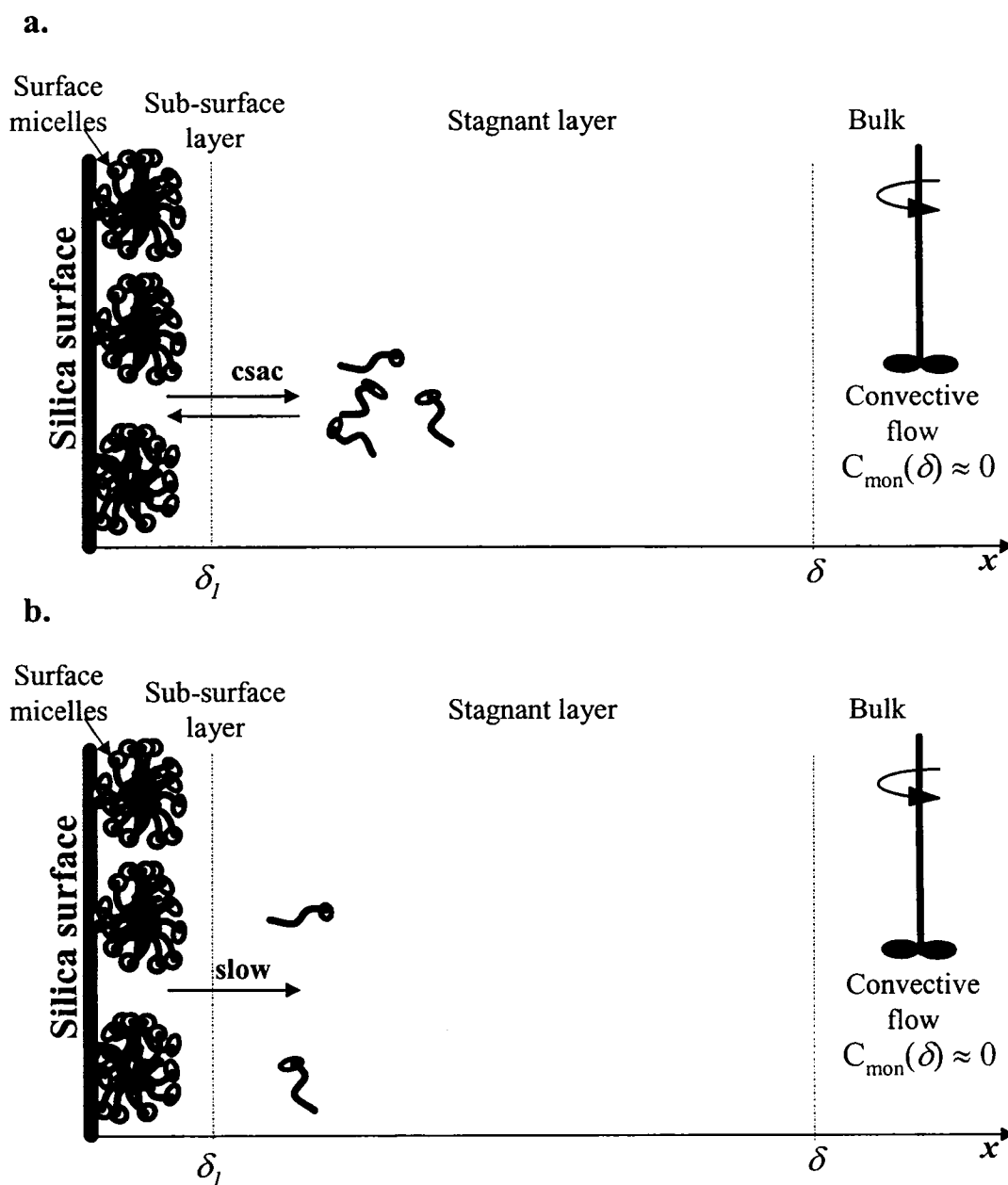


**Figure 2.3** Schematic diagrams of surfactant desorption process from silica surface. This scheme is based on the model proposed by Tiberg *et al.* [33]. The limiting cases are **a.** fast desorption kinetics; and **b.** slow desorption kinetic of the surfactant from the surface.

Therefore,

$$\frac{\partial \Gamma}{\partial t} = -\frac{1}{\delta - \delta_1} D (csac) \quad (2.10)$$

According to eq. 2.10, a diffusion-controlled rate-limiting step would result in a linear decrease in the surface excess ( $\Gamma$ ) with time.

The alternate limiting case identified by Tiberg *et al.* [33] is that the desorption rate is controlled by the decomposition rate of the adsorbed micelles, as shown in Figure 2.3b. Assuming that the concentration of surfactant monomers in the bulk solution is zero ( $c_b \approx 0$ ), the decomposition rate is:

$$\frac{\partial \Gamma}{\partial t} = -k_{d,mic} \Gamma \quad (2.11)$$

where  $k_{d,mic}$  is a rate constant characteristic of the dissociation of the micelles. This rate constant may differ somewhat from the corresponding value for micelles in the bulk solution due to interactions between the adsorbed micelles and the silica surface. Equation 2.11 predicts an exponential decrease in the surface excess with time.

Tiberg *et al.* [33] also observed that an asymptotic amount of nonionic surfactant remained on the silica surface after the micellar decomposition ( $\Gamma_\infty \approx 0.1 \mu\text{mol}/\text{m}^2$ ). Similarly, a residual fraction of adsorbed surfactant has been observed for nonionic surfactants on a polystyrene surface [34] and for cetyltrimethylammonium bromide (CTAB) on a silica surface, where a considerable amount of CTAB was left on the surface after about 4.5 hours of rinsing with running water [35]. The presence of a residual concentration of surfactant after extensive washes ( $\Gamma_\infty > 0$ ) will be an integral part of the data analysis discussed below (eq. 2.12).

In the kinetic studies of Tiberg *et al.* [33], the thickness of the stagnant layer was

estimated to be 100  $\mu\text{m}$ , and the concentration of surfactant in the bulk solution is assumed to be zero ( $c_b \approx 0$ ). Under these conditions, they observed a linear decrease in surface excess (characteristic of eq. 2.10) for the initial and major portion of the desorption of nonionic polyethylene glycol alkyl ether surfactants from silica, and an exponential decrease (eq. 2.11) for the latter portion of the desorption. In our work, the capillary inner diameter is only 50  $\mu\text{m}$  and the volume of the buffer inside the capillary is small (0.6  $\mu\text{L}$ ). Further, the free surfactant leaching from the bilayer during rinsing has to pass through the capillary. This results in accumulation of the free surfactant in the capillary bulk solution which would be significant due to the small capillary volume. Consequently, the concentration of the surfactant monomers in the capillary bulk solution would not be zero, as assumed by Tiberg *et al.* [33]. As a result, it is expected that transport of monomers across a stagnant layer will not be the factor limiting desorption kinetics in our work.

In the present work, the desorption of the DDAB coating from the CE capillary is studied by monitoring the EOF mobility versus the rinse time, as show in Figure 2.2. The EOF is related to the zeta potential, which in turn is directly related to the surface charge density of the bilayer assuming that the surface potential is less than 25 mV [36]. Thus, the EOF reflects the surface excess of surfactant [37]. The data was fit to a single-exponential decay with a non-zero asymptotic value (Prism version 4.00, GraphPad Software Inc, San Diego, CA):

$$\mu_{EOF} = A_1 \exp(-k_{obs}t) + A_\infty \quad (2.12)$$

where  $k_{obs}$  is the observed decay rate of the EOF,  $A_1$  is a fit parameter, and  $A_\infty$  is the

asymptotic value of the EOF.  $A_1$  plus  $A_\infty$  should equal the EOF at time 0 (i.e., the EOF observed prior to flushing the DDAB-containing buffer from the capillary).

### 2.3.2 Effect of Rinse Pressure

Figure 2.2 shows the effect of varying the pressure of the hydrodynamic rinses from 12.4 to 138 kPa (1.8 to 20 psi). The symbols represent the observed EOF, and the curves are the non-linear fit of the data to eq. 2.12. In all cases, the correlation coefficient ( $R^2$ ) was greater than 0.98. The resultant fit parameters are listed in Table 2.1.

The decay rate ( $k_{obs}$ ) clearly shows a strong dependence on the applied pressure. A plot of decay rate ( $k_{obs}$ ) versus rinse pressure is linear (Figure 2.4), with a correlation coefficient ( $R^2$ ) of 0.9998, and an intercept equals zero based on the 95% confidence limit. Alternatively, the decay behavior in Figure 2.2 can be plotted versus the number of capillary volumes of surfactant-free buffer rinsed through the capillary, as shown in Figure 2.5. In volume units, the half lives for all the decays are statistically equivalent (5.8 capillary volumes), regardless of the rinse pressure (Table 2.1). Thus, the dramatic degradation of the DDAB bilayer upon increasing the rinse pressure is related to the increase in volume of running buffer flushed through the capillary, and not on the buffer rinsing time. This suggests that the equilibrium between the free surfactant in the capillary bulk solution and the bilayer has the major influence on the bilayer degradation. Due to the small capillary volume, the leached free DDAB monomers saturate the bulk solution, and an equilibrium between the bilayer and the solution is established. As a consequence, the desorption process would be stopped. However, the introduction of the run buffer into the capillary during rinsing removes the free DDAB which shifts the equilibrium to produce more free DDAB monomers. Further, increasing the buffer

**Table 2.1** Effect of rinsing conditions on DDAB. Desorption modeled using First Order Chemical Kinetics (Equation 2.12).<sup>a</sup>

Rinsing condition	$k_{obs} \times 10^{-3} \text{ min}^{-1}$	$k_{obs} \times 10^{-3} \text{ (cap. vol)}^{-1}$	$A_1 \times 10^{-4} \text{ (cm}^2\text{/Vs)}$	$A_\infty \times 10^{-4} \text{ (cm}^2\text{/Vs)}$	$R^2$
12.4 kPa (1.8 psi)	$72 \pm 3$	$121 \pm 6$	$8.9 \pm 0.1$	$2.1 \pm 0.1$	0.998
34.5 kPa (5 psi)	$195 \pm 9$	$113 \pm 5$	$7.6 \pm 0.1$	$3.1 \pm 0.1$	0.997
69.0 kPa (10 psi)	$414 \pm 39$	$121 \pm 11$	$8.8 \pm 0.4$	$2.2 \pm 0.1$	0.98
138 kPa (20 psi)	$836 \pm 53$	$128 \pm 8$	$9.7 \pm 0.4$	$2.34 \pm 0.07$	0.992
-9 kV	$37.4 \pm 0.9$		$7.92 \pm 0.07$	$2.18 \pm 0.08$	0.9996

<sup>a</sup> Experimental conditions: as in Figure 2.2.

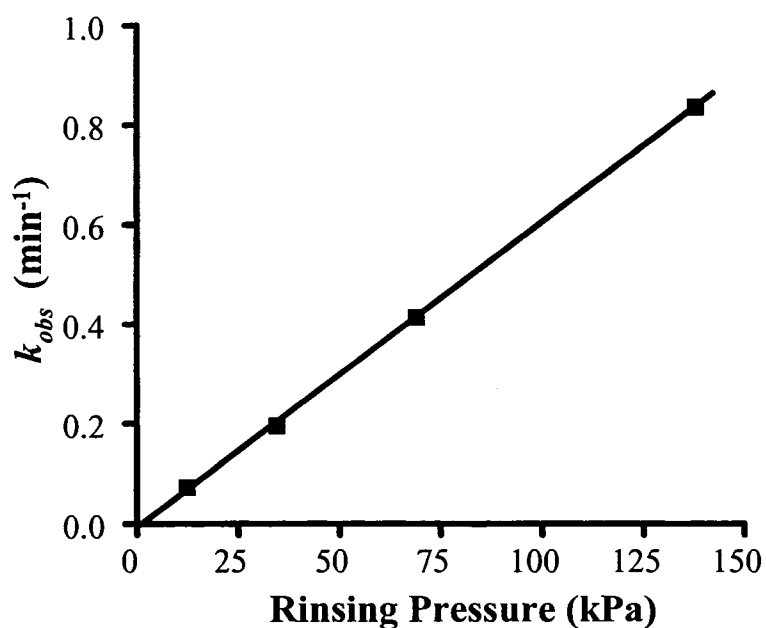


**Figure 2.4** Effect of rinsing pressure on the decay rate constant ( $k_{obs}$ ). **Experimental conditions:** as in Figure 2.2.

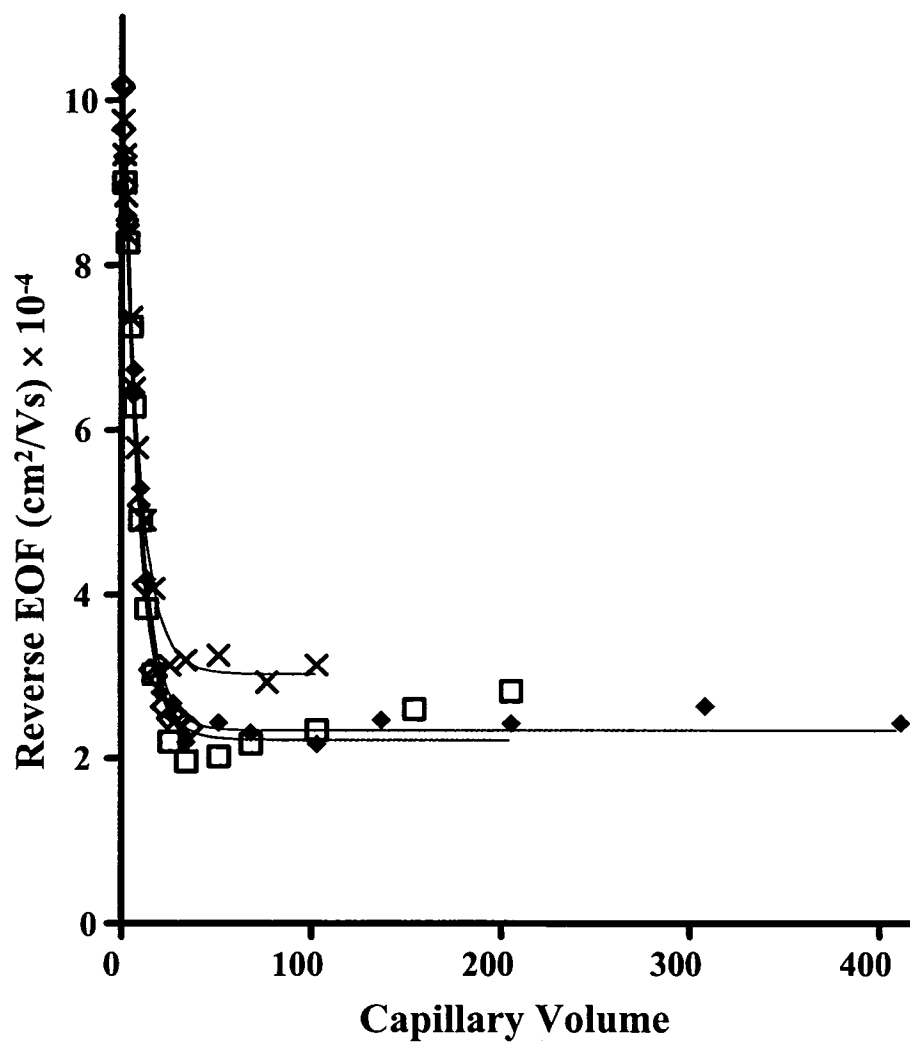


**Figure 2.5** Effect of buffer volume that flow in the capillary during rinsing on the EOF. Rinses using 12.4 kPa ( $\diamond$ ), 34.5 kPa ( $\times$ ), 69.0 kPa ( $\square$ ), and 138 kPa ( $\blacklozenge$ ). Curves are the fit of the data to eq. 2.12. **Experimental conditions:** as in Figure 2.2.

volume flushed through the capillary increases the amount of the free monomers that must leach from the bilayer to reestablish the equilibrium. Since the desorption process does not depend on the rinsing time, further experiments were performed using 138 kPa (20 psi) rinses to minimize the experiment time. Further, the decay rates are quoted in units of reciprocal capillary volume (for the hydrodynamic rinsing) to eliminate any flow rate dependence, unless otherwise stated.

A strong residual reversed EOF is evident in Figure 2.2 for all the conditions explored. The magnitude of the residual reversed EOF is  $2-3 \times 10^{-4} \text{ cm}^2/\text{Vs}$  compared to an initial reversed EOF of about  $11 \times 10^{-4} \text{ cm}^2/\text{Vs}$  (i.e.,  $A_1$  plus  $A_\infty$ ). As discussed above, the presence of residual adsorbed surfactant is consistent with previous studies of surfactant desorption [33-35]. In Figure 2.2 and Table 2.1, there is no correlation between the asymptotic values of the curves ( $A_\infty$ ) and the rinse pressure. A detailed analysis of the asymptotic behavior was not performed, as protein separations performed under such conditions displayed poor efficiencies and recoveries, as will be discussed in Section 2.3.9.

### 2.3.3 Effect of Capillary Diameter

Figure 2.6 shows the effect of the capillary inner diameter on the DDAB coating stability. Capillaries with inner diameters (i.d.) of 25, 50, 75 and 100  $\mu\text{m}$  were used in this study. Due to the difference in the capillary i.d., these experiments were performed using electro-kinetic rinsing to keep the initial linear velocity constant. The first run at each capillary (time 0) was performed with the DDAB in the solution to ensure that equivalent bilayers were formed in the various capillaries. The curves in Figure 2.6 are

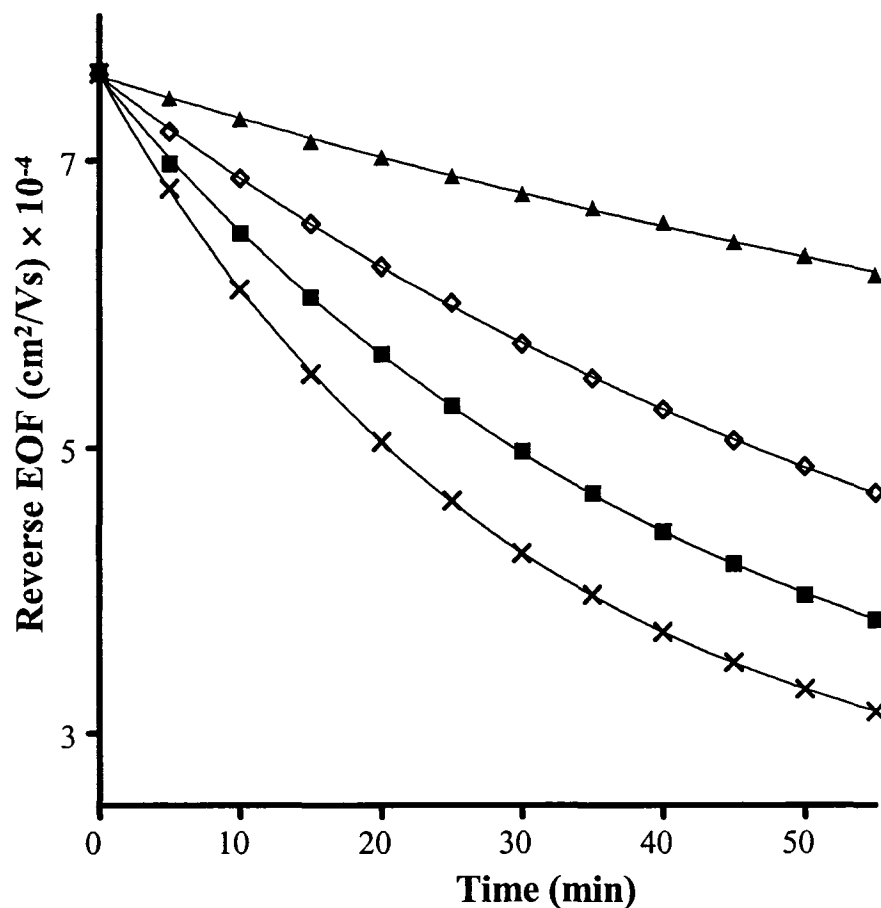


**Figure 2.6** Effect of capillary inner diameter on reverse EOF of DDAB coated capillaries. The capillary inner diameters are 25  $\mu\text{m}$  ( $\blacktriangle$ ); 50  $\mu\text{m}$  ( $\diamond$ ); 75  $\mu\text{m}$  ( $\blacksquare$ ); and 100  $\mu\text{m}$  ( $\times$ ). The curves are the fit of the data to equation 2.12. **Experimental conditions:** applied voltage during EOF measurement,  $-9$  kV; capillary length, 30 cm (20 cm to detector); buffer, 10 mM phosphate at pH 3.0; neutral marker, mesityl oxide;  $\lambda$ , 254 nm; and temperature, 25  $^{\circ}\text{C}$ . The capillary was rinsed with 0.1 mM DDAB-containing solution for 5 min at 138 kPa. The first run at time zero is done with the DDAB buffer in the solution. Note: with DDAB coating, the EOF is directed from anode to cathode and thus CZE is run in reverse mode.

**Table 2.2** Effect of capillary inner diameter on DDAB bilayer. Desorption modeled using First Order Chemical Kinetics (Equation 2.12).<sup>a</sup>

Capillary i.d. ( $\mu\text{m}$ )	$k_{obs} \times 10^{-3}$ ( $\text{min}^{-1}$ )	$A_1 \times 10^{-4}$ ( $\text{cm}^2/\text{Vs}$ )	$A_\infty \times 10^{-4}$ ( $\text{cm}^2/\text{Vs}$ )	$R^2$
25	$7.6 \pm 1.4$	$4.0 \pm 0.6$	$3.6 \pm 0.6$	0.9989
50	$14.2 \pm 0.5$	$5.3 \pm 0.1$	$2.2 \pm 0.1$	0.9999
75	$22.8 \pm 0.6$	$5.31 \pm 0.08$	$2.28 \pm 0.09$	0.9998
100	$32.9 \pm 0.3$	$5.32 \pm 0.02$	$2.28 \pm 0.02$	1.000

<sup>a</sup> **Experimental conditions:** as in Figure 2.6.

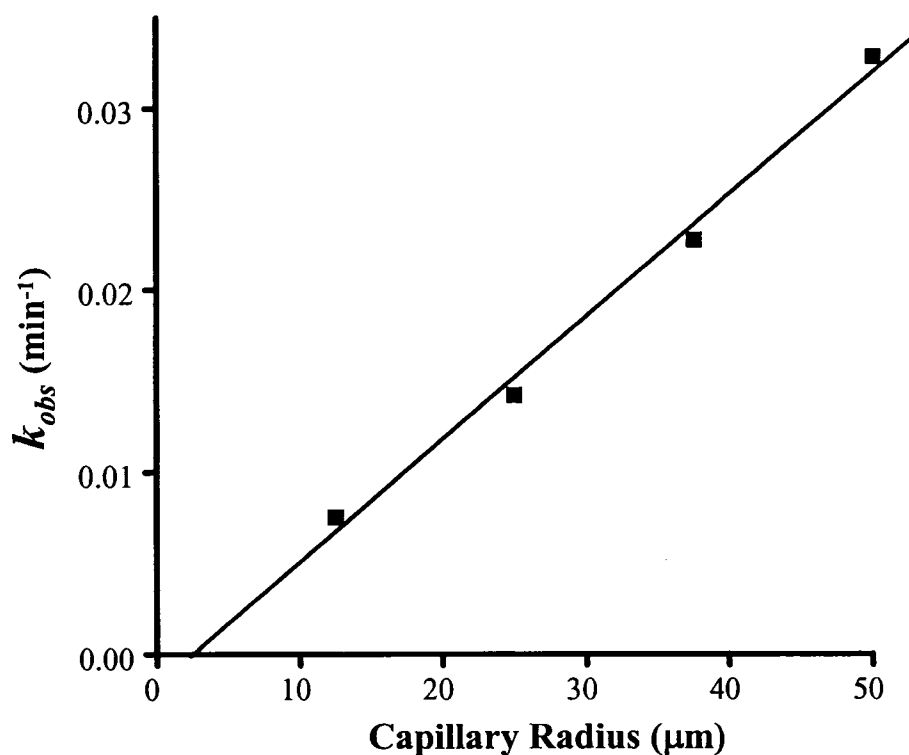


**Figure 2.7** Effect of capillary radius on the decay rate constant ( $k_{obs}$ ). **Experimental conditions:** as in Figure 2.6.

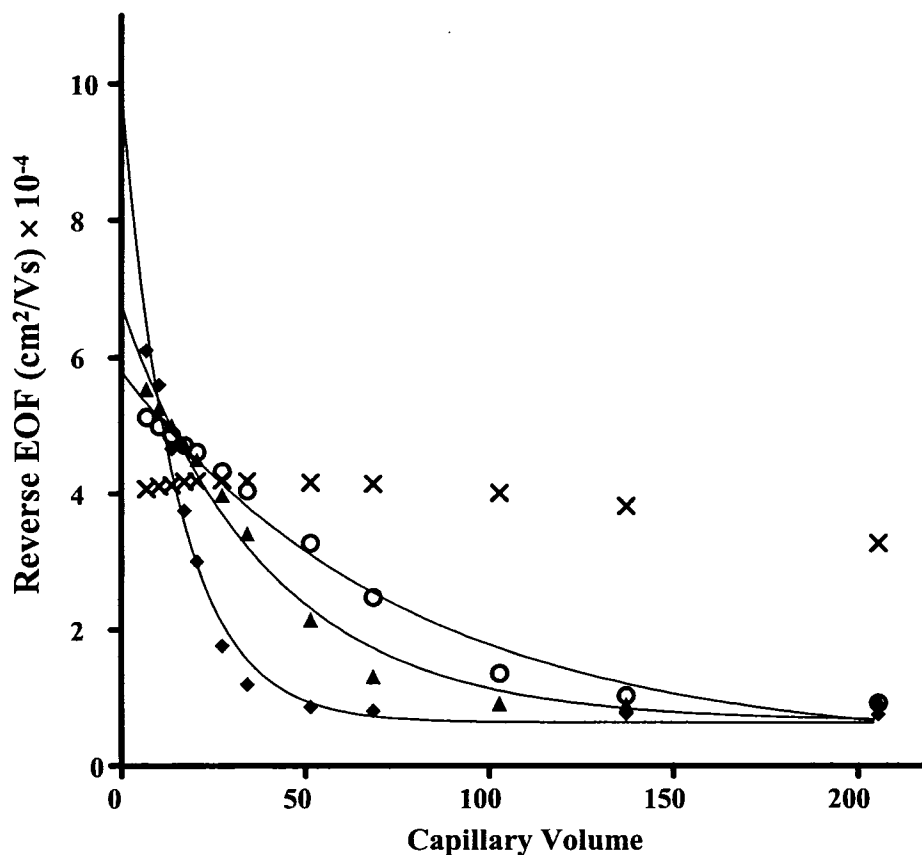
the fit of the data to equation 2.12. The fit parameters, along with the correlation coefficient ( $R^2$ ) for each curve, are shown in Table 2.2.

Figure 2.7 and Table 2.2 show that the decay rate constant ( $k_{obs}$ ) increases dramatically with increasing inner diameter. A plot of decay rate constant as a function of capillary radius is linear as shown in Figure 2.7, with a correlation coefficient ( $R^2$ ) of 0.992, and an intercept equals zero within the 95% confidence limit. Increasing the capillary inner diameter results in a linear increase in the volume-to-surface ratio. Thus, the more rapid decay in the coating stability with increased capillary diameter, as shown in Figure 2.6 and Figure 2.7, is indicative of the greater volume of solution that the DDAB bilayer must saturate as it desorbs. These results are consistent with those obtained in Section 2.3.2. In summary, capillary diameters should be kept narrow to maximize the bilayer stability.

#### 2.3.4 Effect of Buffer Ionic Strength

High ionic strength buffers can be used to minimize protein adsorption. Green *et al.* demonstrated that increasing the buffer ionic strength to 1.0 M greatly reduced the protein adsorption [5]. The buffer cations compete with the proteins for the cation-exchange (silanols) sites on the silica surface. In addition, the high buffer ionic strength reduces the electrostatic interactions among the charged species due to coulombic screening [38]. However, the DDAB surfactant bilayer shields the silanols and reverses the charge of the capillary surface.

The effect of increasing the ionic strength of a pH 3.0 sodium phosphate buffer on the decay of the reverse EOF has been studied. Figure 2.8 shows the variation of the EOF as a function of capillary volumes in sodium phosphate buffer at different ionic



**Figure 2.8** Effect of buffer ionic strength on the reversed EOF of DDAB coated capillaries at day 0. Buffer ionic strength of:  $9 \times 10^{-3}$  M (◆);  $22 \times 10^{-3}$  M (▲);  $44 \times 10^{-3}$  M (○); and  $88 \times 10^{-3}$  M (×). The curves are the fit of the data to equation 2.12. **Experimental conditions:** applied voltage during EOF measurement,  $-9$  kV; capillary,  $30$  cm  $\times$   $50$   $\mu$ m i.d. ( $20$  cm to detector); buffer, sodium phosphate at pH 3.0; neutral marker,  $1$  mM mesityl oxide;  $\lambda$ ,  $254$  nm; and temperature,  $25$  °C. The capillary was rinsed with  $0.1$  mM DDAB-containing solution for  $10$  min at  $138$  kPa. After each run the capillary was regenerated by rinsing with  $1$  M NaOH then recoated again with DDAB solution. Note: with DDAB coating, the EOF is directed from anode to cathode and thus CZE is run in reverse mode.

**Table 2.3** Effect of ionic strength of sodium phosphate buffer at day 0 on DDAB bilayer. Desorption modeled using First Order Kinetics (Equation 2.12).<sup>a</sup>

Buffer ionic strength (M)	cmc (mM)	$k_{obs} \times 10^{-3}$ (cap. vol) <sup>-1</sup>	$A_1 \times 10^{-4}$ (cm <sup>2</sup> /Vs)	$A_\infty \times 10^{-4}$ (cm <sup>2</sup> /Vs)	R <sup>2</sup>
$9 \times 10^{-3}$	0.010	$67 \pm 7$	$9.3 \pm 0.7$	$0.63 \pm 0.16$	0.984
$22 \times 10^{-3}$	0.0037	$27 \pm 3$	$6.1 \pm 0.3$	$0.78 \pm 0.15$	0.985
$44 \times 10^{-3}$	0.0018	$15 \pm 1$	$5.2 \pm 0.3$	$0.63 \pm 0.19$	0.985

<sup>a</sup> Experimental conditions: as in Figure 2.8.

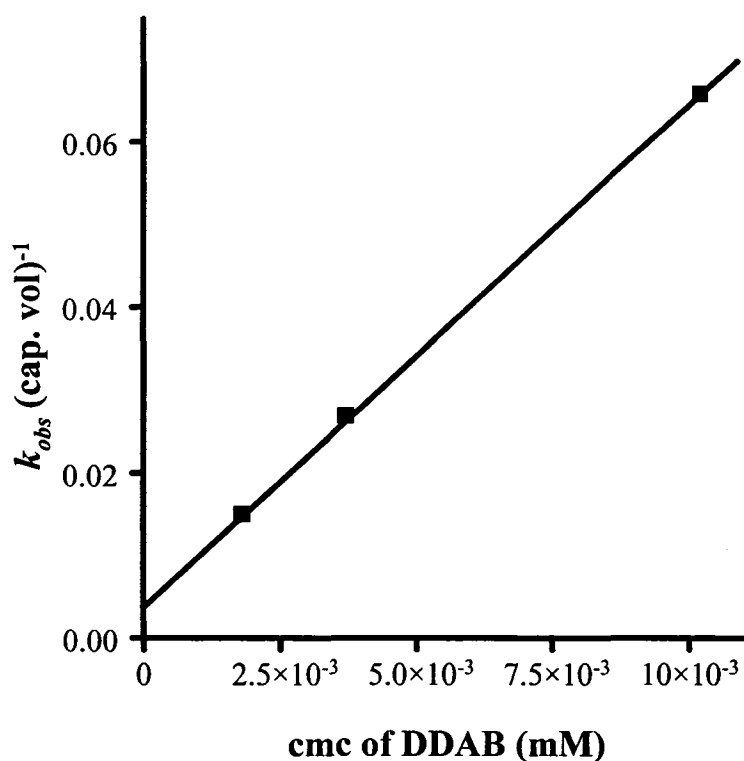


**Figure 2.9** Effect of cmc of DDAB on the decay rate constant ( $k_{obs}$ ). Experimental conditions: as in Figure 2.8.

strength ( $9 \times 10^{-3}$ ,  $22 \times 10^{-3}$ ,  $44 \times 10^{-3}$ , and  $88 \times 10^{-3}$  M). In the presence of surfactant (rinse volume = 0), the reversed EOF displays the expected inverse dependence on the buffer ionic strength [39, 40]. As described above, removal of surfactant from the capillary (rinse times > 0) results in degradation in the DDAB coatings, as reflected by a decrease in the magnitude of the EOF. The curves in Figure 2.8 are the fit of the data to equation 2.12. The resultant fit parameters are shown in Table 2.3. The EOF at the highest ionic strength ( $88 \times 10^{-3}$  M) was too stable to obtain a reasonable fit to equation 2.12.

Increasing the buffer ionic strength is known to reduce the cmc of ionic surfactants by increasing the coulombic screening between the charged headgroup which allows a tighter headgroup packing [41]. Thus, it was hypothesized that the stability to the DDAB coatings may be related to the cmc of the DDAB in solution. The cmc were determined as described in Section 2.2.5 and are listed in Table 2.3, along with the fit parameters from Figure 2.8. A plot of the decay rate constant ( $k_{obs}$ ) as a function of cmc of DDAB in different ionic strengths (Figure 2.9) is linear with a correlation coefficient ( $R^2$ ) of 0.99997 and an intercept equals zero within the 95% confidence limit. Thus, the stability of the bilayer coating can be highly enhanced by any means that reduces the cmc value of the surfactant in solution.

### 2.3.5 Effect of Buffer Counter-ion Nature

Figure 2.10 shows that the coating stability is greater in phosphate than in acetate buffer, consistent with the observations of Westerlund *et al.* [29]. In addition to the ionic strength, the adsorption of the counter-ions onto surfactant headgroups also strongly affects the coulombic screening between the charged headgroups [41]. Increased

coulombic screening allows tighter headgroup packing. Enhanced adsorption between counter-ions in the buffer and cationic surfactants is reflected by a decrease in the cmc [42, 43]. Table 2.4 displays the cmc of DDAB in acetate and phosphate buffers of constant pH (4.0) and ionic strength ( $9 \times 10^{-3}$  M), along with the fit parameters for the degradation of the coating in these buffers obtained from Figure 2.10.

Switching from phosphate to acetate resulted in an increase in the DDAB cmc from 0.010 to 0.014 mM. The magnitude of the reversed EOF also reflects the strength of interaction between anions and the adsorbed cationic surfactants [19]. The faster EOF in acetate than that in phosphate ( $10.0 \pm 0.3$  and  $6.4 \pm 0.2$  cm<sup>2</sup>/Vs, respectively in Table 2.4) is indicative of the weaker interaction between acetate and DDAB than between phosphate and DDAB. Finally, the decay rate constant ( $k_{obs}$ ) in Table 2.4 correlates with both the cmc and the magnitude of the reversed EOF. This indicates that the tendency of a buffer anion to adsorb to the DDA<sup>+</sup> surfactant molecules will strongly affect the stability of DDAB coatings.

### 2.3.6 Effect of Buffer pH

The effect of buffer pH on the degradation of the bilayer coating is also shown in Figure 2.10 and Table 2.4. The ionic strength for the tested buffers was maintained constant at  $9 \times 10^{-3}$  M. Changing the buffer pH has no effect on the charge of the quaternary ammonium headgroup. Also, the cmc of DDAB should not be affected by the change of pH, so long as the chemistry of the counter ion does not change (i.e., H<sub>2</sub>PO<sub>4</sub><sup>-</sup>). This is reflected in the cmc values in Table 2.4. pH greater than 4.7 were not explored as they would contain increasing amounts of HPO<sub>4</sub><sup>2-</sup>, which would alter the cmc. Thus,

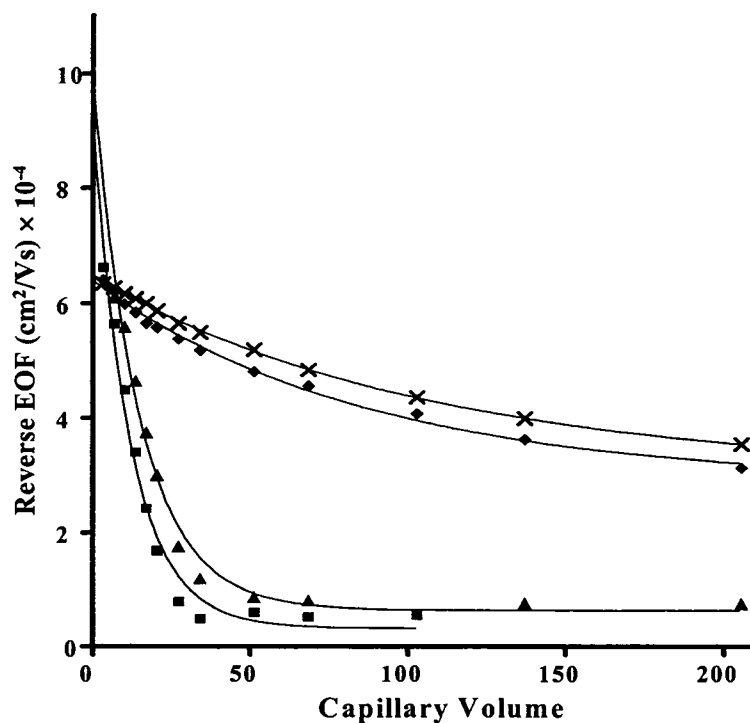


**Figure 2.10** Effect of pH on EOF of DDAB coated capillaries. Sodium phosphate at pH 2.5 (■), pH 3.0 (▲), pH 4.0 (◆), and pH 4.7 (×). **Experimental conditions:** ionic strength of buffers is constant at  $9 \times 10^{-3}$  M; applied voltage is  $-9$  kV; capillary,  $30 \text{ cm} \times 50 \text{ } \mu\text{m}$  i.d. (20 cm to detector); neutral marker, 1 mM mesityl oxide;  $\lambda$ , 254 nm; and temperature,  $25 \text{ }^\circ\text{C}$ . Note: with DDAB coating, the EOF is directed from anode to cathode and thus CZE is run in reverse mode.

**Table 2.4** Effect of buffer type and pH on DDAB bilayer. Desorption modeled using First Order Chemical Kinetics (Equation 2.12).<sup>a</sup>

Buffer system	pH	cmc (mM)	$k_{obs} \times 10^{-3}$ (cap. vol) <sup>-1</sup>	$A_1 \times 10^{-4}$ (cm <sup>2</sup> /Vs)	$A_\infty \times 10^{-4}$ (cm <sup>2</sup> /Vs)	R <sup>2</sup>
Acetate	4.0	0.014	$29 \pm 2$	$8.9 \pm 0.2$	$1.1 \pm 0.2$	0.991
Phosphate	2.5		$83 \pm 9$	$8.9 \pm 0.5$	$0.32 \pm 0.2$	0.98
Phosphate	3.0	0.010	$67 \pm 7$	$9.3 \pm 0.7$	$0.63 \pm 0.16$	0.98
Phosphate	4.0	0.010	$12 \pm 1$	$3.5 \pm 0.1$	$2.9 \pm 0.2$	0.993
Phosphate	4.7		$9.4 \pm 0.4$	$3.42 \pm 0.06$	$3.05 \pm 0.06$	0.9994

<sup>a</sup> **Experimental conditions:** as in Figure 2.10.

under the pH range studied no changes to the DDAB solution aggregation behavior are expected or observed.

In contrast, as shown in Figure 2.10 and Table 2.4, elevating the pH dramatically enhances the stability of the DDAB coatings on silica. Increasing the buffer pH enhances the negative charge of the capillary surface by further dissociating the silanol groups. Therefore, increasing the negative potential of the silica surface would be expected to favor adsorption of cationic surfactants onto the surface. For instance, using atomic force microscopy (AFM), Baryla *et al.* observed that the nearest neighbor distance for spherical CTAB aggregates onto silica decreased from  $13.1 \pm 0.4$  to  $8.3 \pm 0.3$  nm as the pH increased from 3.0 to 5.0 [17]. With DDAB surfactant, a continuous bilayer coating is formed, as observed by Baryla *et al.* [17]. Thus, the enhanced DDAB coating stability is believed to result from the enhanced electrostatic attraction between the  $DDA^+$  molecules and the silica surface.

### 2.3.7 Role of cmc

The significant role of cmc in the bilayer desorption kinetics can be viewed in two ways. Firstly, desorption occurs when the bulk concentration of surfactant is less than the cmc. Once the bulk solution reaches the cmc, the degradation process is terminated, and an equilibrium between the bilayer and the free surfactant monomers in the bulk solution is established. Thus, a decrease in the cmc enables equilibrium to be achieved more rapidly since fewer DDAB monomers are required to reach the cmc value in the bulk solution.

Alternatively, the cmc can be viewed in a thermodynamic manner as the reciprocal of the equilibrium constant for the micellarization process. In this view, a

lower cmc simply reflects a more thermodynamically stable aggregate structure.

Regardless, the stability of the DDAB coatings increases as the cmc decreases, either due to the nature of the counter ion or increased buffer ionic strength. Buffer pH has no effect on the cmc value of the surfactant solution; however, the enhancement of the bilayer stability is due to the increase in the electrostatic interaction between the surfactant monomers and the capillary surface as discussed in the Section 2.3.6.

### 2.3.8 Aging Time

Previously, Pagac *et al.* [30] reported that allowing CTAB to equilibrate with a silica surface (i.e., age) for 24 hours did not affect the desorption of CTAB from the surface. In contrast, Liu *et al.* found that the desorption of cetyltrimethylammonium chloride (CTAC) was strongly dependent on the exposure time of CTAC solution to the substrate [44]. Regardless, CTAB adsorbs onto silica as spherical micelles whereas DDAB forms a bilayer [17]. Thus, the effect of aging the DDAB bilayer on the coating stability was explored.

As observed above, the behavior varied with buffer conditions. For a capillary equilibrated with 0.1 mM DDAB in 10 mM phosphate buffer pH 3.0, the observed desorption rate remained essentially constant ( $t_{1/2} \approx 10$  capillary volumes) for 21 days of aging. However, the residual EOF ( $A_{\infty}$ ) gradually increased from  $(0.63 \pm 0.16) \times 10^{-4}$  on day 0 to  $(2.2 \pm 0.3) \times 10^{-4} \text{ cm}^2/\text{Vs}$  at day 12, and then the EOF became essentially constant at  $(7.56 \pm 0.06) \times 10^{-4} \text{ cm}^2/\text{Vs}$  on day 15, as shown in Figure 2.11. Yet, on days 18-21 the residual EOF returned to its initial values of  $(1-2) \times 10^{-4} \text{ cm}^2/\text{Vs}$  (the dotted lines in Figure 2.11).

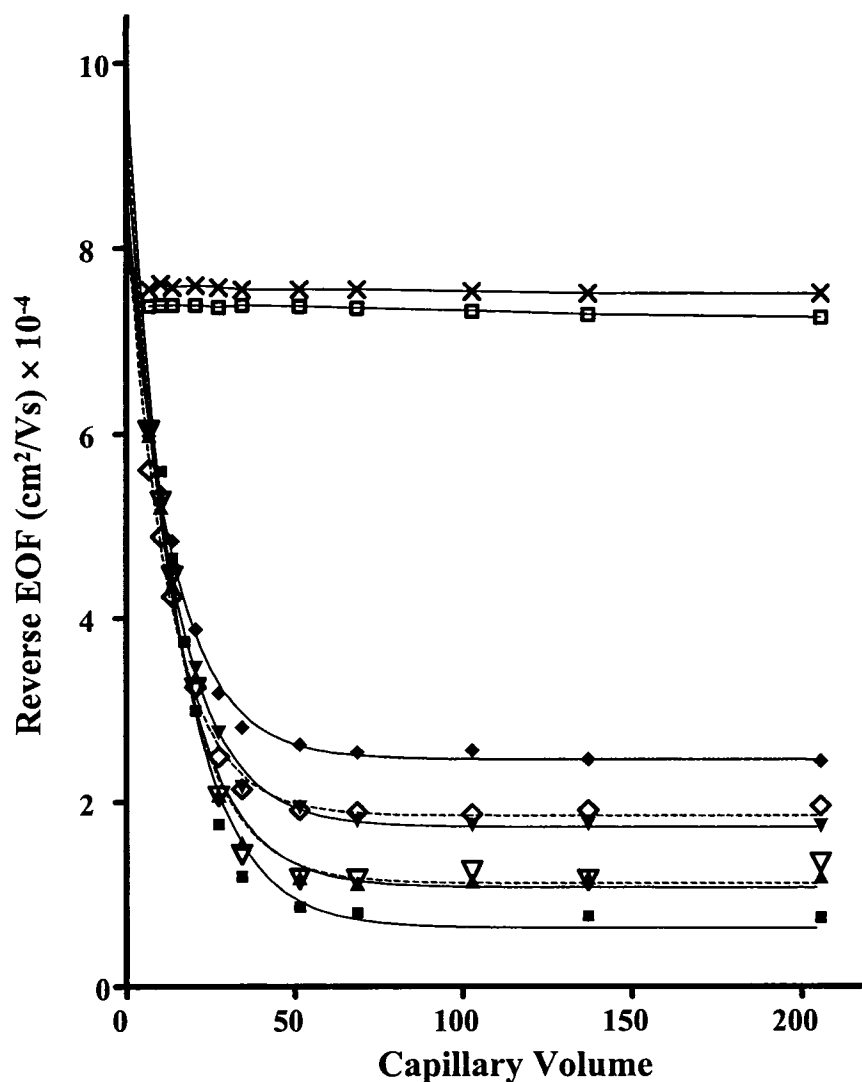


**Figure 2.11** Effect of aging time on EOF of DDAB coated capillaries in sodium phosphate buffer at ionic strength of  $9 \times 10^{-3}$  M and pH 3.0. Day 0 (■); day 4 (▲); day 6 (▼); day 12 (◆); day 15 (□); day 16(×); day 18 (▽) and day 21 (◇). **Experimental conditions:** applied voltage during EOF measurement,  $-9$  kV; capillary,  $30$  cm  $\times$   $50$   $\mu$ m i.d. ( $20$  cm to detector); neutral marker,  $1$  mM mesityl oxide;  $\lambda$ ,  $254$  nm; and temperature,  $25$  °C. New capillary was preconditioned rinsed with  $0.1$  mM DDAB-containing solution for  $10$  min at  $138$  kPa in day 0. After each run the capillary was recoated again with DDAB solution. Between days the capillary was rinsed with DDAB solution and left overnight. Curves are the fit of the data to equation 2.12. Note: with DDAB coating, the EOF is directed from anode to cathode and thus CZE is run in reverse mode.

In contrast, in 100 mM phosphate buffer pH 3.0, the DDAB tends to form a very stable coating almost immediately upon rinsing ( $\times$  in Figure 2.8). However, upon aging the capillary for 24 hours in 0.1 mM DDAB in 100 mM phosphate pH 3.0, the coating becomes essentially permanent with EOF values decreasing by less than 1% over 200 capillary volumes of rinsing, as shown in Figure 2.12. Therefore, the aging time effect on the stability of the DDAB bilayer is significant and the coating becomes permanent at earlier aging times as the buffer concentration increases. In summary, aging of the capillary in DDAB solution did cause some improvements in the coating behavior, but the general trends were consistent with the behavior observed above using fresh capillaries.

### 2.3.9 Protein Separations

To examine the effectiveness of the DDAB bilayer for protein separations, a mixture of four basic proteins (lysozyme, ribonuclease A,  $\alpha$ -chymotrypsinogen A, and cytochrome *c*) were used as test analytes, as recommended by Mazzeo and Krull [45]. Narrow (25  $\mu\text{m}$  i.d.) capillaries were used to maximize the stability of the DDAB coatings. The capillaries were coated with 0.1 mM DDAB in buffer, and then rinsed with buffer void of DDAB for 1 min at 138 kPa (1.5 capillary volumes). Figure 2.13a shows the separation of the four proteins in 5.0 mM acetate buffer pH 5.0. Under these buffer conditions, the DDAB coating would be expected to undergo significant degradation ( $k_{obs} = (85 \pm 6) \times 10^{-3} (\text{cap. vol})^{-1}$  in a 50  $\mu\text{m}$  i.d. capillary). The separation efficiency with this dilute acetate buffer (Figure 2.13a) was very poor ( $N < 125,000$  plates/m), and only three of the four proteins eluted. The absence of the  $\alpha$ -chymotrypsinogen A peak, as well as the tailing of the other proteins, indicates that there is a strong interaction

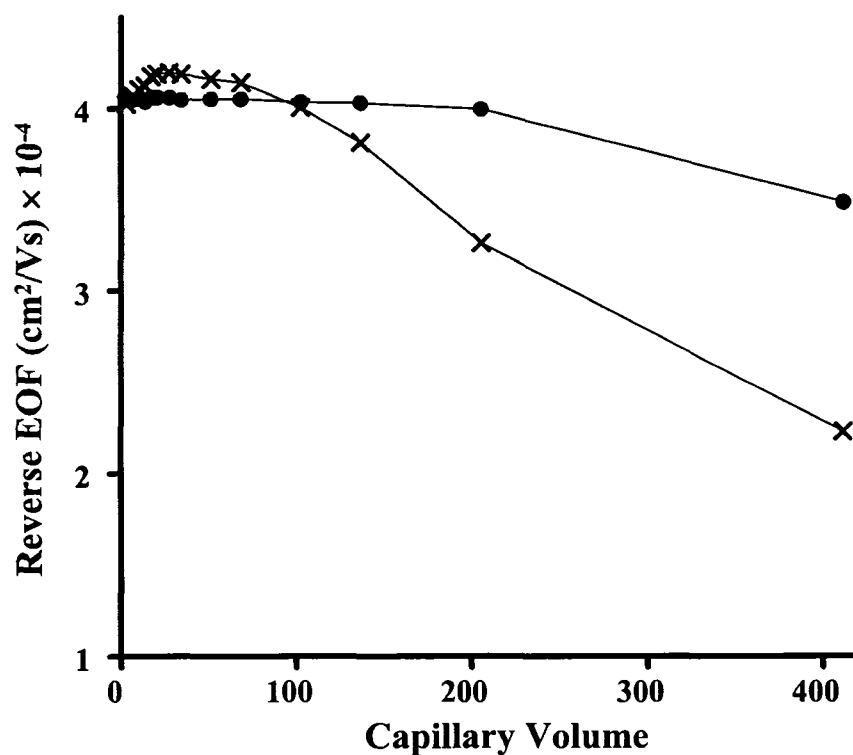


**Figure 2.12** Effect of aging time on the stability of DDAB coated capillaries in sodium phosphate buffer at ionic strength of  $88 \times 10^{-3}$  M and pH 3.0. Day 0 (x); and day 1 (•). **Experimental conditions:** applied voltage during EOF measurement,  $-9$  kV; capillary,  $30 \text{ cm} \times 50 \text{ } \mu\text{m}$  i.d. (20 cm to detector); neutral marker, 1 mM mesityl oxide;  $\lambda$ , 254 nm; and temperature,  $25 \text{ } ^\circ\text{C}$ . New capillary was precondition rinsed with 0.1 mM DDAB-containing solution for 10 min at 138 kPa in day 0. After each run the capillary was recoated again with DDAB solution. Between days the capillary was rinsed with DDAB solution and left overnight. Note: with DDAB coating, the EOF is directed from anode to cathode and thus CZE is run in reverse mode.

between the proteins and the capillary. Similarly, a strong interaction between the proteins and the wall coating was also observed in the residual asymptotic region of the degradation curve due to the presence of less packed bilayer. Increasing the buffer concentration to 50 mM acetate improved the separations, as seen in Figure 2.13b. Efficiencies range from 0.75 to 1.05 million plates/m at  $-2$  kV, which was the optimal voltage for the separation.

Alternately, switching the buffer from acetate to phosphate reduces the EOF (Section 2.3.5) resulting in the separation time increasing from 9 to 17 min, as shown in Figure 2.14a. Peak efficiencies were 0.67-0.76 million plates/m. The primary source of band broadening appears to be longitudinal diffusion. Increasing the electric field strength from 6.7 to 10.0 kV/m, enhances the peak efficiencies to 1.25 million plates/m (Figure 2.14b). The electric field strength was an optimum for the separation.

The reproducibility of the migration time for 10 successive runs with no rinsing between the runs was used to measure the bilayer stability. At 25 mM pH 3.0 phosphate buffer, where the desorption rate ( $k_{obs}$ ) was  $27 \times 10^{-3}$  (cap. vol) $^{-1}$  in 50  $\mu$ m capillary i.d. (Table 2.3), the run to run reproducibility of the migration times was 2.2% RSD. However, during the course of the injections the efficiencies gradually decreased from 0.7 million to 0.26 million plates/m. This implies that the interaction between the analytes and the coating increased gradually as the bilayer decayed. Increasing the buffer concentration to 100 mM phosphate at pH 3.0 (where  $k_{obs}$  was unmeasurable), the migration time reproducibility was better than 0.5% RSD. The peak efficiencies were 0.77-0.86 million plates/m with a reproducibility of less than 4% RSD, except for the lysozyme peak which showed a gradual increase in efficiency from 0.20 million to 0.65

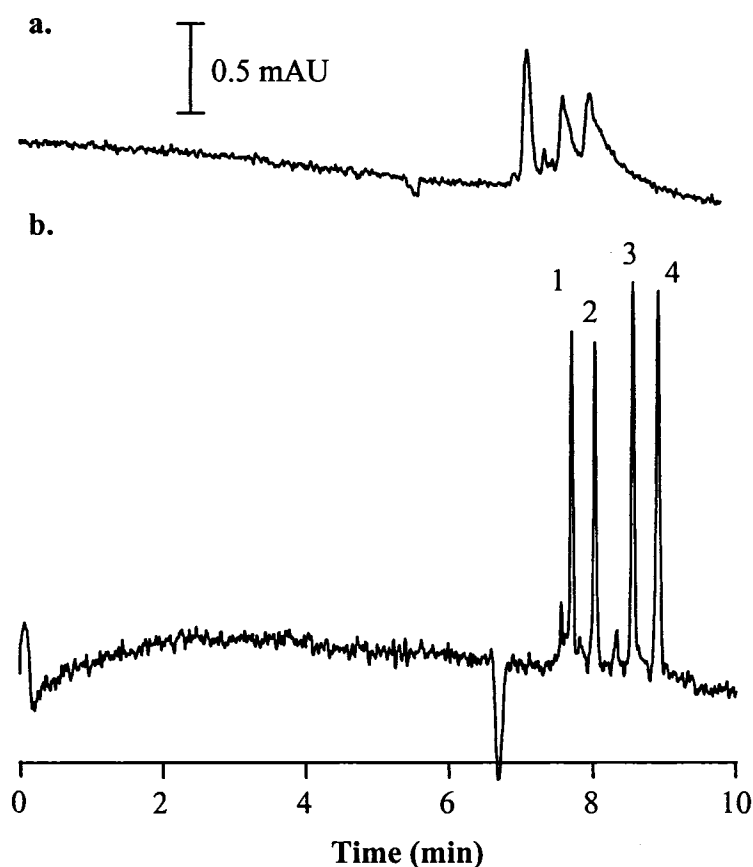


**Figure 2.13** Electropherograms of four proteins in acetate buffer at different concentration: **a.** 5.0 mM; and **b.** 50 mM. Peaks are (1)  $\alpha$ -chymotrypsinogen A, (2) ribonuclease A, (3) cytochrome *c* and (4) lysozyme. **Experimental conditions:** 30 cm  $\times$  25  $\mu$ m i.d. capillary; -2 kV, hydrodynamic injection at 7 kPa for 5 s; buffer pH 5.0;  $\lambda$ , 214 nm; and temperature, 25  $^{\circ}$ C. The capillary was initially rinsed with 0.1 mM DDAB solution dissolved in the running buffer for 5 min at 138 kPa, followed by the running buffer for 1 min at 138 kPa.

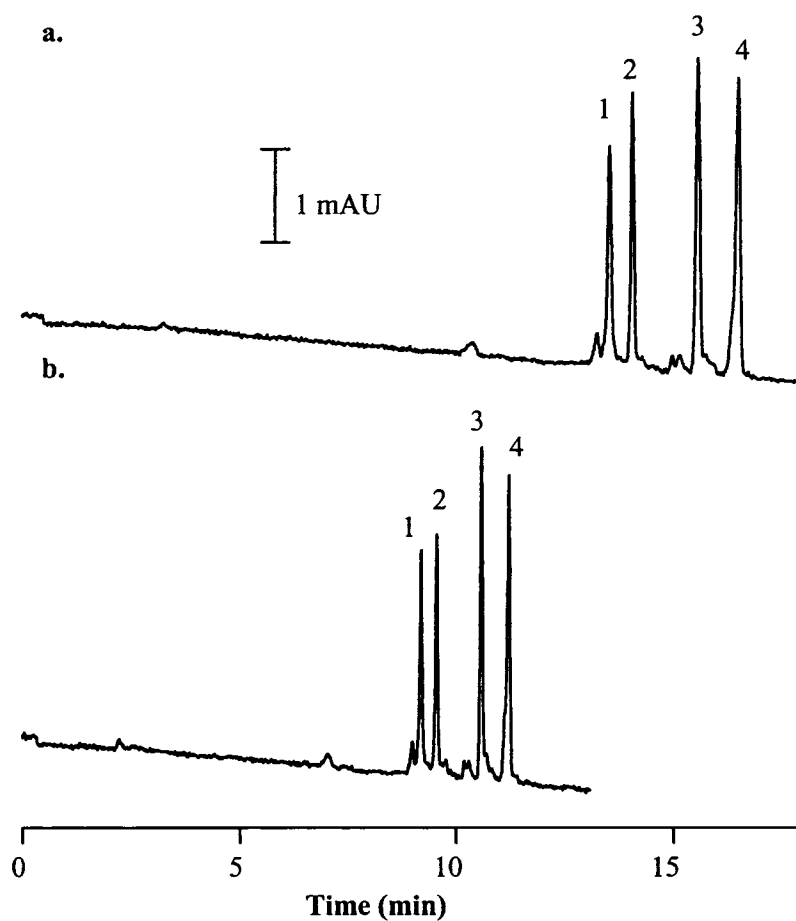


**Figure 2.14** Electropherograms of four proteins in 50 mM phosphate buffer at different voltage: **a.**  $-2\text{kV}$ ; and **b.**  $-3\text{kV}$ . Peaks are (1)  $\alpha$ -chymotrypsinogen A, (2) ribonuclease A, (3) cytochrome *c* and (4) lysozyme. **Experimental conditions:** 30 cm  $\times$  25  $\mu\text{m}$  i.d. capillary; hydrodynamic injection at 7 kPa for 5 s; buffer pH 5.0;  $\lambda$ , 214 nm; temperature, 25  $^{\circ}\text{C}$ . The capillary was initially rinsed with 0.1 mM DDAB solution dissolved in the running buffer for 5 min at 138 kPa, followed by the running buffer for 1 min at 138 kPa.

million plates/m. This indicates that increasing the stability of the DDAB coating reduces the degree of interaction between the proteins and the capillary wall.

Alternatively, increasing the buffer pH of the 25 mM phosphate buffer from pH 3.0 to 5.0 (which increases the coating stability) resulted in a migration time switch between cytochrome *c* and lysozyme. More importantly, the reproducibility of the migration time improved from 2.2% at pH 3.0 to 0.64% RSD at pH 5.0. The efficiencies were also enhanced with values ranging between 0.83 and 0.93 million plates/m, with a reproducibility of less than 7% RSD. The improvement in migration time reproducibility as well as the efficiencies was a result of increasing both the pH and ionic strength of the running buffer. In 50 mM sodium acetate buffer at pH 5.0, similar separations were achieved with a run-to-run migration time reproducibilities of 0.64-0.83% RSD. Efficiencies were between 0.75 and 1.05 million plates/m with a RSD of less than 6% over 10 successive runs. These results are very promising for performing protein separations using DDAB coated capillary with buffers necessary for electrospray ionization mass spectrometry detection.

## 2.4 Conclusions

The double chained cationic surfactant, DDAB, forms a dynamic coating that efficiently prevents protein adsorption onto the capillary wall. The coating is semi-permanent in nature, and the protein separation can be performed in a simple buffer system after removing the excess surfactant from the capillary. The temporal stability of the coating, and thus the efficiencies and reproducibility that are achieved, is improved by those factors that decrease the cmc of DDAB in the buffer. Those factors include

increasing the ionic strength of the buffer and using a buffer that interacts more strongly with quaternary amines (e.g. phosphate rather than acetate). The coating stability is also enhanced by increasing the buffer pH, and decreasing the capillary diameter and the volume of the electrophoretic buffer that flows within the capillary.

## 2.5 References

- [1] Dovichi, N. J., Zhang, J., *Angew. Chem. Int. Ed.* 2000, 39, 4463-4468.
- [2] Lauer, H. H., McManigill, D., *Anal. Chem.* 1986, 58, 166-170.
- [3] Towns, J. K., Regnier, F. E., *Anal. Chem.* 1991, 63, 1126-1132.
- [4] McCormick, R. M., *Anal. Chem.* 1988, 60, 2322-2328.
- [5] Green, J. S., Jorgenson, J. W., *J. Chromatogr.* 1989, 478, 63-70.
- [6] Bushey, M. M., Jorgenson, J. W., *J. Chromatogr.* 1989, 480, 301-310.
- [7] Quigley, W. W. C., Dovichi, N. J., *Anal. Chem.* 2004, 76, 4645-4658.
- [8] Doherty, E. A. S., Meagher, R. J., Albarghouthi, M. N., Barron, A. E., *Electrophoresis* 2003, 24, 34-54.
- [9] Jiang, W., Awasum, J., Irgum, K., *Anal. Chem.* 2003, 75, 2768-2774.
- [10] Belder, D., Deege, A., Husmann, H., Kohler, F., Ludwing, M., *Electrophoresis* 2001, 22, 3813-3818.
- [11] Srinivasan, K., Pohl, C., Avdalovic, N., *Anal. Chem.* 1997, 69, 2798-2805.
- [12] Steiner, F., Hassel, M., *Electrophoresis* 2003, 24, 399-407.
- [13] Hardenborg, E., Zuberovic, A., Ullsten, S., Soderberg, L., Heldin, E., Markides, K. E., *J. Chromatogr. A* 2003, 1003, 217-221.
- [14] Córdova, E., Gao, J., Whitesides, G. M., *Anal. Chem.* 1997, 69, 1370-1379.
- [15] González, N., Elvira, C., Roman, J. S., Cifuentes, A., *J. Chromatogr. A* 2003, 1012, 95-101.
- [16] Baryla, N. E., Lucy, C. A., *J. Chromatogr. A* 2002, 956, 271-277.
- [17] Baryla, N. E., Melanson, J. E., McDermott, M. T., Lucy, C. A., *Anal. Chem.* 2001, 73, 4558-4565.

- [18] Yeung, K. K., Lucy, C. A., *Anal. Chem.* 1997, 69, 3435-3441.
- [19] Lucy, C. A., Underhill, R. S., *Anal. Chem.* 1996, 68, 300-305.
- [20] Baryla, N. E., Lucy, C. A., *Anal. Chem.* 2000, 72, 2280-2284.
- [21] Melanson, J. E., Baryla, N. E., Lucy, C. A., *Trends Anal. Chem.* 2001, 20, 365-374.
- [22] Melanson, J. E., Baryla, N. E., Lucy, C. A., *Anal. Chem.* 2000, 72, 4110-4114.
- [23] Severs, J. C., Smith, R. D., in: Landers, J. P. (Ed.), *Handbook of Capillary Electrophoresis*, CRC Press, Boca Raton, FL 1997, pp. 806.
- [24] Rundlett, K. L., Armstrong, D. W., *Anal. Chem.* 1996, 68, 3493-3497.
- [25] Varghese, J., Cole, R. B., *J. Chromatogr. A* 1993, 652, 369-376.
- [26] Macka, M., Andersson, P., Haddad, P. R., *Anal. Chem.* 1998, 70, 743-749.
- [27] Cunliffe, J. M., Baryla, N. E., Lucy, C. A., *Anal. Chem.* 2002, 74, 776-783.
- [28] Hautala, J. T., Lindén, M. V., Wiedmer, S. K., Ryhänen, S. J., Säily, M. J., Kinnunen, P. K. J., Riekkola, M.-L., *J. Chromatogr. A* 2003, 1004, 81-90.
- [29] Westerlund, D., Mohabbati, S., in 27th International Symposium on High performance Liquid Phase Separations and Related Techniques (HPLC 2003), Nice, France, June 15- 19, 2003.
- [30] Pagac, E. S., Prieve, D. C., Tilton, R. D., *Langmuir* 1998, 14, 2333-2342.
- [31] Atkin, R., Craig, J., Biggs, S., *Langmuir* 2000, 16, 9374-9380.
- [32] Brinck, J., Jönsson, B., Tiberg, F., *Langmuir* 1998, 14, 1058-1071.
- [33] Tiberg, F., Jönsson, B., Lindman, B., *Langmuir* 1994, 10, 3714-3722.
- [34] Geffroy, C., Cohen Stuart, M., Wong, K., Cabane, B., Bergeron, V., *Langmuir* 2000, 16, 6422-6430.

- [35] Atkin, R., Craig, J., Wanless, E. J., Biggs, S., *Adv. Colloid Interface Sci.* 2003, 103, 219-304.
- [36] Grossman, P. D., in: Grossman, P. D. and Colburn, J. C. (Eds.), Academic Press, Inc., San Diego 1992, pp. 3-43.
- [37] Dimov, N. K., Koley, V. L., Kralchevsky, P. A., Lyutov, L. G., Broze, G., Mehreteab, A., *J. Colloid Interface Sci.* 2002, 256, 23-32.
- [38] Li, D., Fu, S., Lucy, C. A., *Anal. Chem.* 1999, 71, 687-699.
- [39] Kennedy, R. T., *Anal. Chimica Acta* 1999, 400, 163-180.
- [40] Issaq, H. J., Atamna, I. Z., Janini, G. M., *Chromatographia* 1991, 32, 155- 161.
- [41] Boström, M., Williams, D. R. M., Ninham, B. W., *Langmuir* 2002, 18, 6010-6014.
- [42] Brady, J. E., Evans, D. F., Warr, G. G., Grieser, F., Ninham, B. W., *J. Phys. Chem.* 1986, 1853-1859.
- [43] Velegol, S. B., Fleming, B. D., Biggs, S., Wanless, E. J., Tilton, R. D., *Langmuir* 2000, 16, 2548-2556.
- [44] Liu, J., Min, G., Ducker, W. A., *Langmuir* 2001, 17, 4895-4903.
- [45] Mazzeo, J. R., Krull, I. S., in: Landers, J. P. (Ed.), *Handbook of Capillary Electrophoresis*, CRC Press, Boca Raton, FL 1994, pp. Chapter. 18.

## **CHAPTER THREE: Enhanced Stability Self-assembled Coatings for Protein Separations by Capillary Zone Electrophoresis through the use of Long Chained Surfactants**

### **3.1 Introduction**

The separation of basic (positively charged) proteins has proven to be particularly challenging in capillary zone electrophoresis due to adsorption of proteins onto the fused silica capillary [1]. Numerous approaches have been explored to minimize this adsorption, including the use of extreme pH [2, 3], high ionic strength [4] and zwitterionic additives [5]. However, the most common approach has been to coat the capillary wall [1]. Coatings can be broadly categorized as [6]: covalently linked polymeric coatings [7-10]; physically adsorbed polymer coatings [11-13]; or small molecule additives (adsorbed surfactants) [14-17]. Detailed discussion on the approaches that minimize protein adsorption is demonstrated in Sections 1.6.

In a recent review, Barron and co-workers stated that covalently bonded coatings are “the most prevalent, and perhaps the most effective, strategy for preventing biomolecule adsorption and improving resolution in the electrophoresis of proteins”. However, adsorbed coatings offer the advantages of the simplicity and a *priori* knowledge of the adsorbent properties [6]. Particularly attractive are “static” or “semi-permanent” adsorbed coatings where the adsorbed material need not be in the run buffer. Ideally, such a coating would be regenerable, i.e., could be totally removed from the

---

\* Aversion of this chapter has been published. Yassine, M. M., Lucy, C. A., *Analytical Chemistry* **2005**, *77*, 620-625

capillary by a simple rinse with acid, base or organic solvent, and then replaced with a fresh layer of adsorbent.

Previously, Melanson *et al.* have demonstrated that two tailed cationic surfactants such as didodecyldimethylammonium bromide (DDAB) form semi-permanent wall coating [18], as shown in Section 1.6.3. The stability of the DDAB coating results from the formation of a bilayer structure at the capillary surface [19]. These coating was very effective for protein separation where efficiencies up to 0.75 million plates/m and recoveries more than 92% can be achieved [18]. However, the capillary should be recoated before each run to maintain high separation efficiency and reasonable migration time reproducibility (Section 1.6.3).

In Chapter Two, I showed that the DDAB bilayers do gradually degrade as the running buffer passes through the capillary. The degradation curve for the DDAB bilayer was obtained by measuring the reverse EOF ( $\mu_{EOF}$ ) as a function of the volume of buffer ( $v_{cap}$ , in dimensionless units of capillary volumes) flushed through the capillary. The obtained degradation curve can be modeled by an exponential decay with non-zero asymptotic value:

$$\mu_{EOF} = A_1 \exp(-k_{obs} v_{cap}) + A_{\infty} \quad (3.1)$$

where  $k_{obs}$  is the observed decay rate of the EOF,  $A_1$  is a fit parameter, and  $A_{\infty}$  is the asymptotic value of the EOF. The rate of degradation is influenced by a number of experimental factors such as the buffer type and concentration [20]. Essentially, greatest stability is achieved under conditions that minimize the critical micelle concentration (cmc) of the surfactant.

In this chapter, the use of longer tailed surfactant analogous of DDAB is explored for the generation of “static adsorbed” or semi-permanent surfactant coatings for protein separations. These surfactants possess lower cmc than DDAB and thus are expected to form highly stable bilayer coatings even with volatile buffers such as ammonium acetate and ammonium formate.

## 3.2 Experimental Section

### 3.2.1 Apparatus

The apparatus utilized in this Chapter was as described in Section 2.2.1.

### 3.2.2 Chemicals

Nanopure 18-M $\Omega$  ultra-pure water (Barnstead, Dubuque, IO, USA) was used to prepare all solutions. Ammonium formate buffers were prepared from ammonium formate salt (BDH, Darmstadt, Germany), and the pH was adjusted using formic acid (BDH). Acetate buffers were prepared using ammonium acetate (BDH), and glacial acetic acid (BDH) to adjust the pH. The cationic surfactants didodecyldimethylammonium bromide (DDAB), dimethylditetradecylammonium bromide (2C<sub>14</sub>DAB), dihexacyldimethylammonium bromide (2C<sub>16</sub>DAB), dimethyldioctadecylammonium bromide (2C<sub>18</sub>DAB) and tridodecylmethylammonium iodide (3C<sub>12</sub>MAI) were used as received from Aldrich (Milwaukee, WI, USA). Chemical structures of these surfactants are shown in Figure 3.1 and their physico-chemical properties are listed in Table 3.1. HPLC-grade methanol (MeOH; Fisher, Fair Lawn, NJ, USA) was used to remove the bilayer coating from the capillary when needed. A solution of 1 mM mesityl oxide (Aldrich) dissolved in water was used as the neutral EOF marker. The proteins lysozyme

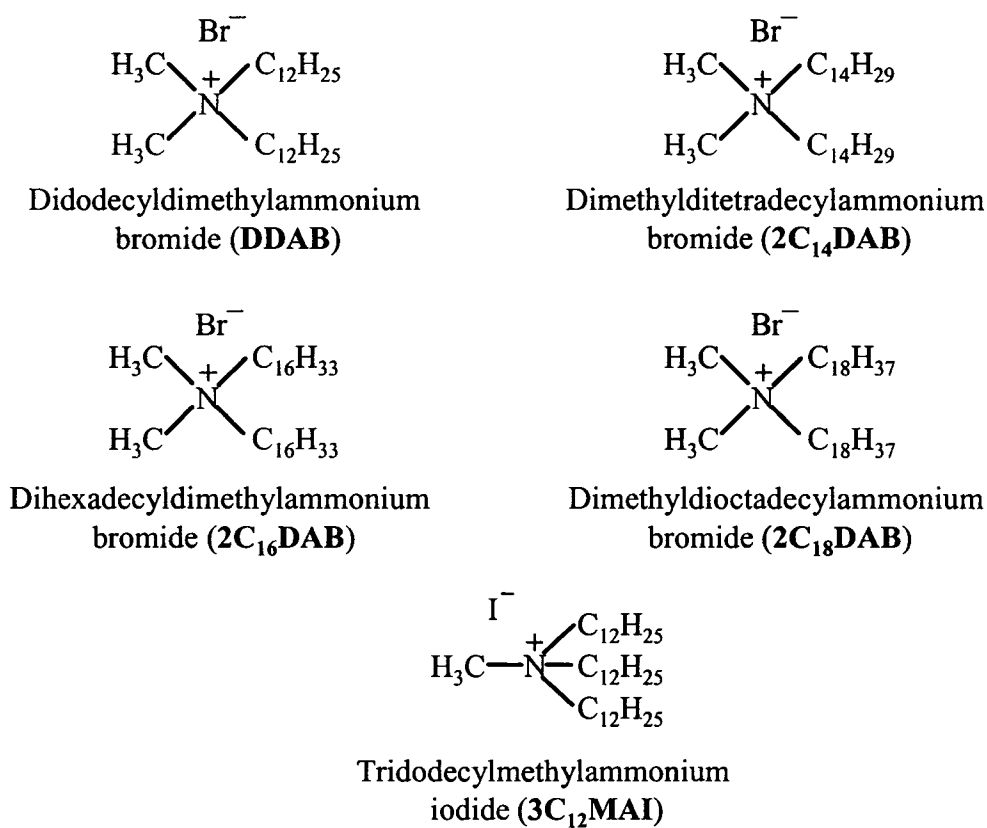


**Figure 3.1** Chemical structures of cationic surfactants used as coatings.

**Table 3.1** Physico-chemical properties of cationic surfactants used as coatings.

Surfactant type	cmc <sup>a</sup> (10 <sup>-3</sup> mM)	Packing parameter <sup>b</sup> ( <i>p</i> )	Chain melting temperature (T <sub>m</sub> ) (°C)
DDA <sup>+</sup> Br <sup>-</sup>	35	0.62	15.8 [21], 16 [22]
2C <sub>14</sub> DA <sup>+</sup> Br <sup>-</sup>	1.6	0.62	29.3 [21], 31 [22]
2C <sub>16</sub> DA <sup>+</sup> Br <sup>-</sup>	0.078	0.62	28.1 [21], 37 [23]
2C <sub>18</sub> DA <sup>+</sup> Br <sup>-</sup>	0.0037	0.62	44.9 [21], 45 [24]
3C <sub>12</sub> MA <sup>+</sup>		0.93	

<sup>a</sup> Determined based on equation 3.2 [25].

<sup>b</sup> Data are taken from reference 25. The values for 2C<sub>18</sub>DA<sup>+</sup> and 3C<sub>12</sub>MA<sup>+</sup> are determined based the formulas in the same reference.

(chicken egg white), ribonuclease A (bovine pancreas),  $\alpha$ -chymotrypsinogen A (bovine pancreas), and cytochrome *c* (bovine heart) were used as received from Sigma (St. Louis, MO, USA), and dissolved in water at a concentration of 0.1 mg/mL of each protein.

### 3.2.3 Preparation of the Surfactant Solutions

DDAB solutions were prepared by adding the surfactant salt to the desired buffer and stirring for 30 min or until a clear solution was obtained. Double chained surfactants with longer hydrocarbon chains ( $2C_{14}DAB$ ,  $2C_{16}DAB$ , and  $2C_{18}DAB$ ), and the triple chained surfactant  $3C_{12}MAI$  are only slightly soluble in water. Thus, we applied the sonicate/stir cycle method [26]. First, the buffer surfactant mixture was sonicated at 50 °C (above the chain melting temperature of  $2C_{18}DAB$ , as shown in Table 3.1) for 20 min. Then, the solution was allowed to rest for 10 min at room temperature with stirring. This sonicate/stir cycle was repeated two times, or until a clear solution was obtained. For instance,  $2C_{14}DAB$  and  $2C_{16}DAB$  surfactants required two and three cycles to dissolve into a clear solution, respectively. However, the surfactants  $2C_{18}DAB$  and  $3C_{12}MAI$  takes at least 6 cycles to form a clear solution.

The  $3C_{12}MAI$  was stored in the dark to prevent iodide photo-oxidation. Also, this surfactant solution had to be re-sonicated every week or before use to re-dissolve a precipitate that formed over time. With the double-chained surfactants, no change in the coating stability was observed for solutions stored for over two months.

### 3.2.4 EOF Measurements

To avoid hysteresis effects, fresh capillaries were used with each new buffer system. New capillaries were flushed with 1 M NaOH for 10 min under high pressure at 138 kPa (20 psi) and then with distilled water for 2 min at 138 kPa. The flushing times

were adjusted according to Poiseuille's equation for capillaries with i.d. other than 50  $\mu\text{m}$  (Section 2.2.3). After the preconditioning steps, the capillary was coated by rinsing with 0.1 mM surfactant-containing buffer for 10 min at 138 kPa. Finally, the capillary was rinsed with the running buffer for 1.5 min at 13.8 kPa (2 psi), corresponding to one capillary volume. The electroosmotic flow ( $\mu_{EOF}$ ) was measured by injection of 1 mM mesityl oxide (neutral marker) in water for 3 s at 3.4 kPa (0.5 psi), followed by applying a constant voltage of  $-9$  kV.

### 3.2.5 Coating Stability

The stability of the surfactant-based coatings was indirectly evaluated by monitoring the EOF as a function of rinsing time. The stability studies were performed using hydrodynamic rinsing method, as described previously in Section 2.2.4. This method was repeated for rinsing times up to 60 min at 138 kPa (corresponding to 415 capillary volumes). The stability of the coating (i.e., EOF) was reported as a function of the number of capillary volumes of run buffer flushed through the capillary.

### 3.2.6 Protein Separations

For protein separations, a fresh capillary of length 30 cm (20 cm to the detector) and 25  $\mu\text{m}$  inner diameter (360  $\mu\text{m}$  outer diameter) was used, unless otherwise stated. The capillary was flushed under a high-pressure rinse (138 kPa) with 1 M NaOH for 20 min, followed by rinsing with water for 5 min at 138 kPa. The coating procedure for the capillary consisted of a 20 min rinse with 0.1 mM surfactant containing buffer, followed by a 1 min rinse (138 kPa) with the electrophoretic buffer to remove the excess surfactant monomers from the capillary. A protein mixture of 0.1 mg/mL was injected using 6.9 kPa (1 psi) for 5 s. The data acquisition was performed using P/ACE station software

(Version 2.3; Beckman) with rate set at 32 Hz for protein separations. Efficiencies were calculated based on the peak width at half-height method, as computed by the P/ACE Station software (Section 2.2.6). Within-day migration time, peak height and peak efficiency reproducibilities were determined for 10 successive injections without regenerating or refreshing the capillary with surfactant. The capillary was simply rinsed with the running buffer (no surfactant) at 138 kPa for 2 min between runs. The day-to-day migration time reproducibility was determined over 5 consecutive days without any regeneration or refreshing of the capillary. The capillary was stored in running buffer overnight.

### 3.3 Results and Discussion

The surfactant bilayer coatings generated herein are characterized by a number of quantitative measures, as recently advocated by Barron and co-workers [6]. Firstly, the EOF stability of the “static adsorbed” or semi-permanent coating is assessed. That is, the coating is formed by rinsing the capillary with surfactant solution. Then, the unsorbed surfactant is flushed from the capillary with run buffer, and the coating stability is assessed using the hydrodynamic rinsing procedure developed in Chapter Two [20]. Where possible, degradation of the EOF was fit to first-order kinetics (eq. 3.1).

Second, the coating performance was assessed based on protein separations of four basic proteins ( $\alpha$ -chymotrypsinogen A, ribonuclease A, cytochrome *c* and lysozyme) recommended by Mazzeo and Krull as model analytes [27]. Protein adsorption can be conceptualized [6, 28] as involving the discrete steps of: 1) protein diffusion through solution to the vicinity of the surface; 2) protein reversibly adsorbing onto the surface; and 3) protein possibly undergoing irreversible adsorption onto the surface. Theoretical

models and simulations have demonstrated that both mass transfer to the capillary wall (step 1) [29, 30], and slow adsorption/desorption kinetics (step 2) [29] of proteins can result in significant peak broadening and possibly tailing. Thus, determination of peak broadening is an important criterion for assessing the effectiveness of a capillary coating. The degree of irreversible adsorption of protein (step 3) can be assessed by measuring the protein recovery [31, 32]. Protein recoveries of 92-100% have been observed for DDAB coatings [18]. Alternatively, long term reproducibility of capillary performance, including efficiency and migration time, is a more operational indicator of low irreversible protein adsorption.

### 3.3.1 Effect of Buffer on EOF

In Chapter Two, I demonstrated that the nature of the buffer counter-ion has a strong influence on the stability of DDAB bilayer coating. Figure 3.2 shows the EOF degradation curves of DDAB coating in ammonium acetate, ammonium formate and phosphate buffers as a function of the number of capillary volumes of run buffer flushed through the capillary. These degradation curves are all well fit by equation 3.1. The resultant fit parameters together with the correlation coefficients ( $R^2$ ) are listed in Table 3.2.

The observed decay rate of the DDAB coating ( $k_{obs}$ ) is greater for acetate buffer than with phosphate buffer, as shown previously in Chapter Two. The lower stability of the DDAB bilayer in acetate buffer has been attributed to the higher cmc of DDAB in acetate than phosphate buffers (cmc value of 0.014 vs. 0.010 mM, respectively). As shown in Figure 3.2 and Table 3.2, the DDAB coating is more stable in ammonium formate than ammonium acetate buffer ( $k_{obs}$  of  $(24 \pm 2) \times 10^{-3}$  vs.  $(30 \pm 2) \times 10^{-3}$

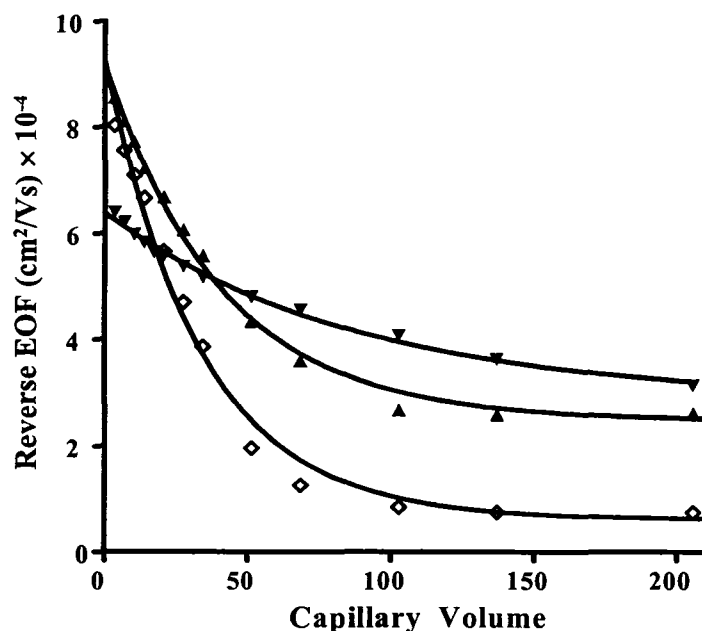


**Figure 3.2** Effect of hydrodynamic rinsing on the EOF of DDAB coated capillaries in different buffers. Buffer used are: ammonium acetate at ionic strength of 10 mM ( $\diamond$ ); ammonium formate at ionic strength of 10 mM ( $\blacktriangle$ ); and sodium phosphate at ionic strength of 9 mM ( $\blacktriangledown$ ). **Experimental conditions:** rinsing pressure is at 138 kPa (20 psi); pH of all buffers is constant at 4.0; applied voltage during EOF measurement,  $-9$  kV; capillary,  $30$  cm  $\times$   $50$   $\mu$ m i.d. (20 cm to detector); 1 mM mesityl oxide;  $\lambda$ , 254 nm; and temperature,  $25$   $^{\circ}$ C. Curves are the fit of the data to equation 3.1. Note: with DDAB coating, the EOF is directed from anode to cathode, and thus CZE is run in reverse mode.

**Table 3.2** Effect of hydrodynamic rinsing on DDAB bilayer. Desorption modeled using First Order Chemical Kinetics (Equation 3.1).<sup>a</sup>

Buffer system	pH	$I$ (mM)	$k_{obs}$ ( $10^{-3}$ cap. vol) $^{-1}$	$A_1$ ( $10^{-4}$ cm $^2$ /Vs)	$A_{\infty}$ ( $10^{-4}$ cm $^2$ /Vs)	$R^2$
Ammonium formate	4.0	10	$24 \pm 2$	$6.7 \pm 0.2$	$2.5 \pm 0.1$	0.995
Ammonium formate	3.0	10	$33 \pm 3$	$9.2 \pm 0.4$	$0.6 \pm 0.2$	0.99
Ammonium acetate	4.0	10	$30 \pm 2$	$8.7 \pm 0.3$	$0.6 \pm 0.2$	0.99
Sodium acetate*	4.0	9	$29 \pm 2$	$8.9 \pm 0.2$	$1.1 \pm 0.2$	0.991
Sodium phosphate*	4.0	9	$12 \pm 1$	$3.5 \pm 0.1$	$2.9 \pm 0.2$	0.993

<sup>a</sup> **Experimental conditions:** as in Figure 3.2.

\* Data from previous work presented in Chapter Two.

(cap. vol)<sup>-1</sup>). This relative stability is consistent with the cmc values for the corresponding dodecyltrimethylammonium salts in distilled water (30.5 mM for acetate and 27.9 mM for formate) [33].

Overall however, DDAB does not form a stable bilayer in either acetate or formate buffers. Also, free DDAB from the degrading bilayer could interfere with detection methods such as electrospray ionization mass spectrometry (ESI-MS). The stability of these bilayer coatings could be improved by increasing the ionic strength of the run buffer [20], but this approach is limited by Joule heating generated within the capillary (Section 1.4.3) and would cause ion suppression in ESI. The desire to make the surfactant bilayer coatings more compatible with ESI-MS was the incentive to find an alternate means of increasing the stability of the bilayer coatings in volatile buffers, such as ammonium acetate and ammonium formate.

Finally, changing the buffer cation from sodium to ammonium did not change the stability of the coatings in acetate buffer (Table 3.2). This is consistent with Atkin *et al.*'s observation that the co-ion ( $K^+$ ,  $Na^+$ , and  $Li^+$ ) had minimal influence on the kinetics of adsorption of CTAB aggregates [34].

### 3.3.2 Effect of Surfactant on EOF

As discussed in Section 1.6, double-chained cationic surfactants with alkyl chains longer than eight carbons form bilayer (vesicle) structures in aqueous solutions [25, 35], and are favored to form bilayers on surfaces. The packing factors ( $p$ ) [36] of the double chained surfactants used in this study are  $\sim 0.62$  (Table 3.1). The length of the alkyl chain has no effect on the packing factors ( $p$ ), as both the volume ( $v_c$ ) and the length ( $l_c$ ) of the

hydrocarbon chain increase proportionally. Thus, all of the double chained surfactants are expected to form bilayers onto silica surface [22].

To achieve greater bilayer stability, a lower cmc is required [20]. Rather than modifying the buffer conditions, the cmc can be lowered by increasing the hydrophobicity of the surfactant tail either by increasing the length or number of the hydrocarbon chains in the surfactant [25, 33, 36]. For double chained surfactants the cmc can be estimated by [25]:

$$\log(\text{cmc}, \text{M}) = 3.495 - 0.6625n \quad (3.2)$$

where  $n$  is the number of carbon atoms in each alkyl chain. Thus, the cmc is estimated to decrease by 21-fold for every two methylenes added to each hydrocarbon chain of the surfactant monomer. Based on the above equation, the calculated cmc values for 2C<sub>14</sub>DAB to 2C<sub>18</sub>DAB range from  $1.6 \times 10^{-6}$  to  $3.7 \times 10^{-9}$  M, as shown in Table 3.1. Figure 3.3 illustrates the stability of coatings formed with 2C<sub>14</sub>DAB, 2C<sub>16</sub>DAB and 2C<sub>18</sub>DAB in 10 mM ammonium formate buffer. No significant degradation (< 3%) is observed for these longer chain surfactants over 415 capillary volumes (~245  $\mu$ L) of continuous rinsing with the run buffer.

Another way to lower the cmc is to increase the number of alkyl chains on the surfactant monomers. This can be achieved by using 3C<sub>12</sub>MAI, a triple chained surfactant. According to the theory of self-assembly of surfactant discussed in Chapter One, the calculated packing parameter ( $p$ ) of 3C<sub>12</sub>MA<sup>+</sup> is 0.93 (Table 3.1). This suggests that 3C<sub>12</sub>MA<sup>+</sup> could form a bilayer structure on the silica surface. Figure 3.3 shows that the reversed EOF for 3C<sub>12</sub>MAI ( $\diamond$ ) is almost constant (< 3% change) during 415 capillary volumes (~245  $\mu$ L) of continuous rinsing with run buffer. Thus, under the experimental

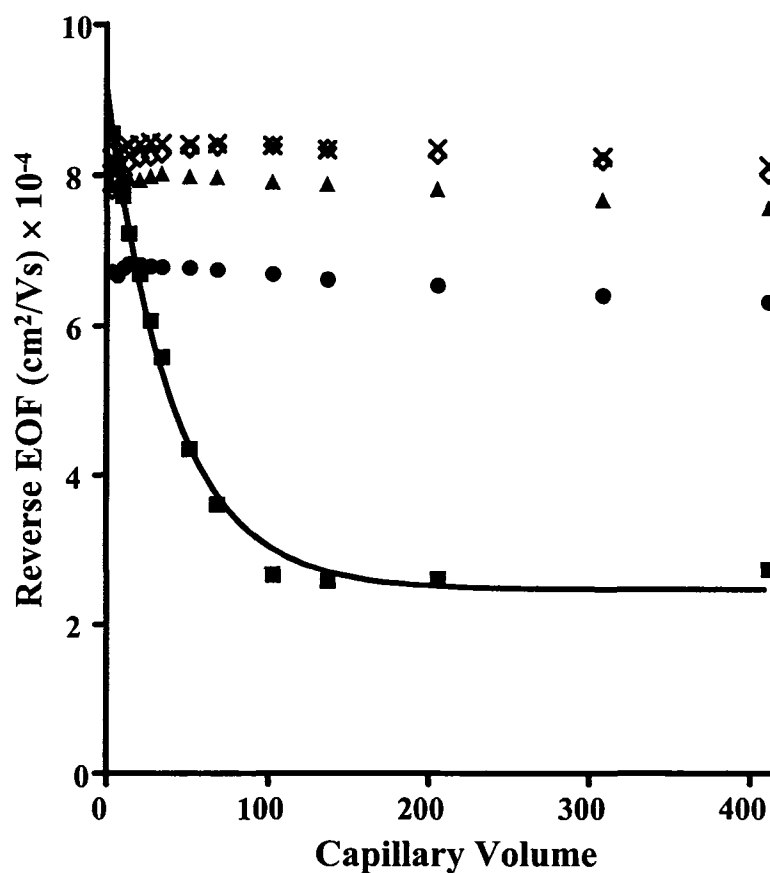


**Figure 3.3** Effect of increasing the hydrocarbon chain length and the number of hydrocarbon chains of the surfactant monomer on the stability of the coatings. Surfactants used are: DDAB (■); 2C<sub>14</sub>DAB (×); 2C<sub>16</sub>DAB (▲); 2C<sub>18</sub>DAB (●); and 3C<sub>12</sub>MAI (◇). **Experimental conditions:** ammonium formate buffer at ionic strength of 10 mM and pH 4.0; applied voltage during EOF measurement, -9 kV; capillary, 30 cm × 50 μm i.d. (20 cm to detector); neutral marker, 1 mM mesityl oxide; temperature, 25 °C; and λ, 254 nm. The capillary was rinsed with 0.1 mM surfactant containing solution for 10 min at 138 kPa. After each run the capillary was regenerated by rinsing with pure methanol and 1 M NaOH then recoated again with surfactant solution. Curve for DDAB is the fit of the data to equation 3.1. Note: with cationic surfactant coatings, the EOF is directed from anode to cathode, and thus CZE is run in reverse mode.

conditions used in Figure 3.3, the stability of the  $3C_{12}MA^+$  coating is indistinguishable from that of  $2C_{14}DAB$ ,  $2C_{16}DAB$  and  $2C_{18}DAB$ .

A second study of coating stability was performed using a wider bore capillary. This allowed a greater buffer volume to be flushed through the capillary, and thereby provides a more severe test of the coating stability [20], as shown in Section 2.3.2. Figure 3.4 shows the EOF degradation curves of the surfactant bilayer coatings as a function of the number of capillary volumes of run buffer flushed through the capillary in 10 mM ammonium acetate buffer using 75  $\mu\text{m}$  i.d capillary. Under these conditions, the reversed EOF for DDAB rapidly decays to its asymptotic value by 60 capillary volumes ( $\sim 80 \mu\text{L}$ ). In contrast, for the  $2C_{14}DAB$  coating the EOF decays by only 10% by 417 capillary volumes ( $\sim 550 \mu\text{L}$ ). Both DDAB and  $2C_{14}DAB$  behavior were fitted to eq. 3.1 with correlation coefficients ( $R^2$ ) better than 0.99, as shown in Table 3.3. Moreover, even under these severe rinse conditions the EOF observed for the  $2C_{18}DAB$  coating was constant (2% random variation, with no evidence of drift) throughout the study, while the EOF of  $3C_{12}MAI$  coating was also constant up to 115 capillary volumes ( $\sim 150 \mu\text{L}$ ), but thereafter decreased by 5%. This indicates that the coating stability follows the order:  $2C_{18}DAB > 3C_{12}MAI \approx 2C_{16}DAB > 2C_{14}DAB \gg DDAB$ .

### 3.3.3 Effect of pH on EOF

Previously, it was observed in Section 2.3 that the stability of DDAB coatings decreased as the buffer became more acidic [20]. This behavior is believed to result from the reduced electrostatic attraction between the surfactant headgroups and the silica surface. This is illustrated in Table 3.2 and Figure 3.5 where decreasing the pH of a formate buffer (10 mM constant ionic strength) from 4.0 to 3.0 causes  $k_{obs}$  to increase

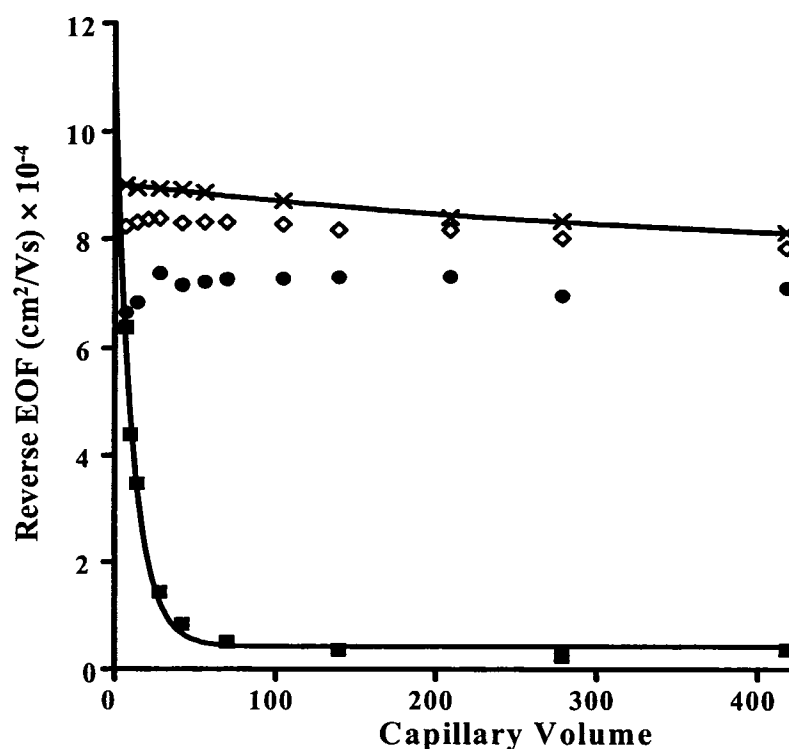


**Figure 3.4** Effect of increasing the capillary inner diameter on the stability of the surfactant bilayer coatings. Surfactant used are: DDAB (■); 2C<sub>14</sub>DAB (×); 2C<sub>18</sub>DAB (●); and 3C<sub>12</sub>MAI (◇). **Experimental conditions:** ammonium acetate buffer at ionic strength of 10 mM and pH 4.0; applied voltage is -9 kV; capillary, 30 cm × 75 μm i.d. (20 cm to detector); neutral marker, 1 mM mesityl oxide; λ, 254 nm; and temperature, 25 °C. The capillary was rinsed with 0.1 mM surfactant containing solution for 10 min at 138 kPa. After each run the capillary was regenerated by rinsing with pure methanol and 1 M NaOH then recoated again with surfactant solution. Curves for DDAB and 2C<sub>14</sub>DAB are the fit of the data to equation 3.1. Note: with cationic surfactant coating, the EOF is directed from anode to cathode, and thus CZE is run in reverse mode.

**Table 3.3** Effect of increasing the capillary inner diameter on the stability of the DDAB and 2C<sub>14</sub>DAB surfactant bilayer coatings. Desorption modeled using First Order Chemical Kinetics (Equation 3.1).<sup>a</sup>

Surfactant	$k_{obs}$ (10 <sup>-3</sup> cap.vol) <sup>-1</sup>	A <sub>1</sub> (10 <sup>-4</sup> cm <sup>2</sup> /Vs)	A <sub>∞</sub> (10 <sup>-4</sup> cm <sup>2</sup> /Vs)	R <sup>2</sup>
DDAB	91 ± 11	11 ± 1	0.4 ± 0.1	0.991
2C <sub>14</sub> DAB	2.7 ± 0.7	1.3 ± 0.2	7.7 ± 0.2	0.994

<sup>a</sup> Experimental conditions as in Figure 3.4.

from  $(24 \pm 2) \times 10^{-3}$  to  $(33 \pm 3) \times 10^{-3}$  (cap. vol)<sup>-1</sup>. That is, at pH 3.0 there is a 90% decrease in the EOF for a DDAB coating over the first 100 capillary volumes of buffer rinse (~60  $\mu$ L). In contrast, with the 2C<sub>14</sub>DAB coating (Figure 3.5) the EOF decreased only 15% over 208 capillary volumes (~125  $\mu$ L). Fitting the degradation curve of 2C<sub>14</sub>DAB coating to eq. 3.1 ( $R^2 = 0.998$ ) yielded a  $k_{obs}$  of  $(3.1 \pm 0.5) \times 10^{-3}$  (cap. vol)<sup>-1</sup>. That is, the 2C<sub>14</sub>DAB coating is about ten times more stable than the DDAB coating, in reasonable agreement with the 21-fold decrease predicted for the cmc. No EOF degradation was observed over 208 capillary volumes (~125  $\mu$ L) of pH 3.0 formate buffer for the 2C<sub>18</sub>DAB coatings, as shown in Figure 3.5.

### 3.3.4 Effect of Surfactant Concentration on EOF

Figure 3.6 shows the effect of the concentration of 2C<sub>14</sub>DAB and 2C<sub>18</sub>DAB in the coating solution on the stability of the bilayer in 10 mM ionic strength formate buffer at pH 3.0. Based on the 95% confidence limit, decreasing the concentration of 2C<sub>14</sub>DAB from 0.1 to 0.005 mM has no effect on the stability (i.e.,  $k_{obs}$ ) of the bilayer coating as shown in Table 3.4. However, longer coating times (at least 20 min) had to be used with the dilute 2C<sub>14</sub>DAB solution to achieve a fully reversed EOF. Similarly, decreasing the concentration of 2C<sub>18</sub>DAB solution from 0.1 mM (●) to 0.005 mM (○) had no effect on the stability of the bilayer coatings, as shown in Figure 3.6. However, the magnitude of the reversed EOF value increased from  $(5.8 \pm 0.2) \times 10^{-4}$  to  $(8.5 \pm 0.2) \times 10^{-4}$  cm<sup>2</sup>/Vs when the 2C<sub>18</sub>DAB solution concentration was decreased. The EOF of the 2C<sub>18</sub>DAB coated capillary with 0.005 mM surfactant concentration solution is comparable to the initial reversed EOF of 2C<sub>14</sub>DAB coating  $(8.8 \pm 0.8) \times 10^{-4}$  cm<sup>2</sup>/Vs. Further, the rinse time necessary to achieve fully reversed EOF did not change with 2C<sub>18</sub>DAB

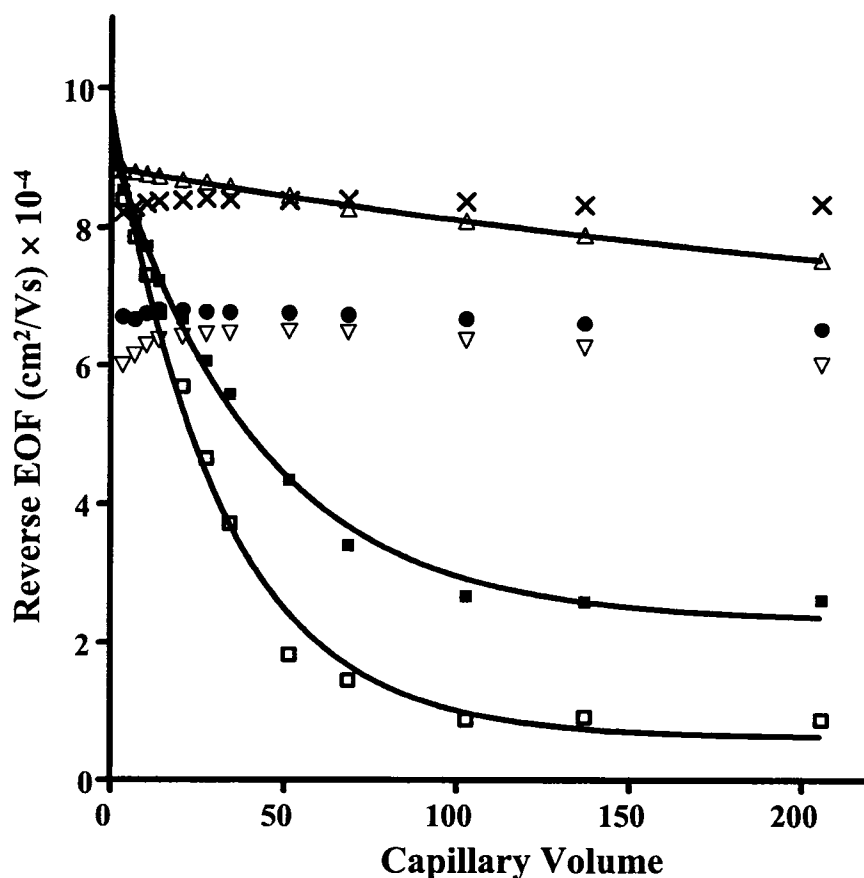


**Figure 3.5** Effect of buffer pH on the stability of the double chained surfactants at pH 3.0 and pH 4.0. Surfactant used at pH 3.0: DDAB ( $\square$ );  $2C_{14}DAB$  ( $\triangle$ );  $2C_{18}DAB$  ( $\nabla$ ), and at pH 4.0: DDAB ( $\blacksquare$ );  $2C_{14}DAB$  ( $\times$ );  $2C_{18}DAB$  ( $\bullet$ ). **Experimental conditions:** ammonium formate buffer at ionic strength of 10 mM; applied voltage during EOF measurement,  $-9$  kV; capillary,  $30$  cm  $\times$   $50$   $\mu$ m i.d. ( $20$  cm to detector); neutral marker,  $1$  mM mesityl oxide;  $\lambda$ ,  $254$  nm; and temperature,  $25$   $^{\circ}$ C. The capillary was rinsed with  $0.1$  mM surfactant containing solution for  $10$  min at  $138$  kPa. After each run the capillary was regenerated by rinsing with pure methanol and  $1$  M NaOH then recoated again with surfactant solution. Curves are the fit of the data to equation 3.1. Note: with cationic surfactant coating, the EOF is directed from anode to cathode, and thus CZE is run in reverse mode.

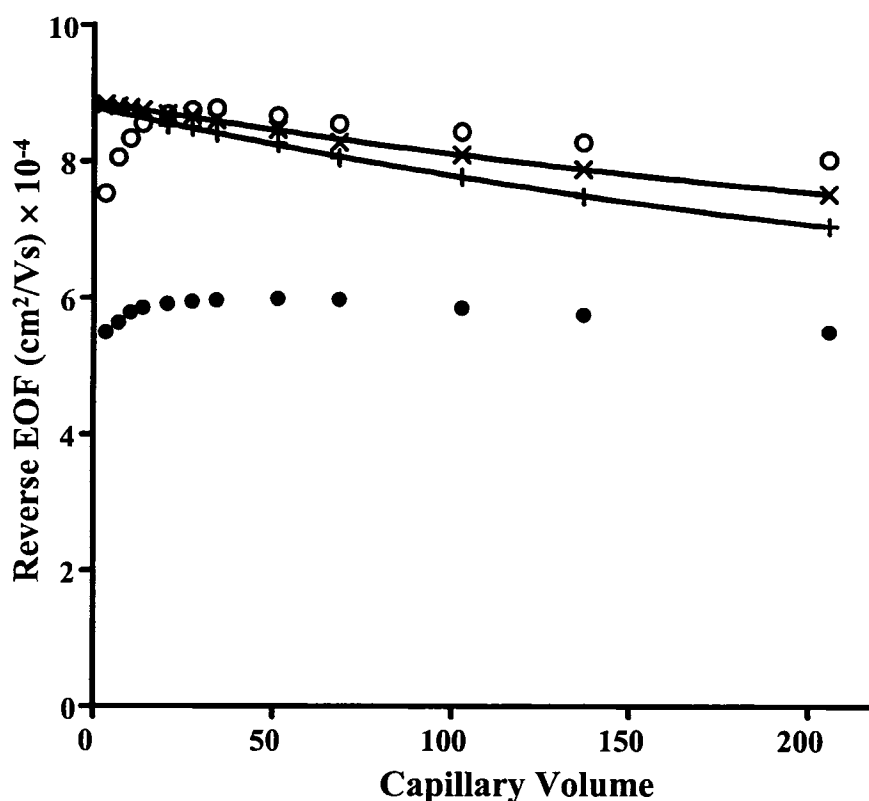


**Figure 3.6** Effect of surfactant concentration on the stability of the bilayer. Surfactant concentration of 0.1 mM: 2C<sub>14</sub>DAB (×) and 2C<sub>18</sub>DAB (●); and concentration of 0.005 mM, 2C<sub>14</sub>DAB (+); and 2C<sub>18</sub>DAB (○). **Experimental conditions:** ammonium formate buffer at ionic strength of 10 mM and pH 3.0; applied voltage, -9 kV; capillary, 30 cm × 50 μm i.d. (20 cm to detector); neutral marker, 1 mM mesityl oxide; λ, 254 nm; and temperature, 25 °C. The capillary was rinsed with 0.1 mM surfactant containing buffer for 10 min at 138 kPa. After each run the capillary was regenerated by rinsing with pure methanol and 1 M NaOH then recoated again with surfactant solution. Curves are the fit of the data to equation 3.1. Note: with cationic surfactant coating, the EOF is directed from anode to cathode, and thus CZE is run in reverse mode.

**Table 3.4** Effect of 2C<sub>14</sub>DAB concentration on the stability of the bilayer. Desorption modeled using First Order Chemical Kinetics (Equation 3.1).<sup>a</sup>

Surfactant	Conc. (mM)	$k_{\text{obs}}$ ( $10^{-3}$ cap. vol) <sup>-1</sup>	$A_1$ ( $10^{-4}$ cm <sup>2</sup> /Vs)	$A_{\infty}$ ( $10^{-4}$ cm <sup>2</sup> /Vs)	$R^2$
2C <sub>14</sub> DAB	0.1	3.1 ± 0.5	2.8 ± 0.4	6.0 ± 0.4	0.998
2C <sub>14</sub> DAB	0.005	3.2 ± 0.6	3.6 ± 0.5	5.2 ± 0.5	0.999

<sup>a</sup> **Experimental conditions:** as in Figure 3.6.

concentration. Regardless, since the coating stability does not depend on the surfactant concentration in the coating solution, 0.1 mM surfactant was used as the coating solution in all other experiments.

### 3.3.5 Protein Separations

Four basic proteins ( $\alpha$ -chymotrypsinogen A, ribonuclease A, cytochrome *c* and lysozyme) were used as model analytes to evaluate the surfactant coatings [27]. Figure 3.7 shows the separation of these proteins in a 50  $\mu\text{m}$  i.d. capillary using the 2C<sub>14</sub>DAB coating. At pH 3.0, the protein peak efficiencies are 0.5 to 0.7 million plates/m. At pH 4.0, the cytochrome *c* and lysozyme almost elute together and the peaks are no longer resolved. Further increasing the pH to 4.5 resulted in a migration order switch between cytochrome *c* and lysozyme. Also the protein peak efficiencies improved to 1.0 million plates/m. Upon decreasing the capillary i.d. to 25  $\mu\text{m}$  (to maximize the stability of the wall coating) [20], comparable peak efficiencies were observed. However, if the protein sample was prepared in 1/10 diluted-buffer, the efficiencies of the protein peaks were enhanced to 1.2 to 1.4 million plates/m, as shown in Figure 3.8a, comparable to the 1-2 million plates/m theoretically predicted [27]. This sample matrix effect suggests that there is some band broadening occurring due to the laminar flow generated by the mismatch of conductivity between the pure water zone and background electrolyte [37]. This band broadening compromises the peak sharpening achieved by sample stacking. Regardless, protein samples prepared in distilled water were used in all further experiments.

Using the triple-chained surfactant 3C<sub>12</sub>MAI (Figure 3.8b) yields a slightly slower separation of 2.3 min compared to a separation time of 2.0 min with 2C<sub>14</sub>DAB coating, as

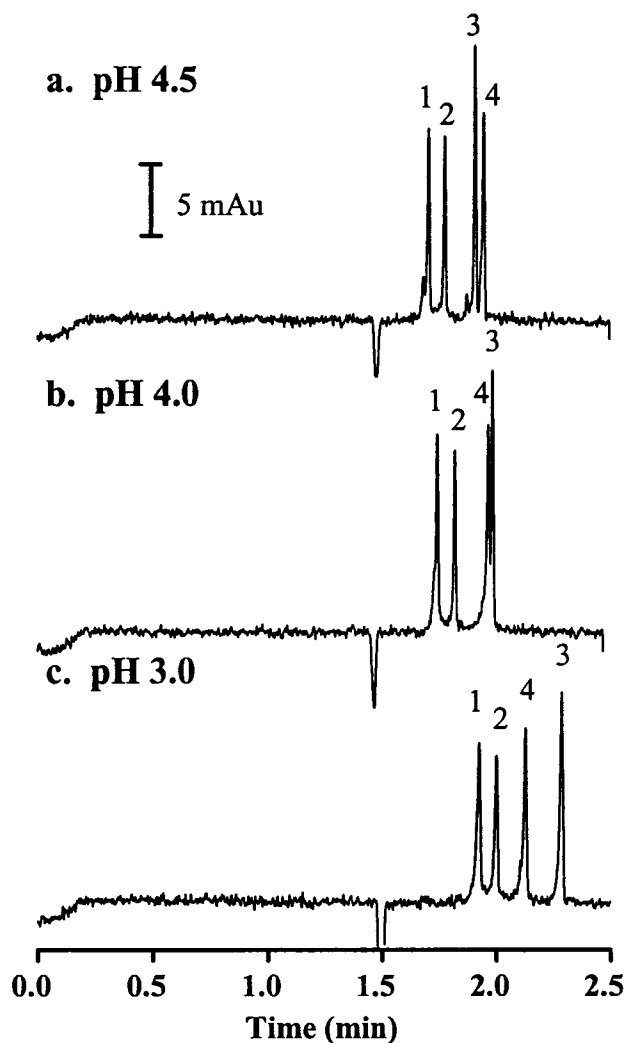


**Figure 3.7** Electropherograms of four cationic proteins using  $2C_{14}DAB$  coatings at different pH: **a.** pH 4.5; **b.** pH 4.0; and **c.** pH 3.0. Peaks: (1)  $\alpha$ -chymotrypsinogen A, (2) ribonuclease A, (3) cytochrome *c* and (4) lysozyme. **Experimental conditions:** 30 cm  $\times$  50  $\mu$ m i.d. capillary; protein sample was dissolved in water; hydrodynamic injection at 2 kPa for 3 s; 50 mM ammonium formate buffer; voltage at  $-10$  kV;  $\lambda$ , 214 nm; and temperature, 25  $^{\circ}C$ . The capillary was initially rinsed with 0.1 mM  $2C_{14}DAB$  solution dissolved in the running buffer for 5 min at 138 kPa, followed by rinsing with the running buffer for 2 min at 13.8 kPa.

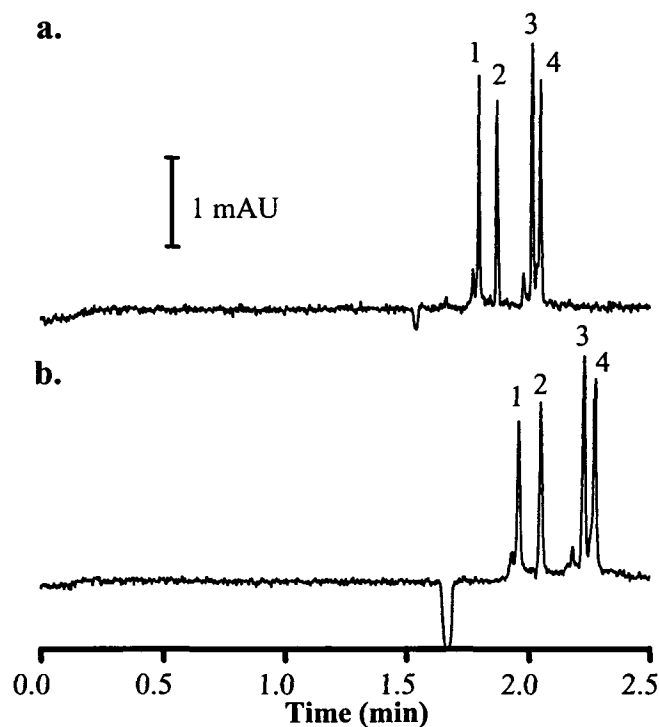


**Figure 3.8** Electropherograms of four cationic proteins using  $2C_{14}DAB$  and  $3C_{12}MAI$ . **a.**  $2C_{14}DAB$  coating, protein sample prepared in 1/10 dilute buffer; and **b.**  $3C_{12}MAI$  coating, protein sample prepared in distilled water. Peaks: (1)  $\alpha$ -chymotrypsinogen A, (2) ribonuclease A, (3) cytochrome *c* and (4) lysozyme. **Experimental conditions:** 30 cm  $\times$  25  $\mu$ m i.d. capillary; 50 mM ammonium formate buffer at pH 4.5; hydrodynamic injection at 7 kPa for 5 s; temperature, 25  $^{\circ}C$ ;  $\lambda$ , 214 nm; and voltage at  $-10$  kV.

**Table 3.5** Migration time of the cationic proteins separated using  $2C_{14}DAB$ ,  $2C_{18}DAB$ , and  $3C_{12}MAI$ .<sup>a</sup>

Coatings	$\mu_{EOF}$ $cm^2/Vs$	migration time (min)				
		$t_{EOF}$	$\alpha$ -chymotrypsinogen A	ribonucleas A	cytochrome <i>c</i>	lysozyme
$2C_{14}DAB$	$6.7 \times 10^{-4}$	1.51	1.77	1.84	1.98	2.02
$2C_{18}DAB$	$4.0 \times 10^{-4}$	2.49	3.27	3.49	4.06	4.22
$3C_{12}TAI$	$6.0 \times 10^{-4}$	1.67	1.97	2.07	2.25	2.29

<sup>a</sup> **Experimental conditions:** as in Figure 3.8.

shown in Table 3.5. This result is consistent with the lower reversed EOF with this surfactant. Efficiencies are ranging between 0.7 and 0.8 million plates/m for sample dissolved in distilled water. As shown in Table 3.5, the separation time of the same protein mixture using 2C<sub>18</sub>DAB coating was about 4.2 min, with efficiencies of only 0.3-0.4 million plates/m. Peak tailing was not evident in any of the electropherograms, indicating that the strong positive charge of the bilayer coating minimizes protein interaction with the capillary wall.

Figure 3.9 demonstrates the reproducibility and stability of the 2C<sub>18</sub>DAB coating. Over 60 successive runs were performed over a 12-day period without ever regenerating or refreshing the capillary. The percent relative standard deviation (% RSD) for the migration time, peak height and efficiency reproducibilities for 10 successive runs per day are shown in Table 3.6. The migration time reproducibility was 0.11-0.84% RSD within-day and 2.3% RSD for between-day (n = 5 days). No general trends in the migration time (*i.e.*, not decreasing or increasing) were evident over the 12-day period (Table 3.7). The peak height reproducibility within each day was ranging between 1.6 and 4.4% RSD. The efficiency (*N*) reproducibility within-day was 3.0-8.7% RSD, with efficiencies varying randomly during the course of the experiment. The high degree of reproducibility suggests that little protein is irreversibly retained on the 2C<sub>18</sub>DAB, consistent with the high recoveries observed previously with DDAB coated capillaries [18, 19]. A similar reproducibility and stability study was performed with the triple-chained surfactant 3C<sub>12</sub>MAI. Fifty successive runs were performed over a 5-day period without ever regenerating or refreshing the capillary. The % RSD for the migration time, peak height and efficiency reproducibilities for 10 successive runs per day are presented

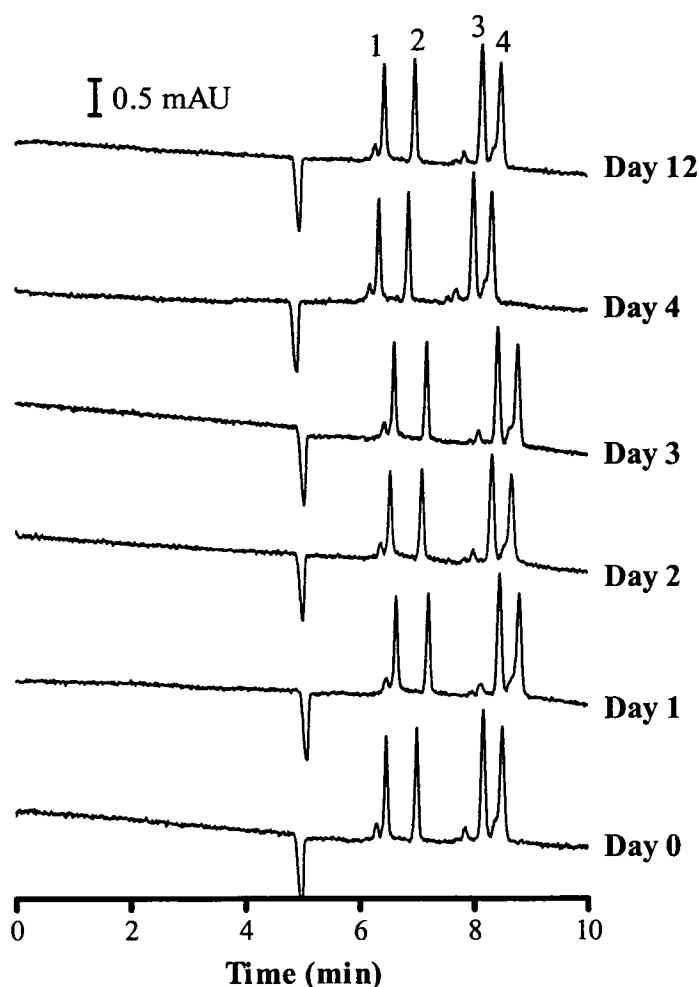


**Figure 3.9** Electropherograms of four cationic proteins with  $2C_{18}DAB$  coated capillary for 12-day period. Peaks: (1)  $\alpha$ -chymotrypsinogen A, (2) ribonuclease A, (3) cytochrome *c* and (4) lysozyme. **Experimental conditions:** 30 cm  $\times$  25  $\mu$ m i.d. capillary; injection at 7 kPa for 5 s; 50 mM ammonium formate buffer at pH 4.5; voltage  $-5$  kV; temperature, 25  $^{\circ}$ C; and  $\lambda$ , 214 nm. The capillary was initially rinsed with 0.1 mM  $2C_{18}DAB$  solution dissolved in the running buffer for 5 min at 138 kPa, followed by rinsing with the running buffer for 2 min at 138 kPa. Between the runs the capillary was rinsed with the run buffer for 2 min at 138 kPa without re-coating with the surfactant solution. The capillary was stored in the running buffer overnight.

**Table 3.6** Migration time reproducibility, peak height reproducibility, and efficiency reproducibility of the cationic proteins separated using 2C<sub>18</sub>DAB coating over a 12-day period.<sup>a</sup>

	Migration time reproducibility % RSD	Peak height Reproducibility % RSD	Efficiency reproducibility % RSD
Day 0	0.64-0.84	3.4-4.4	4.0-4.8
Day 1	0.18-0.24	3.1-3.6	3.7-4.8
Day 2	0.20-0.34	2.3-3.2	3.8-7.9
Day 3	0.75-0.82	1.8-2.9	4.1-7.4
Day 4	0.08-0.11	1.6-3.2	3.6-7.0
Day 12 <sup>b</sup>	0.18-0.35	2.1-2.4	3.0-7.3

<sup>a</sup> **Experimental conditions:** as in Figure 3.9. Ten replicate injections were performed each day.

<sup>b</sup> After day 4 the coated capillary was stored for 7 days in the run buffer.

**Table 3.7** Average migration time within the day for the cationic proteins separated using 2C<sub>18</sub>DAB coating over a 12-day period.<sup>a</sup>

	Average migration time (min)			
	$\alpha$ -chymotrypsinogen A	ribonuclease A	cytochrome <i>c</i>	lysozyme
Day 0	6.50	7.04	8.22	8.55
Day 1	6.65	7.22	8.47	8.82
Day 2	6.58	7.13	8.34	8.68
Day 3	6.62	7.19	8.45	8.79
Day 4	6.35	6.88	8.00	8.33
Day 12 <sup>b</sup>	6.54	7.09	8.32	8.66

<sup>a</sup> **Experimental conditions:** as in Figure 3.9. Ten replicate injections were performed each day.

<sup>b</sup> After day 4 the coated capillary was stored for 7 days in the run buffer.

in Table 3.8. The migration time reproducibility within-day was 0.13-0.61% RSD, and the peak height reproducibility 1.1-6.1% RSD. However, the migration time reproducibility between-day was 3.4% RSD and displayed a gradual increase in the migration times (Table 3.9). More importantly, the peak efficiencies decreased from 0.7-0.8 to 0.3-0.4 million plates/m over the 5-day period. The poorer migration time reproducibility and loss in efficiency indicates that the 3C<sub>12</sub>MAI coating gradually degraded over the 5-day period. This is consistent with the small difference in stability observed for the 3C<sub>12</sub>MAI coating versus the 2C<sub>18</sub>DAB coating in Figure 3.4.

The long-term stability of the 2C<sub>14</sub>DAB coating was expected to be poor. Nonetheless, it was studied due to the high efficiencies achieved with this coating (Figure 3.8). The migration time and peak height reproducibility observed for 14 successive runs on a 2C<sub>14</sub>DAB coated capillary without regeneration were 0.30-0.46 % and 3.4-3.6% RSD, respectively. The efficiencies reproducibility was ranging between 2.3 and 7.7% RSD, with the efficiencies decreasing significantly after 10 runs. Therefore, the capillary needs to be regenerated to resurrect performance. This is done by washing the capillary with pure methanol solution for 5 min followed by rinsing NaOH, water, buffer and then the surfactant solution.

### 3.4 Conclusions

Static adsorbed coatings were generated within fused silica capillaries by flushing the capillary with a 0.1 mM solution of the double-chained cationic surfactants 2C<sub>14</sub>DAB, 2C<sub>16</sub>DAB and 2C<sub>18</sub>DAB as well as the triple-chained surfactant 3C<sub>12</sub>MAI. All of these coatings were semi-permanent, whereby the coating remained intact after the unadsorbed

**Table 3.8** Migration time reproducibility, peak height reproducibility, and efficiency reproducibility of the cationic proteins separated using 3C<sub>12</sub>MAI coating over a 5-day period.<sup>a</sup>

	Migration time reproducibility % RSD	Peak height Reproducibility % RSD	Efficiency reproducibility % RSD
Day 0	0.41-0.42	3.6-6.1	7.4-10.9
Day 1	0.25-0.26	2.0-3.7	2.2-4.8
Day 2	0.51-0.61	1.1-3.7	2.0-5.1
Day 3	0.31-0.32	1.9-3.1	3.6-6.1
Day 4	0.13-0.16	2.0-4.5	5.6-8.2

<sup>a</sup> **Experimental conditions:** as in Figure 3.9. Ten replicate injections were performed each day.

**Table 3.9** Average migration time within the day for the cationic proteins separated using 3C<sub>12</sub>MAI coating over a 5-day period.<sup>a</sup>

	Average migration time (min)			
	$\alpha$ -chymotrypsinogen A	ribonuclease A	cytochrome c	lysozyme
Day 0	6.57	6.89	7.53	7.69
Day 1	6.70	7.03	7.72	7.88
Day 2	6.69	7.03	7.70	7.87
Day 3	6.82	7.18	7.90	8.06
Day 4	7.07	7.45	8.22	8.41

<sup>a</sup> **Experimental conditions:** as in Figure 3.9. Ten replicate injections were performed each day.

surfactant was removed from the capillary. The stability of the coating increased with decreasing the cmc via increasing the hydrophobicity of the surfactant by increasing the length or number of the hydrocarbon chains in the surfactant. For instance, the stability of the long chain surfactants ( $2C_{18}DAB$ ) was very high over a 12-day period without any regeneration of the coating. The migration time reproducibility of  $2C_{18}DAB$ -coated capillary varied by less than 2.3% over 5-day period with no loss in efficiency.

### 3.5 References

- [1] Quigley, W. W. C., Dovichi, N. J., *Anal. Chem.* 2004, 76, 4645-4658.
- [2] McCormick, R. M., *Anal. Chem.* 1988, 60, 2322-2328.
- [3] Lauer, H. H., McManigill, D., *Anal. Chem.* 1986, 58, 166-170.
- [4] Green, J. S., Jorgenson, J. W., *J. Chromatogr.* 1989, 478, 63-70.
- [5] Bushey, M. M., Jorgenson, J. W., *J. Chromatogr.* 1989, 480, 301-310.
- [6] Doherty, E. A. S., Meagher, R. J., Albarghouthi, M. N., Barron, A. E., *Electrophoresis* 2003, 24, 34-54.
- [7] Jiang, W., Awasum, J., Irgum, K., *Anal. Chem.* 2003, 75, 2768-2774.
- [8] Belder, D., Deege, A., Husmann, H., Kohler, F., Ludwing, M., *Electrophoresis* 2001, 22, 3813-3818.
- [9] Srinivasan, K., Pohl, C., Avdalovic, N., *Anal. Chem.* 1997, 69, 2798-2805.
- [10] Steiner, F., Hassel, M., *Electrophoresis* 2003, 24, 399-407.
- [11] Córdova, E., Gao, J., Whitesides, G. M., *Anal. Chem.* 1997, 69, 1370-1379.
- [12] González, N., Elvira, C., Roman, J. S., Cifuentes, A., *J. Chromatogr. A* 2003, 1012, 95-101.
- [13] Hardenborg, E., Zuberovic, A., Ullsten, S., Soderberg, L., Heldin, E., Markides, K. E., *J. Chromatogr. A* 2003, 1003, 217-221.
- [14] Baryla, N. E., Lucy, C. A., *J. Chromatogr. A* 2002, 956, 271-277.
- [15] Yeung, K. K.-C., Kiceniuk, A. G., Li, L., *J. Chromatogr. A* 2001, 931, 153-162.
- [16] Lucy, C. A., Underhill, R. S., *Anal. Chem.* 1996, 68, 300-305.
- [17] Melanson, J. E., Baryla, N. E., Lucy, C. A., *Trends Anal. Chem.* 2001, 20, 365-374.

- [18] Melanson, J. E., Baryla, N. E., Lucy, C. A., *Anal. Chem.* 2000, 72, 4110-4114.
- [19] Baryla, N. E., Melanson, J. E., McDermott, M. T., Lucy, C. A., *Anal. Chem.* 2001, 73, 4558-4565.
- [20] Yassine, M. M., Lucy, C. A., *Anal. Chem.* 2004, 76, 2983-2990.
- [21] Blandamer, M. J., Briggs, B., Cullis, P. M., Kirby, S. D., Engberts, J. B. F. N., *J. Chem. Soc., Faraday Trans.* 1997, 93, 453-455.
- [22] Warr, G. G., Radha Sen, Evans, D. F., Trend, J. E., *J. Phys. Chem.* 1988, 92, 774-783.
- [23] Dubois, M., Zemb, T., *Langmuir* 1991, 7, 1352-1360.
- [24] Kunitake, T., *Angew. Chem. Int. Ed.* 1992, 31, 709-726.
- [25] Svitova, T. F., Smirnova, Y. P., Pisarev, S. A., Berezina, N. A., *Colloids Surf. A* 1995, 98, 107-115.
- [26] Leonenko, Z. V., Carnini, A., Cramb, D. T., *Biochim. Biophys. Acta* 2000, 1509, 131-147.
- [27] Mazzeo, J. R., Krull, I. S., in: Landers, J. P. (Ed.), *Handbook of Capillary Electrophoresis*, CRC Press, Boca Raton, FL 1994, pp. Chapter. 18.
- [28] Ingendoh, A., Karas, M., Hillenkamp, F., *Int. J. Mass Spectrom. Ion Processes* 1994, 131, 345-354.
- [29] Gaš, B., Stedry, M., Rizzi, A., Kenndler, E., *Electrophoresis* 1995, 16, 958-967.
- [30] Schure, M. R., Lenhoff, A. M., *Anal. Chem.* 1993, 65, 3024-3037.
- [31] Towns, J. K., Regnier, F. E., *Anal. Chem.* 1991, 63, 1126-1132.
- [32] Castelletti, L., Verzola, B., Gelfi, C., Stoyanov, A., Righetti, P. G., *J. Chromatogr. A* 2000, 894, 281-289.

- [33] Brady, J. E., Evans, D. F., Warr, G. G., Grieser, F., Ninham, B. W., *J. Phys. Chem.* 1986, 1853-1859.
- [34] Atkin, R., Craig, J., Wanless, E. J., Biggs, S., *Adv. Colloid Interface Sci.* 2003, 103, 219-304.
- [35] Kunitake, T., Kimizuka, N., Higashi, N., Nakashima, N., *J. Am. Chem. Soc.* 1984, 106, 1978-1983.
- [36] Israelachvili, J. N., Mitchell, D. J., Ninham, B. W., *J. Chem. Soc., Faraday Trans. 2* 1976, 72, 1525- 1568.
- [37] Burgi, D. S., Chien, R. L., *Anal. Chem.* 1991, 63, 2042-2047.

## CHAPTER FOUR: Preparative Capillary Zone Electrophoresis using a Dynamic Coated Wide-bore Capillary

### 4.1 Introduction

Currently, two-dimensional gel electrophoresis is the method of choice for preparative protein separations and analyses for proteomic applications [1]. However, this technique is time-consuming, labor-intensive, difficult-to-automate and has low reproducibility [2]. More importantly, it is not possible to extract the whole protein from the gel in its native form, and in some cases the amount extracted is not sufficient for the subsequent protein identification and characterization studies [3]. In addition, the extracted sample must be cleaned to remove sodium dodecyl sulfate. Consequently, extensive efforts have been devoted to the development of preparative non-gel-based techniques to facilitate protein isolation. One of the non-gel electrophoretic methods that has been used for preparative protein separations is capillary isoelectric focusing (CIEF) [4, 5]. Using 100  $\mu\text{m}$  i.d. capillaries, loadings of 0.3  $\mu\text{g}$  of each protein have been achieved [6]. However, the mobilization step in CIEF can distort the pH gradient created in the column during the focusing step resulting in poor reproducibility, longer analysis times and degradation of resolution between the focused zones [5]. Further, proteins with similar isoelectric points cannot be separated using CIEF (estimated resolution is 0.05 pH units [6]). For instance, bovine and horse cytochrome *c* differ by only three amino acid residues which results in their theoretical *pI* differing by only 0.07 [7].

---

\* A version of this chapter has been published. Yassine, M. M., Lucy, C. A., *Electrophoresis* **2006**, 27, 3066-3074.

Capillary zone electrophoresis (CZE) is extensively used to separate a wide variety of ionic species, ranging from amino acids to large biomolecules. Due to its beneficial features including fast, high resolution, high efficiency, automation, ease sample collection and minimal sample pre-cleaning required, CZE is potentially a good candidate as a preparative tool for proteomic applications. Furthermore, CZE separations are performed in free solution, and thus the proteins may be purified and isolated without altering their activity.

Previously, CZE was used for preparative separations of small molecules such as pharmaceutical compounds and peptides mixture [8-13]. For instance, Lee *et al.* employed CZE to separate synthetic peptides ( $M_r$  range from 555 to 2148 [13]) at large scales to prepare sample prior to mass spectrometric analysis. Their studies focused mainly on the effects of capillary inner diameter (50 to 200  $\mu\text{m}$ ) and injected plug length on the separation performance at preparative scales. The 100- $\mu\text{m}$  i.d. capillary was found to be the best choice, with an optimum loading limit of 39-78 pmol of each peptide [9]. Theoretically, sample loading could be significantly increased by utilizing wider capillaries ( $> 100 \mu\text{m}$  i.d.). However, the separations deteriorated with wider capillaries due to extensive broadening caused by Joule heating [14, 15] and siphoning [8], as previously discussed in Sections 1.4.3 and 1.4.5.

The possibility of employing CZE for preparative purposes for protein separations has been discussed from a theoretical viewpoint by Poppe and coworkers [16]. However, prior efforts to perform preparative protein separations by CZE have been hampered by protein adsorption. The interaction between positively charged proteins and the negatively charged silica surface leads to significant band broadening, poor migration

time reproducibility [17] and in severe cases irreversible adsorption of protein onto the capillary surface such that the protein never elutes from the capillary [18]. A detailed discussion on protein separation is present in Section 1.5.

Coating of the capillary walls is the most effective approach to eliminate the electrostatic attraction between cationic proteins and the silica surface. As shown in Section 1.6.3, double chained cationic surfactants, such as didodecyldimethylammonium bromide (DDAB), form semi-permanent wall coatings [19-21]. However, the stability of the DDAB coating was influenced by a number of experimental factors such that the coatings were unstable under some buffer conditions, as discussed in Chapter Two. As demonstrated in Chapter Three, a simple means to increase the stability of the surfactant bilayer was to use longer chained surfactants such as dimethylditetradecylammonium bromide ( $2C_{14}DAB$ ). For instance, the  $2C_{14}DAB$  coating showed no significant degradation over 415 capillary volumes ( $\sim 245 \mu L$ ) in a  $50 \mu m$  i.d. capillary [22]. In contrast, the DDAB coating rapidly degraded in less than 100 capillary volumes ( $\sim 59 \mu L$ ) under the same experimental conditions. Although  $2C_{18}DAB$  coating exhibit the highest stability among the surfactant used in the thesis, the separation time with this coating was more than 1.8 times larger than the separation time achieved by  $2C_{14}DAB$  coating, as shown in Chapter Three. Thus, the  $2C_{14}DAB$  coating is employed in this chapter to shorten the separation time.

This Chapter investigates the potential of wide bore surfactant coated capillaries for protein separations at preparative (picomole) scales using the  $2C_{14}DAB$  coating. The stability of  $2C_{14}DAB$  coatings with wide bore ( $100 \mu m$  i.d.) capillaries will be demonstrated. Further, as the  $2C_{14}DAB$  coatings eliminate adsorption on the capillary

walls, the influences of other broadening mechanisms that accompanied protein separations at large scales are also examined.

## 4.2 Experimental Section

### 4.2.1 Apparatus

The apparatus utilized in this Chapter was as described in Section 2.2.1.

Untreated fused-silica capillaries (Polymicro Technologies, Phoenix, AZ) with a total length of 58 cm (48 cm to the detector), an inner diameter (i.d.) of 100  $\mu\text{m}$  and an outer diameter of 363  $\mu\text{m}$  were used, unless otherwise noted.

### 4.2.2 Chemicals

Nanopure 18-M $\Omega$  ultra-pure water (Barnstead, Dubuque, IO, USA) was used to prepare all solutions. Potassium, sodium, lithium, tetraethylammonium (TEA), and tetrabutylammonium (TBA) phosphate buffers were prepared from phosphoric acid (BDH, Darmstadt, Germany), and the pH was adjusted using potassium, sodium, lithium (BDH), tetraethylammonium and tetrabutylammonium hydroxide (Aldrich, Milwaukee, WI, USA), respectively. Tris and Bis-tris phosphate buffers were prepared by titrating phosphoric acid with a 100 mM solution of ultra-pure tris(hydroxymethyl)aminomethane ( $\text{pK}_a = 8.1$ , Schwarz/Mann Biotech, Cleveland, OH) or bis(2-hydroxyethyl)iminotris(hydroxyl-methyl)methane ( $\text{pK}_a = 6.5$ , Sigma, St. Louis, MO, USA) to pH 7.0, respectively. The ionic strength of the buffers and the effective mobility of the buffer cations were computed using PeakMaster 5.1 [23].

The cationic surfactant dimethylditetradecylammonium bromide (2C<sub>14</sub>DAB) was used as received from Aldrich. The surfactant solution was prepared using the sonicate/

stir cycle method [24] at 50°C. This sonicate/stir cycle was repeated two times for 2C<sub>14</sub>DAB surfactant. HPLC-grade methanol (MeOH; Fisher, Fair Lawn, NJ, USA) was used to remove the bilayer coating from the capillary after each run. Standard proteins bovine heart cytochrome *c* (b-cyt *c*, C3131, M<sub>r</sub> = 12230.70 Da) and horse heart cytochrome *c* (h-cyt *c*, C7752, M<sub>r</sub> = 12360.46 Da) were used as received from Sigma. The theoretical *pI* predicted from their amino acid sequence are 9.52 and 9.59, respectively [7]. These proteins were dissolved in water at concentrations ranging from 0.05 to 50 g/L for each protein. Throughout this chapter, the protein concentrations are reported in g/L for each individual protein.

#### 4.2.3 Coating Procedure

To avoid hysteresis effects, fresh capillaries were used with each new buffer system. New capillaries were flushed with 1 M NaOH for 5 min under high pressure at 138 kPa (20 psi) and then with distilled water for 2 min at 138 kPa. The rinsing times were adjusted for capillaries with i.d. other than 100 μm. After the preconditioning steps, the capillary was rinsed at 138 kPa for 5 min with 0.1 mM surfactant-containing solution to coat the capillary. Finally, before sample injection and application of the electric field, the capillary was flushed with the running buffer for 1.5 min at 20.7 kPa (3 psi), corresponding to about 2 capillary volumes of buffer. After each separation, the capillary was rinsed with pure methanol for 3 min at 138 kPa to remove the surfactant coating from the capillary, followed by rinsing with 1 M NaOH for 3 min at 138 kPa and water for 2 min at 138 kPa. The capillary was then recoated with the surfactant solution, as described above. With wide bore capillaries, coating regeneration is critical before each run to guarantee optimum performance.

#### 4.2.4 Protein Separations

After coating the capillary, the protein sample was hydrodynamically injected into the capillary. Buffers based on phosphate at pH 7.0 were used in this study. This pH was found to be optimum for the separation of the cytochrome *c* mixture [25]. The applied voltage was –10 kV, unless otherwise stated. Direct UV-absorbance detection (Section 1.3.1) was performed at 214 nm for all buffers, except for Bis-tris phosphate where 254 nm was used.

The number of moles of protein injected was calculated by multiplying the protein concentration by the volume injected (Section 1.1). The volume of the sample plug was estimated using the Poiseuille's equation:

$$v_{inj} = \frac{\Delta P \pi r^4 \tau}{8\eta L_t} \quad (4.1)$$

where  $v_{inj}$  is the calculated injection volume ( $m^3$ ),  $\Delta P$  is the pressure gradient across the capillary length ( $Nm^{-2}$ ),  $r$  is the capillary radius in m,  $\tau$  is the time in seconds that the pressure is applied,  $L_t$  is the total capillary length in m, and  $\eta$  is the viscosity of the electrolyte ( $0.891 \times 10^{-3} Nsm^{-2}$  at 25 °C).

The peak asymmetry factor (B/A) was determined from the ratio of the right half (B) over left half (A) of the analyte peak at 10% of its maximum height, as illustrated in Figure 4.1. B/A equal to 1 corresponds to a symmetrical peak, less than 1 is a fronting peak (e.g. Figure 4.1), and greater than 1 is a tailing peak.

Resolution ( $R_s$ ) of the sample components was calculated from its definition, as previously discussed in Section 1.4 (eq. 1.19). The migration time reproducibility for wide bore capillary was calculated by performing 3 successive injections without recoating the capillary with the surfactant solution. Efficiencies were computed by the

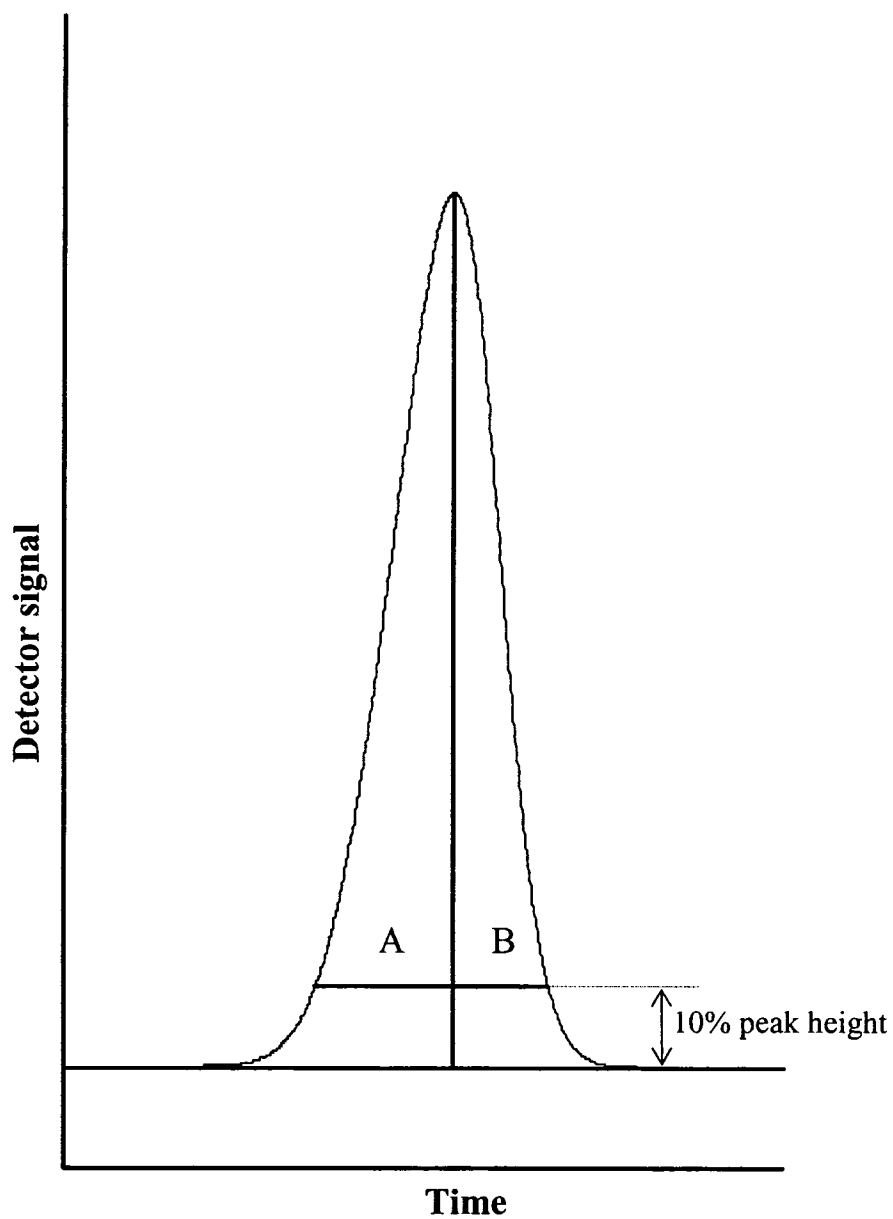


**Figure 4.1** Schematic diagram of a fronting peak showing parameters used to estimate the asymmetric factor ( $B/A$ ).  $A+B$  is the peak width at one-tenth of the maximum peak height.

P/ACE Station software, using the peak width at half-height method (eq. 2.3, Section 2.2.6).

## 4.3 Results and Discussion

### 4.3.1 Protein Separation under Trace Conditions

In theory, the efficiency ( $N$ ) in CZE separations of low concentrations of protein should be limited only by longitudinal diffusion [26], according to:

$$N = \frac{\mu_{app} V}{2D} \quad (4.2)$$

where  $\mu_{app}$  is the apparent electrophoretic mobility of the analyte under consideration,  $V$  is the applied voltage, and  $D$  is the analyte's diffusion coefficient. Thus, increasing the applied voltage will increase the separation efficiency. However, adsorption onto the capillary wall can severely broaden protein peaks, generate substantial tailing and even result in irreversible loss of protein [27-29], as discussed in Section 1.4.5. There are a number of approaches have been developed to eliminate protein adsorption (Section 1.6). Previously in Chapters Two and Three, it was demonstrated that bilayer coatings based on surfactants, such as DDAB [19-21] and 2C<sub>14</sub>DAB [22], yield high efficiency separations of proteins under trace conditions. For instance, efficiencies in excess of one million plates/m, have been reported for injections of 0.1 g/L of cationic proteins such as lysozyme, ribonuclease A,  $\alpha$ -chymotrypsinogen and cytochrome *c*. Furthermore, protein recoveries from bilayer coated capillaries are essentially quantitative [20, 22].

As shown in Figure 4.2 and Table 4.1, efficiencies of 0.80 million plates/m and peak asymmetry factors of 1.0 were achieved for short injections (~1% of the capillary length) of 0.05 g/L h-cyt *c* on a 25  $\mu$ m i.d. capillary. The high efficiency and absence of

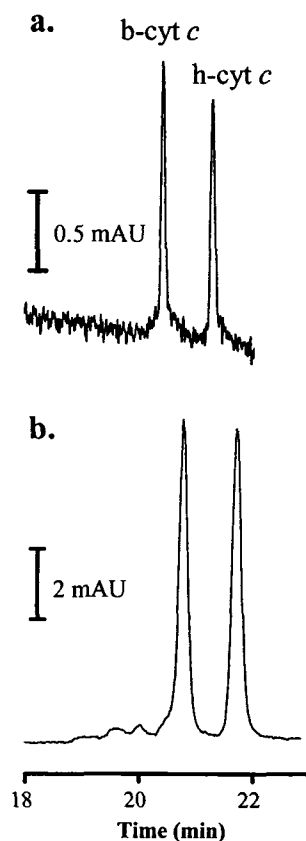


**Figure 4.2** Effect of capillary diameter on electropherograms of trace concentrations of b-cyt *c* and h-cyt *c* using 2C<sub>14</sub>DAB coated capillaries: **a.** 25 µm; and **b.** 100 µm.

**Experimental conditions:** Capillary length 58 cm (48 cm to the detector); the injection plug length was kept constant at 6.2 mm; the analyte was dissolved in water at 0.05 g/L; 50 mM lithium phosphate buffer at pH 7.0; voltage at -10 kV; and  $\lambda$ , 214 nm. The injection condition and the rinsing times were adjusted for the different capillary dimensions.

**Table 4.1** Peak efficiency and peak asymmetry factor of h-cyt *c* separated in 25, 50 and 100 µm i.d. capillaries coated with 2C<sub>14</sub>DAB.<sup>a</sup>

Capillary i.d µm	Current µA	Injection volume nL	Moles of analyte pmol	<i>N</i> Plates/m	B/A
25	-4.5	3	0.012	800 000	1.0
50	-18	12	0.049	700 000	0.97
100	-72	48	0.19	130 000	1.0

<sup>a</sup> **Experimental conditions:** as in Figure 4.2.

the peak tailing indicates that adsorption has been effectively eliminated by the 2C<sub>14</sub>DAB coating. Also, excellent migration time reproducibility (< 0.5% RSD for 10 successive injections without coating regeneration, as shown in Chapter Three) is an additional operational indicator of low irreversible protein adsorption. Hence, the 2C<sub>14</sub>DAB coating successfully minimizes the broadening due to analyte/wall interaction and so is used for all further studies herein.

Ultimately, wider bore (100  $\mu\text{m}$  i.d.) capillaries will be used to maximize loading for the preparative protein separations. The main advantage of increasing the capillary i.d. is to increase the sample loading by increasing the volume of the injection plug without changing the plug length. Switching the capillary i.d. from 25 to 100  $\mu\text{m}$  increases the sample plug volume by 16-fold. However, the current generated inside the capillary also increases 16-fold. Indeed, as the capillary i.d. increases from 25 to 100  $\mu\text{m}$ , the peak efficiency under trace conditions (0.05 g/L of h-cyt *c*) decreases from 0.8 million to 0.13 million plates/m, as illustrated in Figure 4.2 and Table 4.1. Ohm's law plots confirm that the Joule heating is effectively dissipated in the 25  $\mu\text{m}$  i.d. capillary but is significant within the 100  $\mu\text{m}$  i.d. capillary, as discussed in Section 1.4.3.

Adsorption onto the capillary wall is not significant, as indicated by the peak asymmetry factor being  $\sim 1$  regardless of the capillary diameter (Table 4.1). Thus, the decrease in efficiencies in wide bore capillary is due to Joule heating [30-32]. Nonetheless, the h-cyt *c* and b-cyt *c* peaks were well resolved ( $R_s > 2.0$ ), as shown in Figure 4.2. As will be demonstrated in Section 4.3.2, the band broadening under preparative conditions is dominated by factors other than Joule heating.

Finally, another consequence of using wider capillaries is a reduction in the stability of the bilayer coating (Sections 2.3.3 and 3.3.2). With surfactant-based coatings, the coating gradually degrades when the bulk concentration of the surfactant is less than the cmc of the surfactant. Once the bulk solution is saturated with surfactant (bulk concentration equals the cmc), the degradation process stops. The cmc of long chained surfactants, such as  $2C_{14}DAB$ , and the volume of 25 and 50  $\mu\text{m}$  i.d. capillaries are sufficiently low that  $2C_{14}DAB$  coatings are stable for more than 10 successive without recoating the capillary (Section 3.3.5). However, wide bore capillaries substantially increase the volume of solution that must be saturated with surfactant and so the coating stability is diminished [19]. Migration times in the wide bore capillary were stable (1.0% RSD) for 3 successive runs without refreshing the coating between runs, but thereafter showed a gradual drift indicating that the coating was degrading. Thus, with the 100  $\mu\text{m}$  i.d. capillaries used herein, the capillary was regenerated before each run to ensure optimum performance.

#### **4.3.2 Effect of Analyte Concentration under Preparative Conditions**

Figure 4.3 shows the effect of increasing the protein concentration from 0.05 to 10 g/L on the peak shape. The sample plug length was maintained constant at 6.2 mm (1.1% of the total capillary length). At low concentrations ( $\leq 1$  g/L) the peaks were close to Gaussian, with asymmetry factors between 1.1 and 0.9. However, at higher sample concentrations ( $> 1$  g/L) the efficiency decreases significantly and the peaks become increasingly fronted, as shown in Figure 4.3 and Table 4.2. For instance, upon increasing the analyte concentration from 0.05 to 10 g/L, the efficiency decreased sharply from

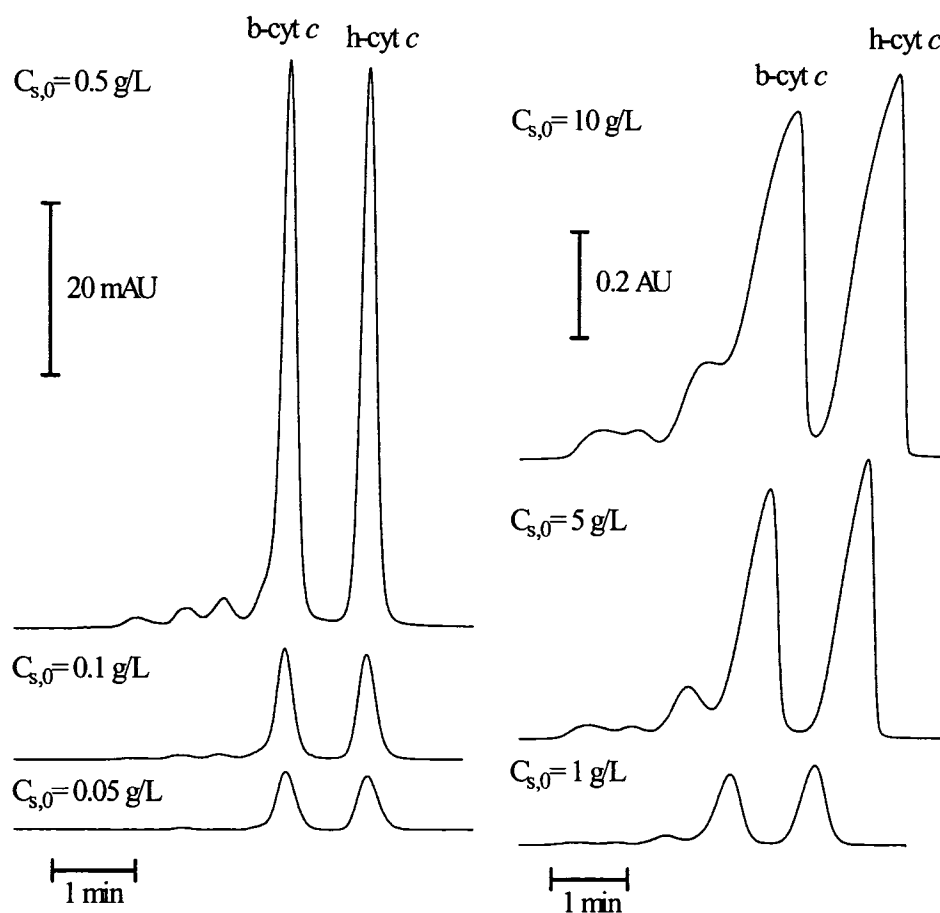


**Figure 4.3** Electropherograms of b-cyt *c* and h-cyt *c* in 100  $\mu\text{m}$  capillary i.d. using  $2\text{C}_{14}\text{DAB}$  coatings at different sample concentrations. The concentration of each protein are reported for each electropherogram in the figure. **Experimental conditions:** capillary length 58 cm (48 cm to the detector); hydrodynamic injection at 3.4 kPa for 3 s; the analytes were dissolved in water; 50 mM lithium phosphate buffer at pH 7.0; voltage at  $-10$  kV; and  $\lambda$ , 214 nm. The capillary was initially rinsed with 0.1 mM  $2\text{C}_{14}\text{DAB}$  solution dissolved in the running buffer followed by rinsing with the running buffer.

**Table 4.2** Peak efficiency and peak asymmetry factor of h-cyt *c* at different concentrations separated using 100  $\mu\text{m}$  i.d. capillary coated with 2C<sub>14</sub>DAB.<sup>a</sup>

Analyte Conc. g/L	Analyte injected pmol	<i>N</i> Plates/m	B/A
0.05	0.19	130 000	1.0
0.1	0.39	125 000	1.1
0.2	0.79	105 000	0.95
0.5	2.0	115 000	0.94
1	3.9	100 000	0.90
2	7.9	65 000	0.68
5	20	30 000	0.38
10	40	20 000	0.24

<sup>a</sup> Experimental conditions: as in Figure 4.3.

130 000 to 20 000 plates/m, with the highest concentrations yielding essentially triangular fronting peaks, B/A = 0.24 (Table 4.2).

The triangular peak shape indicates that the broadening at higher analyte concentrations is dominated by electromigration dispersion [33, 34]. As discussed in Section 1.4.4, electromigration dispersion (EMD) results from differences in the local electric field strength in the analyte zone relative to that in the normal buffer [35]. EMD originates from the difference in the effective mobilities between the analyte and the buffer co-ion, and becomes more significant at higher sample concentrations [33]. When the mobility of the analyte molecules is less than that of the buffer co-ions, the electric field within the sample zone increases at higher analyte concentrations [34]. In our work, the effective mobility of h-cyt *c* is  $+0.68 \times 10^{-4} \text{ cm}^2/\text{Vs}$ , which is substantially less than

that of lithium ( $+3.0 \times 10^{-4} \text{ cm}^2/\text{Vs}$ ). As a result, the velocity of the h-cyt c protein becomes faster in the region with higher protein concentration, and thus a sharp front side is formed in the migration direction. The reversed EOF sweeps the analyte zone to the detector side resulting in the fronting triangular peak.

Based on the discussion in Section 1.4.4, the plate height due to electromigration dispersion ( $H_{\text{EMD}}$ ) is proportional to the analyte injection length ( $l_{\text{inj}}$ ), the sample-to-buffer concentration ratio, and the electromigration dispersion factor ( $k_{\text{EMD}}$ ), as described by eq. 1.35. The electric field strength ( $E$ ) has no effect on the electromigration dispersion as the electric field increases proportionally with the analyte apparent velocity ( $v_{\text{app}}$ ), i.e.,

$$\frac{v_{\text{app}}}{E} = \mu_{\text{app}} \quad (4.3)$$

where  $\mu_{\text{app}}$  is the analyte apparent mobility, and it is constant at constant buffer conditions and temperature. Therefore,

$$H_{\text{EMD}} = \frac{2El_{\text{inj}}C_{\text{s},0}|k_{\text{EMD}}|}{9c_{\text{B}}v_{\text{app}}} = \frac{2l_{\text{inj}}C_{\text{s},0}|k_{\text{EMD}}|}{9c_{\text{B}}\mu_{\text{app}}} \quad (4.4)$$

where  $C_{\text{s},0}$  is the initial analyte concentration, and  $c_{\text{B}}$  is the buffer concentration. In addition, the injection plug length was kept constant at 6.2 mm (1.1% of the total capillary length) to avoid any extra broadening due to injection (Section 1.4.1.1).

In preparative separations, the sample concentration must be kept as high as possible. Thus, other means must be found to reduce the electromigration dispersion. Based on eq. 4.4,  $H_{\text{EMD}}$  can be reduced by increasing the buffer concentration and/or reducing the mobility difference between the analyte and buffer co-ion. These factors will be explored in Sections 4.3.3 and 4.3.4.

### 4.3.3 Effect of Buffer Concentration

As indicated by eq. 4.4, buffer concentration has a critical effect on the electromigration dispersion [10, 33]. Figure 4.4 and Table 4.3 show the effect of increasing the concentration of lithium phosphate (pH 7.0) buffer for preparative (40 pmol of each protein) injections. At low buffer concentrations (10 mM), the protein peaks are very broad and strongly fronting, with asymmetry factors less than 0.1. Not surprisingly, the peaks were not well resolved ( $R_s < 0.75$ ). Increasing the buffer concentration to 100 mM improves the efficiency of h-cyt *c* to 30 000 plates/m and the asymmetry factor to 0.38. At a buffer concentration of 150 mM, the peak shape was improved (B/A of 0.5-0.6); however, the peak efficiency decreased to 22 000 plates/m due to Joule heating. Additionally, the reversed EOF displays the expected inverse dependence on the buffer ionic strength (Table 4.3), causing the separation times to increase [36].

As shown by eq. 4.4, the  $H_{EMD}$  is directly related to the sample-to-buffer concentration ratio ( $C_{s,0}/c_B$ ). At low buffer concentration, the  $C_{s,0}/c_B$  is high due to the large sample concentration needed for preparative purposes. As a result, electromigration dispersion is significant. Increasing the buffer concentration decreases the  $C_{s,0}/c_B$ , which in turn lowers the  $H_{EMD}$ , and thus more symmetrical peaks are produced. As shown in Figure 4.4 and Table 4.3, the enhancement in efficiency at a buffer concentration of 100 mM is due to the reduction of the electromigration dispersion. However, increasing the buffer concentration increases the electric current within the capillary causing substantial Joule heating peak-broadening. In lithium phosphate buffer at 150 mM, for instance, the peak asymmetry factor was 0.5-0.6, but the peak efficiency was less than that observed at

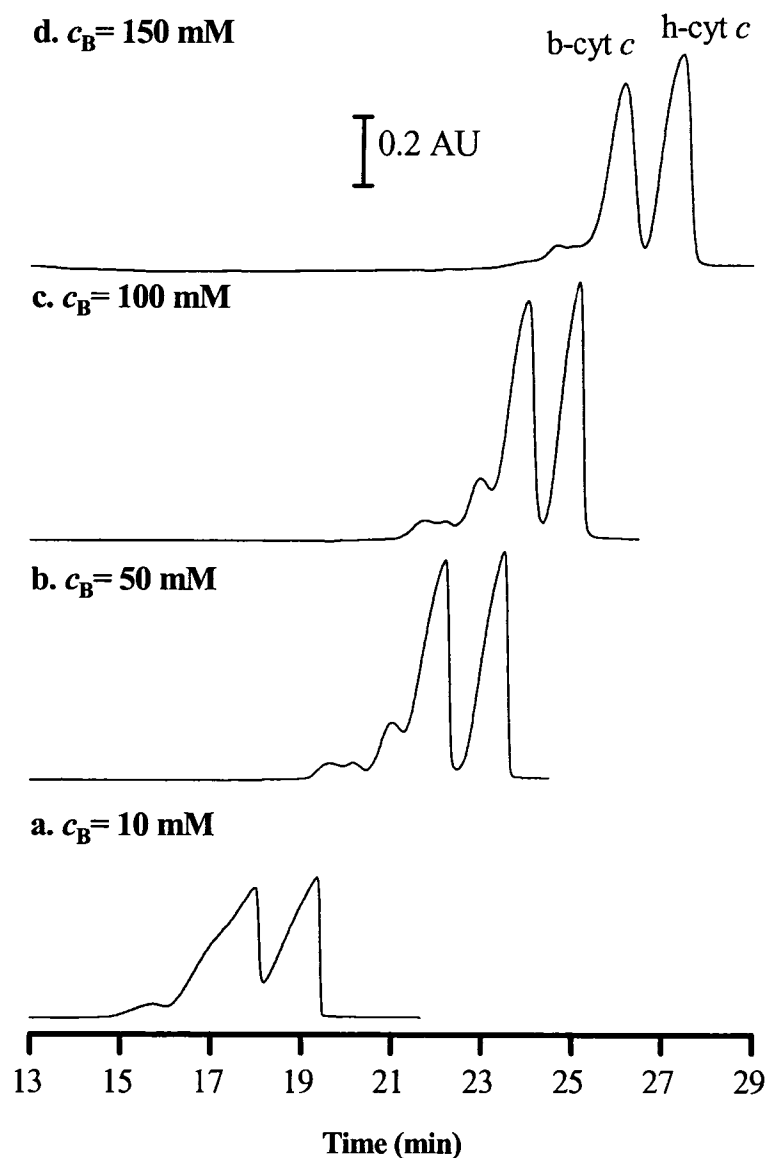


**Figure 4.4** Effect of buffer concentration on electropherograms of b-cyt *c* and h-cyt *c* using a  $2C_{14}DAB$  coating. The buffer concentration for each electropherogram in the figure. **Experimental conditions:** 58 cm  $\times$  100  $\mu$ m i.d. capillary (48 cm to the detector); protein sample was dissolved in water; sample concentration of 10 g/L of each protein; hydrodynamic injection at 3.4 kPa for 3 s (40 pmol of each protein); lithium phosphate buffer at pH 7.0; applied voltage at  $-10$  kV; and  $\lambda$ , 214 nm.

**Table 4.3** Effective mobility of buffer co-ion, effective electrophoretic mobility, and peak asymmetry factor of b-cyt *c* and h-cyt *c* at different buffer concentrations separated by 100  $\mu\text{m}$  i.d. capillary using 2C<sub>14</sub>DAB coating.<sup>a</sup>

Buffer conc. mM	$\mu_{\text{co-ion}}^b$ $\times 10^4$ $\text{cm}^2/\text{Vs}$	$\mu_{\text{EOF}}$ $\times 10^4$ $\text{cm}^2/\text{Vs}$	b-cyt <i>c</i>			h-cyt <i>c</i>		
			$\mu$ $\times 10^4$ $\text{cm}^2/\text{Vs}$	<i>N</i> Plates/m	B/A	$\mu$ $\times 10^4$ $\text{cm}^2/\text{Vs}$	<i>N</i> Plates/m	B/A
10	3.5	3.7	1.1	2 500	<0.10	1.2	5 000	<0.10
50	3.0	2.7	0.57	15 000	0.23	0.68	20 000	0.24
100	2.7	2.4	0.42	25 000	0.38	0.52	30 000	0.39
150	2.5	2.1	0.34	20 000	0.60	0.42	22 000	0.50

<sup>a</sup> **Experimental conditions:** as in Figure 4.4.

<sup>b</sup> The effective mobility of the buffer co-ions were computed based on PeakMaster 5.1 [23].

100 mM buffer (Figure 4.4 and Table 4.3). At high buffer concentration, the Joule heating and electromigration dispersion work antagonistically to each other.

#### 4.3.4 Effect of Buffer co-ion

The effect of the nature of buffer co-ion was studied using a series of pH 7.0 phosphate buffers with a total ionic strength of 105 mM. The amount of protein injected was fixed at 40 pmol for each protein. The shape of the protein peaks was significantly affected by the buffer co-ion (Figure 4.5 and Table 4.4). With a high mobility co-ion as previously discussed, the electromigration dispersion originates from the difference in the effective mobility between the analyte and buffer co-ion. Reducing the mobility difference decreases the  $k_{\text{EMD}}$  which in turn reduces the plate height, as shown in eq. 4.4.

The value of  $k_{\text{EMD}}$  can be calculated from the electrophoretic mobilities of the buffer constituents and the analyte ions according to [16, 37]:

$$k_{\text{EMD}} = \frac{(\mu_a - \mu_s)(\mu_b - \mu_s)}{(-\mu_a + \mu_b)\mu_s} \quad (4.5)$$

where  $\mu_a$ ,  $\mu_b$  and  $\mu_s$  are the mobilities of the buffer co-ion, the buffer counter-ion and the sample, respectively. For all co-ions used in this study, except for Bis-tris<sup>+</sup>, the effective mobility of the analyte is lower than the mobility of the buffer co-ion (Table 4.5), and so fronting peaks are expected. Since the mobility of the Bis-tris co-ion is less than the effective mobility of the analyte, peak tailing was expected. Surprisingly, fronting peaks (B/A=0.85) were observed. Regardless, using a buffer co-ion whose mobility matches that of the proteins reduces the EMD, resulting in the improvement in the peak shape and efficiency in preparative separations. However, solely focusing on the mobility of the buffer co-ion is not sufficient, as the buffer co-ion can cause other adverse effects. For instance, the hydrophobic co-ion tetrabutylammonium (TBA<sup>+</sup>) has a lower mobility than Li<sup>+</sup> (Table 4.4) and so should cause less electromigration dispersion. Indeed, the peak shapes were more symmetrical with TBA<sup>+</sup> than Li<sup>+</sup>. However, use of TBA<sup>+</sup> also dramatically decreased efficiency (< 7 000 plates/m, Table 4.4) and reduced the stability of the bilayer (migration time reproducibility was 20% RSD for 3 successive runs). In contrast, the stability of the bilayer was higher with the hydrophilic Bis-tris<sup>+</sup>, with a migration time reproducibility of 1.0% RSD (n = 3).

#### 4.3.5 Maximizing sample loading

An additional advantage of using low mobility buffer ions is that they reduce the electric current and thus decrease Joule heating. For example, the current generated

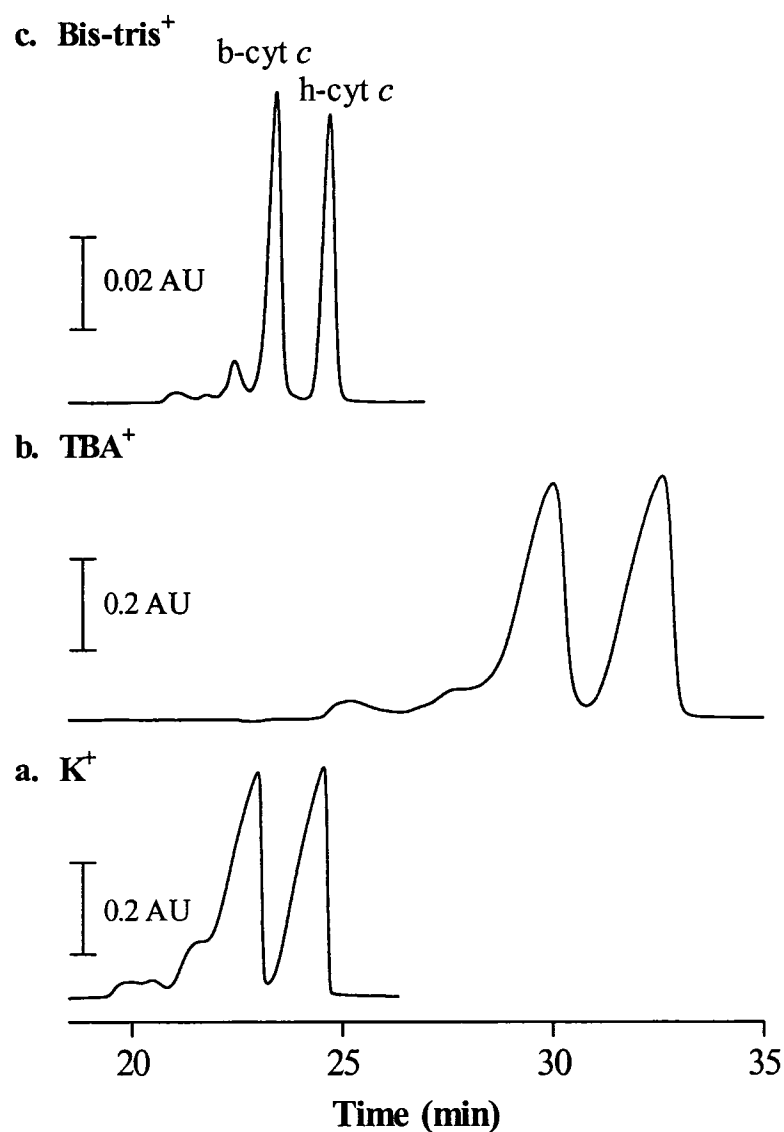


**Figure 4.5** Effect of buffer co-ion on electropherograms of b-cyt *c* and h-cyt *c* using 2C<sub>14</sub>DAB coatings at different buffer co-ions. The type of the buffer co-ion is reported for each electropherogram in the figure. **Experimental conditions:** 58 cm × 100 μm i.d. capillary (48 cm to the detector); protein sample was dissolved in water; sample concentration of 10 g/L of each protein; hydrodynamic injection at 3.4 kPa for 3 s (40 pmol); phosphate based buffer at ionic strength of 105 mM and pH 7.0; voltage at -10 kV; and λ, 214 nm for K<sup>+</sup> and TBA<sup>+</sup> but 254 nm for Bis-tris<sup>+</sup> buffer co-ions.

**Table 4.4** Effective mobility of buffer co-ion, effective electrophoretic mobility, and peak asymmetry factor of b-cyt *c* and h-cyt *c* with different buffer co-ions separated by 100  $\mu\text{m}$  i.d. capillary using 2C<sub>14</sub>DAB coating.<sup>a</sup>

Buffer co-ion	$\mu_{\text{co-ion}}^b \times 10^4 \text{ cm}^2/\text{Vs}$	Current ( $\mu\text{A}$ )	b-cyt <i>c</i>			h-cyt <i>c</i>		
			$\mu \times 10^4 \text{ cm}^2/\text{Vs}$	<i>N</i> Plates/m	B/A	$\mu \times 10^4 \text{ cm}^2/\text{Vs}$	<i>N</i> Plates/m	B/A
K <sup>+</sup>	6.3	-123	0.51	8 000	0.10	0.65	11 000	0.11
Na <sup>+</sup>	4.1	-92	0.53	12 000	0.17	0.65	16 000	0.18
Li <sup>+</sup>	3.0	-72	0.57	15 000	0.23	0.68	20 000	0.24
TEA <sup>+</sup>	2.4	-67	0.50	7 500	0.20	0.61	9 500	0.21
TBA <sup>+</sup>	1.6	-58	0.46	5 500	0.28	0.60	7 000	0.34
Tris <sup>+</sup>	1.9	-53	0.67	35 000	0.43	0.78	45 000	0.44
Bis-tris <sup>+</sup>	0.48	-45	0.60	60 000	0.80	0.71	70 000	0.85

<sup>a</sup> **Experimental conditions:** as in Figure 4.5.

<sup>b</sup> The effective mobility of the buffer co-ions were computed based on PeakMaster 5.1 [23].

inside the capillary with Bis-tris<sup>+</sup> (-45  $\mu\text{A}$ ) was 3-fold lower than that with K<sup>+</sup> (-123  $\mu\text{A}$ ), as shown in Table 4.4. This permits the application of higher electric fields to speed up the separation. Besides, using buffers with low ion mobilities makes it possible to increase the buffer concentration to reduce the EMD. The peak asymmetry factor improved from 0.85 to 0.91 upon increasing the Bis-tris phosphate buffer concentration from 50 to 100 mM, as shown in Figure 4.7 and Table 4.5. More importantly, the resolution increased from 1.8 to 2.0, and thus more sample could be injected and still maintain reasonable resolution ( $R_s \geq 1.4$ ). Elevating the sample concentration to 40 g/L (160 pmol of each protein), the resolution was reduced from 2.0 to 1.4 (Figure 4.7 and

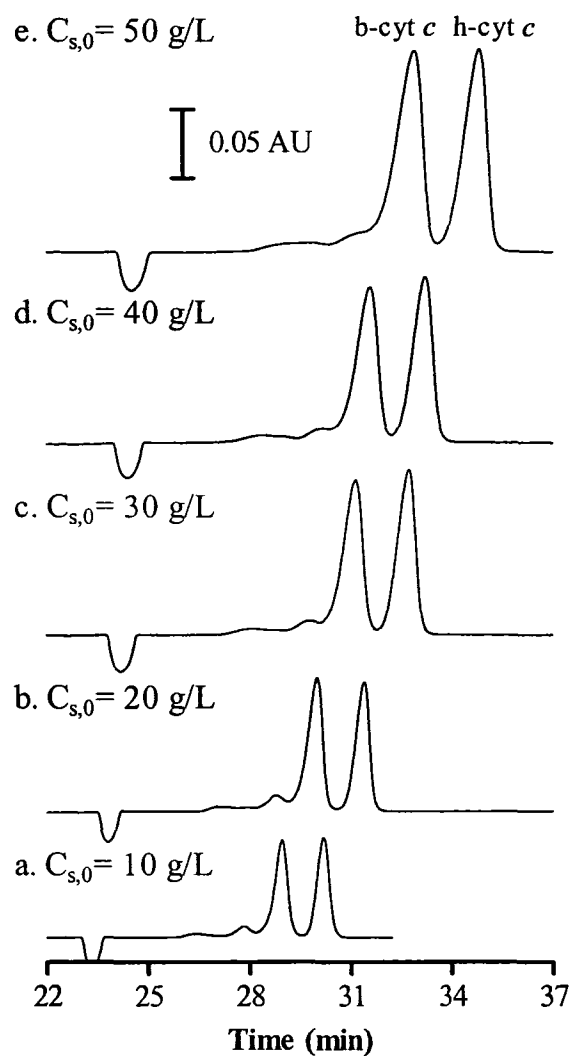


**Figure 4.6** Effect of sample concentration on preparative CZE separations of b-cyt *c* and h-cyt *c* using  $2C_{14}$ DAB coatings. The concentration of each protein was reported for each electropherogram in the figure. **Experimental conditions:** 58 cm  $\times$  100  $\mu$ m i.d. capillary (48 cm to the detector); applied voltage at  $-10$  kV; protein sample was dissolved in water; hydrodynamic injection at 3.4 kPa for 3 s; 100 mM Bis-tris phosphate buffer at pH 7.0; and  $\lambda$ , 254 nm.

**Table 4.5** Sample amount of each protein, resolution, and peak asymmetry factor of b-cyt *c* and h-cyt *c* separated by 100  $\mu\text{m}$  i.d. capillary using 2C<sub>14</sub>DAB coating at different sample concentrations.<sup>a</sup>

Sample conc. (g/L)	Sample injected (pmol)	Resolution	b-cyt <i>c</i>		h-cyt <i>c</i>	
			<i>N</i> Plates/m	B/A	<i>N</i> Plates/m	B/A
10	40	2.0	75 000	0.88	86 000	0.91
20	80	1.8	50 000	0.84	54 000	0.86
30	120	1.6	30 000	0.76	36 000	0.81
40	160	1.4	24 000	0.67	30 000	0.71
50	200	1.2	15 000	0.60	20 000	0.64

<sup>a</sup> **Experimental conditions:** as in Figure 4.6.

Table 4.5). At a sample loading of 200 pmol (sample concentration of 50 g/L), the resolution decreased to 1.2, and cross contamination between the two proteins became significant. Therefore, under these conditions the maximum loading capacity of sample for a single run was 160 pmol for isolation of protein with high purity (> 99 %). This amount of sample loading corresponded to 2.0  $\mu\text{g}$  of each protein, about seven folds more than what was injected in preparative CIEF with 100  $\mu\text{m}$  i.d. capillaries [6], and more than 30-fold compared to the mass of peptides isolated by past preparative CZE methods [9].

#### 4.4 Conclusions

Capillary electrophoresis has successfully been used for protein separation at preparative scales. The problem of low protein recoveries in CE was solved by using surfactant-based coatings. Upon rinsing the capillary with 2C<sub>14</sub>DAB solution, the

surfactant molecules formed a temporally stable bilayer coating which significantly minimized the interaction between the cationic proteins and the capillary wall and thus essentially eliminating protein adsorption. For preparative purposes, the sample loading was increased by utilizing a wide bore capillary (100  $\mu\text{m}$  i.d.). A further increase in the sample loading was also achieved by increasing the sample concentration. However, this approach is accompanied by broadening due to electromigration dispersion (EMD). The buffer concentration and the choice of the buffer co-ion have critical effects on the EMD. Matching the mobilities between the analyte and the buffer co-ion highly reduces the EMD, and near symmetric peak shapes are observed. Optimizing the experimental conditions such as capillary i.d., buffer concentration and buffer co-ions, it is possible to inject as high as 160 pmol of protein, 3250 fold more than what is normally injected in 50  $\mu\text{m}$  i.d. capillaries.

## 4.5 References

- [1] Rabilloud, T., *Proteomics* 2002, 2, 3-10.
- [2] Wang, Y., Balgley, B. M., Rudnick, P. A., Lee, C. S., *J. Chromatogr. A* 2005, 1073, 35-41.
- [3] Keller, B. O., Wang, Z., Li, L., *J. Chromatogr. B* 2002, 782, 317-329.
- [4] Hjertén, S., *J. Chromatogr.* 1985, 347, 191-198.
- [5] Kilár, F., *Electrophoresis* 2003, 24, 3908-3916.
- [6] Minarik, M., Foret, F., Karger, B. L., *Electrophoresis* 2000, 21, 247-254.
- [7] Gasteiger, E., Hoogland, C., Gattiker, A., Duvaud, S., Wilkins, M. R., Appel, R. D., Bairoch, A., in: Walker, J. M. (Ed.), *The Proteomics Protocols Handbook*, Humana Press Inc., Totowa, NJ 2005, pp. 571-607.
- [8] Yin, H., Keely-Templin, C., McManigill, D., *J. Chromatogr. A* 1996, 744, 45-54.
- [9] Gilges, M., Kleemlss, M. H., Schomburg, G., *Anal. Chem.* 1994, 66, 2038-2046.
- [10] Lee, H. G., Desiderio, D. M., *Anal. Chim. Acta* 1999, 383, 79-99.
- [11] Altria, K. D., Dave, Y. K., *J. Chromatogr.* 1993, 633, 221-225.
- [12] Rose, D. J., Jorgenson, J. W., *J. Chromatogr.* 1988, 438, 23-34.
- [13] Lee, H. G., Desiderio, D. M., *J. Chromatogr. B* 1994, 662, 35-45.
- [14] Valko, I. E., Porras, S. P., Riekkola, M.-L., *J. Chromatogr. A* 1998, 813, 179-186.
- [15] Jussila, M., Palonen, S., Porras, S. P., Riekkola, M.-L., *Electrophoresis* 2000, 21, 586-592.
- [16] Cifuentes, A., Xu, X., Kok, W. T., Poppe, H., *J. Chromatogr. A* 1995, 716, 141-156.
- [17] Lauer, H. H., McManigill, D., *Anal. Chem.* 1986, 58, 166-170.

- [18] Towns, J. K., Regnier, F. E., *Anal. Chem.* 1991, 63, 1126-1132.
- [19] Yassine, M. M., Lucy, C. A., *Anal. Chem.* 2004, 76, 2983-2990.
- [20] Baryla, N. E., Melanson, J. E., McDermott, M. T., Lucy, C. A., *Anal. Chem.* 2001, 73, 4558-4565.
- [21] Melanson, J. E., Baryla, N. E., Lucy, C. A., *Anal. Chem.* 2000, 72, 4110-4114.
- [22] Yassine, M. M., Lucy, C. A., *Anal. Chem.* 2005, 77, 620-625.
- [23] Gas, B., Jaros, M., Hruska, V., Zuskova, I., Stedry, M., *LC GC Eur.* 2005, 18, 282-288.
- [24] Leonenko, Z. V., Carnini, A., Cramb, D. T., *Biochim. Biophys. Acta* 2000, 1509, 131-147.
- [25] Yeung, K. K.-C., Kiceniuk, A. G., Li, L., *J. Chromatogr. A* 2001, 931, 153-162.
- [26] Jorgenson, J. W., Lukacs, K. D., *Anal. Chem.* 1981, 53, 1298-1302.
- [27] Schure, M. R., Lenhoff, A. M., *Anal. Chem.* 1993, 65, 3024-3037.
- [28] Doherty, E. A. S., Meagher, R. J., Albarghouthi, M. N., Barron, A. E., *Electrophoresis* 2003, 24, 34-54.
- [29] Ghosal, S., *Anal. Chem.* 2002, 74, 771-775.
- [30] Grushka, E., McCormick, R. M., *J. Chromatogr.* 1989, 471, 421-428.
- [31] Jones, A. E., Grushka, E., *J. Chromatogr.* 1989, 466, 219-225.
- [32] Xuan, X., Li, D., *Electrophoresis* 2005, 26, 166-175.
- [33] Xu, X., Kok, W. T., Poppe, H., *J. Chromatogr. A* 1996, 742, 211-227.
- [34] Beckers, J. L., *J. Chromatogr. A* 1995, 693, 347-357.
- [35] Foret, F., Deml, M., Bocek, P., *J. Chromatogr.* 1988, 452, 601-613.
- [36] Kennedy, R. T., *Anal. Chimica Acta* 1999, 400, 163-180.

- [37] Mikkers, F. E. P., Everaerts, F. M., Verheggen, T. P. E. M., *J. Chromatogr.* 1979, 169, 1-10.

## **CHAPTER FIVE: Off-line Coupling of Preparative Capillary Zone Electrophoresis with Microwave-assisted Acid Hydrolysis for Protein Characterization**

### **5.1 Introduction**

Two-dimensional gel electrophoresis (2D-gel) followed by mass spectrometric identification of proteolytic digestions is currently the workhorse in proteomics [1-4]. However, 2D-gel electrophoresis is time-consuming, labor-intensive, difficult-to-automate and has low reproducibility [5]. Moreover, protein extraction from the gel is not straightforward and requires special methods, which further increase the analysis time. For instance, passive elution requires 4-8 hours to extract the protein from the gel [6], while micro-electroelution requires at least 2 hours [7]. Additionally, all methods of protein extraction from 2D-gels suffer from sample loss [2]. More importantly, sodium dodecyl sulfate (SDS; ~2%) binds extensively to proteins, (approximately one SDS for every two amino acids [8-10]). Thus, it is not possible to extract the whole protein from the gel in its native form [11], and the extracted sample must be cleaned to remove or minimize the amount of the SDS bound to the isolated protein. This sample cleaning step prior the MS analysis is critical to improve the MS signal as the presence of the SDS (< 0.05%) significantly degrades both signal-to-noise ratio and resolution [12-14]. Finally, enzymatic digestion of the protein requires at least 12 hours before the resultant peptide mixture can be analyzed by MS [15, 16].

Capillary zone electrophoresis (CZE) is potentially a good candidate for preparative operations in particularly for proteomic applications. Separations in CZE are

performed in simple buffer solution. Thus, it is possible to purify and collect proteins from a mixture without altering their activity. However, isolation of microscale amounts of separated protein components in CZE is hampered by its small format. Typically, less than 100 femtomoles of protein is injected onto a 50  $\mu\text{m}$  i.d. capillary [17]. Multiple sequential fraction collection can be used to increase the amount of collected analyte [18]. However, this approach is time consuming and impractical.

The introduction of matrix-assisted laser desorption/ionization mass spectrometry (MALDI-MS) [19, 20] has provided a powerful approach for the analysis of small protein amounts and expanded the utility of mass spectrometry to proteomic applications. For instance, mass determination for proteins by MALDI-MS requires less than 100 femtomoles. Coupling of CE with MALDI-MS can be performed either by direct depositing the CE eluent onto the MALDI target [21, 22], or collecting CE fractions and then performing off-line MALDI-MS analysis [17, 23, 24]. The detection limits reported for proteins with CE-MALDI-MS were 0.25 femtomoles by direct sample deposition and 1.2 femtomoles by off-line fraction collection, respectively [17, 21]. Fraction collection approach is more advantageous since a portion of the isolated fractions can be used for mass determination by MALDI, and the rest can be utilized for protein characterization.

Microwave-assisted acid hydrolysis (MAAH) is a simple and rapid method for generating a polypeptide ladder for peptide sequencing of a protein [25, 26]. In MAAH/MALDI, the protein is subjected to a brief (several minutes) acid hydrolysis with the assistance of microwave irradiation. Subsequent mass analysis of the resultant polypeptide ladder enables that each amino acid can be read out from only one spectrum. MAAH requires 10-50 pmol of pure protein [27]. The detection sensitivity of the

MAAH/MALDI technique for small proteins (< 14000 Da) was less than one pmol [26]. Thus, given the loadings demonstrated for preparative CE in Chapter Four, the off-line coupling of CE with MAAH/MALDI has the potential to separate and characterize protein in a short time. In addition, the whole procedure has no complicated steps and is easy to operate.

In this chapter, I investigate the collection and isolation of picomole quantities of pure protein using a commercial CE instrument and MAAH for protein characterization. MALDI/TOF MS was employed to test the purity of the collected fraction.

## 5.2 Background

Previously in Chapter Four, I demonstrated that CE can be utilized for preparative protein separations in 100  $\mu\text{m}$  i.d. capillaries. Semi-permanent double chained cationic surfactant coatings were applied to prevent protein adsorption onto the capillary wall [28-31]. The separation of high concentrations of proteins necessitated increasing the buffer concentration and choosing a buffer co-ion that matched the protein mobility. Under optimal experimental conditions, sample loadings of 40 and 160 pmol of each protein with separation resolution ( $R_s$ ) of 1.4 was achieved using lithium and Bis-tris phosphate buffer, respectively.

In commercial CE instruments, two approaches can be applied to collect the analyte band from the capillary: hydrodynamic [32] and electro-kinetic fractionation [33]. In both techniques, the protein is injected and migrates under the application of an applied electric field, as in a typical CE separation. The voltage is terminated when the protein reaches the outlet of the capillary. In hydrodynamic fractionation, a low pressure

is applied to collect the analyte band in a vial. A disadvantage of this approach is that the separation resolution may significantly deteriorate as a result of the laminar flow generated inside the capillary during collection. In electro-kinetic fractionation, the capillary outlet as well as the electrode must remain in contact with electrolyte solution in the collecting vial to maintain the electric field during fractionation. The analyte band is transported into the collection vial by electromigration of the analyte. As a result of the uniform migration velocities generated by the applied voltage, the separation resolution between the sample components is maintained during fractionation [17, 34].

Both of these techniques require the separation be interrupted before performing the fraction collection. Special instrumentation that enables fraction collection to be performed without interrupting the applied voltage has been described in the literature. For instance, use of an on-column frit allows the electric contact to be maintained during collection [35]. Huang and Zare used such a system to avoid external dilution by buffer in the collecting vial. Alternatively, the electric contact can be maintained during isolation using coaxial sheath-flow, where a stream of fluid flows around the capillary outlet [36]. The analyte exiting from the capillary were transported to the collection vial by the sheath liquid flow. Weinmann *et al.* used such a system for the CE-MALDI-MS analysis of peptides and proteins. Recently, Kobayashi *et al.* [37] employed free flow zone electrophoresis in a 60- $\mu\text{L}$  microchamber (6.5 mm  $\times$  35 mm  $\times$  30  $\mu\text{m}$ ) for collection and isolation of pure fractions from a cytochrome *c*/myoglobin mixture. The free flow electrophoresis has the advantage of continuous collection of analytes. However, the resolution was much lower than the corresponding CE separation [38]. Unfortunately, all of these approaches require special alteration of the instrumentation.

## 5.3 Experimental Section

### 5.3.1 Apparatus

A Beckman-Coulter P/ACE™ MDQ instrument (Fullerton, CA) equipped with a UV absorbance detector was used for all protein separations and fraction collection. Proteins were detected using direct UV-absorption (Section 1.3.1) at 214 nm, unless otherwise stated. Untreated fused-silica capillaries (Polymicro Technologies, Phoenix, AZ) with a total length of 58.0 cm (48.0 cm to the detector), an inner diameter (i.d.) of 100  $\mu\text{m}$ , and an outer diameter of 363  $\mu\text{m}$  were used for the preparative protein separations. The capillary was thermostatted at 25 °C. Data acquisition (4 Hz) and control were performed using P/ACE station software (Version 2.3; Beckman) on a 300-MHz IBM personal computer. 0.2 mL Polymerase chain reaction (PCR) tubes (Rose Scientific Ltd., Edmonton, AB, Canada) were used, after detached the caps, to collect protein fractions during electrokinetic fractionation.

Mass spectral measurements were performed on a Bruker Reflex III MALDI-TOF mass spectrometer equipped with a SCOUT 384 multiprobe inlet (Bremen/Leipzig, German). The instrument is equipped with a pulsed nitrogen laser at 337 nm. Delayed ion extraction was applied to improve the mass resolution of the linear time-of-flight mass spectrometry (TOF-MS). This mode introduces a delay time between ionization and extraction of the ions from the ion source into the drift tube of the analyzer is introduced. The time delay and extraction potential are tuned to minimize the arrival time distribution of the ions at the detector (i.e., to enhance the MS resolution). The spectra were externally calibrated with bovine heart cytochrome *c* (b-cyt *c*, C3131,

$M_r = 12230.70$  Da) as a mass standard. All data were processed with Igor Pro Software package (WaveMetrics, Lake Oswego, OR). Mass spectra shown in the all figures in this Chapter were normalized to the most intense signal in the displayed mass range.

### 5.3.2 Chemicals

Nanopure 18-M $\Omega$  ultra-pure water (Barnstead, Dubuque, IO) was used to prepare all solutions. Lithium phosphate buffer was prepared from phosphoric acid (BDH, Darmstadt, Germany), and the pH was adjusted using lithium hydroxide (BDH). Bis-tris phosphate buffer was prepared by titrating phosphoric acid with a 100 mM solution of ultra-pure tris(hydroxymethyl)aminomethane bis(2-hydroxyethyl)iminotris(hydroxymethyl)methane (Bis-tris; Sigma, St. Louis, MO, USA) to pH 7.0.

The cationic surfactants, dimethylditetradecylammonium bromide (2C<sub>14</sub>DAB) and dimethyldioctadecylammonium bromide (2C<sub>18</sub>DAB), were used as received from Aldrich (Milwaukee, WI, USA). The surfactant solutions were prepared using the sonicate/stir cycle method [39] at 50°C. This sonicate/stir cycle was repeated two times for the 2C<sub>14</sub>DAB surfactant and six times for 2C<sub>18</sub>DAB surfactant to obtain clear solutions. HPLC-grade methanol (MeOH; Fisher, Fair Lawn, NJ, USA) was used to remove the bilayer coating from the capillary after each run. MALDI matrix,  $\alpha$ -cyano- 4-hydroxycinnamic acid, (CHCA), was purchased from Aldrich. Reagents, acetone and acetonitrile (BDH), were used as received. Standard proteins, bovine heart cytochrome *c* (b-cyt *c*; C3131,  $M_r = 12230.70$ ) and horse heart cytochrome *c* (h-cyt *c*; C7752,  $M_r = 12360.46$ ), were used as received from Sigma. These proteins were dissolved in water at 10 g/L unless otherwise stated.

### 5.3.3 Coating Procedure

The coating procedure for the preparative capillaries was as described in Section 4.2.3.

### 5.3.4 Protein Separations

After coating the capillary with 2C<sub>14</sub>DAB or 2C<sub>18</sub>DAB surfactant, the protein sample was hydrodynamically injected into the capillary using 3.4 kPa (0.5 psi) for 3 s. Lithium and Bis-tris phosphate at pH 7.0 were used in this study. The pH was found to be optimum for the separation of the cytochrome *c* mixture, as shown in Chapter Four. The applied voltage was –10 kV unless otherwise stated. Direct detection was performed at 214 nm for the lithium phosphate buffer and at 254 nm for the Bis-tris phosphate buffer. The number of moles of protein injected into the capillary was calculated by multiplying the protein concentration by the volume injected (Section 4.2.4). Resolution ( $R_s$ ) of the sample components was determined from its definition, as previously discussed in Section 1.4 (eq. 1.19).

### 5.3.5 CE Fraction Collection

CE fraction collection of the desired protein band at the outlet of the capillary was performed electro-kinetically into a 0.2-mL PCR tube containing 5  $\mu$ L of dilute (0.01 mM) separation buffer. The electrolyte buffer in the PCR tube is essential to complete the electrical circuit required for the electrophoretic migration of an analyte during fraction collection [33]. The height of the buffer in the PCR tube was about 2 mm (~5  $\mu$ L). To avoid siphoning during fractionation, the buffer of the inlet vial is leveled with the collection PCR tube, as shown in Figure 5.1.

The time within which the protein should be collected is calculated based on the window encompassing the leading and tailing edge of the peak at the UV detector. The time at which the protein band reaches the capillary outlet ( $t_{i,outlet}$ ) is calculated from the migration time corresponding to the leading edge of the protein band as it passes through the detector window ( $t_{i,detector}$ ), according to the following equation assuming that the mobility of the analyte is constant during electrophoresis:

$$t_{i,outlet} = t_{i,detector} \frac{L_t}{L_d} \quad (5.1)$$

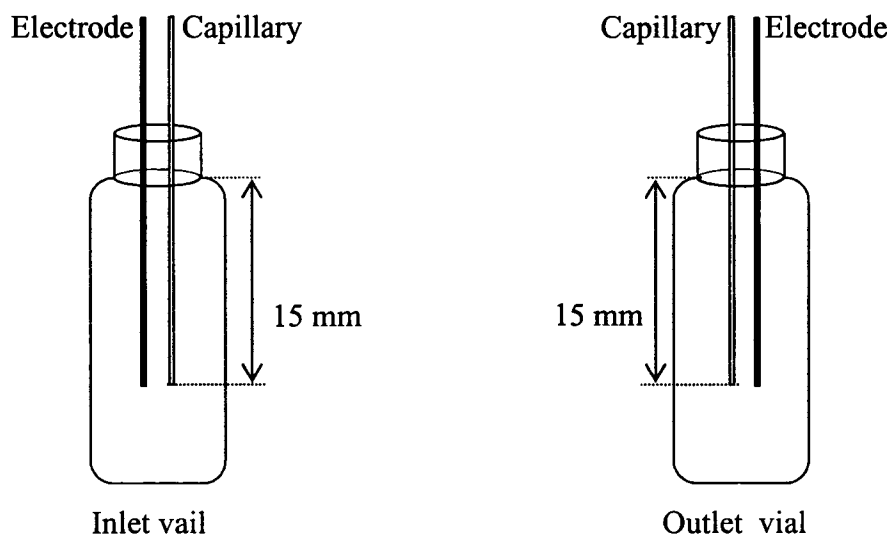
where  $L_t$  is the total length of the capillary (58.0 cm) and  $L_d$  is the capillary length to the detector (48.0 cm). The voltage ramp time was not taken into consideration, since its influence would be negligible given fraction collection started after 28 min.

At time  $t_{i,outlet}$ , the electric field was terminated, and the outlet buffer vial (Figure 5.1a) was replaced by a PCR tube. At the same time, the inlet buffer vial was also replaced with another one-third filled vial, as shown in Figure 5.1b. The electric field was then resumed to collect and isolate the desired protein into the fractionation vial (PCR tube). The time required for electro-kinetic fraction collection ( $w_{collection}$ ) is equivalent to the baseline width of the peak at the capillary outlet ( $w_{b,outlet}$ ), which in turn is computed from the peak baseline width recorded by the detector in time units ( $w_{b,detector}$ ) and corrected for voltage ramp time ( $t_{ramp}$ ), thus:

$$w_{collection} = \left( w_{b,detector} \frac{L_t}{L_d} \right) + \frac{t_{ramp}}{2} \quad (5.2)$$

After collecting the desired fraction, the PCR tube was removed and replaced by the electrophoretic buffer vial, and voltage was applied until the front edge of the next

**a. During separation**



**b. During fraction collection**

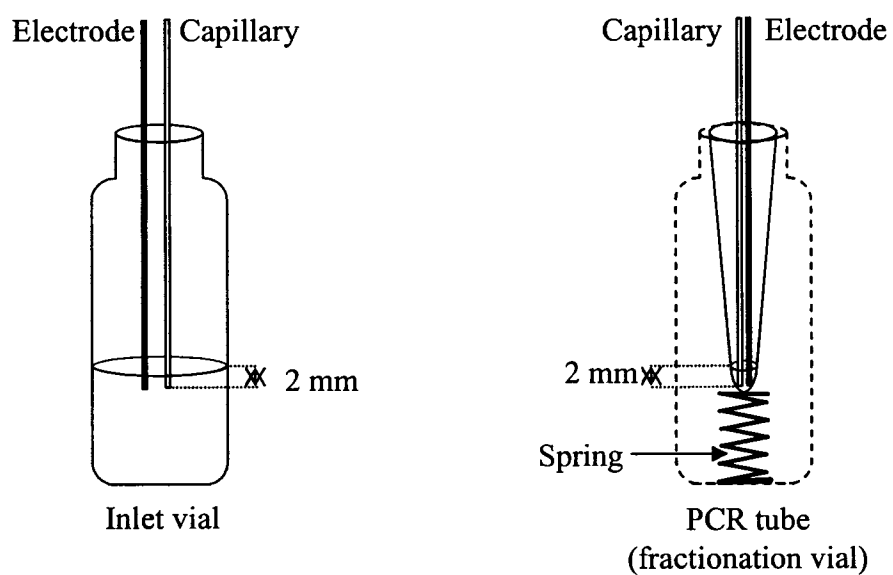


**Figure 5.1** Schematic diagram illustrate the position of the buffer level in the vials during **a.** separation; and **b.** fraction collection.

protein band reached the capillary outlet. If needed, successive fraction collections can be performed by using a new PCR tube for each fraction.

### **5.3.6 Protein Digestion**

The CE fraction was transferred to a non-siliconized Eppendorf centrifuge tube (0.6 mL) and mixed with same volume of 6 M HCl. The centrifuge tube was capped and placed in a 900 W output household microwave oven. Typically, the sample was subjected to microwave irradiation for 2 min [25, 26]. After digestion, the sample solution was dried down completely using a Speed Vac concentrator and was ready for MALDI-MS analysis.

### **5.3.7 Sample Preparation for MALDI-TOF MS Analysis**

The two-layer method with CHCA was used in MALDI-TOF MS protein analysis. In this method, the first layer was prepared as a saturated solution of CHCA in 25% methanol/acetone (v/v). About 0.8  $\mu\text{L}$  of the first layer solution was deposited on the MALDI target and allowed to dry in air. The second layer was a saturated solution of CHCA in 50% acetonitrile/water (v/v). For the protein purity analysis, the solution of the second layer was mixed 1:1 with the protein fraction solution. About 0.4  $\mu\text{L}$  of the mixture solution was deposited on top of the first layer and allowed to air-dry. For the peptide mapping analysis, the dried polypeptide mixture sample was re-dissolved in 0.4  $\mu\text{L}$  of second layer solution and was deposited on the first layer to air dry. On-probe washing was performed by adding a 1  $\mu\text{L}$  droplet of water onto the dried sample spot at room-temperature. After a brief time (> 30 sec), the water droplet was removed by absorbing with a Kimwipe. This washing procedure was performed once on each sample spot.

The MALDI samples and the protein digestion were prepared by Nan Guo from Dr. Liang Li's group at the University of Alberta.

## 5.4 Results and Discussion

CZE separations with wide bore 2C<sub>14</sub>DAB coated capillaries have been utilized for protein mixtures at the preparative scale, as illustrated in Chapter Four. When cationic surfactants are flushed through the capillary, they form a bilayer coating that reverses the charge on the capillary wall. As a consequence, cationic proteins do not adsorb onto the capillary but rather are repelled away from the positively charged capillary wall. However, achievement of high separation efficiency and resolution is dependant on careful attention to other possible sources of broadening.

For instance, during separations with wide bore capillary (100 μm i.d.) the level of buffer in the separation vials is an important parameter that affects the separation performance. As discussed in Section 1.4.5, when the buffer level in the inlet vial is higher or lower than the buffer level in the outlet vial, a pressure induced flow is generated inside the capillary. The parabolic profile of this flow will broaden the flow separated protein bands and thus decrease the efficiency of the separation. The buffer velocity at distance  $x$  from the centre axis of the capillary ( $v_x$ ) can be calculated as

$$v_x = \frac{\Delta P r^2}{8L\eta} (1 - 2r_x^2) \quad (5.3)$$

where  $\Delta P$  is the pressure difference,  $r$  is the internal capillary radius,  $\eta$  is the viscosity of the medium, and  $r_x$  is the normalized radius variable ( $x/r$ ) at distance  $x$  from the central axis of the capillary.

The magnitude of the induced pressure ( $\Delta P$ ) due to siphoning in aqueous electrolyte depends mainly on the level difference of the buffer in the vials and the capillary dimensions (inner radius and length), as shown in eqs. 1.37 and 1.38. Since the linear flow velocity at the center of the capillary is proportional to the square of the capillary radius, the effect of siphoning can be very significant when wide bore capillaries are utilized. Riekkola and coworkers noticed that the siphoning effect became significant with 100  $\mu\text{m}$  i.d. capillaries if there was  $> 4$  mm difference in the buffer level in the separation vials [40]. In our case, the protein separations are performed in 58.0 cm lengths of 100  $\mu\text{m}$  i.d. capillary with the buffer level in the outlet vial that is 13 mm lower than the inlet vial. Under these conditions, the apparent migration time of the neutral marker becomes faster (16.9 versus 18.9 min for the separation with adjusted buffer vial) due to the hydrostatic flow generated inside the capillary. More importantly, the resolution is significantly decreased (from 1.4 to 0.7). The broadening due to siphoning can be eliminated by adjusting the buffer in the separating vials to the same level before the separation is performed. As will be discussed in Section 5.4.1, care must also be taken during the fraction collection steps to avoid similar siphoning broadening.

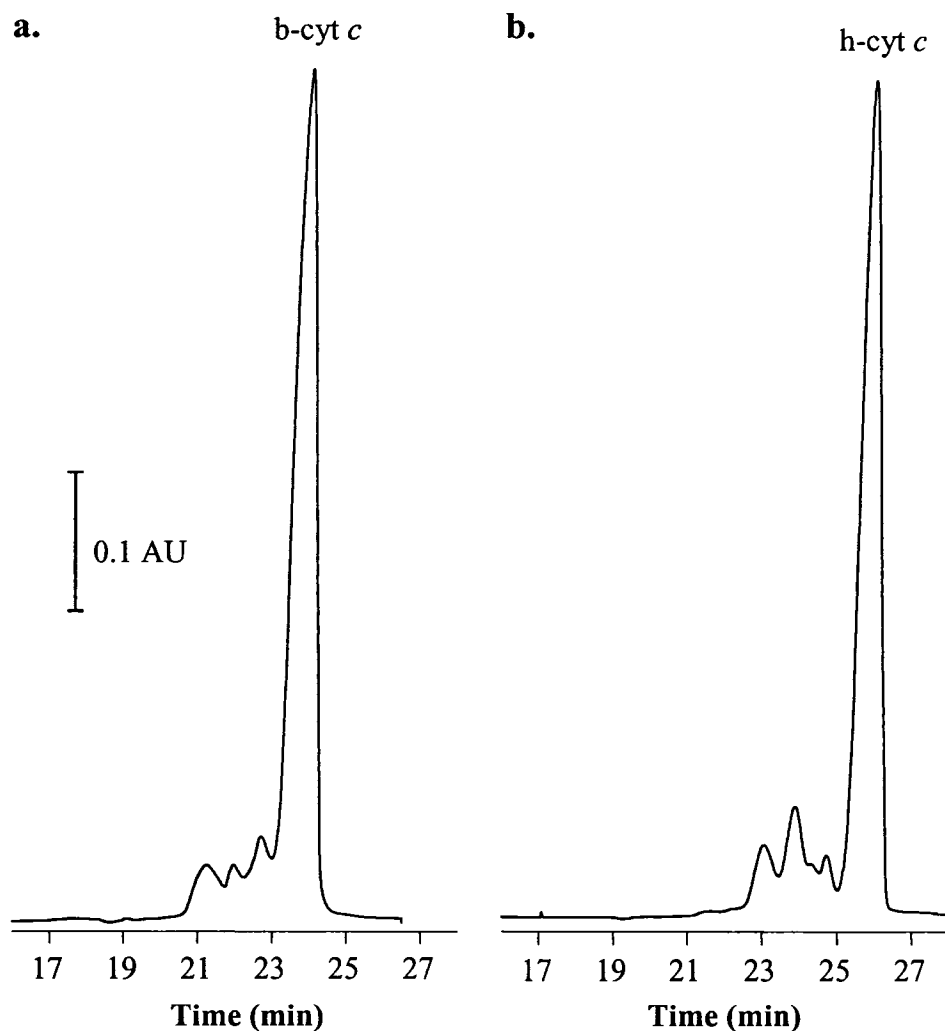
#### 5.4.1 CE Fraction Collection

As shown in Chapter Four, the preparative scale separation was well resolved ( $R_s = 1.4$ ) in 100 mM lithium phosphate buffer. The sample loading (40 pmol of each protein) was within the range required for peptide mapping by microwave assisted acid hydrolysis (MAAH, 10-50 pmol) [27]. Thus, lithium phosphate buffer was employed for initial investigations of preparative CE for MAAH/MS.

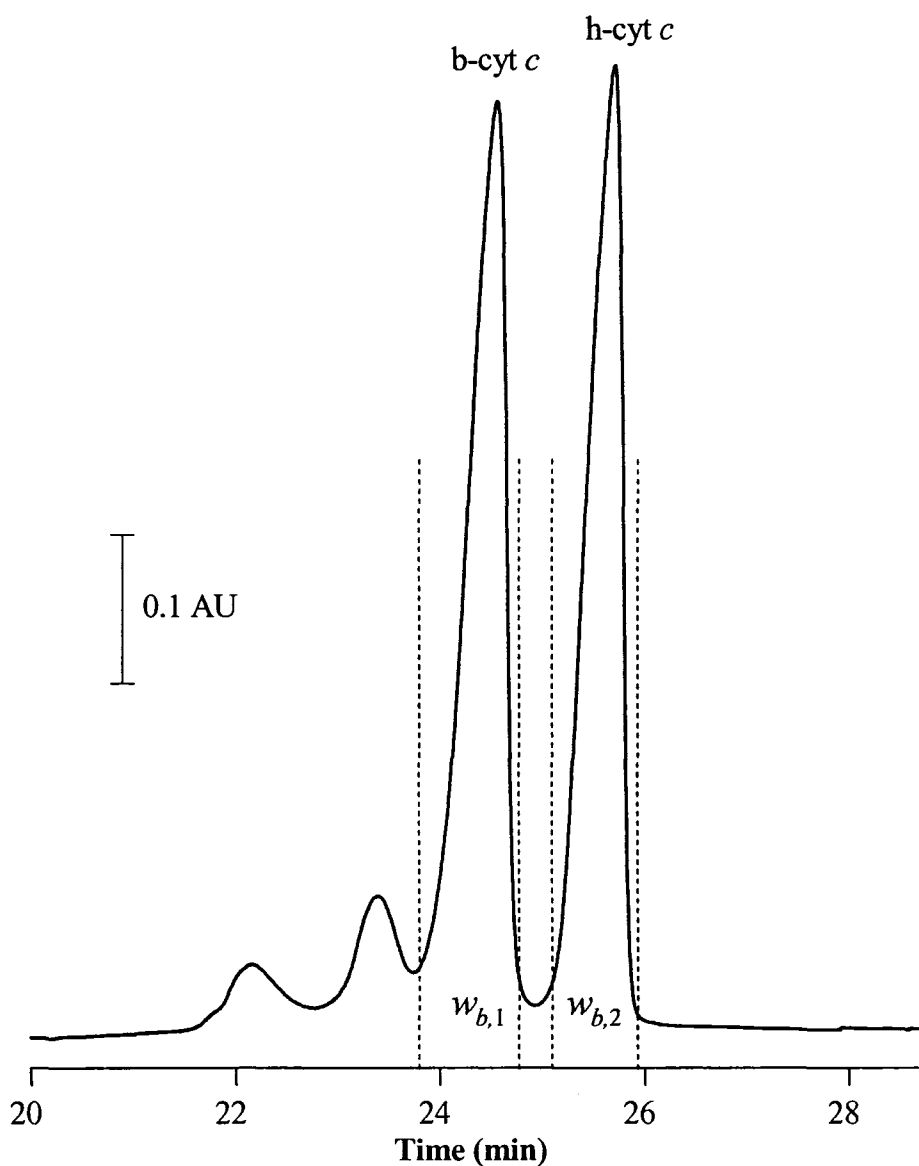
Prior to performing fraction collection, the purity of b-cyt *c* and h-cyt *c* were accessed using CE with a 2C<sub>14</sub>DAB coated capillary (Figure 5.2). In Figure 5.2a, three small peaks (migration times 21.2, 21.9, and 22.7 min) appear before the main b-cyt *c* peak at 24.1 min. Similarly, three small peaks (migration times 23.0, 23.9 and 24.7 min) appear before the h-cyt *c* (26.0 min), as shown in Figure 5.2b. Such small peaks accompanying the b-cyt *c* and h-cyt *c* peaks were previously observed in CE [17, 21, 23], but have not been characterized. The presence of the small peaks in front of the main protein peaks in the electropherograms (Figure 5.2) will introduce a potential problem for isolation and collection of pure protein fractions.

Figure 5.3 shows the separation of a mixture of b-cyt *c* and h-cyt *c* using 100 mM lithium phosphate at pH 7.0 with a 100  $\mu$ m i.d. capillary coated with 2C<sub>14</sub>DAB. Once the protein has been separated and is positioned at the outlet of the capillary, collection of the protein band can be performed either by pushing the band into a collection vial using pressure or an electric field. Hydrodynamic fractionation is simple and more straightforward. However, pressure-induced laminar flow causes significant broadening. Indeed, van Veelen *et al.* observed reduced peak resolution when they applied 3 kPa (0.44 psi) for fraction collection [32]. Therefore, in this work I used electro-kinetic fraction collection to maintain the separation resolution during fractionation and isolate the fractions in a reasonable period of time.

In electro-kinetic fraction collection, the fractionation start time was determined by the appearance of fronting edge of the desired protein band at the detector and accounting for the total-to-detector capillary length ratio, according to eq. 5.1. For instance, the b-cyt *c* peak is first detected at 23.8 min, and thus the fraction time was



**Figure 5.2** Electropherograms of **a.** b-cyt *c*; and **b.** h-cyt *c* using 2C<sub>14</sub>DAB coatings at 100 mM lithium phosphate buffer. **Experimental conditions:** 58.0 cm × 100 μm i.d. capillary (48.0 cm to the detector); applied voltage at -10 kV; individual protein was dissolved in water at concentration of 10 g/L; hydrodynamic injection at 3.4 kPa for 3 s (40 pmol of each protein); buffer pH, 7.0; temperature, 25 °C; and λ, 214 nm.



**Figure 5.3** Electropherogram of b-cyt *c* and h-cyt *c* at  $-10$  kV using  $2C_{14}DAB$  coatings at  $100$  mM lithium phosphate buffer. **Experimental conditions:**  $58.0$  cm  $\times$   $100$   $\mu$ m i.d. capillary ( $48.0$  cm to the detector); protein sample was dissolved in water; sample concentration of  $10$  g/L of each protein; hydrodynamic injection at  $3.4$  kPa for  $3$  s ( $40$  pmol of each protein); buffer pH,  $7.0$ ; temperature,  $25$   $^{\circ}$ C; and  $\lambda$ ,  $214$  nm.  $w_{b,1}$  ( $1.0$  min) and  $w_{b,2}$  ( $0.90$  min) are the baseline width for b-cyt *c* and h-cyt *c* peaks, respectively.

started at 28.8 min ( $23.8 \text{ min} \times \frac{58.0 \text{ cm}}{48.0 \text{ cm}}$ ), as shown in Figure 5.3. At 28.8 min, the electric field for the separation is terminated, and the outlet separation vial is replaced by the PCR tube (fractionation vial), as shown in Figure 5.1.

To make electro-kinetic fraction collection possible, the collection tube must contain electrolyte solution to complete the electric circuit [17, 33, 34, 41]. Generally, the separation buffer has been used as the electrolyte solution in the collecting vial [33, 41]. However, the presence of metal co-ions suppresses the protein or peptide signal in MALDI-TOF MS, which is of particular concern when analyzing low protein or peptide levels [17, 42]. Nevertheless, dilute electrophoretic buffer (0.01 mM) is used to minimize the signal suppression. Typically, 5  $\mu\text{L}$  aliquot of 0.01 mM buffer was used for fraction collection. Use of lower volumes of electrolyte solution (e.g. 3  $\mu\text{L}$ ) for fraction collection was not reliable due to periodic termination of the electric voltage during fractionation.

The separation vials during preparative analysis should contain large buffer volumes to minimize pH change during separation. The buffer pH change in the buffer reservoirs becomes more significant during electrophoretic separations at high electric field, small buffer volumes and large capillary inner diameter [43]. It was demonstrated that a change as small as 0.03 pH unit in the electrophoretic buffer can significantly deteriorate the separation resolution [44]. Therefore, the separation vials were filled to the top with the running buffer ( $\sim 2 \text{ mL}$ ). Under these conditions, the length of the capillary immersed in the inlet and outlet buffer solutions were 15 mm (Figure 5.1a). However, when the PCR tube replaced the outlet vial for fractionation, only 2 mm of the capillary outlet was immersed into the electrolyte solution. Therefore, the buffer level

difference between the inlet vial and the PCR tube would be 13 mm, and thus siphoning flow would occur inside the capillary. As a result, the separated protein bands deteriorate due to the parabolic flow profile as described by eq. 5.3. Furthermore, the timing for fractionation predicted by eqs. 5.1 and 5.2 would be imprecise due to the siphoning flow altering the velocity of the analyte band within the capillary. Therefore, isolation of pure protein fractions would be difficult to perform.

To solve this problem, the inlet vial was replaced during fraction collection with another vial whose buffer level was adjusted to the same level as present in the collection tube. In other words, the buffer level in the inlet vial should be reduced such that the inlet capillary end is inserted only 2 mm under the surface, as shown in Figure 5.1b. Unfortunately, it is not possible to replace the inlet vial during automatic fractionation with the fraction collection program designed for the MDQ CE instrument. Therefore, manual fraction collection was applied to facilitate replacing the adjusted inlet vial.

The baseline width of the peak at the capillary outlet ( $w_{b,outlet}$ ) of the protein band is determined by multiplying the peak baseline width ( $w_{b,detector}$ ) by total-to-detector capillary length ratio.

$$w_{b,outlet} = w_{b,detector} \frac{L_t}{L_d} \quad (5.4)$$

where  $L_t$  is the total capillary length and  $L_d$  is the length of the capillary to the detector. However, the applied voltage needs time to reach the desired set value. This voltage ramp time becomes significant during fractionation since the collection time is small (<1.4 min) [45]. The voltage ramp time in the MDQ CE instrument is 0.2 min. As the voltage increases linearly during the ramp time the corrected observed mobility ( $\mu_{obs,corr}$ ) of the charged species is given by:

$$\mu_{obs,corr} = \frac{L_t L_d}{V_{prog} \left( t_M - \frac{t_{ramp}}{2} \right)} \quad (5.5)$$

where  $V_{prog}$  is the voltage set by the instrument,  $t_M$  is the migration time of the analyte, and  $t_{ramp}$  is the voltage ramp time. Thus, half the ramp time (0.1 min) should be added to each collection time to isolate most of the desired protein band. Voltage de-ramping time was not taken into account since the PCR tube is immediately removed after the electric field is terminated.

After the collection time, the electric field is terminated and the collection tube is removed and replaced by the original outlet vial. The electric field is then resumed until the second fraction reaches the capillary outlet. The second fraction is then collected electro-kinetically into a new collection tube. The dashed lines in Figure 5.3 indicate the time intervals that were used to determine the actual fractions times (the actual start and stop times for fractionation were calculated based on eq. 5.2).

#### 5.4.2 Determination of the Fractions Purity by MALDI-TOF MS

Fraction purity is an important measure of a fraction collection method's ability to isolate separated sample components into discrete fractions. To test for fraction purity, both fraction collected tubes were analyzed with MALDI-TOF MS. The spectra are displayed in Figure 5.4. The  $[b\text{-cyt } c+H]^+$  peak, in the mass spectrum of the first fraction (Figure 5.4a), is equivalent to the mass of protonated b-cyt *c* (12231.70 Da). Immediately to the right of  $[b\text{-cyt } c+H]^+$ , there is a small peak (relative intensity of 15%) at the mass of the protonated h-cyt *c* (12361.46 Da). This indicates that the b-cyt *c* fraction is contaminated by h-cyt *c*. Figure 5.4b shows that the h-cyt *c* fraction is pure, with only

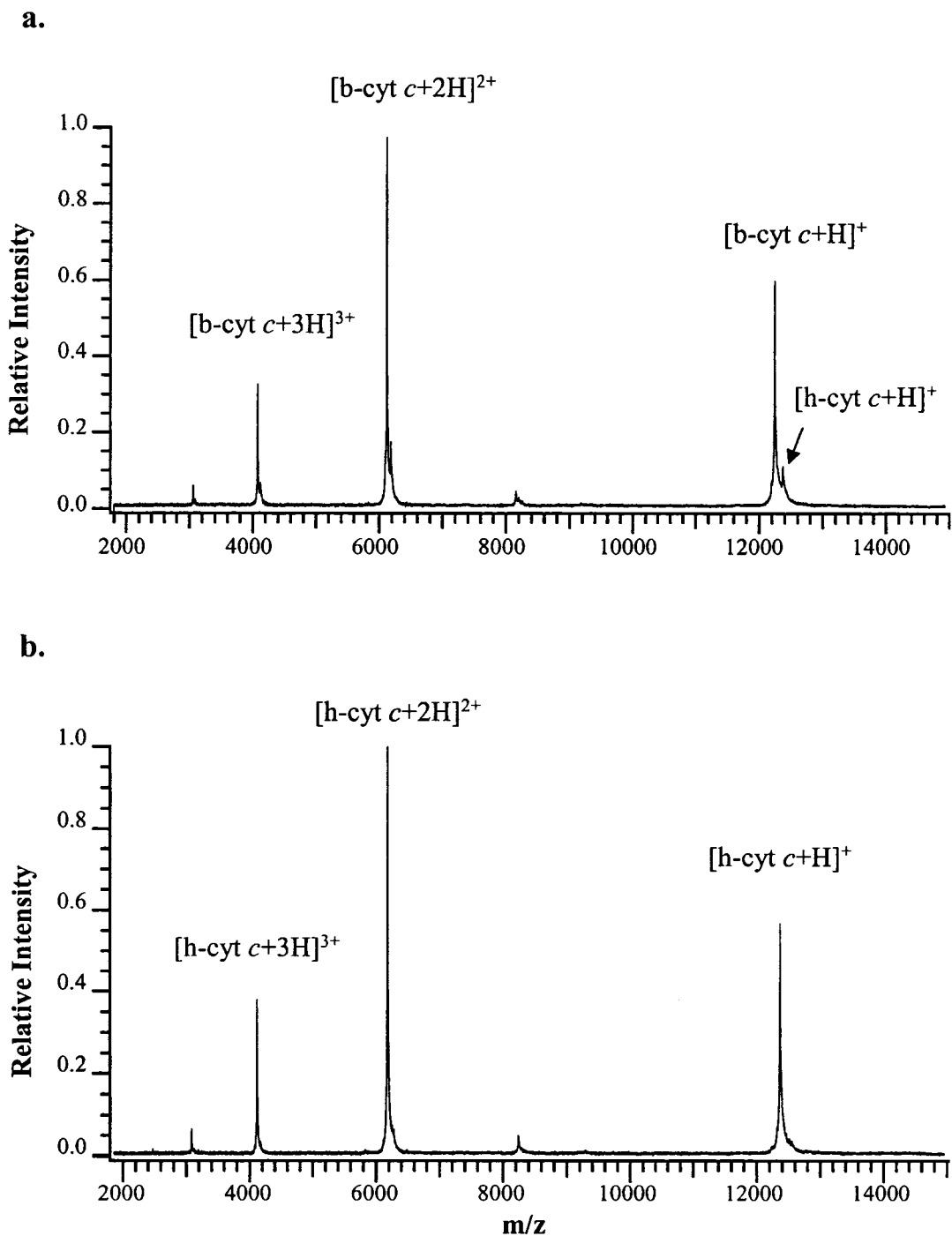


**Figure 5.4** MALDI-TOF mass spectra of the fractions collected from electrophoresis run in Figure 5.3: **a.** spectrum of the first fraction (collection time of 1.3 min), b-cyt *c*; and **b.** spectrum of the second fraction (collection time of 1.2 min), h-cyt *c*.

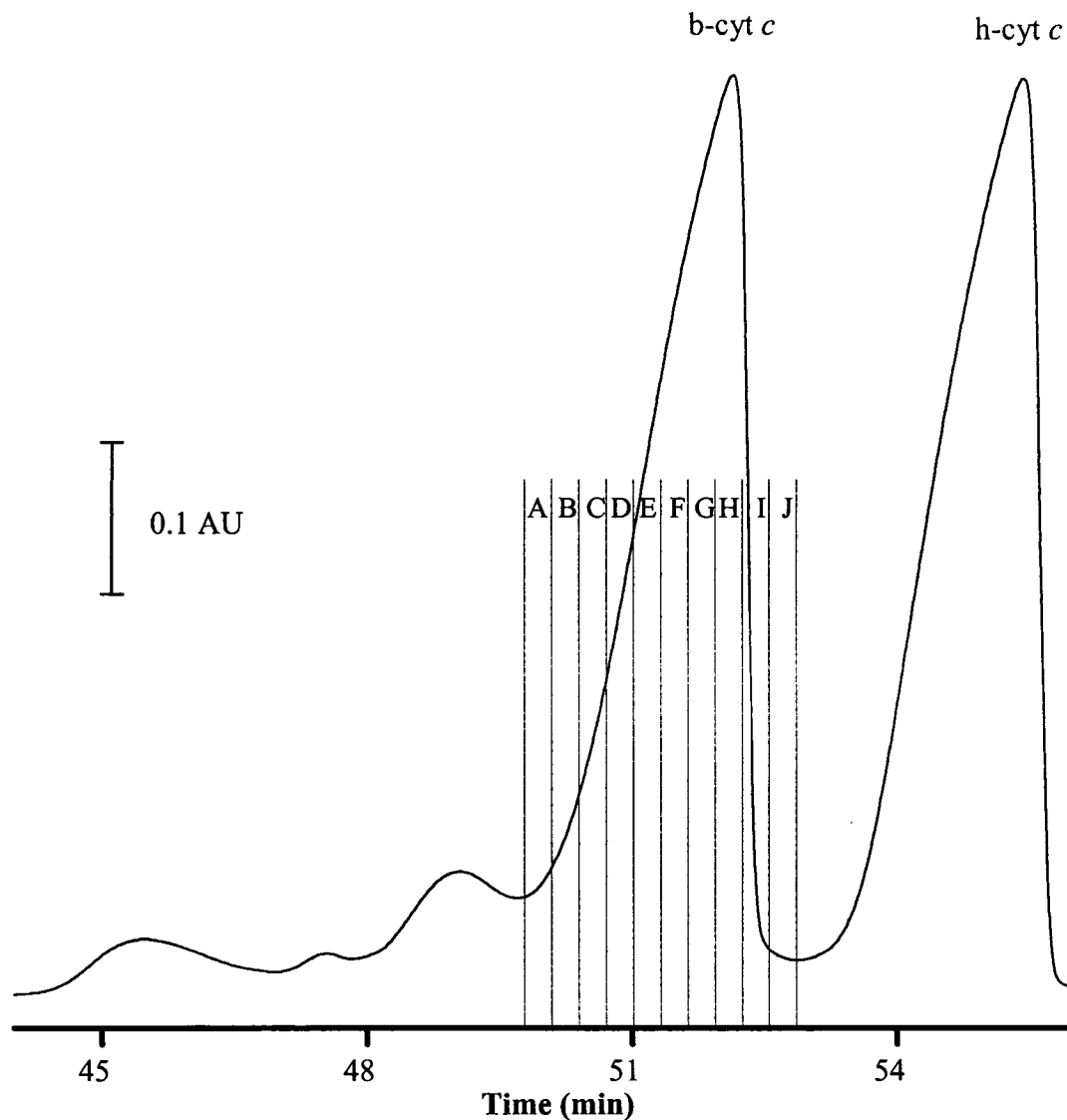
peaks corresponding to single and multiple charged protonated h-cyt *c*. The potential cause of this contamination will be discussed in Section 5.4.3.

#### 5.4.3 Sources of Contamination in the Bovine Protein Fraction

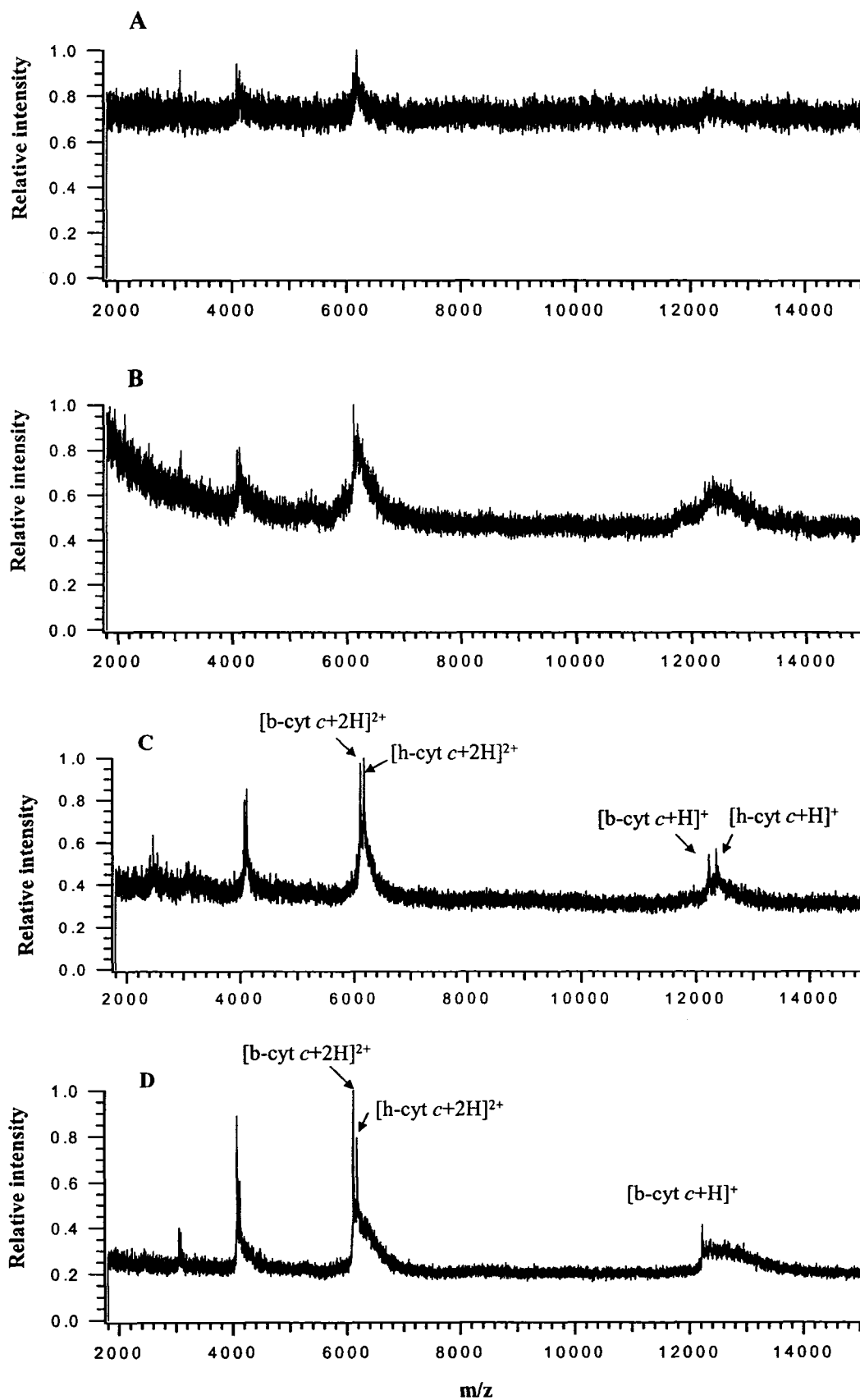
To determine the sources of contamination in the b-cyt *c* peak, a sub-fractionation method was employed. In this method, a preparative separation of a mixture of b-cyt *c* and h-cyt *c* was performed at  $-5$  kV using a  $100\ \mu\text{m}$  i.d. capillary coated with  $2\text{C}_{14}\text{DAB}$ . The b-cyt *c* peak was sub-divided into 10 fractions, as shown in Figure 5.5. The fractionations were performed successively into separate collection vials, each containing  $5\ \mu\text{L}$  of  $0.01\ \text{mM}$  lithium phosphate buffer pH 7.0. The fractionation was started at the time the b-cyt *c* band was predicted to reach the outlet of the capillary at 60.3 min and each fraction was 0.5 min wide.

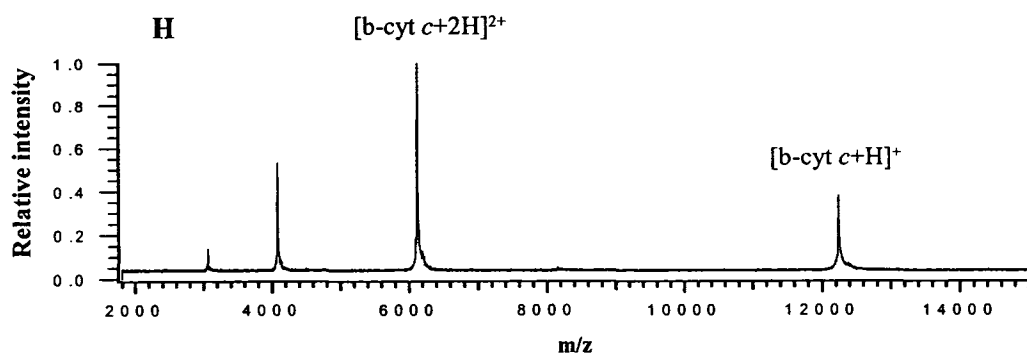
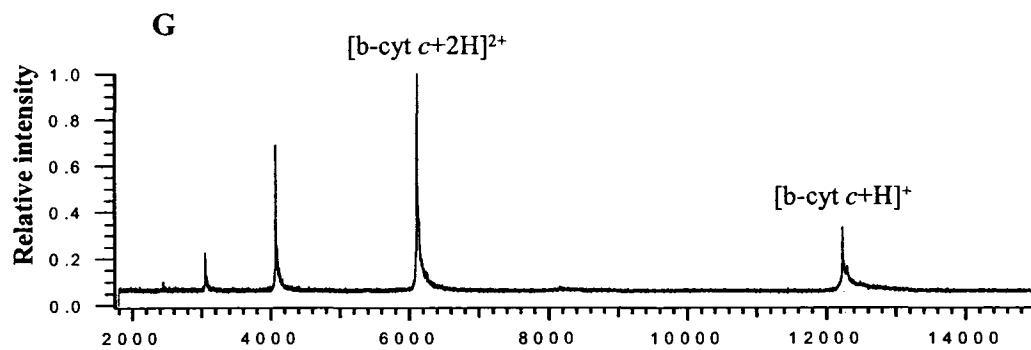
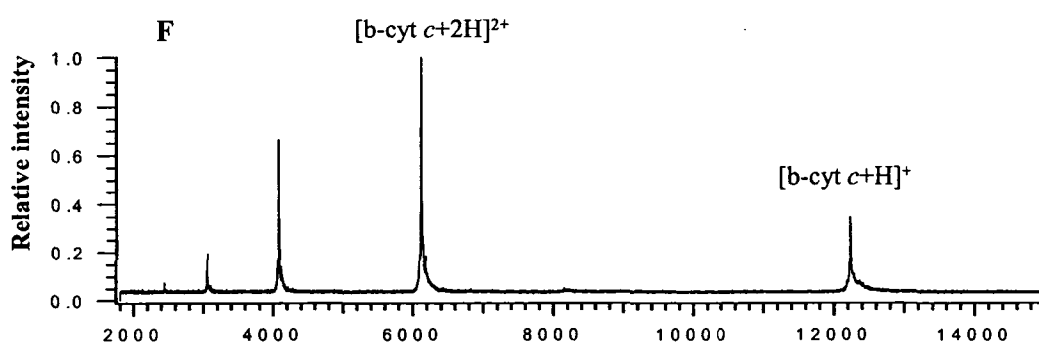
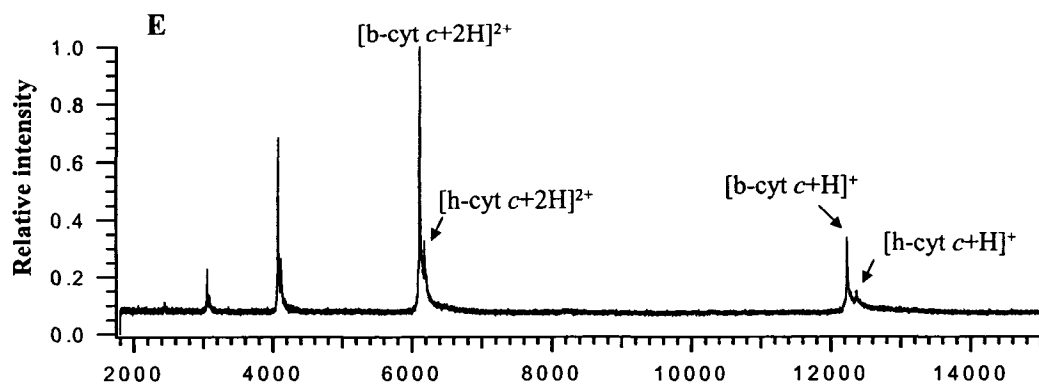
After fraction collection, the fractions were analyzed by MALDI-TOF MS. The resultant spectra are presented in Figure 5.6. The spectra of the first two fractions (A and B) show no protonated b-cyt *c*. Possibly, the MALDI-TOF signal of the small amount of protein present in the collection tube was suppressed by the lithium buffer co-ion [17, 46]. In fractions C to E, the amount of protein gradually increases, as indicated by the improved S/N ( $> 3$ ) within the MALDI spectra in Figure 5.6. Both b-cyt *c* and h-cyt *c* were identified in the spectra from C to E. Fractions F to I exhibit only peaks corresponding to b-cyt *c*, without any interferences from h-cyt *c*. Finally, fraction J shows no peak as this fraction is collected after the b-cyt *c* band exited the capillary.

Although the resolution between b-cyt *c* and h-cyt *c* peaks in this separation is 1.4 (Figure 5.5), some h-cyt *c* contaminates the b-cyt *c* band. If the contamination of b-cyt *c* peak were due to chromatographic peak broadening, later fractions (F-J) would contain



**Figure 5.5** Electropherogram of b-cyt *c* and h-cyt *c* at  $-5$  kV using  $2C_{14}$ DAB coatings at 100 mM lithium phosphate buffer. **Experimental conditions:** 58.0 cm  $\times$  100  $\mu$ m i.d. capillary (48.0 cm to the detector); protein sample was dissolved in water; sample concentration of 10 g/L of each protein; hydrodynamic injection at 3.4 kPa for 3 s (40 pmol of each protein); buffer pH, 7.0; temperature, 25  $^{\circ}$ C; and  $\lambda$ , 214 nm. Dashed lines are the projection of the actual fractions time for b-cyt *c* peak (A-J) collected in separated PCR tubes. Each PCR tube contains 5  $\mu$ L of 0.01 mM lithium phosphate buffer. Actual collection time for each fraction was 0.5 min.





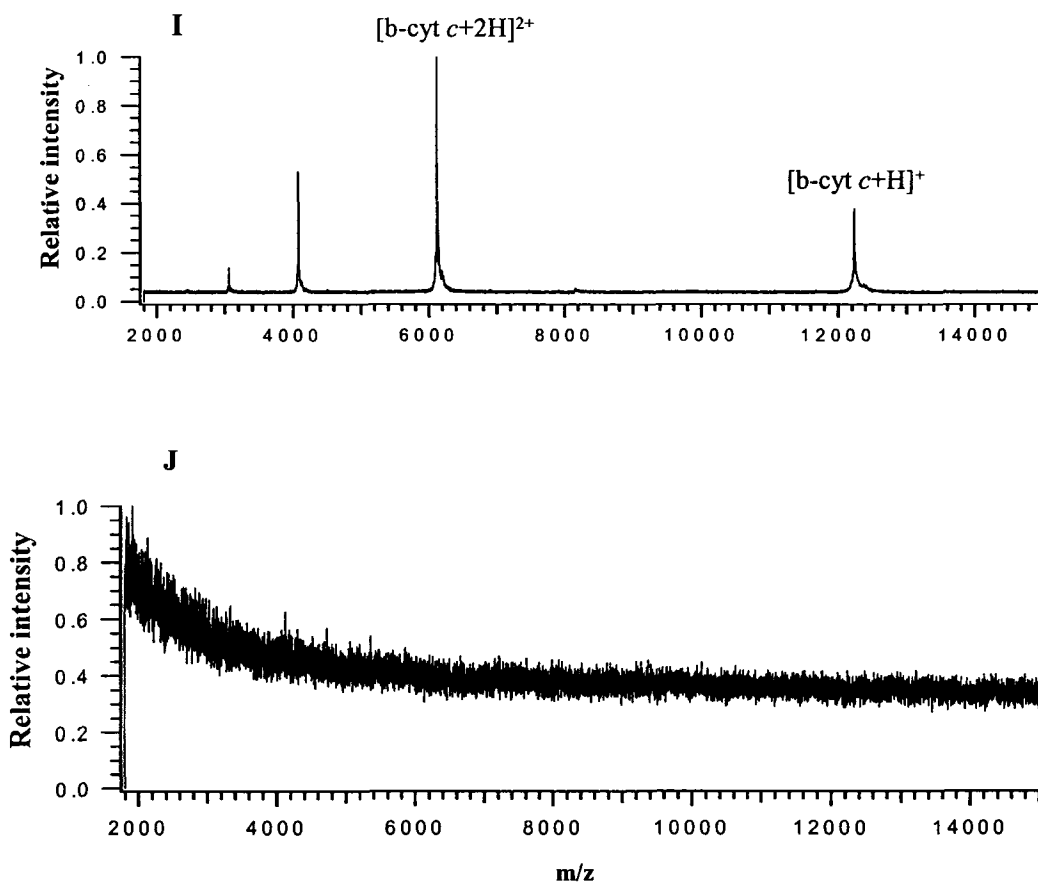


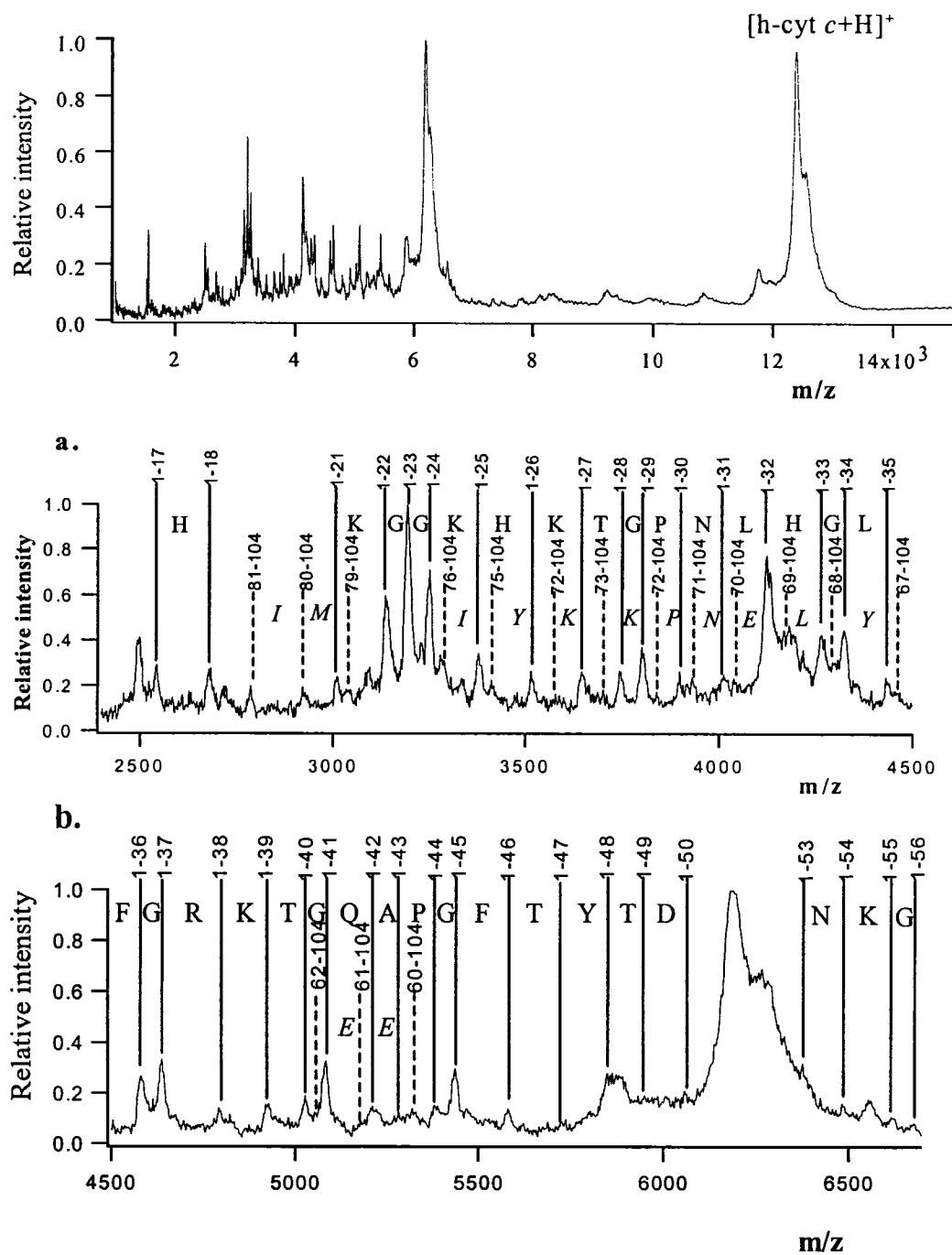
**Figure 5.6** MALDI-TOF mass spectra of 10 fractions (A-J) for b-cyt *c* peak collected from electrophoresis run in Figure 5.5. The fractions were collected in separated PCR tubes each contains 5  $\mu$ L of 0.01 mM lithium phosphate buffer pH 7.0. Actual collection time for each fraction was 0.5 min.

h-cyt *c*, whereas early fractions (C-E) would be purely b-cyt *c*. However, this is not what was observed. Rather fractions C to E (Figure 5.6) were the ones contaminated with h-cyt *c*. This suggests that the small peaks appearing before h-cyt *c* (23.9 and 24.7 min) in Figure 5.2b are h-cyt *c* which migrate slower than the majority of the h-cyt *c* (26 min) and thus contaminate the b-cyt *c* band. Due to the presence of contamination in the b-cyt *c* fraction, only the h-cyt *c* fraction was employed for protein characterization by MAAH.

#### 5.4.4 Microwave-assisted Acid Hydrolysis Analysis

The collected h-cyt *c* fraction was subjected to acid hydrolysis with the assistance of microwave irradiation, as described in Section 5.2.6. The resultant solution was analyzed directly by MALDI-MS, as per Section 5.2.7. The mass spectrum for the h-cyt *c* hydrolyzed fraction is shown in Figure 5.7. The peaks represent polypeptides produced from the acid hydrolysis. Each amino acid can be calculated by the mass difference between the consecutive peptides. The peptide sequence coverage for h-cyt *c* collected in Section 5.3.4 is 44%. The hydrolyzed polypeptides in the expanded spectra (Figure 5.7a and b) are found to be two series of polypeptide ladders containing either N- or C-terminal amino acid of the protein. Predominantly, polypeptides within the mass range 2500-6700 Da are identified with a continuous ladder from polypeptide 1-21 to 1-50 (N-terminal). In addition, a continuous ladder from polypeptide 67-104 to 76-104 (C-terminal) is also identified. However, no polypeptides could be identified at the higher mass range (above 6700 Da).

Due to the absence of the polypeptide peaks in the high mass range, the peptide sequence coverage was only 44%. However, Zhong *et al.* [26] previously demonstrated that peptide sequence coverage of > 95% for pure proteins could be achieved using



**GDVEKGGKKIF VQKCAQCHTV EKGGKHKHTGP NLHGLFGRKT**  
**GQAPGFITYD ANKNKGITWK EETLMLEYLEN PKKYIPGTKM**  
**IFAGIKKKTE REDLIAYLKK ATNE**

**Figure 5.7** The mass spectra of polypeptide ladders of h-cyt *c* fraction collected from electrophoretic run in Figure 5.3. The expanded spectra (a and b) show the labeled peaks for the corresponding peptides from the N-terminal (solid lines and bold letters) and C-terminal (dotted lines and italic letters) of the protein.

MAAH/MALDI. This is considerably higher than the 44% achieved in Figure 5.7. The absence of the high mass polypeptides might be due to surfactants leaching from the bilayer suppressing polypeptide detection. To determine if surfactant suppresses the MALDI signal,  $1 \times 10^{-3}$  to  $4 \times 10^{-3}$  mM  $2C_{14}DAB$  was added to 0.2 g/L solutions of h-cyt *c* and analyzed by MALDI. These surfactant concentrations are near the cmc of  $2C_{14}DAB$  [31], so should be comparable to the free surfactant concentration within the capillary. The results in Table 5.1 show that the mass resolution in the presence of surfactant is equivalent to that observed for protein dissolved in water, whereas the S/N was reduced by a factor of 2. Such a reduction in S/N would not be expected to translate into a complete loss of the high molecular mass polypeptide fragments. In addition, it was previously demonstrated that the presence of sodium dodecyl sulfate surfactant (< 0.1%) had only a small effect on the acid hydrolysis of cytochrome *c* [26]. Thus,  $2C_{14}DAB$  leaching from the capillary does not seem to be the cause of the suppressed MALDI signal.

Alternately, the separation buffer collected along with the protein during the CE fraction collection might suppress the polypeptide signals and thereby reduce the peptide sequence coverage. When fractionation was performed in 100 mM lithium phosphate buffer, the resultant buffer concentration in the collection vial is 3-5 mM. To investigate whether the buffer collected within the vial may affect the MALDI signal, a brief series of solutions of 0.2 g/L h-cyt *c* were prepared in a variety of buffers ranging in concentration from 1-10 mM. Table 5.2 suggests that > 2 mM phosphate causes reduction in the S/N. Furthermore, the amount of the polypeptides in the hydrolyzed mixture is smaller than the protein amount in the collection vial. For instance, the amount of an individual

**Table 5.1** Mass resolution and signal-to-noise ratio (S/N) for 0.2 g/L h-cyt *c* at different 2C<sub>14</sub>DAB surfactant concentrations.<sup>a</sup>

	Mass resolution	S/N
<b>a) water</b>	939	1133
<b>b) surfactant concentration</b>		
1×10 <sup>-3</sup> mM	1086	504
2×10 <sup>-3</sup> mM	1069	723
4×10 <sup>-3</sup> mM	1043	639

<sup>a</sup>**Experimental conditions:** MALDI sample preparation was as described in Section 5.3.7. The number of laser shots was 100 for each sample spot; on-probe washing was performed only once on each sample spot.

**Table 5.2** Mass resolution and signal-to-noise ratio (S/N) for 0.2 g/L h-cyt *c* at different concentrations of lithium and Bis-tris phosphate buffers.<sup>a</sup>

Buffer	Mass resolution	S/N
<b>a) lithium phosphate</b>		
1 mM	976	840
2 mM	865	807
5 mM	1025	422
10 mM	1025	422
<b>b) Bis-tris phosphate</b>		
1 mM	872	1281
2 mM	958	1054
5 mM	1060	636
10 mM	1082	385

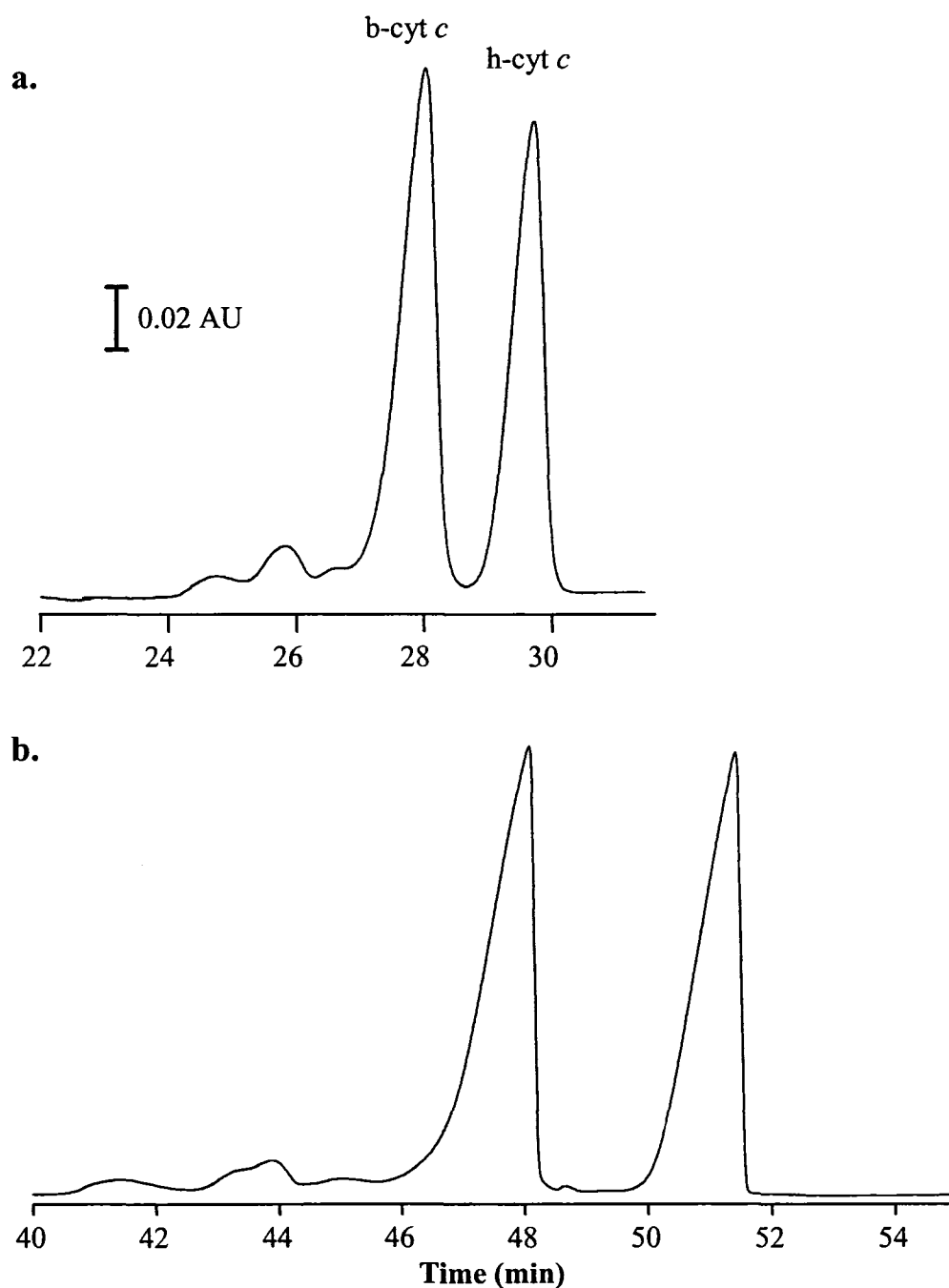
<sup>a</sup>**Experimental conditions:** MALDI sample preparation was as described in Section 5.3.7. The number of laser shots was 100 for each sample spot; on-probe washing was performed only once on each sample spot.

terminal peptide equals the amount of the intact protein hydrolyzed, divided by the number of peptide bonds broken in the protein [26]. Thus, the effect of the buffer is expected to be significant on the hydrolyzed peptides produced from MAAH during MALDI analysis. Increasing the sample loading into the CE and/or reducing the separation buffer concentration should increase the peptide sequence coverage.

However, with lithium phosphate buffer electromigration dispersion limits the protein loading capacity (Chapter Four) and necessitates the use of high buffer concentrations.

#### **5.4.5 MAAH/MALDI with Bis-tris Phosphate Buffer**

The amount of protein loading in the CE can be increased by changing the running buffer. As discussed in Chapter Four, Bis-tris has a low ionic mobility (apparent mobility in 100 mM Bis-tris buffer and pH 7.0 is  $0.36 \times 10^{-4} \text{ cm}^2/\text{Vs}$ ) that closely matches the effective mobility of the proteins used in this study. This mobility match lowers electromigration dispersion allowing a greater amount of protein to be loaded onto the capillary. In addition, Bis-tris phosphate buffer exhibits similar influence on the MALDI ion signals in comparison to lithium phosphate buffer, as shown in Table 5.2. At low Bis-tris phosphate buffer concentration  $\leq 2 \text{ mM}$ , the mass resolution and the S/N were unaffected with values equivalent to that obtained for pure protein dissolved in water. However, at buffer concentration  $> 2 \text{ mM}$ , the S/N is reduced with values comparable to what was obtained with the same concentration of lithium phosphate buffer. Nonetheless, switching the buffer co-ion from lithium to Bis-tris would increase the sample loading without introducing any further negative influence on the MALDI ion signals. Rather, the use of Bis-tris may allow a decrease in the buffer concentration which would improve the MALDI resolution and S/N.

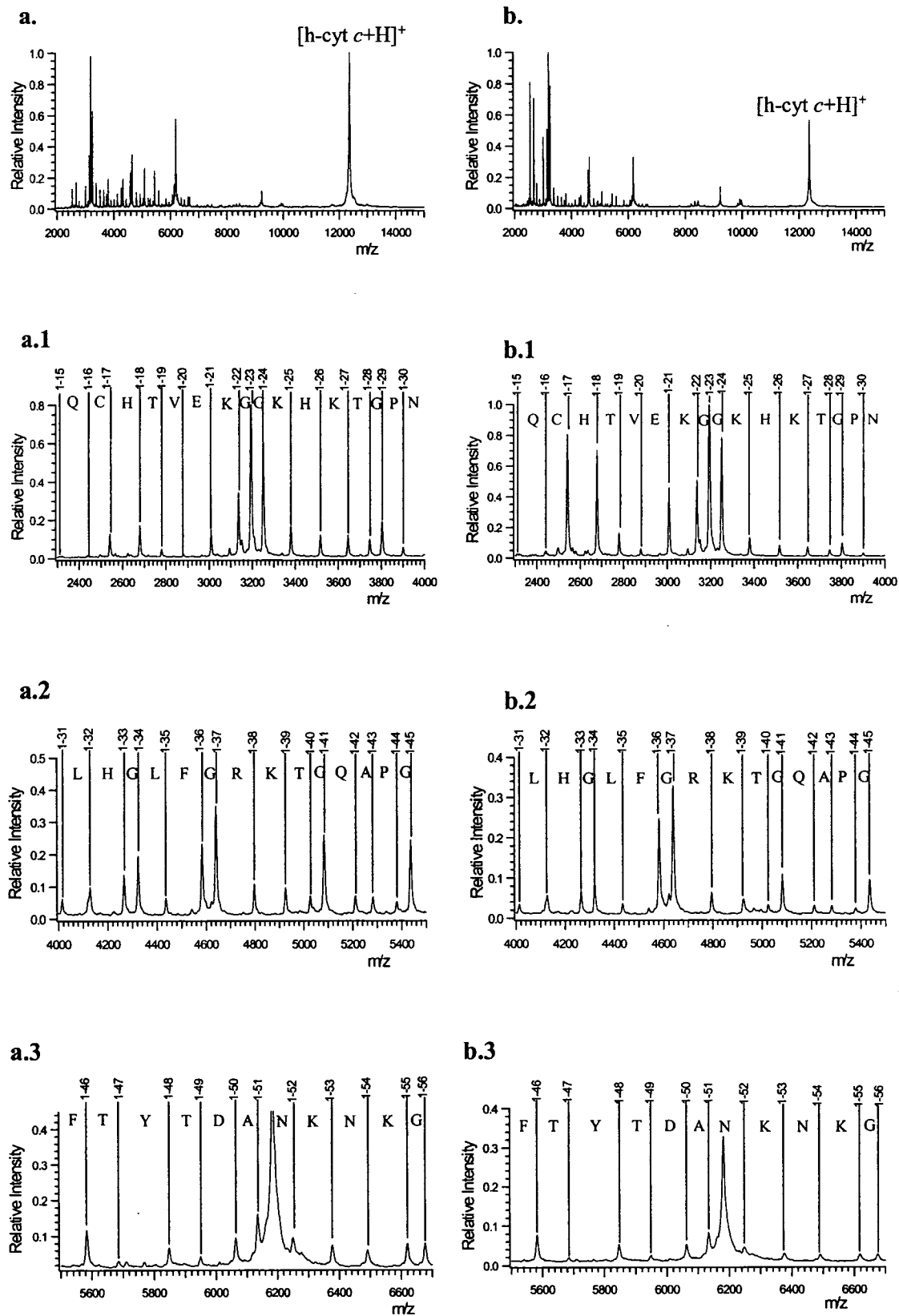


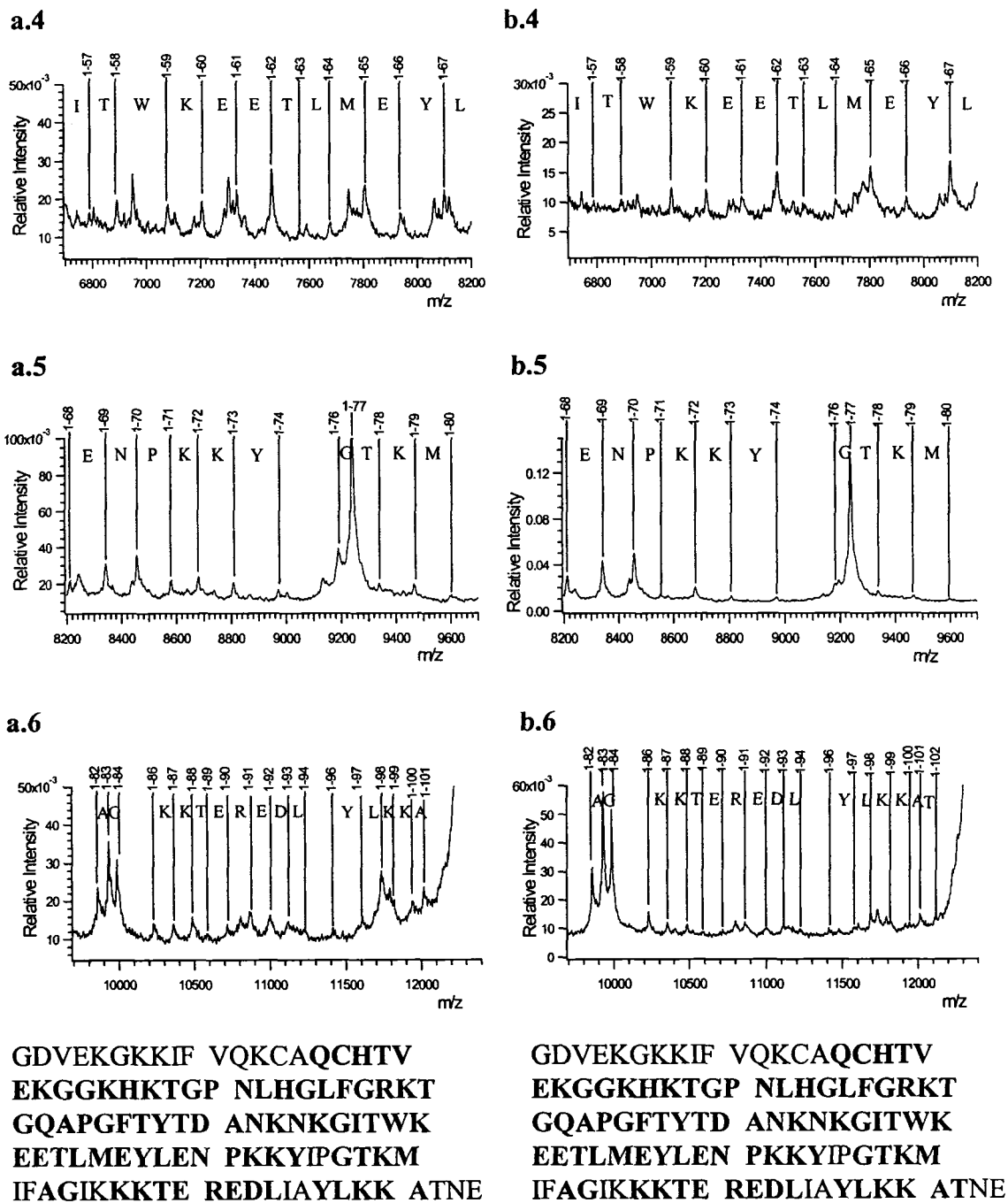
**Figure 5.8** Electropherograms of b-cyt *c* and h-cyt *c* at 100 mM Bis-tris phosphate buffer using two different coatings: **a.** 2C<sub>14</sub>DAB; and **b.** 2C<sub>18</sub>DAB. **Experimental conditions:** 58.0 cm × 100 μm i.d. capillary (48.0 cm to the detector); applied voltage, -10 kV; protein sample was dissolved in water at concentration of 40 g/L of each protein; hydrodynamic injection at 3.4 kPa for 3 s (160 pmol of each protein); buffer pH, 7.0; temperature, 25 °C; and λ, 214 nm.

Figure 5.8a shows the separation of the cytochrome *c* mixture at a concentration of 40 g/L (160 pmol of each protein) using 100 mM Bis-tris buffer using 2C<sub>14</sub>DAB coated capillary. The b-cyt *c* and h-cyt *c* are separated with a resolution of 1.4. The isolation of the h-cyt *c* fraction was performed as described in Section 5.3.5. When the purity of the collected fraction was tested with MALDI, only peaks corresponding to single and multiple charged protonated h-cyt *c* were observed. After the purity test, the h-cyt *c* fraction was subjected to MAAH/MALDI for protein characterization. Figure 5.9a shows that most of the peaks corresponding to polypeptides in the mass range 2300-12400 Da were identified. The peptide sequence coverage at this sample loading was 75% (N-terminal). Although the peptide sequence coverage is increased by increasing the sample loading to 160 pmol versus the 40 pmol in Section 5.4.4, the absence of peptide peaks at 1-1 to 1-14, 1-75, 1-81, 1-85, 1-95, 1-102, and 1-103, makes it difficult to read the amino acid sequence of the entire protein directly from one spectrum.

As inferred from Table 5.2, the introduction of the separation buffer into the collection vial during fractionation has indeed negatively influenced the MAAH/MALDI analysis. Therefore, decreasing the separation buffer concentration would reduce the amount of the buffer introduced to the vial and thus minimize the MALDI signal suppression. However, the resolution between b-cyt *c* and h-cyt *c* in Figure 5.8a is only 1.4. Decreasing the buffer concentration would increase the electromigration dispersion and thus decrease the separation resolution, making collection of a pure protein fraction impossible.

As shown in Chapter Three (Table 3.5), the EOF with a 2C<sub>18</sub>DAB coating was lower than that with 2C<sub>14</sub>DAB coating. As the separation of proteins in Figure 5.8a is





**Figure 5.9** Mass spectra of polypeptide ladders of h-cyt *c* fractions collect from electrophoretic runs using two different coatings: **a.** 2C<sub>14</sub>DAB; and **b.** 2C<sub>18</sub>DAB. The fractions were collected from electrophoretic runs in Figure 5.8. The expanded spectra a.1-a.6 and b.1-b.6 show the labeled peaks for the corresponding peptides from the N-terminal of the protein.

performed in the counter-EOF mode, a lower EOF should yield a greater resolution, as illustrated by eq. 1.23. Therefore, the buffer concentration with a 2C<sub>18</sub>DAB coated capillary could be reduced without altering the sample loading.

#### 5.4.6 Effect of 2C<sub>18</sub>DAB Surfactant on MAAH/MALDI

To examine the effect of the 2C<sub>18</sub>DAB surfactant on the MAAH/MALDI, the protein analysis was performed under the same buffer conditions, as in Section 5.4.5. Figure 5.8b shows the separation of the cytochrome *c* mixture at a concentration of 40 g/L (160 pmol of each protein). Both b-cyt *c* and h-cyt *c* are separated in about 52 min. This longer migration time is expected for a counter-EOF separation where the EOF and analyte mobility are well matched [47]. The peaks of both b-cyt *c* and h-cyt *c* are more fronted ( $B/A = 0.18$  and  $0.21$  respectively) with the 2C<sub>18</sub>DAB coating than that with the 2C<sub>14</sub>DAB coating ( $B/A = 0.65$  and  $0.74$  respectively). Equation 4.4 predicts that the electromigration dispersion would be greater with the 2C<sub>18</sub>DAB coating as a result of the slower apparent mobility of the analytes ( $\mu_{app}$ ). However, the separation resolution between b-cyt *c* and h-cyt *c* increased to 2.2 due to the slower electroosmotic flow obtained using the 2C<sub>18</sub>DAB coating.

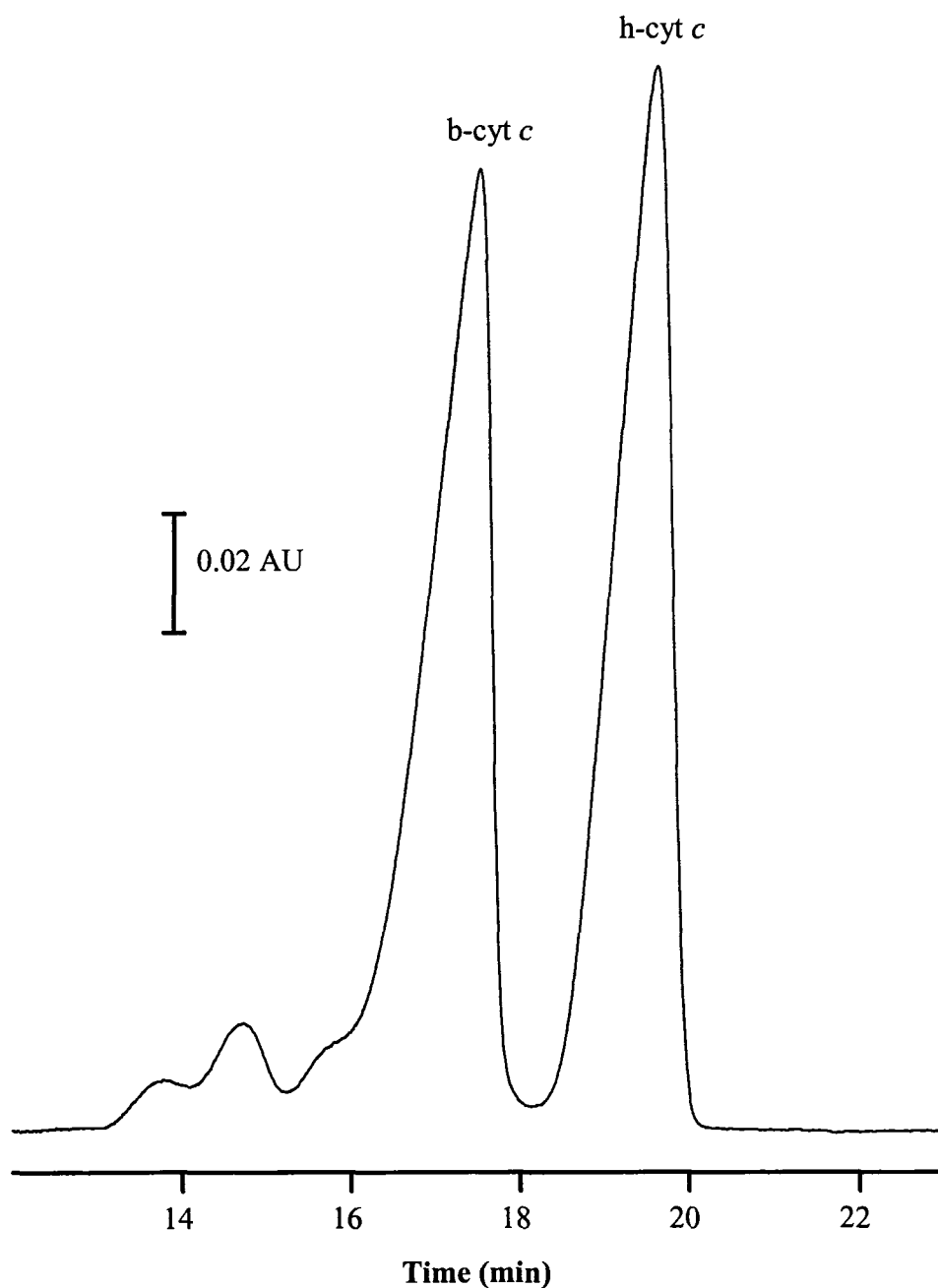
The spectrum of the hydrolyzed resultant mixture of the h-cyt *c* fraction obtained by MAAH/MALDI with the 2C<sub>18</sub>DAB coating is shown in Figure 5.9.b. The sequence coverage achieved is 76% (N-terminal), comparable to what was obtained with 2C<sub>14</sub>DAB coating at same sample loading (Section 5.4.5). This indicates that the surfactant coating has only a minor influence on the MAAH/MALDI method, consistent with the preliminary results in Section 5.4.4. This is also consistent with previous demonstration of the tolerance of the MAAH technique to common additives such as surfactants [26].

#### 5.4.7 Effect of Buffer Concentration on MAAH/MALDI

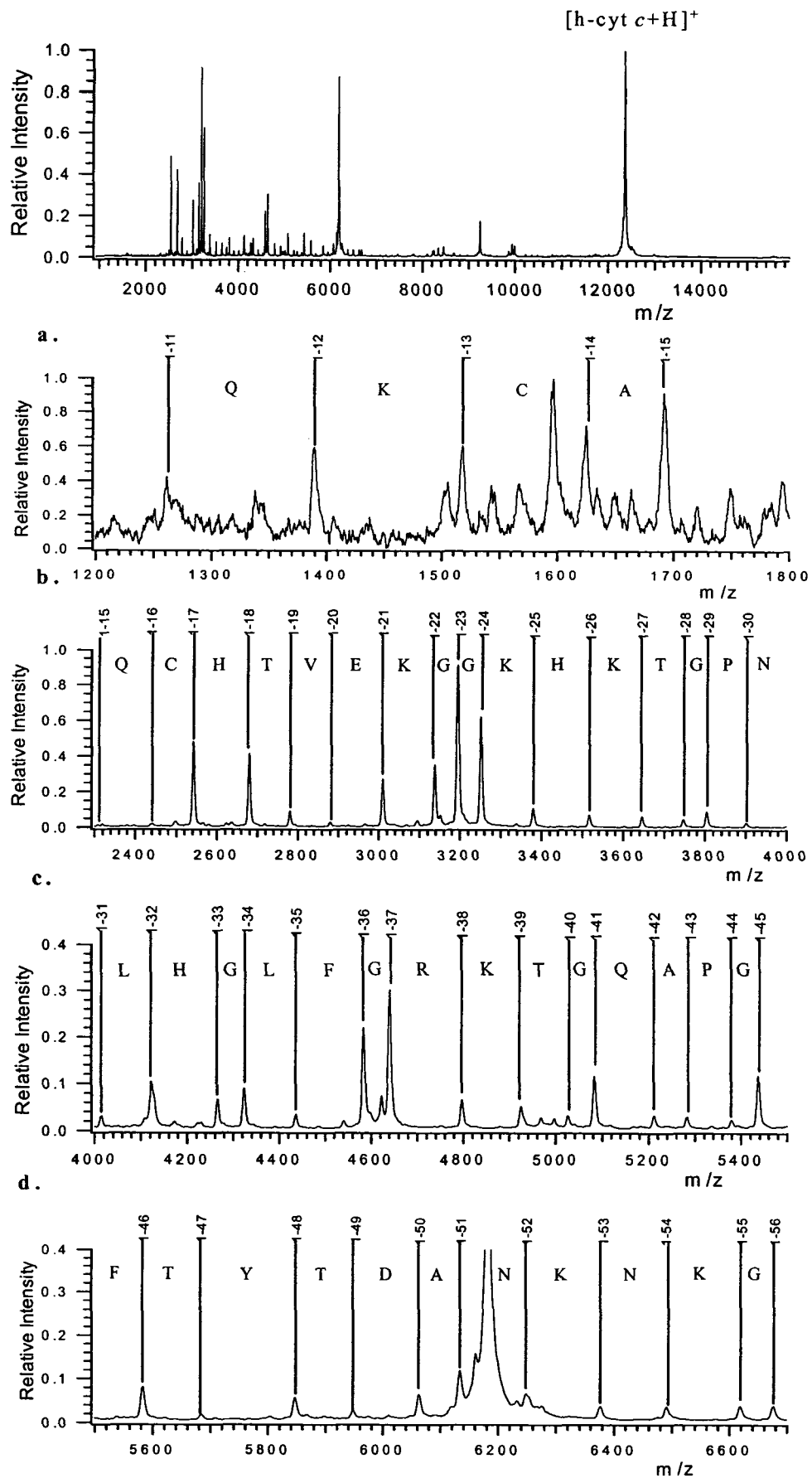
The advantage of utilizing the 2C<sub>18</sub>DAB coatings rather than the 2C<sub>14</sub>DAB coating is that the separation resolution of the protein mixture is higher. This allows the buffer concentration to be decreased while still maintaining a reasonable separation resolution. Furthermore, a low buffer concentration allows the applied voltage to be increased, thereby reducing the analysis time. Figure 5.10 shows the separation of the protein mixture at a concentration of 40 g/L (160 pmol of each protein) in 25 mM Bis-tris phosphate buffer with the 2C<sub>18</sub>DAB coating at -20 kV (-10 kV was used in Figure 5.8). The separation resolution between b-cyt *c* and h-cyt *c* was 1.4. In addition, the separation time was decreased to 20 min due to the increased applied voltage.

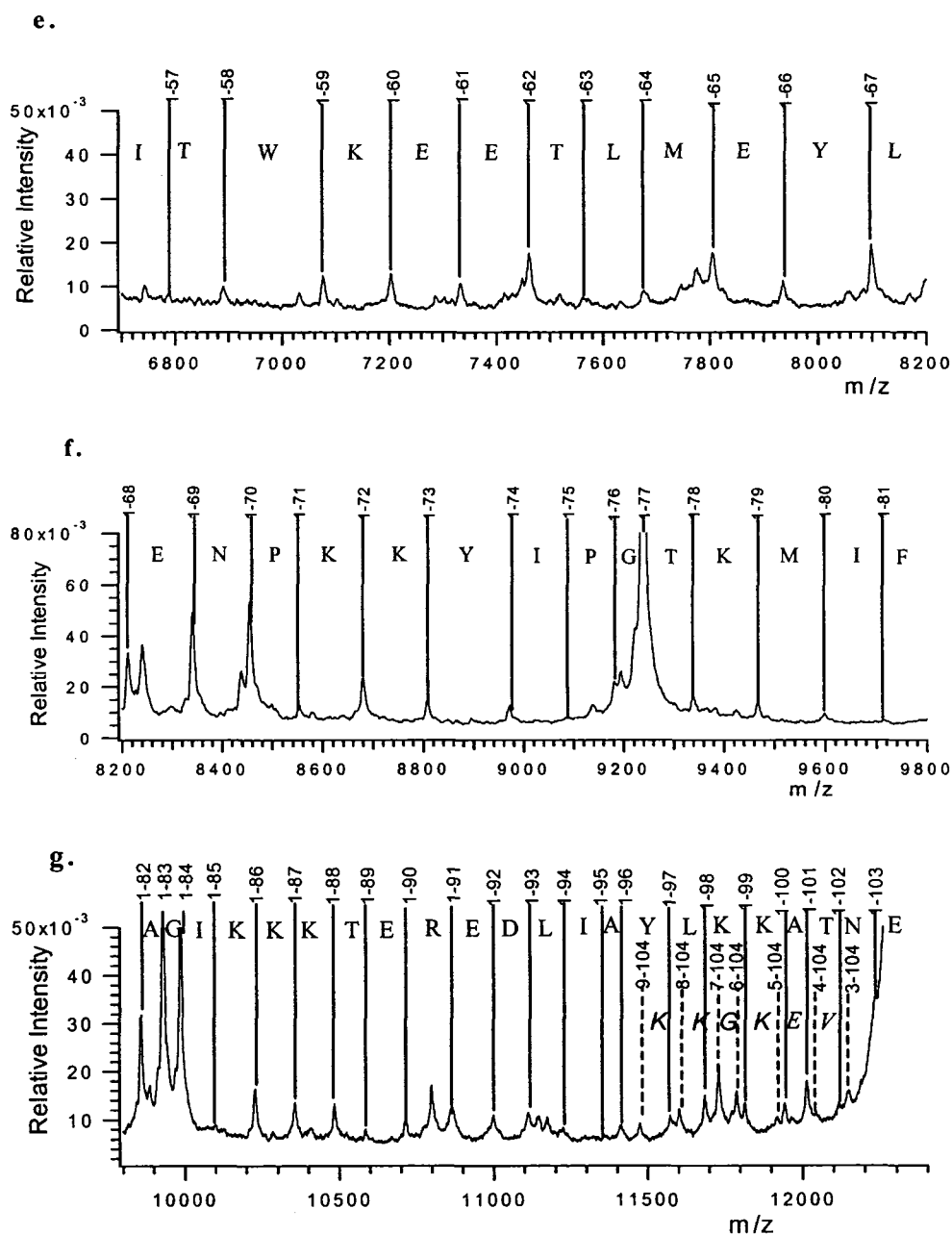
Figure 5.11 shows the polypeptide mixture from the MAAH/MALDI of the h-cyt *c* fraction. As shown in the expanded spectra (Figure 5.11 a-g), all polypeptides with masses larger than 1200 Da from the N-terminal were detected as a continuous ladder. Seven additional C-terminal polypeptides within high mass range were also identified. The peptide sequence coverage for h-cyt *c* collected from CE separation with 25 mM Bis-tris phosphate buffer was 95% (combined N-terminal and C-terminal). This compares very favorably with the combined N- and C-terminal coverage achieved for neat protein solutions [25].

The enhancement of the peptide sequence coverage using CE-MAAH/MALDI was mainly due to the decrease of the separation buffer concentration in the collection vial. During fractionation, a considerable amount of the separation buffer was introduced into the collection vial and thus suppressed the polypeptide signals. This signal suppression reduced the peptide sequence coverage of the protein at separation 100 mM



**Figure 5.10** Electropherogram of b-cyt *c* and h-cyt *c* at 25 mM Bis-tris phosphate buffer using 2C<sub>18</sub>DAB coatings. **Experimental conditions:** 58.0 cm × 100 μm i.d. capillary (48.0 cm to the detector); applied voltage at -20 kV; protein sample was dissolved in water at concentration of 40 g/L of each protein; hydrodynamic injection at 3.4 kPa for 3 s (160 pmol of each protein); buffer pH, 7.0; temperature, 25 °C; and λ, 254 nm.





**GDVEKGGKKIF VQKCAQCHTV EKGKHKHTGP NLHGLFGRKT**  
**GQAPGFITYD ANKNKGITWK EETLMEYLEN PKKYIPGTKM**  
**IFAGIKKKTE REDLIAYLKK ATNE**

**Figure 5.11** Mass spectrum of polypeptide ladder of h-cyt *c* fraction collect from electrophoretic run in Figure 5.10. CE separation performed using 2C<sub>18</sub>DAB coated capillary in 25 mM Bis-tris phosphate buffer at pH 7.0. The expanded spectra a-g show the labeled peaks for the corresponding peptides from the N-terminal amino acid (solid lines and bold letters) and C-terminal (dotted lines and italic letters) of the protein. Note: only the polypeptide peaks that are not identified from the N-terminal were labeled from the C-terminal in this Figure.

Bis-tris phosphate buffer. Decreasing the separation buffer concentration 4-fold enabled more peptides to be detected which increased the sequence coverage from 76 to 89% (N-terminal). Further decreasing the concentration of the separation buffer to 10 mM reduced the separation resolution to 0.95 for a 40 g/L loading. Thus, isolation of pure protein fractions at high sample loading could not be performed with 10 mM Bis-tris buffer. Thus, isolation of pure protein fractions at high sample loading could not be performed with Bis-tris buffer concentration less than 25 mM. Nonetheless, using CE separation with 25 mM Bis-tris phosphate buffer the polypeptides from 1-11 to 1-104 (N-terminal) were identified continuously from a single spectrum (Figure 5.11a-g). In addition, seven more polypeptides from 3-104 to 9-104 (C-terminal) were also identified in the same spectrum (Figure 5.11g).

This peptide sequence coverage is very high compared to what can be achieved with other peptide mapping methods using MALDI/ TOF MS. For instance, peptide mapping after enzymatic digestion typically provides, at most, a sequence coverage of 40-50% [16]. In addition, 2D-gel separations, and their associated subsequent extractions and cleaning are laborious and time-consuming [5-7]. Finally, enzymatic digestion of the isolated for protein prior to MS characterization requires at least 12 hours [15, 16]. In contrast, the analysis time of the entire CE-MAAH/MALDI process- including protein separations, collection and characterization- was less than one hour. This is at least 20 times less than required for 2D-gel combined by mass spectrometric characterization of proteolytic digestion. In addition, CZE separations are performed in free buffer solution, and thus the proteins may be purified and isolated with no sample pre-cleaning.

## 5.5 Conclusions

CZE has been demonstrated to be a useful tool for preparative fraction collection of proteins. Parameters, such as voltage ramp time and the buffer level during fractionation, should be taken into consideration upon using wide bore capillary to improve the quality of the collected fractions. Pure horse cytochrome *c* fraction was collected and isolated from the preparative CE. Collection of pure bovine cytochrome *c* was hampered by contamination from horse cytochrome *c*.

Microwave-assisted acid hydrolysis (MAAH) provided a rapid method for characterization of pure proteins. Preparative CE has the ability to collect pure protein at the picomole scale. Off-line coupling fast CE separation with MAAH/ MALDI, protein mixture can be separated and characterized. The analysis including protein separations, fraction isolation and protein identification, could be performed within one hour, and the method is easy to operate with no complicated steps involved. Using buffer with a mobility matching that of the protein, the CE sample loading can be increased to 160 pmol. Increasing the buffer concentration (100 mM) is necessary to reduce broadening due to electromigration dispersion at preparative scales. However, the introduction of the separation buffer into the collection vial during fractionation has a significant negative influence on MAAH/MALDI, and reduces the sequence coverage for the examined protein. Reducing the buffer concentration four-fold, the sequence coverage achieved by coupling CE with MAAH/MALDI at sample loading of 40 g/L was 95%.

## 5.6 References

- [1] Görg, A., Weiss, W., Dunn, M. J., *Proteomics* 2004, 4, 3665-3685.
- [2] Stutz, H., *Electrophoresis* 2005, 26, 1254-1290.
- [3] Gevaert, K., Vandekerckhove, J., *Electrophoresis* 2000, 21, 1145-1154.
- [4] Zhu, H., Bilgin, M., Snyder, M., *Annu. Rev. Biochem.* 2003, 72, 783-812.
- [5] Wang, Y., Balgley, B. M., Rudnick, P. A., Lee, C. S., *J. Chromatogr. A* 2005, 1073, 35-41.
- [6] Cohen, S. L., Chait, B. T., *Anal. Biochem.* 1997, 247, 257-267.
- [7] Clarke, N. J., Li, F., Tomlinon, A. J., Naylor, S., *J. Am. Soc. Mass Spectrom.* 1998, 9, 88-91.
- [8] Reynolds, J. A., Tanford, C., *Proc. Natl. Acad. Sci. USA* 1970, 66, 1002-1007.
- [9] Nelson, C. A., *J. Biol. Chem.* 1971, 246, 3895-3901.
- [10] Molloy, M. P., *Anal. Biochem.* 2000, 280, 1-10.
- [11] Keller, B. O., Wang, Z., Li, L., *J. Chromatogr. B* 2002, 782, 317-329.
- [12] Jeannot, M. A., Zheng, J., Li, L., *J. Am. Soc. Mass Spectrom* 1999, 10, 512-520.
- [13] Zhang, N., Doucette, A., Li, L., *Anal. Chem.* 2001, 73, 2968-2975.
- [14] Rundlett, K. L., Armstrong, D. W., *Anal. Chem.* 1996, 68, 3493-3497.
- [15] Zhu, K., Kim, J., Yoo, C., Miller, F. R., Lubman, D. M., *Anal. Chem.* 2003, 75, 6209-6217.
- [16] Yoo, C., Pal, M., Miller, F. R., Barder, T. J., Huber, C., Lubman, D. M., *Electrophoresis* 2006, 27, 2126-2138.
- [17] Yeung, K. K.-C., Kiceniuk, A. G., Li, L., *J. Chromatogr. A* 2001, 931, 153-162.
- [18] Boss, H. J., Rohde, M. F., Rush, R. S., *Anal. Biochem.* 1995, 230, 123-129.

- [19] Karas, M., Bahr, U., Hillenkamp, F., *Int. J. Mass Spectrom. Ion Processes* 1989, 92, 231-242.
- [20] Karas, M., Bahr, U., *Trends Anal. Chem.* 1990, 9, 321-325.
- [21] Zhang, H., Caprioli, R. M., *J. Mass Spectrom.* 1996, 31, 1039-1046.
- [22] Preisler, J., Hu, P., Rejtar, T., Karger, B. L., *Anal. Chem.* 2000, 72, 4785-4795.
- [23] Walker, K. L., Chiu, R. W., Monnig, C. A., Wilkins, C. L., *Anal. Chem.* 1995, 67, 4197-4204.
- [24] Keough, T., Takigku, R., Lacey, M. P., Purdon, M., *Anal. Chem.* 1992, 64, 1594-1600.
- [25] Zhong, H., Marcus, S. L., Li, L., *J. Am. Soc. Mass Spectrom.* 2005, 16, 471-481.
- [26] Zhong, H., Zhang, Y., Wen, Z., Li, L., *Nat. Biotechnol.* 2004, 22, 1291-1296.
- [27] Li, L., in, Edmonton, May, 2005 (personal communication).
- [28] Melanson, J. E., Baryla, N. E., Lucy, C. A., *Anal. Chem.* 2000, 72, 4110-4114.
- [29] Baryla, N. E., Melanson, J. E., McDermott, M. T., Lucy, C. A., *Anal. Chem.* 2001, 73, 4558-4565.
- [30] Yassine, M. M., Lucy, C. A., *Anal. Chem.* 2004, 76, 2983-2990.
- [31] Yassine, M. M., Lucy, C. A., *Anal. Chem.* 2005, 77, 620-625.
- [32] van Veelen, P. A., Tjaden, U. R., van der Greef, J., Ingendoh, A., Hillenkamp, F., *J. Chromatogr.* 1993, 647, 367-374.
- [33] Rose, D. J., Jorgenson, J. W., *J. Chromatogr.* 1988, 438, 23-34.
- [34] Murray, K. K., *Mass Spectrom. Rev.* 1997, 16, 283-299.
- [35] Huang, X., Zare, R. N., *Anal. Chem.* 1990, 62, 443-446.

- [36] Weinmann, W., Parker, C. E., Deterding, L. J., Papac, D. I., Hoyes, J., Przybylski, M., Tomer, K. B., *J. Chromatogr. A* 1994, 680, 353-361.
- [37] Kobayashi, H., Shimamura, K., Akaida, T., Sakano, K., Tajima, N., Funazaki, J., Suzuki, H., Shinohara, E., *J. Chromatogr. A* 2003, 990, 169-178.
- [38] Kasicka, V., Prusik, Z., Sazelova, P., Jiracek, J., Barth, T., *J. Chromatogr. A* 1998, 796, 211-220.
- [39] Leonenko, Z. V., Carnini, A., Cramb, D. T., *Biochim. Biophys. Acta* 2000, 1509, 131-147.
- [40] Valko, I. E., Porras, S. P., Riekkola, M.-L., *J. Chromatogr. A* 1998, 813, 179-186.
- [41] Lee, H. G., Desiderio, D. M., *J. Chromatogr. A* 1994, 686, 309-317.
- [42] Keller, B. O., Li, L., *J. Am. Soc. Mass Spectrom.* 2000, 11, 88-93.
- [43] Bello, M. S., *J. Chromatogr. A* 1996, 744, 81-91.
- [44] Kenndler, E., Friedl, W., *J. Chromatogr.* 1992, 608, 161-170.
- [45] Williams, B. A., Vigh, G., *Anal. Chem.* 1995, 67, 3079-3081.
- [46] Bergman, A.-C., Bergman, T., *FEBS Letters* 1996, 397, 45-49.
- [47] Terabe, S., Yashima, T., Tanaka, N., Araki, M., *Anal. Chem.* 1988, 60, 1673-1677.

## CHAPTER SIX: Summary and Future Work

### 6.1 Summary

This thesis has demonstrated the stability of the semi-permanent coating can be highly enhanced by altering the experimental conditions. Careful control of physical and chemical factors enabled generation of highly stable and efficient semi-permanent coatings for protein separations (Chapters Two and Three). Further, the high stability achieved by the semi-permanent coating was the basis of utilizing CZE for preparative operations for protein separations as well as collecting and isolating pure protein fractions in the picomole range for characterization with MAAH/MALDI method (Chapters Four and Five).

In Chapter Two, I showed that the didodecyldimethylammonium bromide (DDAB) surfactant coating degraded in a first order kinetic fashion as the electrophoretic buffer passes through the capillary. As the run buffer passes through the capillary, it removed the free surfactant from the bulk solution in the capillary. Thus, more surfactant molecules had to leach from the bilayer to reestablish the equilibrium between the bilayer and the bulk solution inside the capillary. This reduced the charge density on the capillary wall and as a consequence reduced the EOF. Decreasing the capillary inner diameter reduced the volumetric flow of the buffer through the capillary and thus minimized surfactant bleeding from the bilayer. Buffer pH had an indirect effect on the stability of the DDAB coating. Enhancing the degree of ionization of the silica surface, by elevating the buffer pH, increased the stability of the coating. More important were the effect of chemical factors such as buffer ionic strength and the nature of the counter-

ion. These factors impacted on the coating stability through their influence on the surfactant critical micelle concentration (cmc). Increasing the buffer ionic strength decreased the cmc of the surfactant solution and thereby increased the stability of the DDAB coating.

A more direct means to increase the stability of the bilayer was to decrease the cmc of the surfactant by increasing the volume of the hydrocarbon region of the surfactant monomers (Chapter Three). This was done by either increasing the length of the hydrocarbon tail, i.e., long double chained surfactants, or increasing the number of hydrocarbon chains, i.e., triple chained surfactant. These coatings are simply performed by rinsing the capillary with the surfactant containing solution for a short time (< 5 min). The excess surfactants were removed by flushing the capillary with run buffer. The bilayer coatings formed by these surfactants were very stable and exhibited high separation efficiencies for cationic proteins. Using dimethylditetradecylammonium bromide ( $2C_{14}DAB$ ) coating in 50 mM ammonium formate buffer at pH 4.5, protein separations were achieved in about 2 min with efficiencies of 1.4 million plates/m. The stability of the long chained surfactants, in particular dimethyldioctadecylammonium bromide ( $2C_{18}DAB$ ), was very high, with reproducibility less than 0.84% RSD within the day and less than 2.3% RSD from day-to-day (5 days), without the need to recoat the capillary between runs.

In Chapter Four, long chained surfactant coated wide-bore capillaries (100  $\mu\text{m}$  i.d.) were utilized for protein separations at the preparative scale. For preparative operation, wide bore capillaries (100  $\mu\text{m}$  i.d.) were essential to increase the sample loading without increasing the sample plug length. Long chained surfactant coating was

found to be stable in the wide bore capillary and thus significantly reduced the broadening due to adsorption. At low protein concentrations ( $\leq 1$  g/L), symmetrical peaks were obtained indicating that protein adsorption was highly minimized. Further increase in the sample loading was accomplished by increasing the protein concentration. However, at high protein concentrations electromigration dispersion became the dominant source of broadening and the peak shape distorted to triangular fronting. Electromigration dispersion was minimized by increasing the buffer concentration and thus decreased the sample-to-buffer concentration ratio. Yet, this approach was limited by Joule heating broadening. Matching of the mobility of the buffer co-ion to that of the protein resulted in dramatic improvements in the efficiency and peak shape. This mobility match significantly lowers the electromigration dispersion, allowing more proteins to be injected onto the capillary. Bis-tris co-ion has a low ionic mobility that matches the effective mobility of the proteins examined in Chapter Four. Using 100 mM Bis-tris phosphate buffer at pH 7.0 with a 100  $\mu\text{m}$  i.d. capillary, the sample loading capacity in a single run was 2.0  $\mu\text{g}$  of each protein, 3250 fold more than what was normally injected into 50  $\mu\text{m}$  i.d. capillaries.

Off-line coupling of preparative CE with MAAH/MALDI for protein characterization was demonstrated in Chapter Five. This coupling, CE with MAAH/MALDI, offers a simple and powerful method for protein separation and characterization in a short time. The analysis, including protein separation, fraction isolation and protein identification, was performed within an hour. Moreover, the method was easy to operate with no complicated steps involved. The timing of the fraction collection was controlled using manual electrokinetic fractionation. The buffer level in the inlet and collection vial

was adjusted to avoid siphoning and improve the quality of the fractions collected from wide bore capillary.

The choice of the buffer conditions was critical for both preparative CE and the MAAH/MALDI method. Utilizing high buffer concentration with co-ion mobility matching that of the protein, the CE sample loading was increased to 160 picomoles of each protein. High buffer concentration was necessary to reduce broadening due to electromigration dispersion. However, at high buffer concentrations a considerable amount of buffer was introduced into the collection vial during fractionation, which reduced the peptide sequence coverage obtained by MAAH due to MALDI signal suppression. The peptide sequence coverage achieved by MAAH/MALDI for protein fraction collected from preparative CE in 100 mM Bis-tris separation buffer was 76% (N-terminal) at a sample loading of 40 g/L of each protein. Reducing the separation buffer concentration to 25 mM, the peptide sequence coverage was increased to 89% (N-terminal) at the same sample loading.

In conclusion, modification of the capillary surface is essential to prevent protein adsorption onto capillary surface and improve separation performance. Long chained surfactant coatings provide an efficient and economical method for protein separations in capillary electrophoresis. The coating procedure of these surfactants is simple, reproducible and yields high coating stability under severe rinsing conditions in aqueous buffer. Furthermore, the high stability of these coatings in wide bore capillaries permits use of CE for preparative protein separations. Optimizing the experimental conditions, such as buffer concentration, and buffer co-ions, allows high protein concentrations to be injected into the capillary for protein characterization using MAAH/MALDI technique.

## 6.2 Future Work

### 6.2.1 On-line ESI-MS

CE-ESI MS is a powerful analytical method allowing fast separation and detection. Commonly, covalently bonded coatings are a frequent choice for surface modification to prevent peptide and protein adsorption onto the silica surface [1]. Dynamic surfactant coatings are an attractive alternative for covalently bonding coatings because of the simplicity of coating formation. However, single chained surfactants are not compatible with ESI-MS [2]. The presence of the free surfactant molecules in the running buffer suppresses the protein signal and thus decreases the sensitivity of the ESI MS. In addition, adsorption of the surfactant onto the counter-electrode (nozzle) decreases the sensitivity over time [3].

Double chained surfactant, DDAB, form a semi-permanent coating, where surfactant need not be present in the run buffer [4, 5]. However, the DDAB bilayers do gradually degrade as the running buffer passes through the capillary, as shown in Chapter Two. The free DDAB from the degrading bilayer could interfere with electrospray ionization mass spectrometry (ESI-MS). Although the stability of these bilayer coatings could be improved by increasing the ionic strength of the run buffer, this approach is limited by Joule heating generated within the capillary and would cause ion suppression in ESI.

As shown in Chapter Three, the long chained surfactants such as  $2C_{14}DAB$  and  $2C_{18}DAB$  as well as triple chained surfactant,  $3C_{12}MAI$ , formed semi-permanent coatings. These surfactants produced high stability coatings in volatile buffers and exhibited high separation efficiencies for cationic proteins. Due to their high stability, it

is expected that the surfactant coatings would be compatible with electrospray ionization (ESI). Further, utilizing the volatile buffers, such as ammonium formate and ammonium acetate, would be suitable for electrospray ionization process [6].

Coupling CE to MS via ESI would be a valuable separation technique not only for proteins but also for peptide mixtures. Utilizing cationic surfactant-based coatings give the advantage of altering the selectivity of proteins and peptides by changing the separation buffer conditions. In addition, employing the CE-ESI-MS to analyze the resultant peptide mixtures from the microwave digestions would be beneficial to reduce suppression of the peptide signals experienced by the nonvolatile buffers. Thus, it is expected that the separation of the polypeptide mixture produced from MAAH by using surfactant coated capillaries with volatile buffer coupled to the ESI-MS, would improve the signal-to-noise ratio of the polypeptide peaks. Furthermore, the mass range for detecting polypeptides with the MAAH/MALDI method is limited to 14000 Da. This limit is attributed to the problem associated with peptide detection and not to the hydrolysis process [7]. Thus, utilizing CE-ESI-MS would expand the applicability of the MAAH for large proteins (>14000 Da), and full peptide sequence coverage could be achieved.

### **6.2.2 EOF Control for Preparative CZE Applications**

It is well known that the EOF can modify the separation resolution and speed of analysis time. The EOF is often desirable for fast separations since the flat flow profile does not hinder the separation efficiency. However, differences in the analyte mobility are accentuated when the EOF flows against the analyte mobility. For instance, high resolution separations are achieved when the magnitude of the counter EOF is

comparable to that of the analyte [8, 9]. Therefore, control of the EOF is important to optimize the separation resolution of closely migrating analyte components. In addition, by suppressing the EOF it is possible to separate the both cationic and anionic proteins.

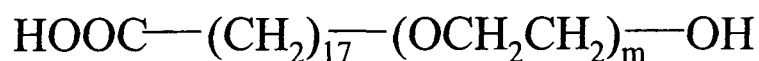
Polyethylene glycol has been utilized as dynamic coating since it forms a neutral hydrophobic coating. Upon adsorption onto the silica surface, polyethylene glycol can effectively suppress the EOF as a result of screening the silanols at the capillary surface [10]. In addition, these coatings exhibited excellent resistance to protein adsorption [11, 12]. However, the adsorption of polyethylene glycol held to the surface by weak interactions, such as van der Waals forces and hydrogen bonding [10]. Thus, the coating can be easily removed from the capillary surface in between the runs.

Recently, MacDonald et al. [13] demonstrated that a stable surface coating can be formed in 50  $\mu\text{m}$  i.d. capillary by mixing  $2\text{C}_{18}\text{DAB}$  surfactant with polyoxyethylene stearate (Figure 6.1a). In the mixed  $2\text{C}_{18}\text{DAB}$ /polyoxyethylene 40 stearate coating, the cationic surfactants adsorbed to the silica surface via electrostatic interaction. However, polyoxyethylene 40 stearate headgroups extend from the top surface of the bilayer into the solution and suppress the EOF by creating a hydrophilic surface. The EOF was found to be 10 times less than that observed for  $2\text{C}_{18}\text{DAB}$  coatings alone. The major advantage of this mixed surfactant/polymer coating is that both cationic and anionic proteins can be separated with excellent efficiency. In addition, the resolution separation between proteins was higher than that achieved with cationic surfactants alone.

For preparative purposes, a wide bore capillary is necessary to increase the sample loading of proteins, as shown in Chapter Four. Since polyoxyethylene stearate has a single hydrophobic tail (Figure 6.1a), the stability of the bilayer is expected to be

highly reduced when a wide bore capillary is utilized, due to the high volumetric flow generated inside the capillary. Polyethylene glycol dialkyl ether,  $2C_nE_m$  (Figure 6.1b), such as 1,2-di-O-octadecyl-rac-glycerol-3-( $\omega$ -dodecaethylene glycol),  $2C_{18}E_{12}$ , are double chained nonionic surfactants that aggregate in aqueous solution to form vesicle like structures [14, 15]. By mixing  $2C_{18}DAB$  with the nonionic surfactant  $2C_{18}E_{12}$ , it is expected that the produced surfactant coating would be stable in the wide bore capillary, due to the high hydrophobic interaction between the two surfactants. Increasing the ratio of the neutral surfactant to that of  $2C_{18}E_{12}$ , the charge density of the coating decreases,

**a.**



**b.**

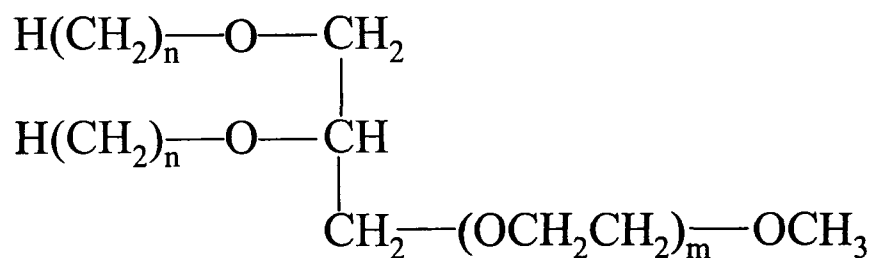


**Figure 6.1** General structure of **a.** polyoxyethylene stearate; and **b.** dialkyl polyoxyethylene ether surfactant of the  $2C_nE_m$  family.

and thus the EOF is also reduced. The advantage of this approach is that proteins can be separated with high resolution, and thus closely migrating protein components can be isolated at preparative scales. More importantly, anionic proteins can also be separated by increasing the ratio of the neutral surfactant to suppress the EOF. Thus, the preparative CE applications can be extended to isolate and collect anionic proteins at preparative scale levels for characterization using MAAH method.

### 6.3 References

- [1] Simpson, D. C., Smith, R. D., *Electrophoresis* 2005, 26, 1291-1305.
- [2] Rundlett, K. L., Armstrong, D. W., *Anal. Chem.* 1996, 68, 3493-3497.
- [3] Varghese, J., Cole, R. B., *J. Chromatogr. A* 1993, 652, 369-376.
- [4] Baryla, N. E., Melanson, J. E., McDermott, M. T., Lucy, C. A., *Anal. Chem.* 2001, 73, 4558-4565.
- [5] Melanson, J. E., Baryla, N. E., Lucy, C. A., *Anal. Chem.* 2000, 72, 4110-4114.
- [6] Klampfl, C. W., *Electrophoresis* 2006, 27, 3-34.
- [7] Zhong, H., Zhang, Y., Wen, Z., Li, L., *Nat. Biotechnol.* 2004, 22, 1291-1296.
- [8] Terabe, S., Yashima, T., Tanaka, N., Araki, M., *Anal. Chem.* 1988, 60, 1673-1677.
- [9] Yeung, K. K.-C., Lucy, C. A., *Anal. Chem.* 1998, 70, 3286-3290.
- [10] Preisler, J., Yeung, E. S., *Anal. Chem.* 1996, 68, 2885-2889.
- [11] Prime, K. L., Whitesides, G. M., *Science* 1991, 252, 1164-1167.
- [12] Pale-Grosdemange, C., Simon, E. S., Prime, K. L., Whitesides, G. M., *J. Am. Chem. Soc.* 1991, 113, 12-20.
- [13] MacDonald, A. M., Lucy, C. A., *J. Chromatogr. A* 2006, on line.
- [14] Harvey, R. D., Heenan, R. K., Barlow, D. J., Lawrence, M. J., *Langmuir* 2004, 20, 9282-9290.
- [15] Harvey, R. D., Heenan, R. K., Barlow, D. J., Lawrence, M. J., *Chem. Phys. Lipids* 2005, 133, 27-36.